Inhibition of UDP-Glucose Dehydrogenase by 6-Thiopurine and its Oxidative Metabolites: Possible mechanism for its interaction within the Bilirubin excretion pathway and 6-Thiopurine associated toxicity

by

Chamitha Janani Weeramange

B.Sc., Wichita State University, 2013

AN ABSTRACT OF A DISSERTATION

submitted in partial fulfillment of the requirements for the degree

DOCTOR OF PHILOSOPHY

Department of Chemistry
College of Arts and Sciences

KANSAS STATE UNIVERSITY
Manhattan, Kansas

2018

Abstract

6-Thiopurine (6TP), or 6-mercaptopurine, is an actively prescribed drug in the treatment of acute lymphocytic leukemia since 1952. Although 6TP has beneficial and promising therapeutic uses, severe toxicities are associated with its use such as jaundice and hepatotoxicity. These toxicities are due to the higher level of accumulation of bilirubin within the body. The bilirubin pathway involves the conjugation of water-insoluble bilirubin to two equivalents of UDP-glucuronic acid (UDPGA) forming the water-soluble and excretable bilirubin diglucuronide species. The glucuronidation of bilirubin is catalyzed by the UDP-glucuronosyl transferase (UGT) enzyme, and the formation of substrate UDPGA is catalyzed by the UDP-glucose dehydrogenase enzyme (UDPGDH).

The therapeutic activity of 6TP comes from two main routes: methylation of the thiol of 6TP and formation of a deoxy-6-thioguanosine triphosphate mimic that is incorporated into DNA resulting in apoptosis. In conjugation to its therapeutic metabolism, there are also detoxification pathways operating simultaneously that significantly reduce its therapeutic activity. In this pathway, oxidative metabolites of 6TP such as 8-hydroxyl-6-thiopurine (6TP-8OH), 6-thioxanthine (6TX) and 6-thiouric acid (6TU) can be formed by xanthine oxidase. It has been observed that the body retains 6TU well beyond 24-hour post 6TP treatment. Therefore, we proposed that the observed toxicity from 6TP administration comes from either 6TP or its oxidative excretion metabolites' ability to inhibit one or both enzymes (UDPGDH, UGT) in the bilirubin excretion pathway. To investigate the toxicity resulting from the 6TP administration about these two enzymatic steps, inhibition analysis of these oxidative metabolites on UDPGDH was assessed using a robust UV-Vis method. The inhibition profile made with regards to varying UDP-glucose showed weak to no inhibition of 6TP towards UDPGDH with a K_i of 288 μM.

However, 6TU, (the primary oxidative metabolite which is oxidized at C2 and C8) has increased inhibition towards UDPGDH with K_i of 7 μM. Inhibition was also observed with 6TX (oxidized at C2) and 8-OH-6TP (oxidized at C8) with K_i values 54 and 14 μM, respectively. To further confirm the results of the UV-Vis assessment, inhibition studies were carried out using an HPLC method that was developed and validated to separate all the analytes in the UDPGDH catalyzed reaction. Inhibition studies were performed via the HPLC method showed K_i values of 105 μM and 5 μM for 6TP and 6TU, respectively, towards UDPGDH.

To assess the inhibition studies towards the UGT enzyme, an HPLC method was developed for the simultaneous determination of bilirubin and its mono/diglucuronides. The inhibition studies were carried to assess the formation of glucuronides and consumption of UDPGA in the presence of the inhibitors using the HPLC method developed. Neither 6TP nor 6TU were shown to inhibit UGT. Also, inhibition studies were carried out *in vivo* animal model, which further confirmed that 6TP and 6TU do inhibit UDPGDH, but no effect on UGT activity. With these results, we discovered that both 6TP and its oxidative metabolites inhibit UDPGDH. Furthermore, it was observed that C2 and C8 positions of 6TP are important for the toxicity towards UDPGDH.

With the goal of developing a single multi-enzymatic assay, another HPLC method was developed to assess the UDPGDH and UGT catalyze reactions together. This method can be used as a standard method to assess interference of any molecule on bilirubin excretion. Given the findings in this study, efforts are being directed towards the synthesis of 8-substituted 6TP analogs that are proposed to retain its therapeutic efficacy but have limited to no toxicity.

Inhibition of UDP-Glucose Dehydrogenase by 6-Thiopurine and its Oxidative Metabolites: Possible mechanism for its interaction within the Bilirubin excretion pathway and 6-Thiopurine associated toxicity

by

Chamitha Janani Weeramange

B.Sc., Wichita State University, 2013

A DISSERTATION

submitted in partial fulfillment of the requirements for the degree

DOCTOR OF PHILOSOPHY

Department of Chemistry
College of Arts and Sciences

KANSAS STATE UNIVERSITY
Manhattan, Kansas

2018

Approved by:

Major Professor
Ryan J. Rafferty, Ph.D.

Copyright

Abstract

6-Thiopurine (6TP), or 6-mercaptopurine, is an actively prescribed drug in the treatment of acute lymphocytic leukemia since 1952. Although 6TP has beneficial and promising therapeutic uses, severe toxicities are associated with its use such as jaundice and hepatotoxicity. These toxicities are due to the higher level of accumulation of bilirubin within the body. The bilirubin pathway involves the conjugation of water-insoluble bilirubin to two equivalents of UDP-glucuronic acid (UDPGA) forming the water-soluble and excretable bilirubin diglucuronide species. The glucuronidation of bilirubin is catalyzed by the UDP-glucuronosyl transferase (UGT) enzyme, and the formation of substrate UDPGA is catalyzed by the UDP-glucose dehydrogenase enzyme (UDPGDH).

The therapeutic activity of 6TP comes from two main routes: methylation of the thiol of 6TP and formation of a deoxy-6-thioguanosine triphosphate mimic that is incorporated into DNA resulting in apoptosis. In conjugation to its therapeutic metabolism, there are also detoxification pathways operating simultaneously that significantly reduce its therapeutic activity. In this pathway, oxidative metabolites of 6TP such as 8-hydroxyl-6-thiopurine (6TP-8OH), 6-thioxanthine (6TX) and 6-thiouric acid (6TU) can be formed by xanthine oxidase. It has been observed that the body retains 6TU well beyond 24-hour post 6TP treatment. Therefore, we proposed that the observed toxicity from 6TP administration comes from either 6TP or its oxidative excretion metabolites ability to inhibit one or both enzymes (UDPGDH, UGT) in the bilirubin excretion pathway. To investigate the toxicity resulting from the 6TP administration about these two enzymatic steps, inhibition analysis of these oxidative metabolites on UDPGDH was assessed using a robust UV-Vis method. The inhibition profile made with regards to varying UDP-glucose showed weak to no inhibition of 6TP towards UDPGDH with a K_i of 288 μM.

However, 6TU, (the primary oxidative metabolite which is oxidized at C2 and C8) has increased inhibition towards UDPGDH with K_i of 7 μM. Inhibition was also observed with 6TX (oxidized at C2) and 8-OH-6TP (oxidized at C8) with K_i values 54 and 14 μM, respectively. To further confirm the results of the UV-Vis assessment, inhibition studies were carried out using an HPLC method that was developed and validated to separate all the analytes in the UDPGDH catalyzed reaction. Inhibition studies were performed via the HPLC method showed K_i values of 105 μM and 5 μM for 6TP and 6TU, respectively, towards UDPGDH.

To assess the inhibition studies towards the UGT enzyme, an HPLC method was developed for the simultaneous determination of bilirubin and its mono/diglucuronides. The inhibition studies were carried to assess the formation of glucuronides and consumption of UDPGA in the presence of the inhibitors using the HPLC method developed. Neither 6TP nor 6TU were shown to inhibit UGT. Also, inhibition studies were carried out *in vivo* animal model, which further confirmed that 6TP and 6TU do inhibit UDPGDH, but no effect on UGT activity. With these results, we discovered that both 6TP and its oxidative metabolites inhibit UDPGDH. Furthermore, it was observed that C2 and C8 positions of 6TP are important for the toxicity towards UDPGDH.

With the goal of developing a single multi-enzymatic assay, another HPLC method was developed to assess the UDPGDH and UGT catalyze reactions together. This method can be used as a standard method to assess interference of any molecule on bilirubin excretion. Given the findings in this study, efforts are being directed towards the synthesis of 8-substituted 6TP analogs that are proposed to retain its therapeutic efficacy but have limited to no toxicity.

Table of Contents

List of Figures

List of Tables

Acknowledgments

First, I would like to express my sincere gratitude to my major advisor, Dr. Ryan J. Rafferty for his valuable support and guidance throughout these years. His supervision and encouragement has been key to accomplish many goals in my Ph.D. life, and I am honored to introduce myself, as his first Ph.D. student.

I would like to thank, my committee members, Dr. Christopher Culbertson, Dr. Santosh Aryal and Dr. Seong-O Choi, for their kind support and always been there for me from the beginning. I appreciate their contribution of time and ideas that helped me during my stay in KSU.

I also want to give my special thanks to Dr. James Mott at Shimadzu instruments, Mr. Tobe Eggers, Dr. Leila Maurman, and Mr. Ron Jackson for helping me whenever I need technical support. I also take this opportunity to thank Dr. Medha Gunarathana, Ms.Tuyen Nguyen, Mrs. Wasu Hulangamuwa. Ms. Prathibha Desman and Mr. Anthony Fatino for their loving friendship and support.

My deepest gratitude goes to my family for their encouragement and being there for me always.

Dedication

In dedication to my loving Amma and Thaththa!

Chapter 1 - **Introduction**

Blood stem cells are made within bone marrow and these stem cells can be divided into myeloid stem cells and lymphoid stem cells.[1] Myeloid stem cells mature to red blood cells, platelets, and granulocytes; while lymphoid stem cells develop into lymphoblast cells, which can eventually can be turned in to three types of lymphocytes such as B, T and natural killer cells. The uncontrolled proliferation of these lymphocytes, especially the B or T origins in the body result in the acute lymphoblastic leukemia (ALL). The high level of leukemic cells in the body is toxic to healthy white blood cells, red blood cells and platelets that cause infection, bone pain, anemia, and bleeding in patients. It is also discovered that in less than 10% of patients with ALL that this cancer can also spread into the central nervous system.[2] The pathogenesis of ALL is normally higher in children younger than 5 and adults over 50. The estimated new cases of ALL in the United States in year 2017 was 5970, including 3350 in male and 2620 in females. The overall death cases estimated at 1440 from ALL including 800 in men and 640 in women.[1]

Treatment regimens for ALL include chemotherapy, radiation therapy, stem cell transplant and targeted therapy. When looking at the treatment options for an individual, the patient first needs to be screened for their chromosomal abnormalities that frequently come with ALL. Over the years, it has been observed that chromosomal abnormalities are associated with ALL and the most common is the Philadelphia chromosome (Ph).[3-4] This is also known as BCR/ABL rearrangement where chromosome 9 and chromosome 22 fuses the breakpoint cluster region (BCR) and the Abelson (ABL) respectively. The important fact about this fused gene is that it encodes for chimerical oncoprotein activity, which is similar to tyrosine kinase activity. Tyrosine kinase is known to up-regulate many oncoproteins downstream of many cells signaling pathways that lead to uncontrolled cell growth and division. The Ph+ ALL patients are identified with two

essential biomarkers, which are CD25 and the chain of interleukin 2 (IL-2) receptor complex. Ph+ patients can be treated with tyrosine kinase inhibitors (TKIs) based chemotherapy.[5-6]

The treatment of ALL is done in phases, which includes: induction, consolidation, and remission. During the induction phase, it is expected that all the leukemic cells in the body will be destroyed.[7] The consolidation phase, the patient undergoes treatment that will support to destroy any remaining leukemic cells that can regrow. In the maintenance therapy, patients are treated with therapies in longer period to avoid the relapse.[7] In each of these treatment regiments, therapies are conducted with the combination of drugs. For example, in the induction therapy patients are given vincristine, prednisone, cyclophosphamide, doxorubicin, and L-asparaginase over a 4-6-week period. In the consolidation phase, cytarabine and methotrexate are used, and in maintenance therapy, 6TP, methotrexate, steroids, and vincristine; intrathecal methotrexate are used for the treatments.[8-9]

For patients in whom ALL has spread to the central nervous system (CNS), while the standard of care therapies are employed in each of the three cases above, sanctuary therapy is also performed. This therapy is also known as CNS prophylaxis would be carried out and involves treatments that targets the CNS where any leukemic cells can be hidden, and treatments are given in high doses to the brain as standard doses of chemotherapy are not sufficient to kill leukemic cells in the brain and spinal cord.[8, 10] Up to 10% of all patients with advanced cancer has a high risk of brain metastasis and will develop the cancer in CNS.[10]

As discussed above, multiple drugs are currently being employed in the well-designed treatment phases (induction, consolidation, maintenance) against ALL **(Figure 1-1)**. However, studies have shown that multi-drug chemotherapy regiments, plus the TKIs for Ph+ ALL have

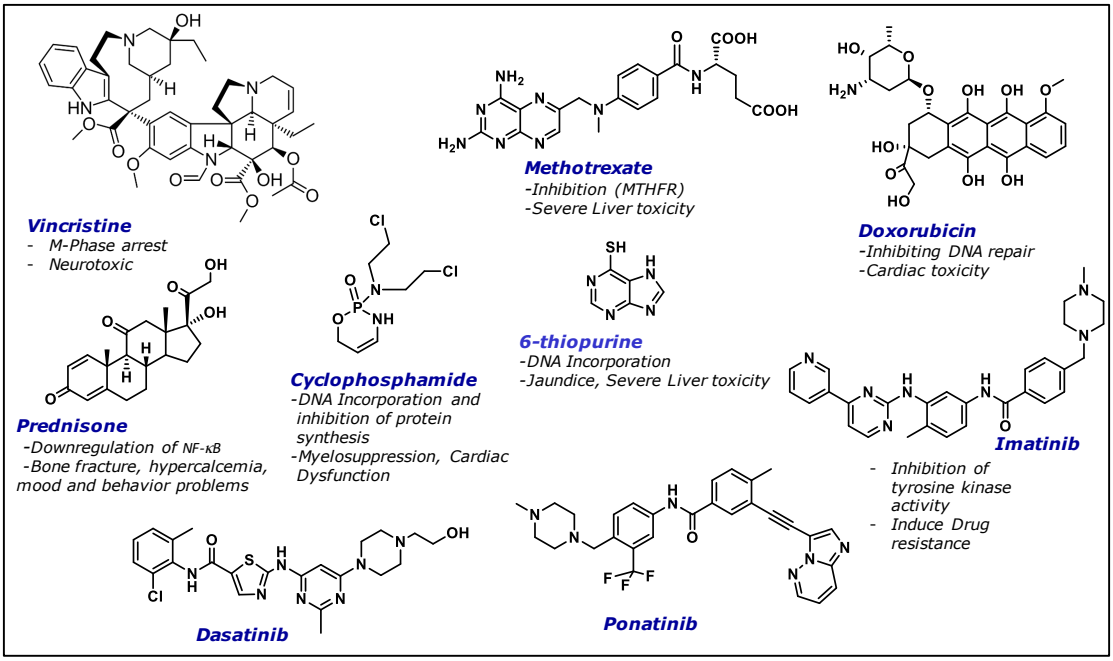

Figure 1-1. Chemical structures of drugs that use for acute lymphoblastic leukemia in different treatment regiments.

only resulted in three-year survival of 50% or more in patients.[1] Each of these treatments have failed to decrease the projected thousands of deaths, mostly due to the fatal toxicity associated with the treatments or discontinuation of therapy and frequent drug resistance. For example, vincristine is a one of the drug use in the chemotherapy for ALL, whose mode of action is by microtubule depolymerization resulting in M-phase arrest and apoptosis.[11] However, the primary drawback associated with its use is neurotoxicity as its administration causes autonomic and peripheral sensory-motor neuropathy.[1, 11] This is caused by the damage of the peripheral nerves which cause the pain and numbness in hands and feet.

Prednisone is another essential drug in the treatment of ALL. It can bind to the glucocorticoid receptors in the cytoplasm, which will lead to the receptors to homodimerize and transfer into the nucleus. In the nucleus, these receptors interact with the glucocorticoid elements and eventually repress the activity of the transcription factors that up-regulate protein-1 (AP-1) or nuclear factor-κB (NF-κB). This process would inhibit cytokine production, induce cell cycle

arrest and apoptosis.[1,12] Furthermore, as it has a higher half-life and CNS penetration, prednisone is a better candidate for CNS leukemia. However, it can also cause many adverse effects such as bone fracture, hypercalcemia, osteonecrosis, mood and behavior problems.[12]

Toxicological studies have shown that cyclophosphamide elucidates its cytotoxicity by binding to DNA and inhibiting protein synthesis. Myelosuppression and cardiac dysfunction are reported as its adverse side effects.[13] On the other hand, doxorubicin, a potent chemotherapeutic agent, imparts its therapeutic activity by inhibiting topoisomerase II enzyme-mediated DNA repair and damaging cellular membrane with free radicals. But the primary limitation associated with its efficacy is cardiac toxicity.[14]

Asparaginase is another promising therapeutic agent used in the induction treatment regimens that is known to break down asparagine into aspartic acid and ammonia in leukemic cells. Asparagine is essential for protein synthesis and cell survival. The lack of cellular asparagine results in cancer cell death. One of the significant disadvantages of asparaginase is its hypersensitivity that leads to the inactivation of the drug by antibodies in the patient's body. Also, the byproducts, aspartic acid, and ammonia coming from the deamination process causes neurological side effects leading to coma onset.[15]

Imatinib, dasatinib, and ponatinib are tyrosine kinase inhibitors that have been used to treat Ph+ ALL and these drugs have been resulted in the complete remission in 90% of the Ph+ patients. But, the drawbacks associated with these drugs are the induction of resistance in patients mostly due to the ABL gene mutations present in Philadelphia chromosome.[16]

6-Thiopurine (6TP) has a proven record in the remission of ALL by acting as a nucleotide mimic for DNA incorporation resulting in a base-pair mismatch and cell death upon cell cycle checkpoint assessment.[17] However, there are also well-documented toxicities associated with its

use. While some 6TP administration related toxicities have been answered, several causes of significant side effects have not been identified such as jaundice and severe hepatotoxicity.

As mentioned previously, there are many drugs in the treatment of ALL, but the efficacy of these treatments is significantly reduced due to major side effects. With each of these treatments different degrees of structure-activity relationship (SAR) studies have been undertaken in the efforts of reducing said toxicities. However, many of these studies have included the commonly assumed major metabolic pathways of interest, or of need in the drugs mode of action. Given the urgent need for new anticancer therapies, at times, these SAR studies can be rushed and are conducted with limited biological scope. As such, many of the reported toxicities are not correctly identified to the drug of interest and the pathway responsible. Of the reported drugs employed in the treatment of ALL, we have chosen to focus on our efforts on the toxicology elucidation of the toxicities associated with 6TP and to use these studies as the guiding principles for analog construction that enhance its therapeutic activity **(**see **Figure 2-6)**.[18]

The metabolism of 6TP can be break down to two pathways: therapeutically active and inactive oxidative metabolites inside the body.[19] These inactive oxidative metabolites may have contributed to the severe side effects come with the 6TP administration. Here in, the 6TP mechanism of action, bilirubin excretion pathway and our postulated hypothesis is discussed.

1.1. 6TP Metabolism and its Mode of Toxicity

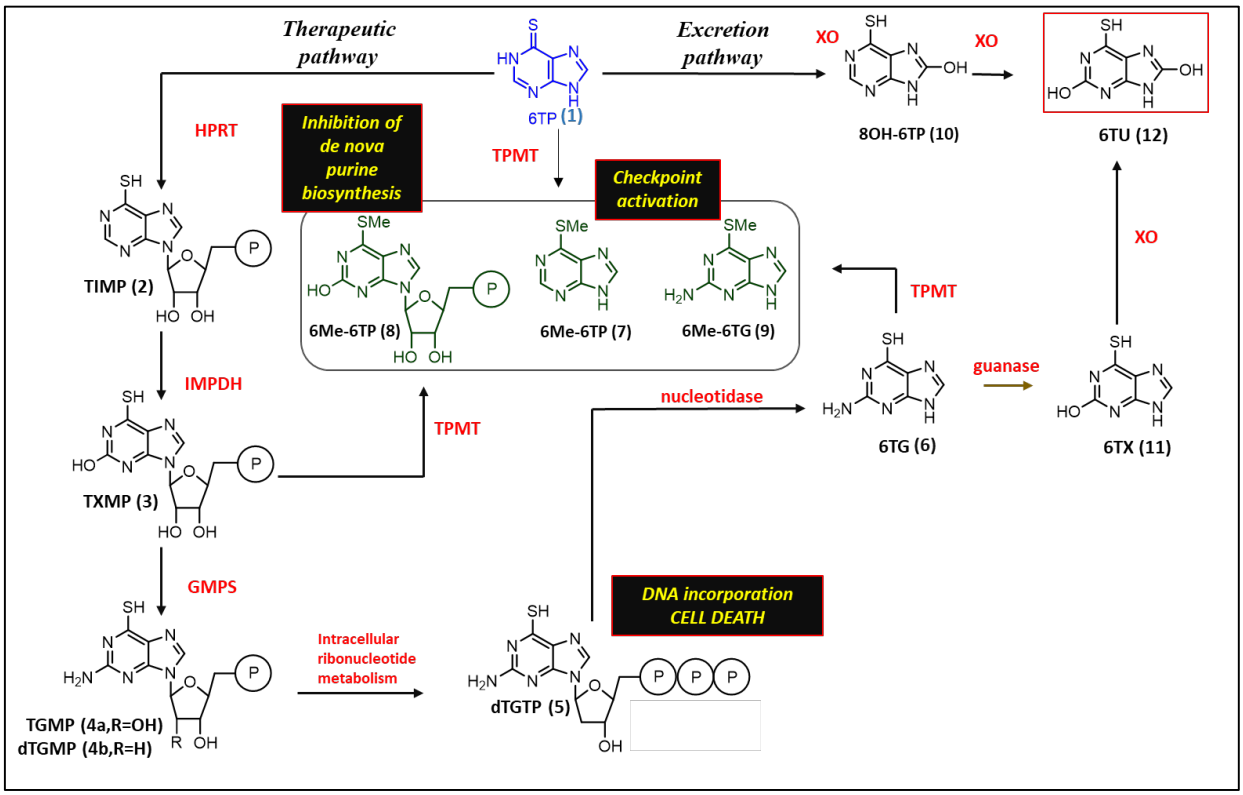

Figure 1-2. Therapeutic metabolism of 6TP (**1**) and TIMP (**2**) into the dTGTP, a mimic of dGTP for DNA incorporation that results in cell death from base pair mismatch. Various side metabolic routes of 6TP are presented: i) methylation forming 6-Me-6TP (7) and 6Me-6TG (9) that induces checkpoint activation triggering cell death from the dTGTP incorporation, and ii) methylation of TIMP (**2**) forming 6-MeTIMP (**8**) that inhibits *de novo* purine biosynthesis. Formation of 6-thiouric acid (**12**) is achieved through degradation of **4b** and direct oxidation from 6TP by xanthine oxidase (XO).

The therapeutic activity of 6TP (**1**) comes from two main routes: methylation of the thiol of 6TP (**7**) and formation of a deoxythioguanosine triphosphate mimic (dTGTP (**5**) illustrated in **(Figure 1-2)**. The former metabolite is formed through the methylation of the thiol by thiopurine methyltransferase (TPMT) and has no direct therapeutic activity.[20] The latter is formed through a cascade starting with the phosphoribosylation of 6TP (**1**) by hypoxanthine-guanine phosphoribosyltransferase (HPRT) to access thioinosinic acid (TIMP, **2**). Two key-fates diverge from TIMP (**2**), both leading to the therapeutic efficacy.[21-23] En route to its primary therapeutic

pathway, **2** is converted to thioxanthine monophosphate (**3**) by inosine monophosphate dehydrogenase (IMPDH). This is normally the rate-limiting step of the pathway, but it has been found that the activity of IMPDH is higher in malignant lymphoblasts and myeloblasts compared to normal lymphocytes.[24] Interestingly, 6TP has been shown to cause an induction of IMPDH which results in a four-fold increase of DNA incorporation of the deoxythioguanine mimic (**5**). Formation of the thioguanine monophosphate nucleoside (**4a**) is accomplished by guanosine monophosphate synthetase (GMPS). This step also allows for the formation of the deoxyribose (**4b**).[21-23] Kinase steps convert both **4a** and **4b** into their corresponding triphosphate forms of RNA and DNA (**5**), respectively. Cell death via 6TP administration occurs through the incorporation of the nucleotide **5**, which mimics and competes with endogenous guanosine nucleotides, into DNA. The incorporation of **5** into DNA results in base-pair mismatching and the cell undergoing apoptosis. However, cell death via this mechanism is not immediate.[25] Multiple passages of the S-phase are required to allow for sufficient dTGTP's to be incorporated into DNA; upon checkpoint activation, recognition of the mismatch base pairing is revealed.[26-28] Enhanced checkpoint activation with 6TP-administration comes from the methylated thiol species **7** and **9**, formed from the methylation of 6TP (**1**) and 6-thioguanine (**6**, 6TG), respectively. Both methylated species have no cytotoxic properties themselves, but both induce checkpoint activation allowing for the identification of mismatching DNA sequences resulting in apoptosis.[27] In addition to methylation forming its checkpoint activating species, the methylation of **2** by TPMT forms 6Me-TIMP (**8**), which has been proven to inhibit *de novo* purine biosynthesis.[27, 29] Through this inhibition an increased cellular uptake of purines follows, which include 6TP. The increased influx of 6TP allows for increased DNA incorporation of **5** that increases the rate at which apoptosis occurs.

In conjunction with its therapeutic metabolism, there are also detoxification pathways operating simultaneously that greatly reduce the bioavailability of 6TP. En route to dTGTP (**5**), dTGMP (**4b**) can be used as a substrate for nucleotidases and nucleosidases that results in the formation of 6TG (**6**), which can further be converted to 6-thioxathine (**11**) by guanase. Xanthine oxidase (XO) then oxidizes the C8 position to form the 6-thiouric acid (6TU, **12**), which is the terminal excretion metabolite of 6TP.[30] The formation of 6TU can be accomplished directly from 6TP through oxidation by XO, a species that is retained by the body well beyond 24-hours post 6TP treatment.[25] It is through this pathway that an excess of 6TP can be redirected, thus preventing the formation of 6Me-TIMP and dTGTP for therapeutic activity. Suppression in the formation of 6TU can be accomplished through a combination therapy with XO inhibitors, such as allopurinol.[31] However, said combination results in new and greater toxicity that requires a lower dosage of 6TP. Keeping in mind that high concentrations of dTGTP are required to cause cell death, the resulting 6TP decrease with the allopurinol co-treatment allows for cells to be rescued from this mode of cell death.[31-32] Likewise, the decreased administration of 6TP also directly reduces the *de novo* purine biosynthesis inhibition caused by 6Me-TIMP, further diminishing its therapeutic efficacy. As such, the combination therapy of XO inhibitors with 6TP fails to produce a beneficial treatment strategy.

1.2. 6TP Clinical Implications

In contrast to 6TP anticancer activity, there also well-documented toxicities associated with its use. Considering the reported clinical implications, single nucleotide polymorphism associated with thiopurine methyltransferase (TPMT) on 6TP administration should be considered.[33-34] The TPMT gene is found in the majority of the human genome, as two wild-type homogeneous alleles as well as the heterozygous variant that have nonfunctional variant allele and a wild-type allele.

These heterozygous patients have been identified as the patients who need dose reduction in the treatment of 6TP. As such, if the standard dose were given to patients it would lead to acute myelosuppression. Therefore, TMPT gene variation has been used to identify patients at high risk for 6TP toxicity.

Also, inosine triphosphate pyrophosphate (ITPA) induced genetic polymorphism has been involved in the treatment of 6TP adjusted to TPMT genotype. In this case, patients that undergo TPMT individualized 6TP administration have shown a higher probability of having fibril neutropenia if they have the heterozygous allele for the ITPA.[35] Furthermore, nucleoside transporters,MRP4 or SLC29A1, have shown to accumulate active metabolites of 6TP.[35-36]

Besides these clinically addressed 6TP associated toxicities, the most reported toxicity associated with the 6TP administration is jaundice which is described by a high accumulation of bilirubin in the body.[37-39] Jaundice results in the yellowing of the skin, eyes, neurotoxicity, hepatotoxicity and organ failures that can be life-threatening. The average person forms 2.5 mg/dL bilirubin amount in the body for a day. The clinical outcomes of 22 case studies reported by the U.S drug-induced liver injury network (DILIN), shows that 6TP administration has caused jaundice in 73% of the patients and that is most common among the other side effects. In this study, it was reported that bilirubin level inside the body had reached 7.5-13.4 mg/dL from the average healthy bilirubin level at 2.5 mg/dL. These toxicities were reported with 25-300 mg/day 6TP dose over 6 month period.[40] These reported toxicities lead us to think about how 6TP administration affects bilirubin metabolism and excretion process.

1.3. Bilirubin Metabolism and Excretion

Oxygen is transported throughout our body by hemoglobin, which consists of heme group and myoglobin protein. Heme is a prosthetic group that contains four tightly bound pyrrole rings via methenyl groups, and in the center, there is a Fe^{2+} which can bind and transport O_2 and CO_2.[41] When red blood cells are lysed, hemoglobin is released and degraded into heme and globin protein. The heme group can be catalyzed by heme oxygenase to form biliverdin which is eventually turning in to bilirubin in the presence of biliverdin reductase enzyme **(Figure 1-3)**.[42-43]

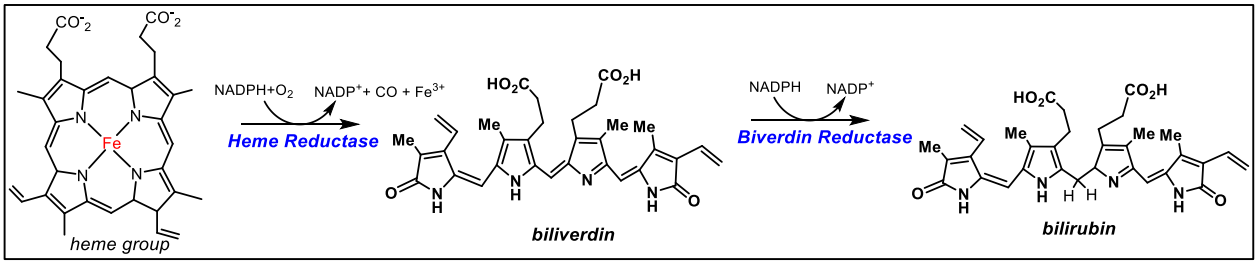

Figure 1-3. Biological degradation of heme groups producing bilirubin via biliverdin. This process required O_2 and reduction via the use of NADPH.

Although bilirubin contains two propionic acid chains and internal N atoms, it is water-insoluble, non-polar molecule. This lower polarity can be explained by the internal H bonding that is formed between the carboxyl group of the propionic acid and the N atoms in the core structure of bilirubin.[41] The carboxyl groups of the propionic acid residues should be attached to two of the UDP-glucuronic acid (UDPGA) molecules, to make bilirubin more water-soluble **(Figure 1-3)**. This glucuronidation step is essential to disrupt the internal H bond formation of bilirubin molecule and make it more of a polar, water-soluble molecule for excretion from the body through bile. Therefore, bilirubin needs to be transferred to the liver and processed under two enzymatic catalytic reactions. Binding of albumin to the unconjugated form of bilirubin take it to the liver for these modification.[41]

When looking at the bilirubin excretion mechanism in detail, the conjugation of UDPGA to unconjugated bilirubin (UCB) is catalyzed by the specific isoform of UDP-glucuronosyl transferase, UGT1A1 in the liver. This enzyme is expressed by UGT family which is also responsible for expression of other eight UGT isoforms.[41, 44] All eight UGT isoforms have a conserved exons 2 to 5 in the 3' end, and UGT1A1 contains a unique single exon unit that has specificity to bind to bilirubin moiety.

On the other hand, the substrate UDPGA for the glucuronidation is facilitated by the UDP-glucose dehydrogenase enzyme that is responsible for the conversion of UDP-Glucose (UDPG) to UDPGA **(Figure 1-4)**. UDPGA has its key roles in various biosynthetic pathways and in cellular detoxification process. It is a donor substrate for different UGTs that promotes incorporation of glucuronosyl moiety into small molecules in xenobiotic metabolism.[45] In addition UDPGA also act as a precursor for biosynthesis of different carbohydrates such as UDP-xylose and L-ascorbate.[46] UDPGDH catalyze two fold oxidation of UDPG using NAD^+ as the oxidant to produce UDPGA.[45]

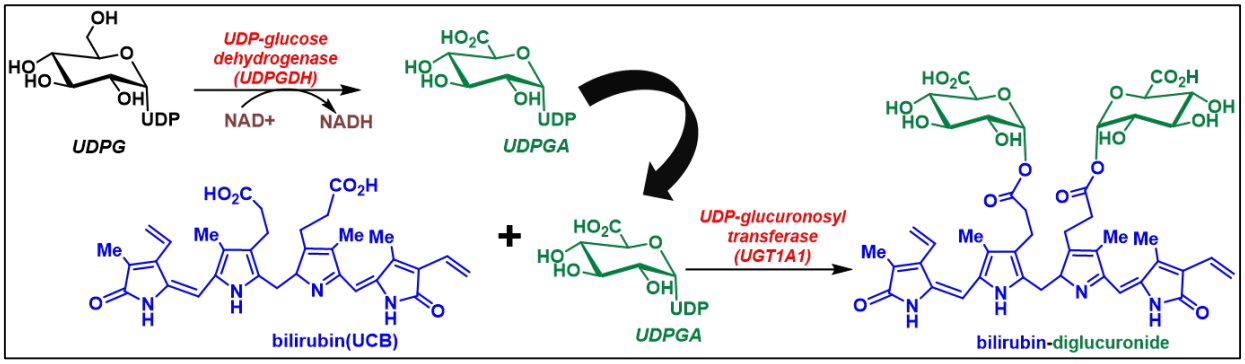

Figure 1-4. Formation of the excretable bilirubin diglucuronide species from the conjugation of bilirubin with two UDPGA units.

When looking at the rate of the glucuronidation many factors influence the rate of this process in addition to the UGT activity. [47-48] Reinke et al, identified that the glucuronidation process could be altered with different nutrition states. However, the nutritional manipulation does

not affect the transferase enzyme. Therefore, the most logical way of interpreting the cause of the rate difference of glucuronidation under varying nutritional state is the supply of UDPGA via the UDPGDH catalyzed reaction.[48]

There is about 96% of bilirubin is in its unconjugated form in the body.[41] Even though the bilirubin concentration increases with the high turnover of heme degradation due to disease conditions like leukemia, the rate of bilirubin conjugation remains the same. But the conversion of bilirubin to its di-glucuronide form is essential for its excretion as high level of bilirubin causes the number of complication in the body.

1.4. Proposed Hypothesis

While 6TP has been demonstrated to possess potent therapeutic activity in the treatment of various diseases, it is also plagued with severe liver toxicity and jaundice onset. The latter is a result of increased levels of bilirubin in the body. To date, there have been no investigations into any possible role in which 6TP affects the bilirubin excretion pathway. Therefore, we postulate that toxicity arises through the inhibition UDPGDH and/or UGT; the former is responsible for UDPGA supply for glucuronidation and the latter for the formation of the bilirubin-diglucuronide species. Furthermore, it is hypothesized that inhibition of one or both enzymatic steps is instigated by 6TP and its known excretion metabolites. This study outlines the work into investigating the possible route of toxicity resulting from the 6TP administration about these two key enzymatic transformations.

Chapter 2 - **Background**

2.1. Diagnosis of 6TP Hepatotoxicity

There are two case reports where it has been tried to track the causes of hepatotoxicity coming from 6TP.[37] In case 1, a 46-year-old woman was given 6TP (100 mg/day) as an immunosuppressant. Five months later, the patient showed severe jaundice condition with total bilirubin level at 11.7 mg/dL in the body. In addition to jaundice, she suffered from nausea and vomiting. Due to the severe liver toxicity, 6TP administration was discontinued and as a result bilirubin levels returned to normal levels **(Figure 2-1)**. In the case study II, when a 53-year-old woman was administrated with 6TP (75 mg/day), after one-month period she also developed jaundice with 8 mg/dL bilirubin concentration. As shown in **Figure 2-2**, when the medication discontinued, the liver function got back to normal with right bilirubin level.

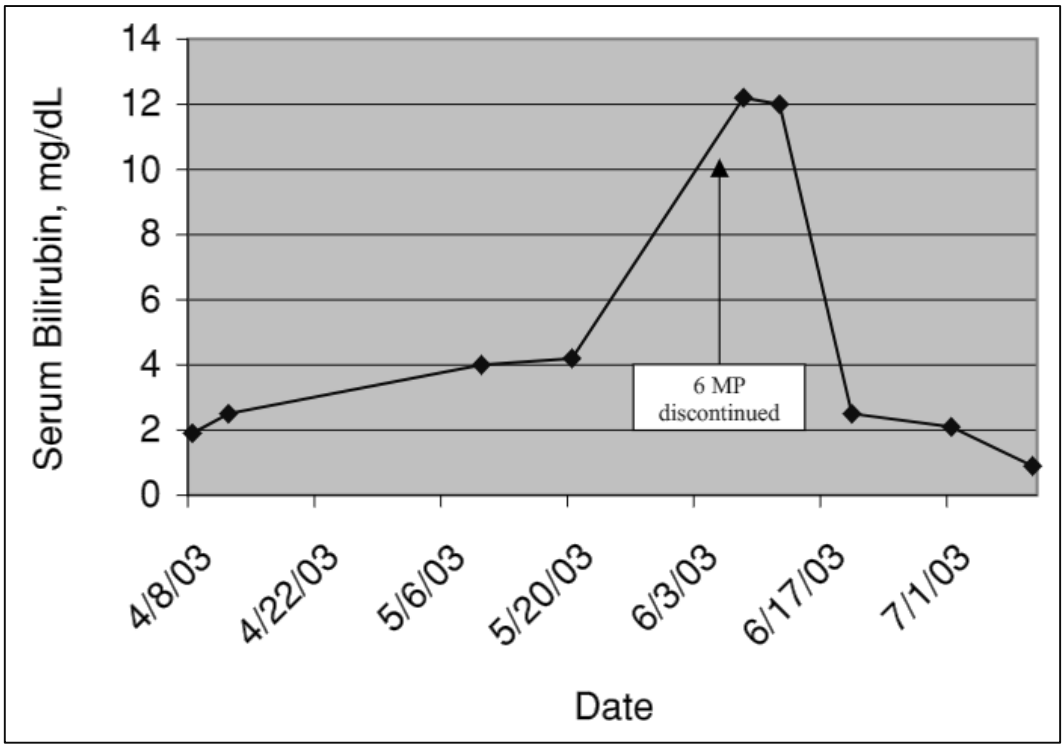

Figure 2-1. Trend of serum bilirubin level in case report 1 with the 6TP administration.[37]

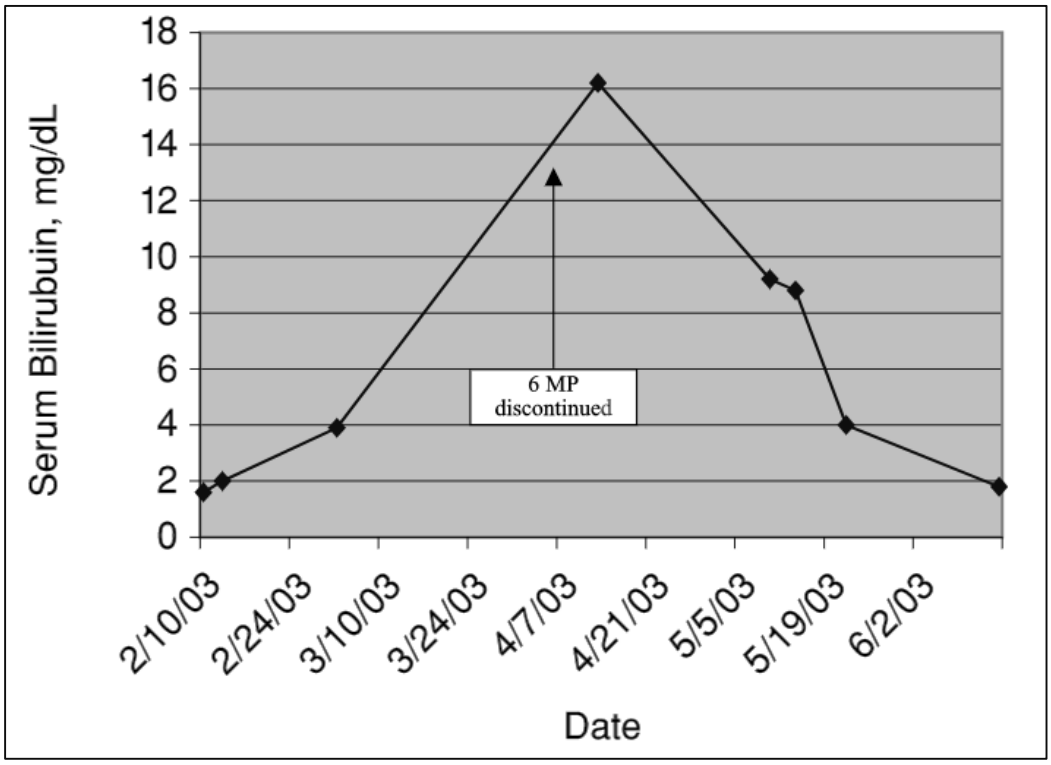

Figure 2-2. Trend of serum bilirubin level in case report 2 with the 6TP administration.[37]

In these two case reports, level of 6TP metabolites such as 6TG **(6)** and 6Me-6TP **(7)** was quantified in the patients. It was found that the 6TP metabolites levels correlate with the toxicity associated with 6TP administration. The 6TG **(6)** levels were observed within the normal range (210-400 pmol per $8x10^8$ red blood cells) in both patients at 270 and 344 pmol per $8x10^8$ red blood cells respectively[37].

In contrast, 6Me-6TP **(7)** was found at higher than 5700 pmol per $8x10^8$ red blood cells, which is significantly elevated in comparison to the toxic thresh-hold value at 6000 pmol per $8x10^8$ red blood cells. Here, it was postulated that 6Me-6TP **(7)** accumulation and disposition cause the renal function and it may be contributed to the hepatotoxicity.

Likewise, many studies in the literature have proposed 6TP administration induced liver toxicity and jaundice is due to the high level of 6Me-6TP,[37-39] but failed to look into the connection with the bilirubin excretion pathway.

2.2. Proposed Mechanisms on High Bilirubin Levels in Clinical Conditions

Hyperbilirubinemia levels in the body can cause a toxic condition such as jaundice, hyperbilirubinemia, kernicterus, Crigler-Najjar syndrome, Gilbert's syndrome and even death.[49-53] Although these conditions can develop due to pathological conditions like hemolysis, dyserythopoiesis, enzyme deficiency (genetic polymorphism), it is well observed that the drug-associated toxicities mostly induce the elevation of serum bilirubin in the clinical conditions.

UGT catalyzed bilirubin glucuronidation is the rate limiting step for bilirubin excretion. Therefore, disturbed conjugation of bilirubin to UDPGA results in high bilirubin accumulation in the body.[54] Due to the undeveloped UGT expression at birth, neonates who are 3-4 days old can get jaundice as the bilirubin concentration get high in the body. Also, a mutation in the exon of UGT, responsible for binding of UDPGA, results in Crigler-Najjar disease in Japanese individuals caused by elevated level of bilirubin.[55] Besides, it was reported that hypothyroidism also causes a decreased level of UGT levels in rats.[56]

Despite these internal causes, UGT levels have been affected by external causes as well. It was reported that molecules like phenobarbital, spironolactone, glutethimide, rifampicin are capable of enhancing the UGT activity, thereby decrease the serum bilirubin level.[57] At the same time, atazanavir, amitriptyline, ketoconazole, regorafenib, sorafenib are known UGT inhibitors which lowering down the bilirubin conjugation to UDPGA which subsequently increase the unconjugated bilirubin.[58]

Once bilirubin is degraded from the heme group, it circulates in the blood as albumin-bound form, which will eventually be taken into the liver hepatocytes by basolateral membrane transporter (OATP1B1). This liver-specific transporter could bind to the negatively charged substrates like bilirubin. However, some drugs can inhibit OATP1B1 (HMG-CoA reductase inhibitors) thereby decreasing binding to the bilirubin. In this case, the unconjugated bilirubin concentration will increase in the body as the amount of bilirubin uptake into the liver is decreased.[59]

On the other hand, UDPGDH activity is also a critical factor for glucuronidation as it is the enzyme responsible for the formation of UDPGA that is needed for bilirubin conjugation. When looking at drug-induced UDPGDH inhibition, high dose of acetaminophen was found to inhibit the UDPGDH activity in the liver and decrease UDPGA production significantly.[60] Besides, piperine was also found to inhibit UDPGDH activity in the liver.[61]

Furthermore, piperine showed non-competitive inhibition of UDPGDH and inhibition constant was observed at 6 μM and 16 μM with varying concentration of NAD^+ and NADH respectively. Also, the structure-activity comparison with piperine analogs has shown that conjugated double bonds are essential for its inhibitory activity upon UDPGDH **(Figure 2-3)**.[61] As shown in the example, functional groups like double bonds affect inhibition greatly. With this concept, investigating the oxidative metabolites of the 6TP could lead to understand its toxicity.

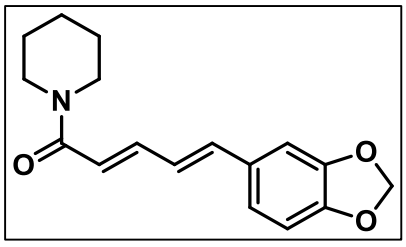

Figure 2-3 Piperine Structure. Structure-activity comparison of piperine analog shows that conjugated double bonds are essential for its inhibition on UDPGDH.

2.3. 6TP Combination Therapy with Allopurinol

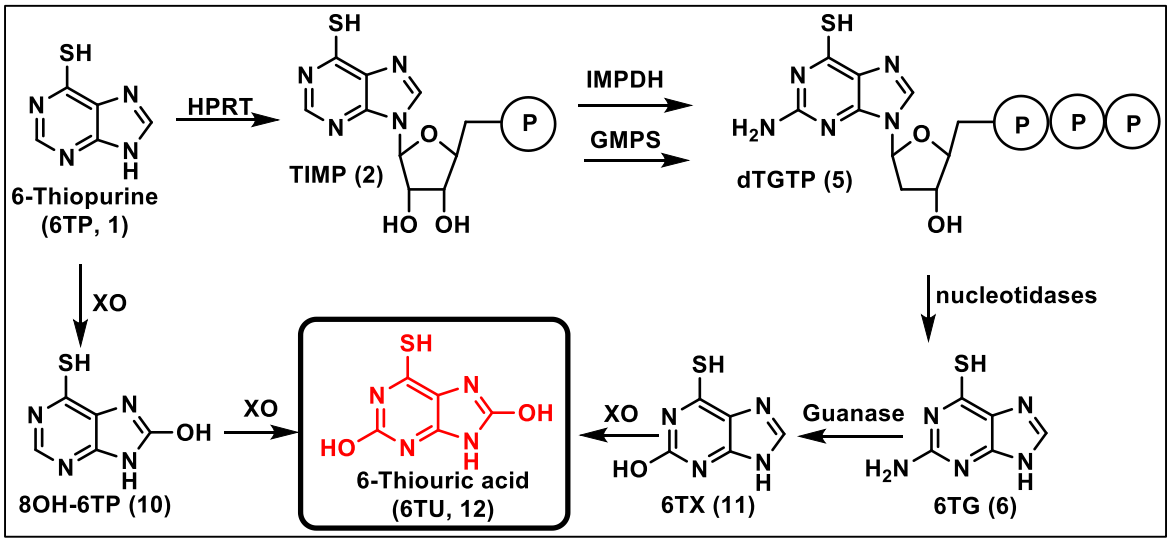

Figure 2-3. Formation of 6-thiouric acid (12) through two pathways: from degradation of one of the intermediates of the therapeutic pathway (5) and direct oxidation from 6TP by xanthine oxidase (XO).

In conjunction to its therapeutic metabolism, there are also detoxification pathways operating simultaneously that significantly reduce the bioavailability of 6TP, shown in **Figure 2-4.** En route to dTGTP (**5**) can be used as a substrate for nucleotidases and nucleosidases that results in the formation of 6TG (**6**), which can further be converted to 6-thioxathine (**11**) by guanase. Xanthine oxidase (XO) then oxidizes the C8 position to form the 6-thiouric acid (6TU, **12**), which is the terminal excretion metabolite of 6TP.[30] The formation of 6TU can be accomplished directly from 6TP through oxidation by XO, a species that is retained by the body well beyond 24-hours post 6TP treatment.[25] It is through this pathway that an excess of 6TP can be redirected, thus preventing the formation of 6Me-TIMP and dTGTP for therapeutic activity. Suppression in the formation of 6TU can be accomplished through a combination therapy with XO inhibitors, such as allopurinol.[31] However, said combination results in new and higher toxicity that requires a lower dosage of 6TP. Keeping in mind that high concentrations of dTGTP are required to cause cell death, the resulting 6TP decrease with the allopurinol co-treatment allows for cells to be rescued

from this mode of cell death.[31-32] Likewise, the decreased administration of 6TP also directly reduces the *de novo* purine biosynthesis inhibition caused by 6Me-TIMP, further diminishing its therapeutic efficacy. As such, the combination therapy of XO inhibitors with 6TP fails to produce a beneficial treatment strategy.

2.4. 6TP and its Analog Synthesis

In the aim of synthesizing compounds that can insert into DNA and act as an anticancer drug, Hitching's group focused on designing purine and pyrimidine antagonists.[62] As such, a number of purines were synthesized that were modified about the amino group of the adenine with various aliphatic, aromatic and heterocyclic amines. In these studies, the treatment of hypoxanthine **(13)** with phosphorus pentasulfide led to 6TP **(1) (Figure 2-5)**. Also, 6TP can be synthesized via 6-chloropurine **(28)** in the same fashion.[62-63] In this synthetic procedure, **28** is refluxed in acetonitrile and thiourea for 90 minute, which results in a yellow precipitate that needs to be refluxed in ethanol to obtain 6TP **(1)**. 6TP was the first chemotherapy agent that was shown to incorporate in DNA and suppress cancer cell proliferation.[64]

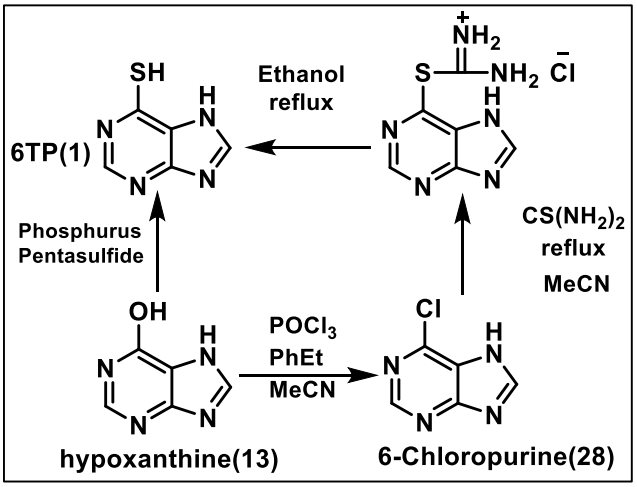

Figure 2-4. Synthetic route of 6TP from hypoxanthine (**13**) and 6-chloropurine (**28**).

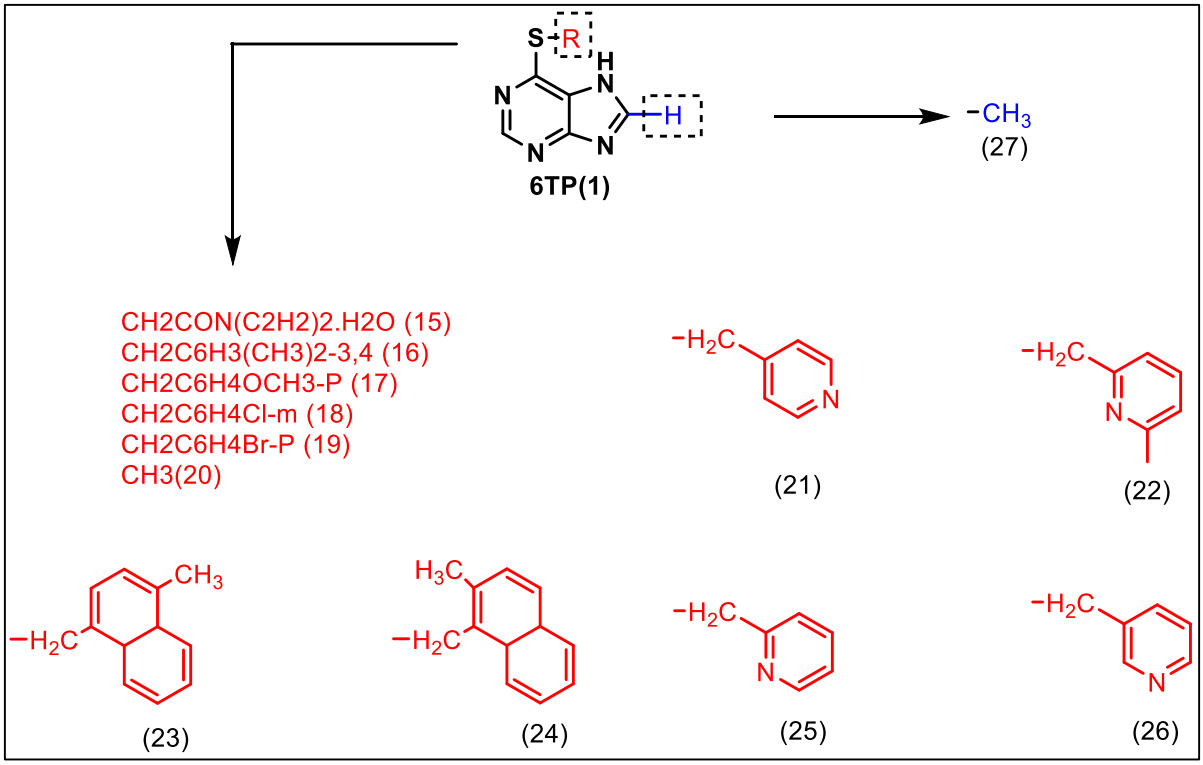

Figure 2-5. Examples of synthesized analogs of 6TP.

During the past six decades, 6TP has been modified in many ways. It has been considered as an excellent lead compound for SAR, and various derivatives of 6TP have been synthesized to enhance its bioactivity.[18, 64] It has been modified about thiol group as well as about C8 position adding a methyl group. Modification in thiol group has given superior therapeutic activity compared to 6TP. [65-66] Importantly, analogs made with different naphthyl derivatives (compound **21** to **26** in **Figure 2-6**) have shown to inhibit S phase cell cycle arrest, and mitochondria dependent cell apoptosis in HepG2 cells.[65] However, biological activity of 8-Me-6TP has not been reported.

2.5. Methods for Kinetic Assays for UDPGDH

UDPGA and NADH are produced in the UDPGDH catalyze reaction by using two equivalents of NAD^+. Assessment of NADH and UDPGA in this enzymatic catalytic reaction is

important for the kinetic analysis of UDPGDH. There are many protocols that describe methods for assessing UDPGDH activity. Here are some of the main methods previously developed.

Two fluorescence procedures have been developed to assay the activity of UDPGDH.[67-68] The enzyme incubation was performed identically, following the protocols of Singh *et al.* for their enzymatic production of UDPGA. Tissue extracts were incubated at 35 °C for 10 min in 0.1 mL of 5 mM glycine and 20 mM sodium phosphate, pH 8.7, with various concentrations of substrates in a total volume of 3 mL. Once 10 min elapsed from the addition of UDPGDH, 0.1 mL of 0.1 M Tris-HCl, pH 7.3, containing 20 mM $MgCl_2$, 0.1% Triton X-100, 0.2 mM UDP-Xylose, 0.05 mM 3-hydroxybenzo[*a*]pyrene, and 0.5 mg/mL guinea pig liver microsomal protein was added to each incubation medium and allowed to incubate for an additional 30 minutes. Both studies require the derivatization of UPDGA, which is performed by 3-hydroxybenzo-[*a*]pyrene in methanol to yield the corresponding glucuronylbenzo[*a*]-pyrene. Unreacted 3-hydroxybenzo[*a*]pyrene was extracted by the addition of 0.8 mL of 0.4 M NaCl and 6 mL of 2:1 chloroform:methanol. The aqueous phase was removed and analyzed via fluorometry. Burrows and Clintron (1983) reported the optimal wavelengths for the derivatived glucuronic acid to be 382 nm and 424 nm for excitation and emission, respectively.[68] Singh *et al.* reported optimal wavelengths for the glucuronic acid derivative to be 378 nm and 425 nm for excitation and emission, respectively.[67] The only difference that might address the excitation wavelength difference is that Burrows and Clintron performed a second chloroform/methanol extraction.

Gainey and Phelps (1975) performed kinetic studies upon UDPGDH via UV detection.[69] Enzymatic activity was assessed in a 1 cm cuvette at 31 °C containing 100 μmol glycine-NaOH buffer, pH 8.7, 1 μmol of NAD^+, 1 μmol of UDPG and variable amounts of UDPGDH to a final volume of 1 mL. The cuvette was preincubated at the desired temperature for 2.5 minutes prior to

the addition of UPDG, which initiated the reaction. Kinetics determination was performed by monitoring the change in absorbance at 340 nm, the optimal wavelength for NADH.

Grubb *et al.* (1993) developed an HPLC method for the separation and detection of UDPGA in 45 minutes.[70] The method, unlike its predecessors, did not require the derivatization of UDPGA, nor allow for possible purine interferences in monitoring the production of NADH due to is chromatographic separation. Incubation protocols required the addition of homogenate equivalent to $5x10^5$ cells to be placed in a 2 mL glass vial that contained 0.1 M glycine buffer, pH 8.7, and 1.25 mM NAD^+. The reaction was initiated by the addition of UDPGA to give a final concentration of 250 μM and a final volume of 275 μL. The vial was capped and vortexed for 10 s and placed in a shaking water bath at 37 °C for 1 hour. Termination of the reaction was done by heat treatment at 100 °C for 2 min with the vial cap still in place. A 40 μL aliquot of the incubation sample was injected onto an Alltech Hypersil ODS (4.5 x 150 mm) C-18 analytical column for separation of the substrates and products from the enzymatic reaction. Chromatographic separation was achieved by gradient elution, which used two mobile phase systems. System A comprised of 40 mM ammonium phosphate and 5 mM tetrabutyl ammonium dihydrogen sulfate, pH 7.16 and system B was comprised of system A containing 50% acetonitrile (v/v). Separation of substrates and products was performed with a gradient program at a flow rate of 0.5 mL/min. Mobile phase composition was 95% system A and 5% system B for the first 25 minutes. After which system B was increased to 35% over a ten-minute period and returned to 5% over ten minutes. Kinetics were determined based upon the production of UDPGA, eluted at 24 minutes, with monitoring the wavelength 262 nm with a UV detector.

Chapter 3 - **Experimental Section**

3.0 Supplies and Materials

3.0.1 Chemicals and Reagents

All standard chemicals used in this study were the highest grades available and were purchased through Sigma-Aldrich (Saint Louis, MO, USA), VWR (Radnor, PA, USA), or Fisher Scientific (Denver, CO, USA). Specialized reagents were purchased through specific vendors. Glycylglycine (gly-gly: G1127), ß-nicotinamide adenine dinucleotide (NAD^+: N1636), uridine 5'-diphosphoglucose (UDPG disodium salt: U4625), uridine 5'-diphosophoglucuronic acid (UDPGA: U6751), uridine 5'-diphosphoglucose dehydrogenases (UDPGDH: U6885), 6-thiopurine monohydrate (6TP), 6-thioguanine (6TG, A4882), 6-thioxanthine (6TX, T8125), bilirubin (including three mixed isomers, B4126), 4,5-diamino-6-hydroxypyrimidine hemisulfate salt (D19303), alamethicin (A5361), and pooled rat liver microsomes (M9066) were purchased 1,2-dibromotetrachloroethan, Regorafenib, Sorafenib, Alcohol dehydrogenase from Saccharomyces cerevisiae, sodium L-lactate, sodium pyruvate, para-methoxybenzyl chloride, from Sigma-Aldrich. L-Lactate Dehydrogenase (Roche), 6-Mercaptopurine-2-ol (6-TX, QA-6668) was purchased from Combi-Blocks, and 6-thiouric acid (6-TU, SC-213040) from Santa Cruz Biotechnology. HPLC-grade water was obtained by passing distilled water through a reverse osmosis system followed by treatment with a Thermo Scientific Barnstead Smart2Pure 3UV purification system (Fisher, 10-451-045), herein referred to as nanopure water. 6-chloropurine was purchased from AK scientific.

3.0.2 Equipment

All standard consumable supplies used in this study were purchased from VWR or Fisher Scientific. Specific equipment utilized in this work are: 1) Hewlett-Packard 8452 Diode Array UV/Vis spectrophotometer (Palo Alto, CA, USA) equipped with a Lauda Brinkman Ecoline RE 106 E100 circulating water bath purchased from VWR, 2) HPLC system consisting of an CBM-20A/20Alite system controller, SIL-20AHT Auto sampler, SPD-20A, SPD-20AV UV-Vis Detector, LC-20AT Solvent delivery module, CTO-20A Column Oven, DGU-20A3R Degassing unit and LC-20AD/20AT Gradient Valve Kit purchased from Shimadzu Scientific Instruments (Kyoto, Japan), and 3) all incubated reactions were performed with a Labcare America PRECISION water bath model 25 purchased from Fisher Scientific. All HPLC separations were performed on a Discovery C18 analytical column, 4.6 mm x 100 mm, 5 μm particle size (504955-30) along with the respective guard column (59576) purchased from Sigma-Aldrich. Nuclear Magnetic Resonance Spectral Analyses: NMR spectra were obtained for all compounds using a 400 MHz Varian spectrometer. The chemical shifts are given in parts per million (ppm) relative to DMSO at δ 2.50 ppm for proton spectra

3.0.3 Software

Data was processed, and all figures and tables constructed via the program Prism 7.02 for Mac, GraphPad Software (La Jolla, CA, USA). All chemical structures were prepared with ChemDraw Professional 16.0 by PerkinElmer (Waltham, MA). All statistical calculations within this body of work was performed by the treatment of two-way factorials (positive and negative controls, design structure of RCBD, and T-tests) with Statistical Analysis System (SAS) software for Windows (Cary, NC, USA). All NMR data was processed via Mestrelab Research software Mnova 10.0.

3.1 Experimental Design and Protocols for UDPGDH Assessment

3.1.1. Assessment of UDP-Glucose Dehydrogenase Activity via UV/Vis Method

The assessment of UDPGDH was first accomplished through UV/Vis detection. The limiting factor in the employment of this spectrometry method is that the purines of interest interfere with the molar absorptivity of NAD^+ and NADH. It is possible to compensate for this interference by using lower levels of the purines that are non-interfering towards the detection of NAD^+ and NADH at 340 nm. Assessment in this fashion is indirectly measuring the inhibition of the 6TP and its excretion, and synthetic analogs.

Standard preparation: A 0.50 M Gly-Gly buffer (pH 8.7 at 25 °C) was prepared by dissolving 1.62 g of Gly-Gly in 22 mL nanopure water, pH adjusted to 8.7 with 9 M potassium hydroxide and then diluted to 25 mL with nanopure water all while being shaken at 25 °C. Solutions of UDPG and NAD^+ were prepared by dissolving 1.7 mg and 4.5 mg, respectively, into nanopure water resulting in 2 mM and 10 mM solutions, respectively. Each of the purines was screened independently for concentration levels that are non-interfering. Preparation of the 0.1 mM 6TU solution was done by dissolving 1.8 mg into 95.5 mL of nanopure water, pH was adjusted to 9.5 with a 2 M sodium hydroxide solution (for solubility), pH adjusted to 7.5 with a 0.5 M hydrochloric acid solution (a dilute solution of HCl is required to prevent thiol oxidation), and then diluted to 100 mL. In an analogous fashion, samples of 6TP, 6TX, and 8Me-6TP were prepared. A 5 unit/mL UDPGDH solution was prepared by dissolving 0.11 mg of UDPGDH in 0.8 mL of 0.5 M Gly-Gly while stirring; once dissolved, the solution was diluted to volume with gly-gly in a 1 mL volumetric flask. All solutions were kept at 4 °C when not in use.

Data Analysis: Absorption data points were plotted in Microsoft Excel, linearly regression lines obtained via Excel, and inhibition values through the plotting of each purine concentration verses its slope from each individual data set.

Procedure: Spectrometric analysis was performed on a Hewlett-Packard 8452 Diode Array UV/Vis spectrometer equipped with a Lauda Brinkman Ecocline RE 106 E100 circulating water bath. The water bath was maintained at 25 °C and the diode array was set at 340 nm, both were allowed to warm up 10-minutes prior to analysis. To a 1 mL cuvette, 300 mL of 0.5 M Gly-Gly (0.15 M final concentration), nanopure water, varying NAD^+ and UDPG concentration in varying inhibitor concentrations were added and placed in the diode array for a 2 min thermal equilibration. Once 1.5 minutes elapsed, the instrument was zeroed to obtain an initial rate change in absorbance versus time. The reaction was initiated by addition of 20 μL of the UDPGDH solution. Thorough mixing by inversion of the cuvette was performed as quickly as possible and then placed in the holder for analysis. The reaction was monitored from 20 to 120 seconds after enzyme addition, and the slope was calculated from 20 to 40 seconds using the diode array software.

Inhibitor Assessment – Saturating NAD^+ varying UDPG concentration: For each analysis, the cuvette was prepared in the same fashion as outlined above. The final concentration of the components of the mixture were 150 mM Gly-Gly, 0.1 unit/mL UDPGDH, 3 mM NAD^+ and varied concentrations of 0.1, 0.05, 0.025 and 0.02 mM of UDPG, obtained from stock solution addition. Nanopure water was used as a variable component to ensure that a final volume of 1 mL was obtained. Inhibitor analysis of the four purines was performed at two concentrations: 50 and 100 μM for 6TP, 20 and 50 μM for 6TX and 8OH-6TP, and 5 and 10 μM for 6TU, obtained from their corresponding stock solutions. Each assessment was performed in triplicate. The average of the three were plotted and the slopes were used to determined inhibition values.

Saturating UDPG varying NAD^+ concentration: In an analogous protocol as described for NAD^+ saturating conditions (above), inhibitor analysis of UDPGDH was performed under UDPG saturating conditions (0.6 mM) with varying concentration of NAD^+.

3.1.2. HPLC Method Development for UDPGDH Inhibitor Assessment

Assessment of 6TP and its excretion metabolites in a direct fashion was accomplished via a HPLC method for separation and quantification and an enzymatic method for substrate assessment.

HPLC Method Development for Separation of UDPGDH substrates and products: Employing a Shimadzu analytical HPLC system the separation of both substrates and products were accomplished in 24-minutes, during which separation and column washing was performed. See detailed rationale as to specifics of the method in Chapter 4 (**Figure 4-5**).

Glycyl-glycine Buffer Preparation: 0.50 M gly-gly buffer (pH 8.7 at 25 oC) was prepared by dissolving 2.1 g of glyglycine in 22 mL of nanopure water. The pH was adjusted to 8.7 with 9 M potassium hydroxide then diluted to 25 ml in a 25 ml graduated cylinder.

Substrate and Product Standard Preparations: Solutions of 5.0 mM UDPG, 1.0 mM UDPGA, and 1.0 mM NADH were prepared by dissolving 15.3,3.2,3.5 mg, respectively, in nano pure water and diluted to 5 mL in volumetric flasks. A 10.0 mM NAD^+ solution was prepared by dissolving 33.2 mg of NAD^+ in 0.5ml of 0.50 M glycylglycine buffer and diluted to 5.0 ml with nano pure water. 6.8 units of UDPGDH were dissolved in 6.8 mL Gly-Gly buffer, pH at 8.7.

Procedure: The method commenced with the pre-equilibration of the Discovery Reverse-Phase column with an 80:20 organic to aqueous mobile phases at a flow rate of 0.5 mL/min at a constant temperature of 35 °C. The aqueous phase consisted of 8 mM imidazole and 5 mM tetrabutyl ammonium hydrogen sulfate (TBAHS) at a pH 6.5. Preparation of this buffer system

was accomplished by dissolving 0.545 g of imidazole and 1.7 g of TBAHS in 980 ml of nanopure water (herein referred to as System A) and the organic phase was composed of HPLC grade methanol (herein referred to as System B). The pH was adjusted to 6.5 with 0.1 M NaOH and then diluted to volume in 1 L with nanopore water. Analysis was performed using UV/Vis detection at a wavelength of 262 nm.

The HPLC method developed employed a gradient mobile phase profile for separation and quantification, as shown in **Figure 3-1**. The method commenced with the column pre-equilibrated at 90:10 (noted as system A-aqueous to system B-organic) held for three-minutes, then raised to 60:40 over one-minute and held for six-minutes, and then lowered over 2.7 minutes to 90:10 and held for 10 minutes for column regeneration. The total length of the run is 23.70 minutes and allowed for baseline separation of all substrates and products at constant elution points within the method. The substrates and products (UDPG, NAD^+, UDPGA, and NADH) were all prepared as described below.

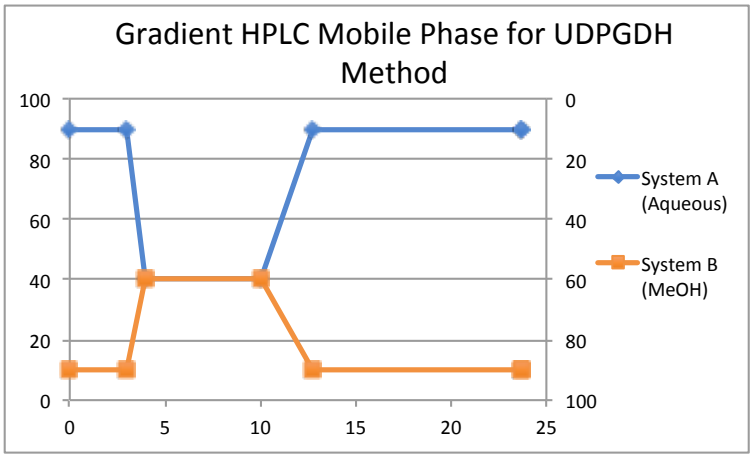

Figure 3-1. Gradient profile for the developed HPLC Method with detection at 262 nm, flow rate 0.5 mL/min, and the mobile phase consisting of imidazole/TBAHS for the aqueous phase and methanol for the organic phase.

3.1.3. HPLC Method Validation Procedure

Validation of the method was performed in adherence with the International Council for Harmonization of Technical Requirements for Pharmaceuticals for Human Use (ICH Guidelines), which covered the specific guidelines set forth by both the United Stated FDA and US Pharmacopeia Guidelines. Rationale as to the need to adhere to such strict guidelines is for the future potential of the described work for clinical translation of new analogs developed through this research. The specific points of the guidelines and how they were assessed are described below.

Selectivity: The method was evaluated for selectivity by analyzing the mixture of four analytes in the UDPGDH catalyzed reaction. Furthermore, blank sample (the incubation sample in the absence of UDPGDH) and a control sample (incubation sample in the presence of UDPGDH) were also evaluated.

Linearity & Sensitivity: Calibration curves for each of the analytes were constructed to determine linearity. For this purpose, different concentrations of each individual component standard solutions (NAD^+, NADH, UDPG, UDPGA) were prepared by doing serial dilution. The HPLC measurement of the peak area average of six replicates versus concentration of the analyte was used to obtain the calibration curve. LOD and LOQ values were used to determine sensitivity of the method. LOD is the ability of analytical method to detect the lowest concentration of the analyte. LOQ is the lowest concentration of the analyte that can be quantitatively determined with acceptable precision and accuracy. The LOD and LOQ values were determined by the following equation **(Figure 3-2)** according to ICH guidelines.

LOD= 3.3 * S/slope	LOQ= 10 * S/slope
S- standard deviation of response Slope- slope of the regression line	

Figure 3-2 Equations for limit of detection (LOD) and limit of quantification (LOQ) and defined abbreviations.

Accuracy: Assessment of accuracy of the method was accomplished by the analytical method to the true value. It was determined for these 4 analytes (UDPG(A) and NAD(H)) by using the standard addition technique. Spiked samples were prepared at three levels over a range of 80-120% of the target concentration. Per the recommendation of the ICH method, the mean recoveries were targeted to obtain 100+/-2% at each concentration level for each analyte independently.

Robustness: Organic solvent composition and flow-rate were changed to compare the system suitability parameters to ensure the integrity of the analytical procedure. To determine the robustness of the current method, the effect of flow rate was studied at 0.4 and 0.6 mL/min in comparison to the employed 0.5 mL/min. Decreasing and increasing the percentage of methanol in 10 % units assessed the effects of mobile phase.

3.1.4. Enzymatic Formation of UDPGA via UDPGDH

The in vitro assessment of the formation, as well as the determination of the range of linearity of production for inhibition assessment was performed. The in vitro system was composed of 1 mM NAD^+, 400 μM UDPG, and 150 mM Gly-Gly buffer (all prepared from stock solutions) and was incubated at 37 °C for 5 minutes before the addition of UDPGDH (final enzyme concentration of 0.01 unit/mL). The addition of nanopure water was used to maintain constant volume. The addition of the enzyme was assumed to be the time zero point for assessment. Aliquots were removed every minute for 15-minutes in 300 μL portions and transferred to a 2 mL Eppendorf tube. This tube was then immediately placed into a pre-equilibrated sand bath at 87 °C

to heat shock and degrade the enzyme for three minutes. The protocol of aliquot removal, transfer, and placement in the sand bath was reproducible with a minor time variation of 15 seconds. The enzymatic production of both NADH and the desired UDPGA via this method is shown in **Figure 3-3** below.

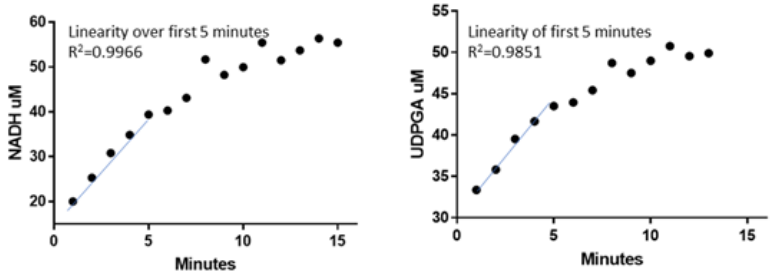

Figure 3-3. Reaction progression curve of UDGPDH catalyzed reaction – quantification of products NADH and UDPGA as a function of time. Each analyte is an average of three independent runs with standard error bars (not visible due to the size of the deviation).

Substrate and product thermal stability was assessed by placing each analyte into an Eppendorf tube and subjected to the sand bath thermal conditions for 10 minutes. While the enzyme degradation was complete at 3-minute, further thermal stability was investigated to illustrate the methods robustness. Aliquots were removed from tube containing the individual analyte and analyzed via the HPLC method developed for this enzymatic process. Results are shown below in **Figure 3-4**.

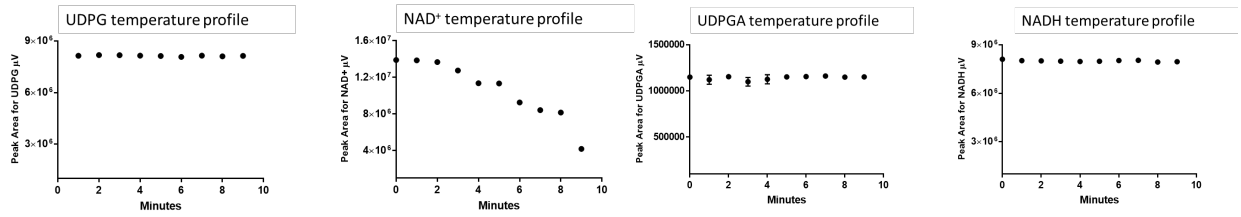

Figure 3-4. Thermal stability of analytes of the UDPGDH enzymatic reaction as assessed by the developed HPLC assay. Each analyte is an average of three independent runs with standard error bars (not visible due to the size of the deviation).

3.1.5. Enzyme Kinetics for Direct UDGPDH Assessment

Inhibitor Assessment of UDPGDH by 6TP and 6TU – Saturating NAD^+ varying UDPG concentration: For each analysis, test tubes were prepared in the same fashion outlined below. Final concentration of the components of the mixture were 150 mM Gly-Gly, 0.1 unit/mL UDPGDH, 3 mM NAD^+ and varied concentrations of 0.1, 0.05, 0.025 and 0.02 mM of UDPG, obtained from stock solution addition. Nanopure water was used as a variable component to ensure that a final volume of 0.5 mL was obtained. Inhibitor analysis of the two purines was performed at two concentrations: 50 and 100 μM for 6TP, and 5,15 μM for 6TU, obtained from their corresponding stock solutions. Each reaction was started by adding the enzyme and the reaction was carried out at 37 °C for 4 minutes followed by 3-minute heat shock. UDPGA levels were quantified using the developed HPLC method. Each concentration point of UDPGA was done in triplicate and the associated velocity of the reaction was calculated and plotting the reciprocals of each afforded the Lineweaver-Burke plots. As previously described, plotting the slopes of the lines verses the concentration of purine allowed for the determination of the K_i for both 6TP and 6TU. The slopes of the curves were plotted against NAD^+ concentration in Graph Pad Prism 7.02 to obtain the K_m and V_{max} values.

3.2. Design and Protocols for UDP-Glucuronosyl Transferase (UGT) Assessment

Standard preparation: A bilirubin stock solution was prepared by dissolving bilirubin in 100% dimethyl sulfoxide to yield a concentration of 2 mM, the stock solution was aliquoted, and stored at –70 °C until use. A 25 mM UDPGA stock solution was prepared by diluting 8 mg to 0.5 mL with nanopure water, and a 10 mg/mL alamethicin solution was prepared by taking 5 mg and diluting to 500 μL with methanol. Preparation of the 100 mM potassium dihydrogen phosphate

buffer was done by dissolving 2.3 g of KH_2PO_4 into 80 mL of nanopure water, pH adjusted to 7.4 with 1 M HCl and diluted to volume in a 100-mL volumetric flask.

3.2.1. HPLC Method Development for Bilirubin and Bilirubin Mono- and Di-Glucuronide

Procedure: Bilirubin and its glucuronide were separated on a Discovery C18 analytical column, 4.5 mm x 100 mm, 5 μM particle size with guard column. A dual mobile phase was employed; the aqueous phase consisted of an 8 mM imidazole & 2.5 mM TBAHS buffer at a pH of 6.5 in nanopure water and acetonitrile as the organic phase. A gradient elution profile was employed for full separation at a flow rate of 0.5 mL/min, the method begins at 10% acetonitrile and increases to 50% over 8 minutes, held for 5.5 minutes, increased to 95% over 4.5 minutes, held for 10 minutes, returned to 10% over 4 minutes and held at 10% for 2 minutes to allow for column regeneration as shown in **Figure 3-5**. The detection wavelength was 450 nm with a sample injection volume of 5 μL. The combined peak area for bilirubin (sum of the three isomers) was plotted relative to the concentration prepared for the generation of a working standard curve.

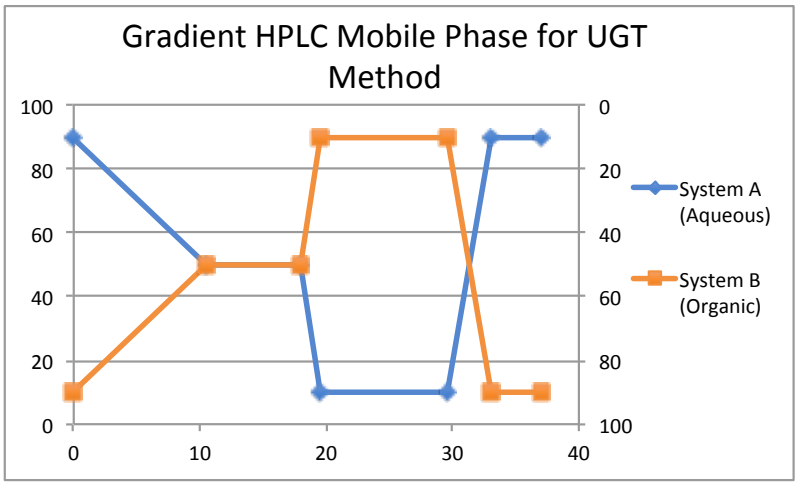

Figure 3-5. Gradient profile for the HPLC method developed for the separation and quantification of the UGT enzymatic reaction.

3.2.2. Bilirubin HPLC Method Validation

Assessment of accuracy of the method was accomplished by the analytical method to the true value per the same protocols as described above for the UDPGDH HPLC method validation. It was determined for UCB by using the standard addition technique. Spiked samples were prepared at three levels over a range of 80-120% of the target concentration. Per the recommendation of the ICH method, the mean recoveries were targeted to obtain 91-94% at each concentration level for UCB.

3.2.3. Quantification of Bilirubin, Mono- & Di-glucuronide, and UDPGA Levels

Standard curves for both bilirubin and UDPGA were constructed and used for the quantification of each species. Bilirubin was quantified directly from the generated standard curve. A total of ten peaks for the glucuronide species, including their isomers were detected in the incubation samples. Peak assignment and identification of UCB, BMG1, BMG2, BDG and their isomers were based on their lipophilicity and polarity, as well as the elution pattern, chromatographic peak position and relative retention time from previous reports. The calibration curves for bilirubin were used to determine the concentration of the mono- and di-glucuronide species employing the gradient HPLC bilirubin method described above. Quantification of UDPGA levels was determined through the use of the constructed standard curve within the isocratic HPLC method developed for UDGPA.

3.2.4. Bilirubin Glucuronide Formation

Bilirubin glucuronidation was performed at 37 °C in a shaking water bath. All steps taken were performed in the lowest light conditions possible; the glucuronide formed was found to be unstable to ambient lighting. The following was added to an Eppendorf tube to achieve the final concentrations indicated, final volume 200 μL: potassium phosphate buffer (50 mM, pH 7.4),

bilirubin (10 μM), $MgCl_2$•$6H_2O$ (0.88 mM), rat liver microsomes (RLM, 100 μg of protein/mL), alamethicin (22 μg/mL), and allowed to pre-incubated for 2 min. Addition of UDPGA (3.5 mM), referred to as the zero-time point, initiated the reaction. The mixture was allowed to shake at 37 °C for each of the time course experiments. To each reaction 600 μL of ice-cold methanol containing 200 mM ascorbic acid was added to terminate the enzymatic reaction, vortexed for 2 min, and then centrifuged at 12,000 rpm for 10 min. The supernatant was then analyzed by the developed gradient HPLC protocol for separation and quantification of UCB, BMG1, BMG2, and BDGs.

3.2.5. Validation of Bilirubin Glucuronide Formation

Quantification of UCB, BMG1&2 and BDGs were performed post the quenching of UGT, which was performed by immersing the Eppendorf tube with the reaction mixture in a cold-water bath for two min. No ascorbic acid was used, as the residual material would quench the glucuronidase enzyme to be added. To this sample 0.1 mg/mL glucuronidase enzyme was added, inverted (x3), and then analyzed by the HPLC protocol developed to quantify the levels of bilirubin and BMG1&2 and BDGs for formation confirmation.

3.2.6. Inhibitor Assessment of Bilirubin Glucuronide Formation

Employing the same protocol, delineated above for the formation of the bilirubin glucuronide species, inhibitor assessment was performed. To an Eppendorf tube, 6-thiopurine or 6-thiouric acid (50 and 75 μM final concentrations) was added alongside a control (no purine added) and allowed to pre-incubate for 2 min. Addition of UDPGA initiated the reaction for each of the time course experiments. The gradient HPLC method was employed for the 45-min time course experiments for the quantification of the glucuronide species. For experiments in which UDPGA was analyzed, the incubation protocol for the formation was altered as follows: 300 μL

final volume, 2.5 μM of bilirubin, 260 μM of UDPGA was employed to start the reaction, no alamethicin was employ as UDPGA was being assessed rather than the bilirubin species, and the enzyme was quenched with heat (87 °C). Quantification of UDPGA for the 1, 12, and 15-hour time course experiments was performed by the isocratic HPLC method described above.

3.3 Combined HPLC Method for UDPGDH and UGT Unified Assessment

3.3.1. Optimization of the Merging of the HPLC Methods for UDPGDH and UGT

The method commenced with the column pre-equilibrated at 90:10:00 (noted as system A-aqueous system B-methanol C-acetonitrile) held for three-minutes, then raised to 60:40:00 over one-minute and held for 6.5 minutes, allowing for baseline separation of all substrates and products of UDPGDH catalyzed reaction at constant elution points at 262 nm wavelength **(Figure 3-6)**. Then lowered over a minute to 90:10:00 while changing to 450 nm. At this point system is brought to 50:00:50 over 8 minutes and then increased to 95% of acetonitrile (05:00:95) over 4.5 minutes and held for 10 minutes allowing the elution of peaks for BDG, BMG and UCB. The system was then returned to initial conditions of 90:10:00 and held for 7 minutes to allow for column regeneration while the wavelength was returned to 262 nm. The sample injection volume was 5 mL and the aqueous phase consisted of an 8 mM imidazole & 2.5 mM TBAHS buffer at a pH of 6.5.

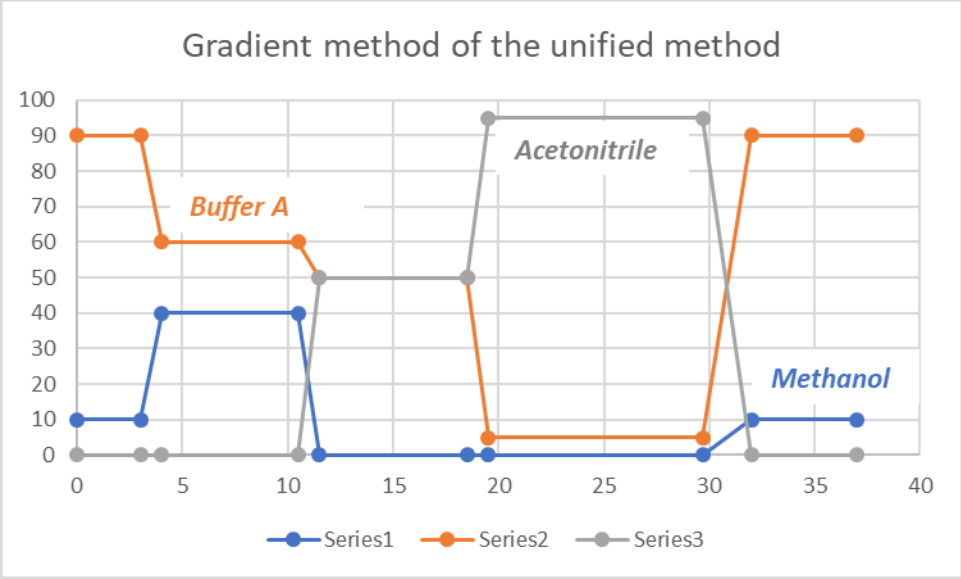

Figure 3-6. Triphasic gradient HPLC method for the unified assessment of UDPGDH and UGT.

3.3.2. UDPGA and Bilirubin Glucuronide Formation in Dual Enzymatic System and Quantification of the Products by Unified HPLC Method

Bilirubin glucuronidation was performed at 37 °C in a shaking water bath. All steps taken were performed in the lowest light conditions possible; the glucuronide formed was found to be unstable to ambient lighting. The following was added to an Eppendorf tube to achieve the final concentrations indicated, final volume 500 µL: Gly-Gly buffer (150 mM pH 6.5) NAD^+ (1 mM), UDPG (5 mM), potassium phosphate buffer (50 mM, pH 7.4), bilirubin (10 µM), $MgCl_2 \cdot 6H_2O$ (0.88 mM), rat liver microsomes (RLM, 304 µg of protein/mL (4.4 U/mL)), alamethicin (22 µg/mL), and allowed to pre-incubated for 2 min. Addition of UDPGDH (0.002 U/mL to 0.01 U/mL), referred to as the zero-time point, initiated the reaction. The mixture was allowed to shake at 37 °C for 45 minutes. To each reaction 1.5 mL of ice-cold methanol containing 200 mM ascorbic acid was added to terminate the enzymatic reaction, vortexed for 2 min, and then centrifuged at

12,000 rpm for 10 min. The supernatant was then analyzed by the unified HPLC protocol for separation and quantification of UCB, BMG1, BMG2, BDGs, and UDPGA.

3.3.3. Inhibitor Assessment of UDPGA and Bilirubin Glucuronide Formation by unified method

Employing the same protocol delineated above for the formation of the bilirubin glucuronide species and UDPGA inhibitor assessment was performed. To the Eppendorf tube, 6-thiopurine, 6-thiouric acid (75 μM final concentrations) or sorafenib, regorafenib (50 μM final concentrations) was added alongside a control (no purine added) and allowed to pre-incubate for 2 min. Addition of UDPDH initiated the reaction. The unified HPLC method was employed for the 45-min time course experiments for the quantification of the UDPGA and glucuronide species.

3.4 In Vivo Studies

All in vivo animal model studies were completed at the University of Texas-Southwestern. Sprague Dawley Rats were used in the study, four rats per experimental condition. Hepatocytes investigations as well as rat studies were completed per standard institutional protocols.

3.5 Synthesis of 6-Thiopurine Analogs

Synthesis of various 6-thiopurine analogs was accomplished through established literature procedures directly, as well as from the development of new combined synthetic methodology building upon previously reported efforts towards various purine systems.

3.5.1. Synthesis of 8-OH-6-Thiopurine

From commercially available 4,5-diamino-6-hydroxypyrimidine, thiol installation about the C6 position was accomplished under standard employed protocols with Lawesson's reagent in a 43% yield as shown in Scheme 3.1. Following a Traube synthesis protocol, 4,5-diamino-6-thiopyrimidine was heated with urea in muffle furnace until the mixture underwent a molting

process. The reaction was worked up under acid-base conditions followed by recrystallization to afford the desired 8OH-6-thiopurine in a 65% yield. The product matched reported characterization data.

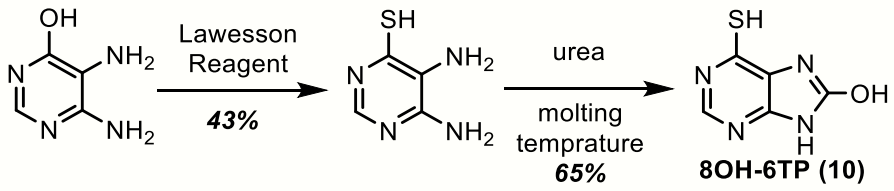

Scheme 3-1. Traube synthesis of substituted purines.

3.5.2. Route Development for the Construction of Various C8 Substituted 6TP Analogs

The synthesis of C8-substituted 6-thiopurine analogs was accomplished through the blending of two previous routes accessing similar, yet structurally different purine systems (See Chapter 2 for further details upon the previous work on purine synthesis). Shown in Scheme 3.2 is the general route established for the construction of 6-thiopurine analogs. The general synthetic route developed commenced with the PMB protection of 6-chloropurine (**28**) to afford the N-9 PMB protected purine (29) in 47%. An additional 33% of the N-7 protected purine was also obtained, and could be further elaborated onto the desired material, but has not been explored in this work. De-protonation of the C8 hydrogen was accomplished with a prepared solution of LDA followed by the addition of 1,2-dibromo-1,3,3,3-tetrachlorethane that allowed for the addition of a bromine upon the C8 position via a E2 mechanism in 78% yield accessing (**30**). The treatment of this functionalized C8 bromine purine with thiourea under reflux provided the nucleophilic additional product **31** that was immediately subjected to reflux in ethanol to provide the 8-bromo-6-thiolpurine *N9*-paramethoxybenzyl compound (**32**) in 87%. Subjecting this material to concentrated sulfuric acid in toluene provided the desired C8 bromine substituted 6-thiopurine

analog 8-Br-6TP (**33**) in 81% yield. Detailed procedures on the formation of this compound can be found in the supplemental section (Chapter 6) of this work. From the route developed, multiple analogs are envisioned to be accessible through the manipulation of this route.

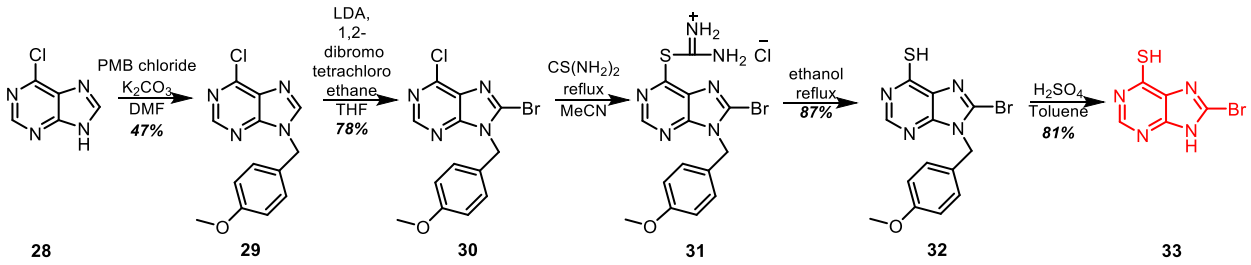

Scheme 3-2. Synthetic route employed accessing 8-substituted-6-TP analogs from 6-chloropurine.

Chapter 4 - **Results and discussion**

4.1 Inhibition Assessment of 6TP and Excretion Metabolites towards UDPGDH

Recalling our central hypothesis that either 6-thiopurine (6TP) or one, or multiple, of its excretion metabolites could be responsible for the reported toxicity associated with its therapeutic administration, efforts were directed towards studying their effects upon UDP-glucose dehydrogenase (UDPGDH) and UDP-glucuronosyl transferase (UGT). While previous efforts in the elucidation of toxicity from 6TP has been undertaken, none have focused upon the bilirubin pathway as the key source of toxicity. Both UDPGDH and UGT are key, and critical enzymes within the bilirubin pathway (as discussed in chapter 1 of this work). In the efforts to probe if our working hypothesis is correct, efforts were focused on the construction of a rapid method to assess inhibition towards UDPGDH. Said enzyme is proposed to be the critical enzyme responsible for the reported 6TP associated toxicity.

4.1.1. Direct UDPGDH Inhibition Assessment: UV/Vis Method Development

Assessment of activity/inhibition of NAD(P)-dependent dehydrogenase catalyzed reactions is commonly and routinely performed by UV/Vis spectrometry methods by monitoring absorbance changes at 340 nm. The only caveat to performing assessment of activity in this fashion is that any substrate/inhibitors to be screened must not absorb at 340 nm. If wavelength overlap is present, it can make it difficult, or even impossible to determine if there are any substrate/inhibitor effects upon the enzymatic reaction. Purines, such as 6-thiopurine and its main excretion metabolites absorb at 340 nm and therefore prevent assessment of enzymatic activity in commonly employed assays. To overcome the interfering signal, we found that if the purines were screened in sufficiently low concentration, such that the magnitude of their absorbance at 340 nm is

relatively non-interfering, that inhibition studies could be performed against UDPGDH in a rapid and reproducible fashion. Through spectral experimentation the following allowable maximum concentrations were found that had negligible interference at 340 nm: 100 μM for 6TP, 50 μM for 6TX, and 10 μM for 6TU. Lower concentrations were then analyzed for generation of inhibition profiles for 6TP, 6TU, and 6TX toward UDPGDH. Inhibition was assessed through saturation kinetics, in which either UDPG or NAD^+ was saturating while the other substrate concentration was variable.

Inhibition profiles for 6TP, 6TU, and 6TX against UDPGDH with varying UDPG and saturating NAD^+ is shown in **Figure 4-1 A-C**, and varying NAD^+ with saturating UDPG is shown in **Figure 4-1 D-F**. For each purine screened, three separate experiments were performed: no purine, and purine at both low and high concentration levels. From the analysis with no purine, under both varying UDPG and NAD^+ conditions, the K_m and V_{max} were calculated. Determination of the K_i was accomplished by plotting the slope from each independent analysis set versus the concentration of purine, and then taking the negative-inverse value of the x-intercept. The table insert within **Figure 4-1** summarizes the respective K_i, K_m, and V_{max} values for each purine in respect to both varying and saturating concentrations of UDPG and NAD^+ concentrations.

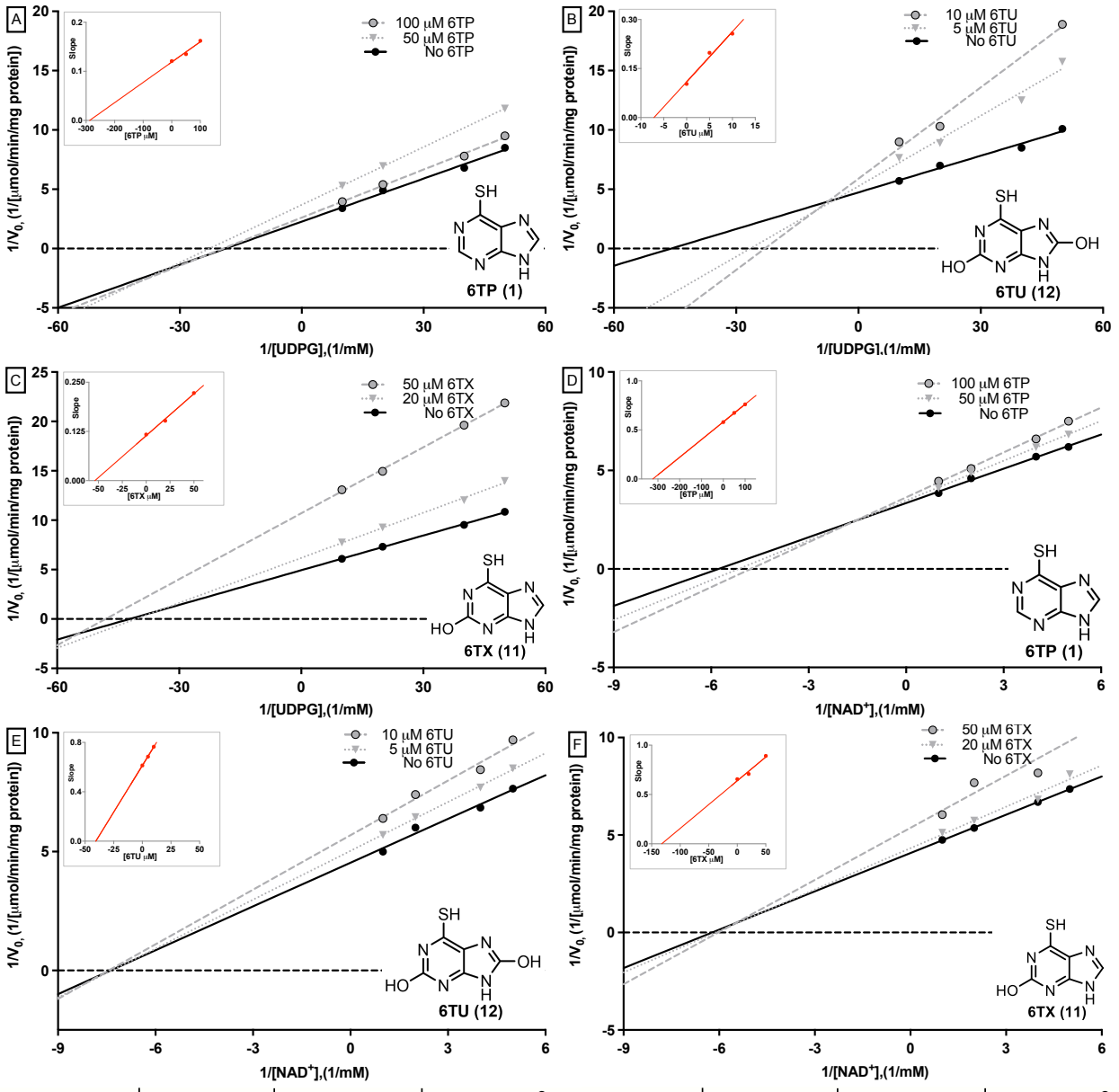

Tabular Summary from Inhibitor Assessment	6-Thiopurine (R_1 = H, R_2 = H)	6-Thiouric acid (R_1 = OH, R_2 = OH)	6-Thioxanthine (R_1 = OH, R_2 = H)
K_i (μM)	288	7	54
K_m (μM)	18.76	45.97	42.16
V_{max} (μmol/min)	1.19	0.57	0.55

Varying UDPG, Saturating NAD^+

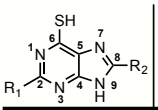	6-Thiopurine (R_1 = H, R_2 = H)	6-Thiouric acid (R_1 = OH, R_2 = OH)	6-Thioxanthine (R_1 = OH, R_2 = H)
K_i (μM)	323	40.5	133
K_m (μM)	5.77	7.39	6.20
V_{max} (μmol/min)	0.81	0.59	0.66

Varying NAD^+, Saturating UDPG

Figure 4-1. Inhibition assessment towards UDPGDH by various 6TP excretion metabolites through Lineweaver-Burk plot analysis under UDPG varying NAD^+ saturating conditions. A) Concentrations of 6TP, varying UDPG, screened were 0, 50, & 100 μM with slopes of each line 0.121, 0.135, 0.1623 respectively. Plotting slopes versus concentration afforded a regression line of y=0.000413x+0.1188. B) Concentrations of 6TU, varying UDPG, screened were 0, 5, & 10 μM with slopes of each line 0.103, 0.198, 0.2565 respectively. Plotting slopes versus concentration afforded a regression line of y=0.0154x+0.1091. C) Concentrations of 6TX, varying UDPG, screened were 0, 20, & 50 μM with slopes of each line 0.117, 0.152, 0.223 respectively. Plotting slopes versus concentration afforded a regression line of y=0.0021x+0.1143. D) Concentrations of 6TP, varying NAD^+, screened were 0, 50, & 100 μM with slopes of each line 0.580, 0.674, 0.760 respectively. Plotting slopes versus concentration afforded a regression line of y=0.0018x+0.5813. E) Concentrations of 6TU, varying NAD^+, screened were 0, 5, & 10 μM with slopes of each line 0.614, 0.685, 0.765 respectively. Plotting slopes versus concentration afforded a regression line of y=0.0154x+1091. E) Concentrations of 6TX, varying NAD^+, screened were 0, 20, & 80 μM with slopes of each line 0.655, 0.708, 0.891 respectively. Plotting slopes versus concentration afforded a regression line of y=0.0048x+6387.

To our surprise, 6TP was shown to have the lowest inhibition towards UDGPDH in comparison to its other two commercially available excretion metabolites (6TU & 6TX) assessed. Under saturation NAD^+ conditions, representing the most biomimetic compared to saturating UDPG, which is a substrate produced and rapidly used within the body, 6TU was shown to possess the most potent inhibition towards UDPGDH. Interestingly, 6TX was shown to have a modestly comparable K_i, relative to the poor inhibition of 6TP, to 6TU. The only difference between these two excretion metabolites is that 6TU possess a hydroxyl at the C8 position, whereas 6TX is non-substituted. Both 6TU and 6TX have a hydroxyl at the C2, and while this interesting, little to no alterations about this position can be considered. As, the therapeutically activity compound from 6TP results from the formation of the 6-thioguanosine nucleotide mimic, which requires the installation of an amino group at C2. Thus, even if the C2 position is found to cause the toxicity resulting from 6TP administration, no alterations or substitutions at this position is possible due to the nucleotide formation requirements. Given the results in hand, the lack of a C8 hydroxyl in 6TX and a drop in inhibition begs the question; what is the effect of the C8 position within 6TP in

regards to both toxicity and inhibition towards UDPGDH. To answer this, the C8 hydroxyl-6TP is required for assessment. While this compound is commercially available, it is cost prohibitive for academic studies. As such, the synthesis of 8-OH-6TP was undertaken via the established and well-reported Traube route for purine construction.

4.1.2. Synthesis of 8-OH-6-thiopurine and UDPGDH Inhibition Profiling

To assess the full effects of hydroxylation about the C2 and C8 positions (purine numbering shown in the **Figure 4-1** table insert) of 6TP excretion metabolites, the synthesis of 8OH-6TP was undertaken from reported procedures in 28% yield over two-steps **(Figure 4-2)**. In an analogous fashion to the three purines described above, 8OH-6TP was assessed for inhibition towards UDPGDH. **Figure 4-3** outlines the inhibition of the C8 hydroxylated purine under varying UDPG concentration **(Figure 4-3A)** and varying NAD^+ concentration **(Figure 4-3B)**. In regard to both, 8OH-6TP was found to inhibit UDPGDH more potently than 6TX (varying about the position of hydroxylation) and comparably to 6TU. The K_i with respect to varying UDPG was found to be 14 μM and with respect to varying NAD^+ 32.5 μM (summarized in **Figure 4-3**-table insert).

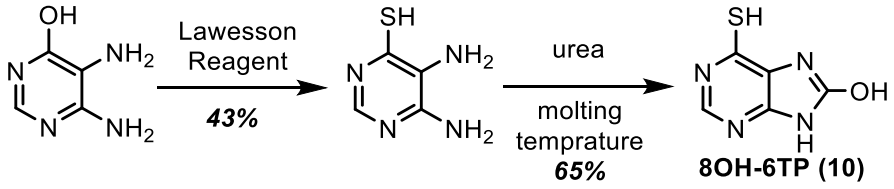

Figure 4-2. Synthesis of 8OH-6TP via a modified Traube approach. Thiol installation through Lawesson reagent upon commercially available 4,5-diamino-6-hydroxylpyrimidine with subsequent purine formation via condensation with urea.

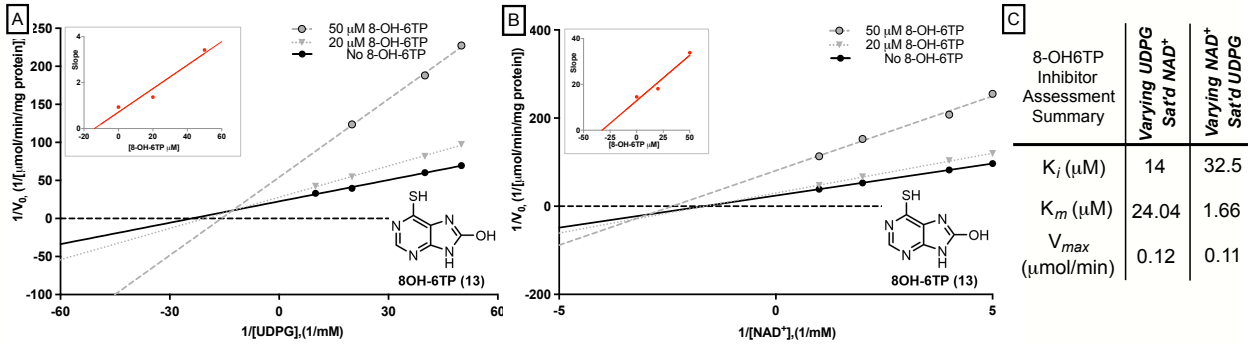

Figure 4-3. Lineweaver-Burk inhibitor assessment of 8OH-6TP under varying UDPG saturating NAD^+ conditions (left), varying NAD^+ saturating UDPG (center), and inhibitor summary (right). Concentrations of 8OH-6TP screened were 0, 20, & 50 μM under both condition with slopes of each line for varying UDPG 0.9365, 1.368, 3.422, respectively, and varying NAD^+ 14.54, 18.12, 33.81, respectively. Plotting slopes versus concentration afforded a regression line of y=0.0512x+0.7142 for varying UDPG and y=0.3963x+12.91 for NAD^+.

With the synthesis of 8-OH-6TP and its inhibition studies toward UDPGDH complete, along with 6TP, 6TX, and 6TU, we have been able to conclude that it is the C8 position within 6TP that is responsible for the greatest inhibition of UDPGDH and possibly causing the reported toxicity with its therapeutic administration. Most importantly, given that the C8 position plays no role in the formation of the 6-thioguanosine nucleotide, this position is amendable to synthetic manipulation for analog construction in the efforts to creating a new 6TP analog that retains its therapeutic character but diminished, if not eliminated toxicity. While these initial finds are a giant step forward in the understanding of 6TP toxicity, and can guide new analog construction, these results are based upon non-direct assessment of inhibition. To solidified and corroborate these finds a direct method is needed. As such, efforts towards the development of a HPLC method was undertaken and described below.

4.1.3. Direct UDPGDH Inhibition Assessment: HPLC Method Development

Building upon preliminary data collected in our laboratory towards the development of an HPLC method to assess UDPGDH activity, efforts were placed towards the optimization of a

basic HPLC method. Employing a reverse-phase HPLC Discovery C-18® column and a dual mobile phase method basic separation of the substrates (UDPG and NAD^+) and products (UDPGA and NADH) was achieved, but without baseline separation of the analytes nor a desired three-minute window to allow for cellular contaminants to elute from future in vivo studies. As such, efforts towards the development of a new robust HPLC assay was undertaken with three critical aspects that must be met: 1) possess a three-minute elution window for cellular contaminants, 2) baseline-separation of all analytes for full quantification of each, and 3) no derivatization of the analytes being required.

Method Development: Employing a mobile phase consisting of a buffer aqueous phase (Imidazole and tetrabutuyl ammonium sulfate, System A), organic phase (methanol, System B), wavelength of 262 nm, column oven temperature constant at 35 °C, and a flow rate of 0.5 mL/min method optimization was performed and guided by the three critical aspects (mentioned above). For the aqueous phase, it was found that an 8 mM imidazole buffer supplemented with 5 mM tetrabutyl ammonium hydrogen sulfate (TBAHS-ion pairing agent) at a pH of 6.5 gave the best separation of the analytes when used in conjunction with methanol. While numerous other mobile phases, specifically different buffers, were explored in this work only the efforts employing the imidazole/TBAHS will be discussed in this dissertation as this combination allowed for each of the three critical aspects to be met.

Isocratic Method Attempts: In the aims of creating a robust method, it was first thought that employing an isocratic method would allow for rapid column equilibration pre- and post-sample injection as well as decrease issues/complications with analyte elution within changing mobile phase compositions. As such, multiple efforts were attempted for an isocratic separation of the analytes (UDPG(A) & NAD(H)), a sample composed of all four were used, employing both

nanopure water, imidazole, and imidazole/TBAHS as the aqueous phase and methanol as the organic phase. As illustrated in **Figure 4-4**, no baseline separation of the four analytes was observed with any combination of aqueous phases at 262 nm, with a flow rate of 1.0 mL/min. The last attempt, shown in purple (top chromatograph line) was run at 0.5 mL/min, which gave the best separation at this time.

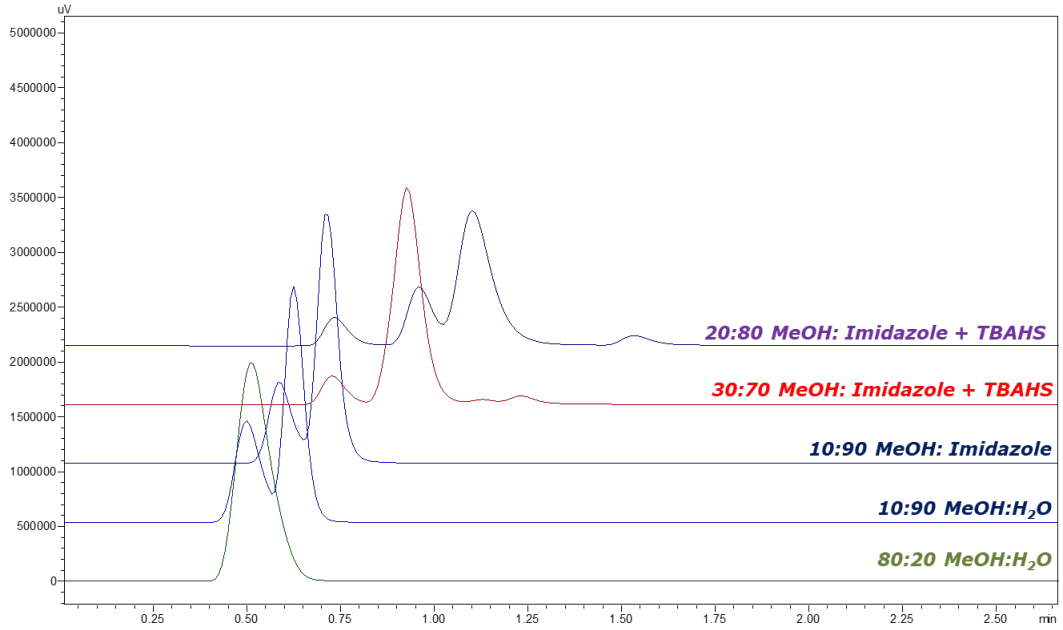

Figure 4-4. Summary of isocratic HPLC methods attempted for the separation of UDPG(A) and NAD(H) using a combination of aqueous phase buffer (imidazole and imidazole/TBAHS), methanol as the organic phase, and alterations of flow rate.

All attempted isocratic condition failed to provide base line separation of the four analytes. Therefore, investigations into a gradient mobile phase system were undertaken. While undertaking these studies, an addition criteria point was added: the separation of analytes and the regeneration of the column needed to be accomplished within 25 min or less. Rationale for this new addition was for analysis speed. After applying number of variations through changing temperature, flow-rate, mobile phase gradient, the final HPLC method with 8 mM imidazole, 5 mM TBAHS in water at pH 6.5 and methanol mobile phase resulted in baseline separation of four components of interest

(Figure 4-5). The retention time for UDPGA is longer than the other 3 analytes. NAD^+ peak is detected first, secondly the UDPG peak and thirdly the NADH. The entire separation time for these four analytes take 9.7 minutes and it was determined that the column should be equilibrated at 10% methanol for another 10.5 minutes in order to maintain its reproducibility. Altogether the HPLC analytical method gradient takes 23.70 minutes. Other gradient systems attempted are presented in the supplemental chapter of this dissertation.

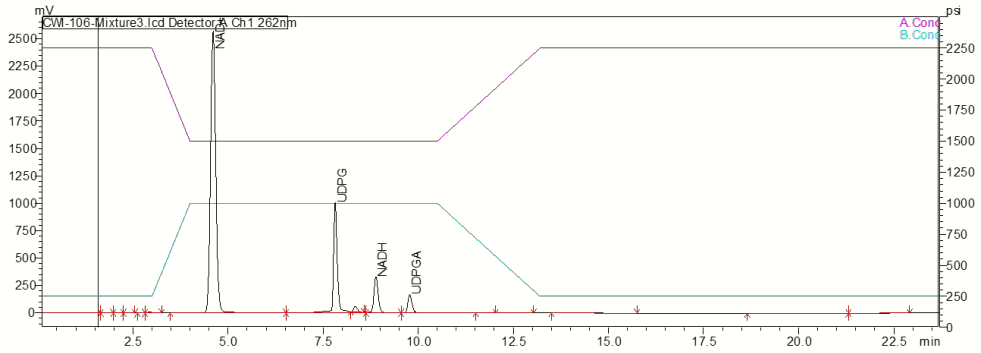

Figure 4-5. Chromatogram illustrating the analyte standards: UDPG(A) and NAD(H).

The identification of each analyte was performed by single agent analysis, as illustrated in **Figure 4-6**. Higher concentration of NAD^+ and UDPG and lower of NADH and UDPGA were employed to mimic biological conditions for future in vivo investigations.

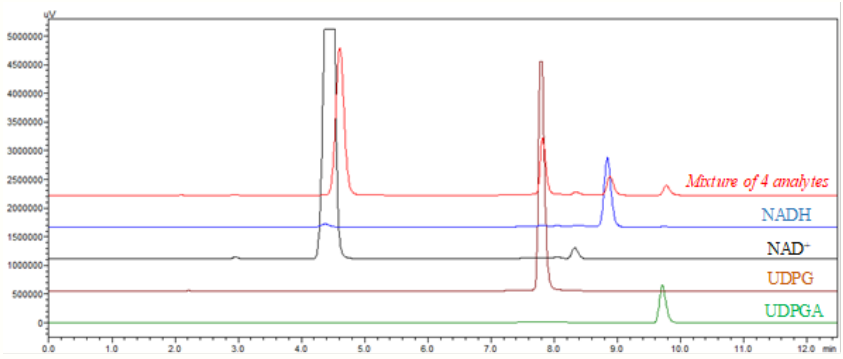

Figure 4-6. Chromatograms of individual analyte standards and a mixture sample illustrating peak identification.

4.1.4. HPLC Method Validation

Validation of the HPLC method was required, given the nature of the work being undertaken. The investigations into the modification of a known therapeutic would require the following of ICH guidelines. This includes all methods of assessment of possible drug candidates. As such, the full validation per ICH guidelines for the HPLC method was undertaken. ICH guidelines are used to verify that the resolution and repeatability of the instrument are adequate for the analysis to be performed. System suitability parameters include the following: 1) plate count, 2) tailing factors, 3) resolution, 4) repeatability (%RSD), and 5) retention time. For each of these, six repetitions are required for their assessment.

The parameters to be measured and the recommended limits are shown in Table 4.1. Capacity factor or the retention factor is defined as quantity of solute in the mobile phase (S) divided by the quantity in the mobile phase (M). The quantity of solutes in each phase is equal to its concentration C_s or C_m times the volume of the phase V_s or V_m, respectively. Therefore $k` = C_s V_s / C_m V_m$; k' is a very important property to interpret and improve for quality of separation. The capacity factor should exceed 2 as recommended by FDA. In this method, all the three components show that k is greater than 2, except for the NAD^+ that is at 1.3. Given that these recommended values are for the pharmaceutical analysis of drugs in clinical trials, and that our current assessment if for in vitro work, this lower than desired value is acceptable. System repeatability reflects the reproducibility of peak area at constant concentration of all analytes in the method. ICH values recommend that the %RSD value be less than 15%, in our methods the highest value is 0.4%. The resolution is the separation of two peaks. For better resolution larger difference in peak retention or narrower peaks need to be seen. Better resolution is obtained between the four components of interest under this method. The relative retention time for each solute is the time from the sample

injection to the appearance of the top of the peak in the chromatogram. The retention times for NAD^+, UDPG, NADH, and UDPGA are 4.35, 7.82, 8.82, and 9.75 respectively. These retention times are detected within less than 0.42 % RSD for more than ten repetitions. The actual peaks in a chromatogram usually have symmetrical Gaussian shape. Tailing factor shows how far it depart from it actual shape. Typically tailing factor should be less than 2 and the 4 components of interest show the value less than 2. The relative ability of column to furnish narrow peaks is described as column efficiency and is defined by the plate number N. In general, it should be more than 2000 and the analytes give higher plate number than the recommended value as shown in Table 4.1.

Parameters	Recommendations	NAD^+	UDPG	NADH	UDPGA
Capacity Factor (K')	k>2.0	1.3	2.9	3.4	3.8
Repeatability	RSD<1% for N>5 is desirable, Bio analytical assays can go up to 15%	0.4144	0.2331	0.0665	0.1479
Relative Retention		4.35 ± 0.41%	7.82 ± 0.01%	8.82 ± 0.06%	9.75 ± 0.14%
Resolution	R of > 2 between the peak of interest and the closest eluting potential interference	7.6	15.6	2.7	4.5
Tailing factor (T)- Actual tailing of the peak	T 0f < 2	1.072	1.322	1.169	1.276
Theoretical Plates (N)	In general, should be > 2000	5536	36547	31870	41470

Table 4-1. Results from the system suitability parameters assessment of the HPLC method for UDPGDH.

With the system suitability parameters complete, all (except one) within the desired accepted ranges, it can be concluded that the instrument is validate for the assay being performed. Next, method validation was performed, which includes: 1) selectivity, 2) linearity & sensitivity, 3) accuracy, and 4) robustness.

Selectivity: The representative chromatograms for the mixture of four analytes in the UDPGDH catalyzed reaction is shown in **Figure 4-5** & **4-6**. Peak assignment and identification of analytes were confirmed with the standard addition method. All these analytes were efficiently separated on the HPLC via a reverse phase column, in which no interference was observed. The repeatability, or the precision (N>5) of the peak areas of NAD^+, UDPG, NADH and UDPGA were in a range of 0.06-0.41% RSD. The resolution between the peak of interest and the closest eluting potential interference peak, should be greater than 2, and was found to be 2.7 in this method. The number of theoretical plates (N) should be greater than 2000, and it was found that this method possesses more than 5000 theoretical plates for all analytes (Table 4.1). With these parameters, it can be concluded that the HPLC method exhibits good selectivity and high resolution.

Linearity & Sensitivity: The regression equations for calibration curves **(Figure 4-7)** and LOD, LOQ values for the four analytes are shown in **Table 4-2**. The HPLC method shows good linearity for each of four analytes and the correlation coefficients greater than 0.9983 for the four calibration curves.

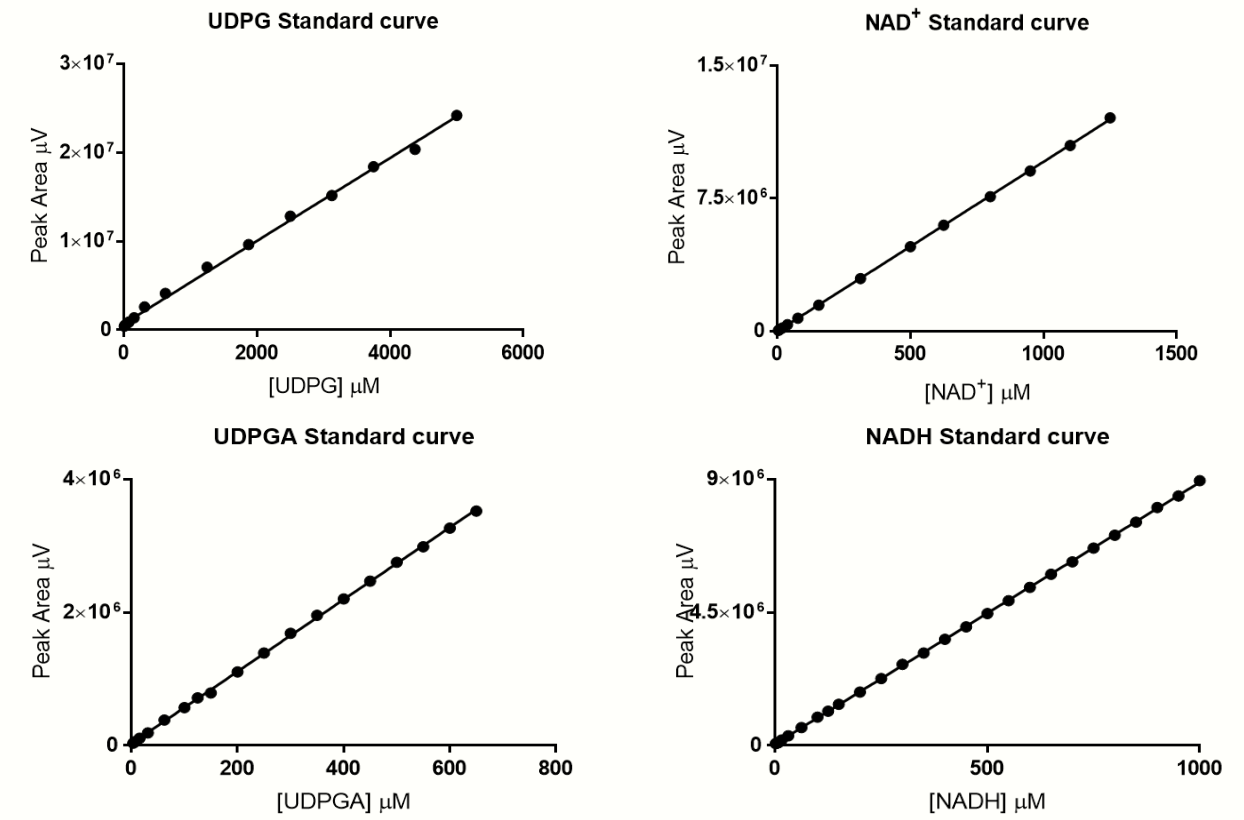

Figure 4-7. Calibration/Standard Curves for UDPG(A) and NAD(H). Regression lines, correlation coefficients, limits of detection (LOD) and quantification (LOQ) for each analyte is presented in Table 4-2 below.

	UDPGA	NADH	NAD^+	UDPG
Equation for regression line	Y=5414.2x+29611	Y=8847.5x+52542	Y=9568.5x-8985.6	Y=4499.6x + 1E+06
Correlation Coefficient	$R^2 = 0.9997$	R^2=0.9999	$R^2 = 0.9999$	$R^2 = 0.9983$
LOD	13.0 µM	7.8 µM	10.3 µM	0.27 µM
LOQ	39.5 µM	23.7 µM	31.4 µM	0.825 µM

Table 4-2. Regression equations, correlation coefficients, LOD, and LOQ for four analytes of the UDPGDH HPLC method developed.

Accuracy: The method was validated for FDA guidelines for the analysis of drugs in biological fluids. The assay results showed that all intra- and inter-day accuracies for the four analytes were more than 95% in both at low, medium, high concentration levels **(Table 4.3 A-D)**

UDPGA μM	Intra-day assay			Inter-day assay		
	Conc. Assayed	Recovery	RSD%	Conc. Assayed	Recovery	RSD%
320.7	320.7	100.0	0.1	319.4	99.6	0.9
296.5	296.2	100.1	0.2	296.3	100.1	0.1
275.5	275.0	100.2	0.3	275.5	100.1	0.5

Table 4-3A. Intra- and inter- day accuracy for UDPGA (n=3).

UDPG μM	Intra-day assay			Inter-day assay		
	Conc. Assayed	Recovery	RSD%	Conc. Assayed	Recovery	RSD%
511.4	514.8	100.7	0.4	509.3	99.6	0.7
471.1	470.7	99.9	0.6	472.1	100.2	0.1
433.7	432.4	99.7	0.1	431.8	99.5	0.1

Table 4-3B. Intra- and inter- day accuracy for NADH (n=3).

NADH μM	Intra-day assay			Inter-day assay		
	Conc. Assayed	Recovery	RSD%	Conc. Assayed	Recovery	RSD%
316.1	315.2	99.7	0.1	315.3	99.7	0.1
291.2	290.5	99.8	0.2	291.0	99.9	0.2
267.9	268.0	100.0	0.4	268.5	100.2	0.2

Table 4-3C. Intra- and inter- day accuracy for UDP (n=3).

NAD^+ μM	Intra-day assay			Inter-day assay		
	Conc. Assayed	Recovery	RSD%	Conc. Assayed	Recovery	RSD%
585.3	565.2	96.6	0.6	559.8	95.6	0.3
523.5	509.6	97.3	1.1	506.6	96.7	1.3
479.9	462.5	96.4	1.8	463.3	96.5	2.5

Table 4-3D. Intra- and inter- day accuracy for NAD^+ (n=3).

Robustness: Organic solvent composition and flow-rate were changed to compare the system suitability parameters to ensure the integrity of the analytical procedure. To determine the robustness of the current method, the effect of flow rate was studied at 0.4 and 0.6 mL/min rather than the employed 0.5 mL/min. Decreasing and increasing the MeOH percentages by 10% increments assessed the effect of mobile phase condition. Number of theoretical plates and tailing factor was monitored relative to UDPGA. No significant difference in variable parameters was observed under these conditions **(Table 4-4)**, which indicate the method is robust.

	Flow Rate (mL/min)	System Suitability Results							
		Plate count				UDPGA tailing			
		NAD^+	UDPG	NADH	UDPGA	NAD^+	UDPG	NADH	UDPGA
1	0.4	6023	29728	28782	34443	1.158	1.354	1.237	1.465
2	0.5	5224	30924	29809	36307	1.174	1.33.	1.213	1.366
3	0.6	4678	31088	30808	37609	1.16	1.319	1.215	1.350

Change in Organic mobile phase (MeOH)	System Suitability Results							
	Plate count				UDPGA tailing			
	NAD^+	UDPG	NADH	UDPGA	NAD^+	UDPG	NADH	UDPGA
10% less	4916	30450	29902	30206	1.167	1.326	1.220	1.388
Actual	5224	30924	29809	36307	1.174	1.333	1.213	1.366
10% more	5710	31000	29478	36366	1.205	1.344	1.215	1.366

Table 4-4. Robustness of the method: Number of theoretical plates and tailing factor was monitored relative to UDPGA. No significant difference in variable parameters were observe under these conditions changed, which indicate the method is robust.

With the validation of the method performed, and validate to the highest levels outlined by ICH, the method developed can be employed in the direct assessment of 6TP and its excretion metabolites to validate our UV/Vis method findings.

4.1.5. UDPGDH Enzymatic Assessment

With a suitable and verified method in place for the quantification of the analytes from the UDPGDH catalyzed reaction, in vitro analysis of the enzymatic reaction was developed to assess inhibitory activity of 6TP and 6TU. Prior the inhibition study, the condition must be developed to ensure inactivation of UDPGDH in the enzyme reaction to prevent non-desired UDPGA production after the 3-minute denaturation process, which is performed by placing samples in a 87 °C sand bath. In addition to ensuring that UDPGDH was denatured, and not producing additional UDPGA/NADH, the thermal stability of the products of the reaction needed to also be assessed.

For, if the sand bath temperatures resulted in UDPGA degradation the enzymatic assay would be unable to correct assess inhibition or activity of the enzymatic reaction.

To validate that UDPGDH was denatured using our sand bath method, 87 °C for 3 min, the enzymatic reaction was run for the formation of UDPGA. Aliquots were removed and assessed for quantification immediately after the sand bath treatment, then again 20 min and 60 min later all in triplicate. No change in UDPGA levels were observed, thus supporting and validating that the thermal sand bath conditions are sufficient to denature UDPGDH in its entirety.

Analyte thermal stability assessment was performed by placing analyte samples in Eppendorf tubes in the sand bath at 87 °C for a 10-minute period. While the enzymatic reaction will only be subjected to the sand bath for three-minute, longer evaluation was done to ensure not only stability but also reproducibility. Shown in **Figure 4-8**, UDPG(A) were shown to be thermal stable for the entire 10 minutes and bath period, with aliquots removed every minute and assessed via the developed HPLC method. NADH was also shown to be thermal stable, but NAD^+ unfortunately, yet not unexpectedly was seen to degraded after three-minutes. The degradation of NAD^+, while unfortunate, does not negatively impact the method being developed.

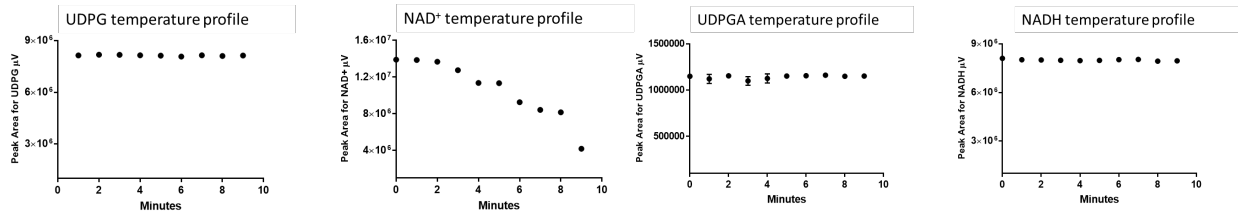

Figure 4-8. Thermal stability assessment of UDPG(A) and NAD(H). Each analyte is an average of three independent runs with standard error bars (SEBs). Many SEBs are not visible due to small value of the error.

To ensure that all UDPGA detected in the method came from the enzymatic conversion of UDPG to UDPGA via UDPGDH a validation of the reaction was performed. A reaction of UDPG and NAD^+ where placed in the appropriate buffer system in the shaking water bath. Prior to

UDPGDH addition an aliquot was removed and assessed for UDPGA and NADH. After the addition of UDPGDH another aliquot was removed 10-minutes later and assessed via the developed HPLC method. Shown in **Figure 4-9** are the results from this UDPGA formation validation study. In the absence of UDPGDH, neither UDPGA nor NADH are observed, but after the addition of the enzyme production of these two products are observed.

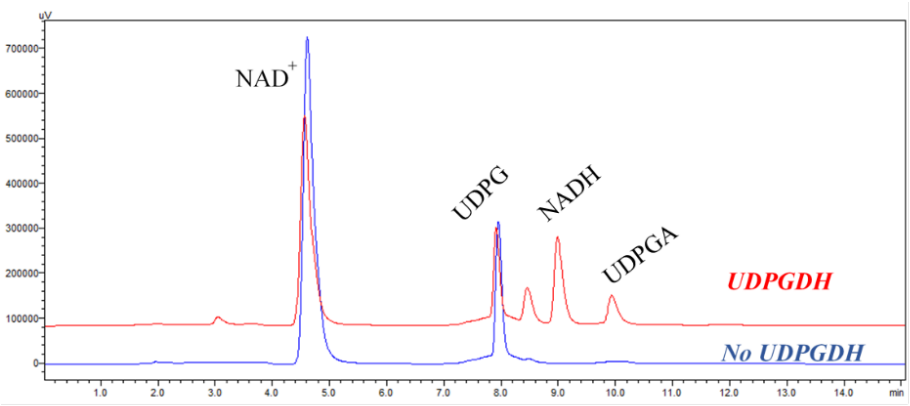

Figure 4-9. Representative chromatograms for formation of UDPGA, NADH in vitro UDPGDH catalyzed reaction mixture.

With a robust HPLC method in place, validation of the thermal stability of analytes, proof in the enzymatic production of UDPGA from UDPG the next step was to determine the range of linearity in the production of UDPGA in our enzymatic method. To accomplish this, the enzymatic reaction was run over a 15-minute period, during which aliquots were removed and assessed for both NADH and UDPGA concentrations every minute. Samples were analyzed in triplicate. Shown in **Figure 4-10** are the progression curves for both NADH and UDPGA. These graphs reveal that there is a five-minute linearity window in the production of both NADH and UDPGA, which can be used for inhibition assessment of 6TP, its excretion metabolites, and future analogs in a direct quantification fashion.

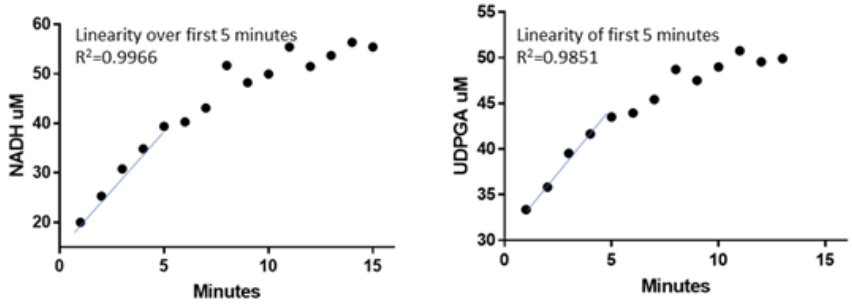

Figure 4-10. Reaction progressive curve for the formation of UDPGA and NADH. Each analyte is an average of three independent runs with standard error bars (SEBs). Many SEBs are not visible due to small value of the error.

4.1.6. Direct Inhibition Assessment of UDPGDH by 6TP and 6TU

It is of importance to recall that 6TP was shown to have a K_i of 288 μM and 6TU a K_i of 7 μM towards UDPGDH under saturating NAD^+ and varying UDPG levels as observed in our indirect UV/Vis method. With the development of our robust and validated HPLC method, construction of our UDPGDH enzymatic assay protocol the assessment of both 6TP and 6TU can be accomplished in a direct fashion. Employing three various concentrations of 6TP (0, 50, & 100 μM) under saturating NAD^+ conditions assessment of inhibition towards UDPGDH was performed and assessed via the developed HPLC assay. Lineweaver-Burk plots were obtained from the determination of UDPG concentrations at various purine concentrations verses the velocity of the reaction (assuming 3.5 mg of protein based upon unit of enzyme from the supplier). Plotting the slopes of these three lines verses the concentration of the purine allows for the determination of the K_i value. The Linweaver-Burke plots for 6TP and 6TU are shown in **Figures 4-11** and **4-12**.

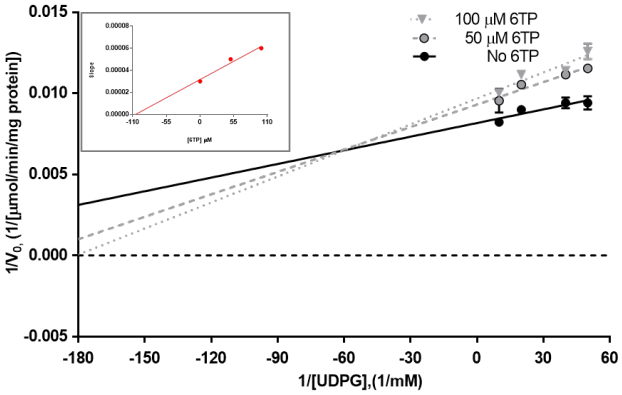

Figure 4-11. Lineweaver-Burk plots for inhibitor assessment of 6TP towards UDPGDH, quantified by HPLC method**.** Each analyte is an average of three independent runs with standard error bars (SEBs). Many SEBs are not visible due to small value of the error.

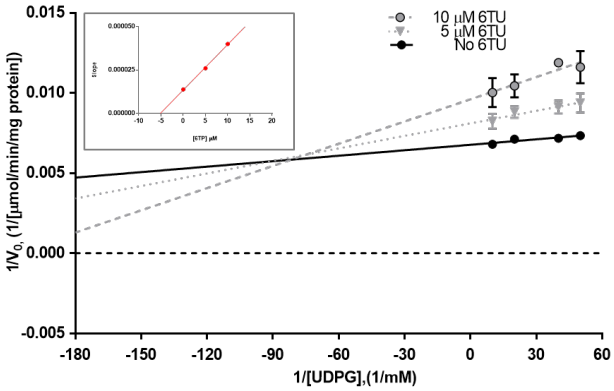

Figure 4-12. Lineweaver-Burk plots for inhibitor assessment of 6TU towards UDPGDH, quantified by HPLC method. Each analyte is an average of three independent runs with standard error bars (SEBs). Many SEBs are not visible due to small value of the error.

From this direct method of inhibitor assessment, it has been found that 6TP possesses a K_i of 106 µM and 6TU 5.2 µM (Table 4.5). In comparison to the non-direct method, both 6TP and6TU are shown to have stronger inhibition towards UDPGDH, further supporting our hypothesis.

Inhibitor	Inhibition Studies for NAD^+ Saturation		
	Equation for the Inhibition Curve	R^2 for the Curve	K_i (μM)
6TP **(1)**	y = 3.0e-007x + 3.167e-005	0.964	105.6
6TU **(12)**	y = 2.6e-006x + 1.35e-005	0.998	5.2

Table 4-5. Inhibition assessment 6TP and 6TU towards UDPGDH as assessed by the direct HPLC method.

From both the indirect and direct methods of UDPGDH assessment, we can conclude that 6TP and its excretion metabolites possess inhibition towards this first enzymatic step of the bilirubin pathway. Furthermore, based upon the results from the indirect method and the synthesis and evaluation of 8-OH-6TP we can conclude that the C8 position is of key interest in both the onset of toxicity as well as the future construction of 6TP analogs. Based upon these findings, thus far, we can have concluded that our hypothesis of 6TP and/or its excretion metabolites do in fact possess inhibition towards UDPGDH to a degree that could be correlated to the associated onset of toxicity from 6TP administration.

4.2. Assessment of UDP-Glucuronosyl Transferase – 6TP and 6TU Inhibition Studies

Determination of any inhibition by either 6TP and/or 6TU, representing the two extremes of inhibitors towards UDPGDH, towards UDP-glucuronosyl transferase (UGT) was performed next. While the production of UDPGA is directly impacted by both 6TP and 6TU, the question that remains is, are these levels still sufficient to allow conjugation with bilirubin for excretion and does 6TP and/or 6TU directly inhibit this transferase step. To answer this, a HPLC method was required as that commercially available bilirubin quantification keys do not discriminate between bilirubin and its mono- and di-glucuronide forms.

4.2.1. HPLC Method Development

Building upon the reported literature for HPLC assays towards UGT, an enhanced method was developed that allows for the baseline separation of the unconjugated bilirubin (UCB), and its three conjugated forms (BMG1, BMG2, and BDG). Employing the gradient method, outlined in chapter 3, separation of the analytes and column regeneration can be achieved within 33-minutes. Unlike the methods for UDPGDH, the wavelength was changed to 450 for bilirubin quantification. The same wavelength can be used for all of the bilirubin analytes as the chromophore remains unaltered in each of the four-bilirubin species. Shown in **Figure 4-13** is the chromatogram from the developed HPLC method for the assessment of UGT.

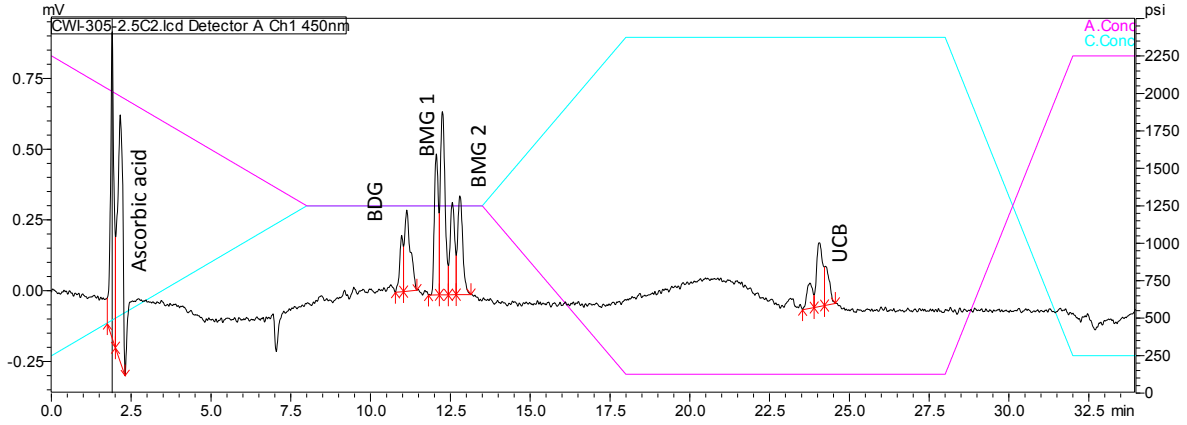

Figure 4-13. Chromatogram of UGT catalyzed reaction for the formation of mono- (BMG1/2) and di-(BDG) glucuronides from unconjugated bilirubin (UCB).

4.2.2. HPLC Method Validation

As with the UDPGDH method, validation of the UGT method was undertaken, but only in the aspect of accuracy. The detailed validation outlined in the UDPGDH method verifies that that instrument is well suited to perform the methods developed, and as such the same level of validation was not performed for the UGT method. Given the aims of the UGT method, assessment

of inhibition, accuracy was assessed. The %RSD, shown in Table 4.6, was shown to be greater than 90% for all three trials. As such, the method was confirmed to be valid.

Trial	Level (%)	Sample Conc. μM	Amount (μM) of Std. Added	True Con. (μM)	Found Con. (μM)	% Recovery
1	120	5	6	5.2	4.9	94 ±9
2	100	5	5	5	4.5	90 ±2
3	80	5	4	4.7	4.3	91 ±9

Table 4-6. Accuracy validation of the UGT method as outlined by ICH guidelines.

4.2.3. Inhibition Effects of 6TP and 6TU upon UGT

Further investigation into the bilirubin detoxification pathway led to inhibition studies of 6TP and 6TU towards UGT1. Only 6TP and 6TU were screened, as they represented the two extremes of inhibition towards UDPGDH with regards to varying UDPGA concentrations. To assess inhibition, an HPLC method was developed that allowed for the separation and quantification of all substrates and products from the UGT reaction. While there are reported methods to assess the activity of this transferase reaction, our method developed includes universal applications of each, as well as new aspects. This method allows for the full separation and quantification for all bilirubin glucuronide species and unconjugated bilirubin, as well as applications into inhibition assessment.

Shown in **Figure 4-14** line A are the three isomers of unconjugated bilirubin (UCB) from 23.6-24.2 min. Line B shows the three isomers of the bilirubin diglucuronide (BDG) species at 11.2-11.4 mins and the various bilirubin monoglucuronides (BMG1&2) from 12.3-13.2 mins. To validate the formation of the various glucuronide species, a separate reaction was run and then

treated with glucuronidase, which removes the glucuronic acid upon the various forms of the bilirubin glucuronide species forming unconjugated bilirubin and glucuronic acid. Line C is obtained post glucuronidase treatment of the formed glucuronide species from line B. With the results from **Figure 4-14**, the formation of the glucuronide species is thereby confirmed and in extension confirms the validity of the method developed for separation of substrates and products.

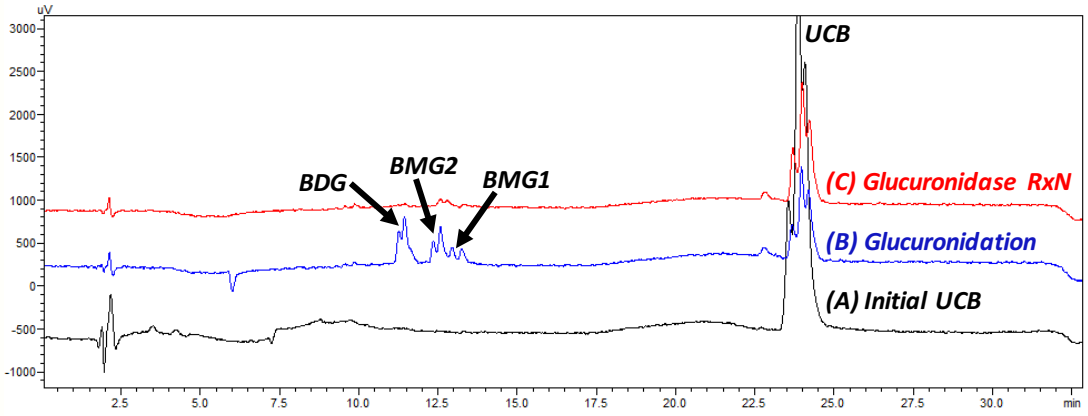

Figure 4-14. Chromatogram illustrating the unconjugated bilirubin starting material (line A), products (line B), and proof of conjugated bilirubin formation via selective enzyme degradation (line C).

Standard curves for both the mono- and di-glucuronide species was unattainable, given that both species are both light and thermally sensitive and have been found to degrade rapidly. To this end, the bilirubin standard curve **(Figure 4-15-left)** was employed given that the same chromophore species is present within UCB, BMG1&2, and BDG. To determine the range of linearity within the enzymatic reaction, the reaction progressive curve investigations were undertaken. It was found that the consumption of bilirubin, and therefore the production of the conjugated bilirubin species possesses a linear range of 45-minutes.

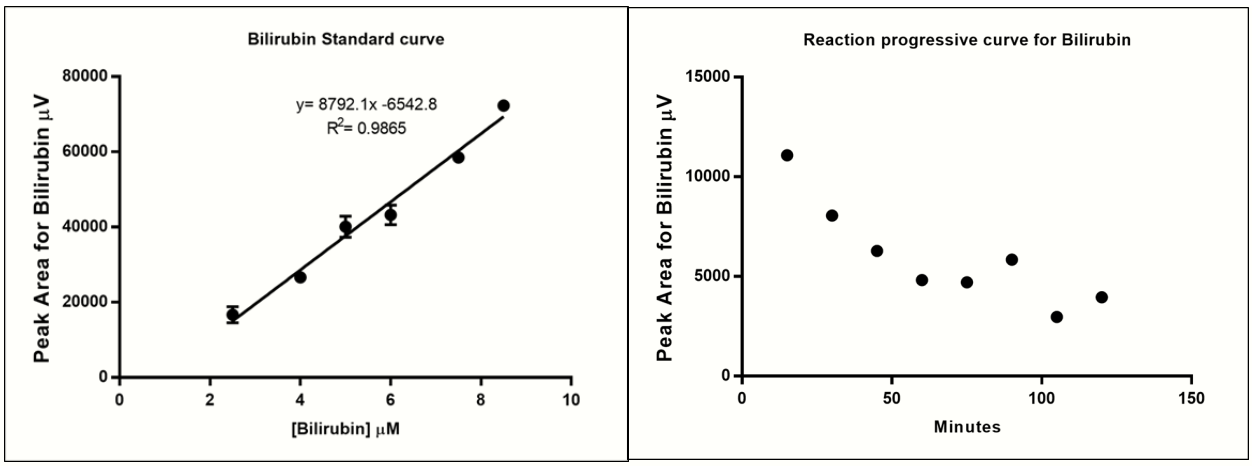

Figure 4-15. (Left) Bilirubin standard curve. (Right) Reaction progressive curve for UGT. Each analyte is an average of three independent runs with standard error bars (SEBs). Many SEBs are not visible due to small value of the error.

Inhibition assessment of 6TP and 6TU was performed at 50 and 75 μM for both purines over a 45-minute incubation period. Outlined in **Figure 4-16** are the levels of the BDG, the various BMG1&2, and UCB when treated with 50 and 75 μM of 6TP. Inhibition investigations by 6TU at the same conditions are shown in **Figure 4-17**. The apparent values for the formation of BMGs, BDG, and remaining UCB showed no significant difference ($P>0.05$) in the presence and absence of 6TP and 6TU. All statistical calculations are presented within the supplemental chapter of this work. Stability of the glucuronide species could present doubt in the accuracy of the quantification and in turn the validity of the inhibition profiles obtained. Therefore, assessment of inhibition by indirect means of a stable species could further validate the findings from the glucuronide study.

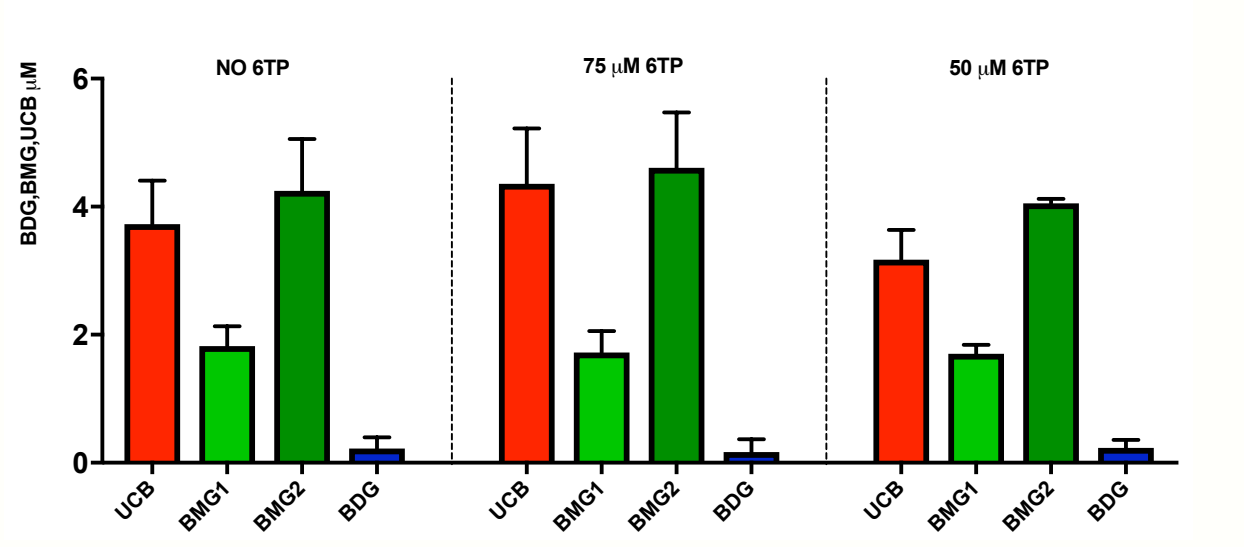

Figure 4-16. Inhibition studies of UDP-glucuronosyl transferase (UGT) by 6TP at 50 and 75 μM. Levels of unconjugated bilirubin (UCB), monoglucuronide bilirubin (BMG1 & BMG2), and diglucuronide bilirubin (BDG) quantified through the bilirubin standard curve. Each analyte is an average of three independent runs with standard error bars (n=3).

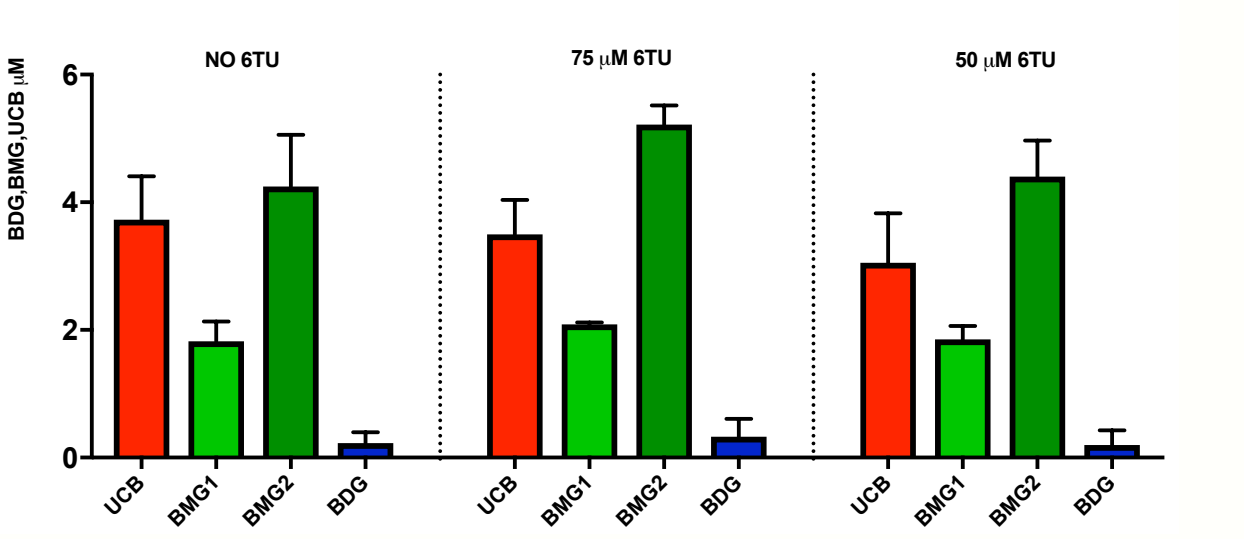

Figure 4-17. Inhibition studies of UDP-glucuronosyl transferase (UGT) by 6TU at 50 and 75 μM. Levels of unconjugated bilirubin (UCB), monoglucuronide bilirubin (BMG1 & BMG2), and diglucuronide bilirubin (BDG) quantified through the bilirubin standard curve. Each analyte is an average of three independent runs with standard error bars (n=3).

Due to the well-reported and documented instability of the glucuronide species, monitoring and quantifying UDPGA levels assessed activity of UGT. The previous HPLC method for glucuronide quantification was not applicable for UDPGA quantification due to the elution of

UDPGA at a gradient point in the method. However, the first HPLC method developed for assessment of UDPGDH could be employed for the quantification of UDPGA for UGT activity and inhibition studies. Successful conjugation of bilirubin to either one or two UDPGAs will form the desired glucuronide species, and upon any degradation of these thermally and light reactive species will result in the return of UCB and glucuronic acid. The glucuronic acid will have a different retention factor in comparison to UDPGA. Therefore, any decrease in UDPGA levels directly corresponds to the formation of the glucuronide species. Thermal stability of UDPGA is key for this method and was determined by incubating UDPGA in the reaction media over a 15-hour period (shown in **Figure 4-18** with comparison between UDPGA and mixture with no enzyme added at 37 °C).

Three time-course experiments were performed (1, 12 & 15-hours) in which UDPGA concentrations were determined by HPLC analysis **(Figure 4-18)**. When the reaction was performed in the absence of any inhibitors, concentrations of UDPGA dropped to 241 μM after 1-hour, 110 μM after 12-hours, and 17 μM after 15-hours from the initial 260 μM (validated by aliquot removal prior to the start of the reaction). Levels of UDPGA were found to be relatively the same when testing inhibition by 50 and 75 μM of 6TP: 241 & 242 for 1 hour, 130 & 128 for 12 hours, and 20 & 20 for 15 hours, respectively. Inhibitor assessment of 6TU towards UGT afforded similar results to 6TP and the control when screened at 50 and 75 μM of 6TU: 243 & 241 for 1 hour, 128 & 125 for 12 hours, and 20 & 16 for 15 hours, respectively. The apparent UDPGA levels at the end of the reaction showed no significance difference ($P>0.05$) in the presence and absence of 6TP and TU. All statistical calculations are presented within the supplemental chapter of this work.

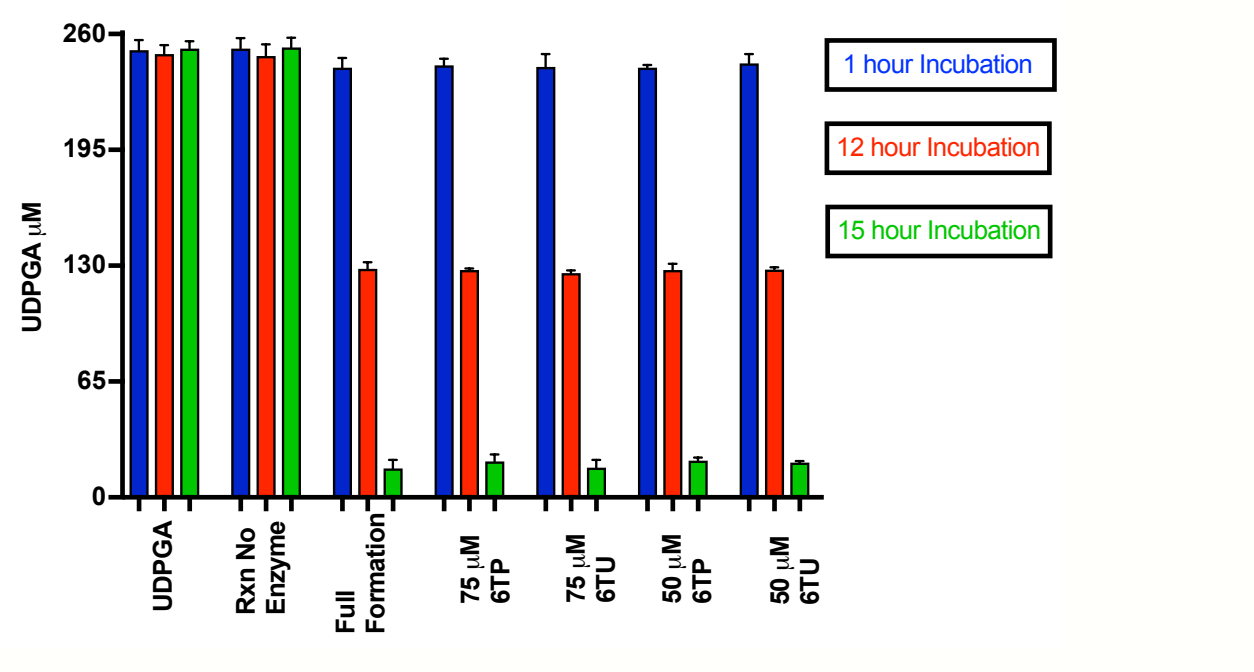

Figure 4-18 Assessment of UGT inhibition by 6TP and 6TU at 75 and 50 µM over three time-course experiments of 1, 12 and 15-hours. One-hour incubations are triplicates of triplicates, 12-hour are triplicates, and 15-hours are triplicates of duplicates.

To ensure that our UGT enzymatic method is working properly, given that no inhibition by either 6TP or 6TU was observed, assessment by known UGT inhibitors was undertaken to serve as a control to illustrate the soundness of the method. Two known inhibitors of UGT were chosen to assess inhibition of UGT, sorafenib and regorafenib. Inhibitor assessment of these two inhibitors, 50 µM in DMSO, revealed strong inhibition relative to the control system, only DMSO was added with no inhibitor **(Figure 4-19 left)**. Given that a unified method for the assessment of bilirubin activity will be developed (to be discussed below) that will include both UDPGDH and UGT, both of these inhibitors were screened against UDPGDH for possible interference/inhibition. As illustrated in **Figure 4.19 right**, neither compound at 50 µM in DMSO was shown to have any significant inhibition, within the limits of standard deviation, towards UDPGDH relative to controls where only DMSO was added.

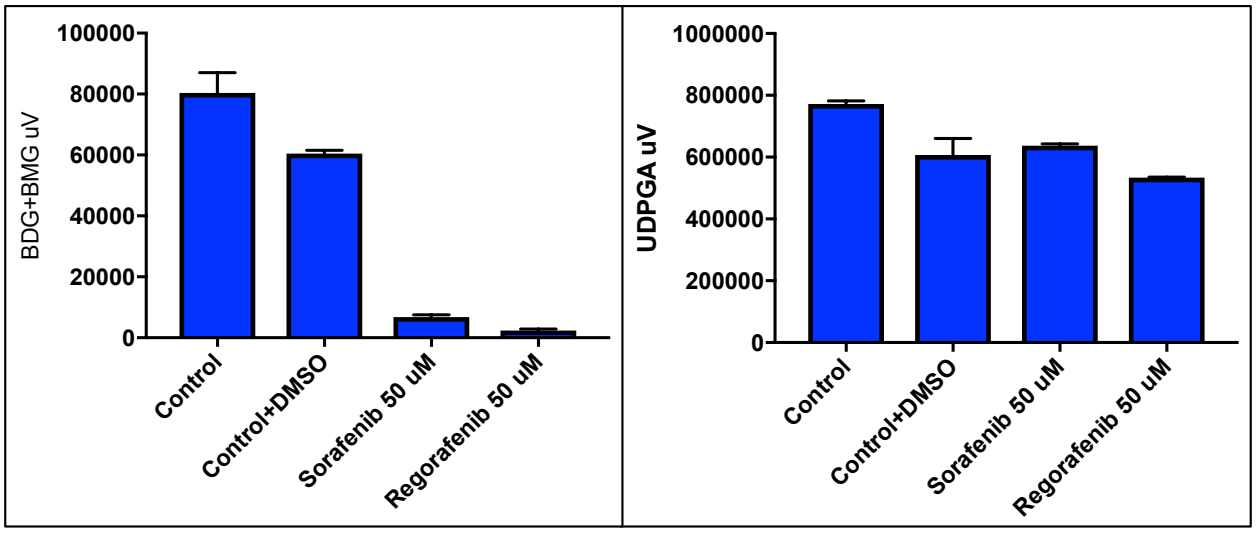

Figure 4-19. Inhibitor assessment of known UGT inhibitors sorafenib and regorafenib towards UGT (left) and UDPGDH (right). Inhibitors were dissolved in DMSO, as such controls with no inhibitors used had the same volume of DMSO added for direct comparison of the inhibition assessments. Each analyte is an average of three independent runs with standard error bars (SEBs). Many SEBs are not visible due to small value of the error. (n=3)

With these findings of no inhibition by either 6TP or 6TU towards UGT, we can conclude that the inhibition via UDPGDH is the sole inhibition point within the bilirubin pathway that could result in the 6TP associated toxicities resulting from its therapeutic use. Recalling the hypothesis behind this study, that 6TP and/or its excretion metabolites inhibit either/both UDPGDH or UGT resulting in toxicity, we can conclude based upon the in-direct and direct methods of UDPGDH and UGT assessments that we have proven this hypothesis to be true; at least in vitro.

4.3. Unified HPLC Method for UDPGDH and UGT Assessment

Given the identification of UDPGDH as the key enzyme within the bilirubin pathway that is inhibited by 6TP and its excretion metabolites, but also noting that while UDPGA is still produced from UDPGDH the underlying question that remains is if the levels of UDPGA produced is sufficient for bilirubin clearance by UGT. Keeping in mind the goal of the project is for the construction of new 6TP analogs that retains its therapeutic activity, but with limited or

eliminated toxicity, assessment of said analogs in a single unified assay would prove useful. No such method has been developed, nor has an in vitro method for the bilirubin pathway that would allow direct assessment and quantification of inhibition been developed or discussed in the literature. While the levels of UGT within the body remain relatively constant, UDPGDH is variable, not only in a person-to-person comparison, but also to physiology demands. As such, while the development of a unified HPLC method for single analysis is achievable, the development of a dual enzymatic system will prove more difficult.

Unified HPLC Method Development for UDPGDH and UGT: While two separate methods for the assessment of UDPGDH and UGT have been developed and successively shown to determine inhibition, efforts were directed towards merging the two methods into a single unified assessment tool for the bilirubin pathway. Given the similarities of the two methods, both using an imidazole/TBAHS (purposely done so) and reverse-phase column, the merging of the two methods was accomplished rapidly, once minor differences were reconciled. While the UDPGDH method requires a wavelength of 262 nm and the UGT at 450 nm, the wavelengths can be switched, along with adequate time for detector zeroing, within the unified method. The full method details are described within chapter 3, but key points will be addressed here. While the UDPGDH method employs methanol for the organic phase, the UGT method requires acetonitrile for UCB, BMG1/2, and BDG elution. This issue was resolved with the introduction of acetonitrile with equal reduction of methanol post the elution of UDPGA (last analyte of interest from the UDPGDH reaction) as shown in **Figure 4-20**. Both the mono- and di-glucuronide species was eluted post this organic phase substitution, as shown in **Figure 4-21**. Further increasing the acetonitrile percentage allowed for the elution of UCB species, after which the column was returned to the starting conditions with enough time included for column regeneration.

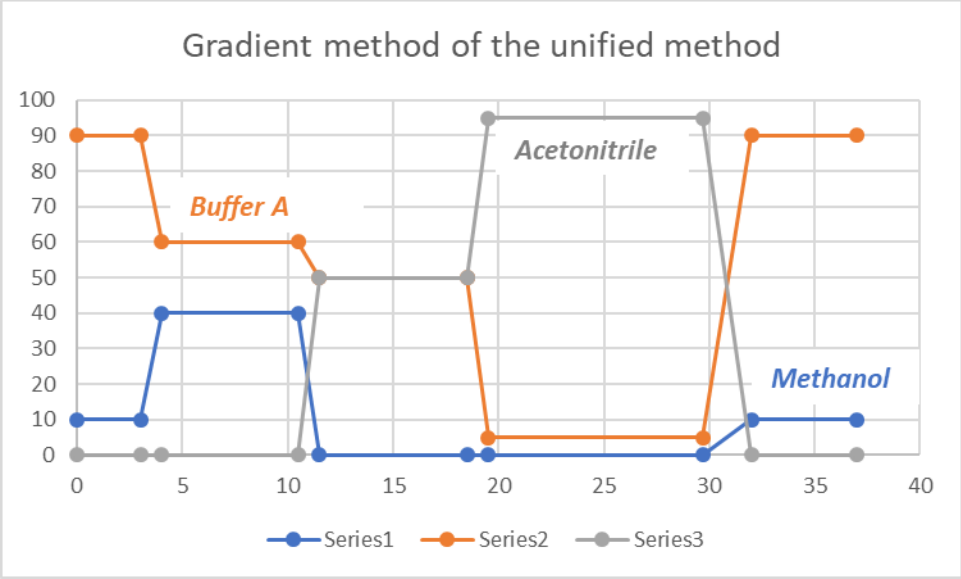

Figure 4-20. Tri-phasic gradient HPLC method for the unified assessment of UDPGDH and UGT.

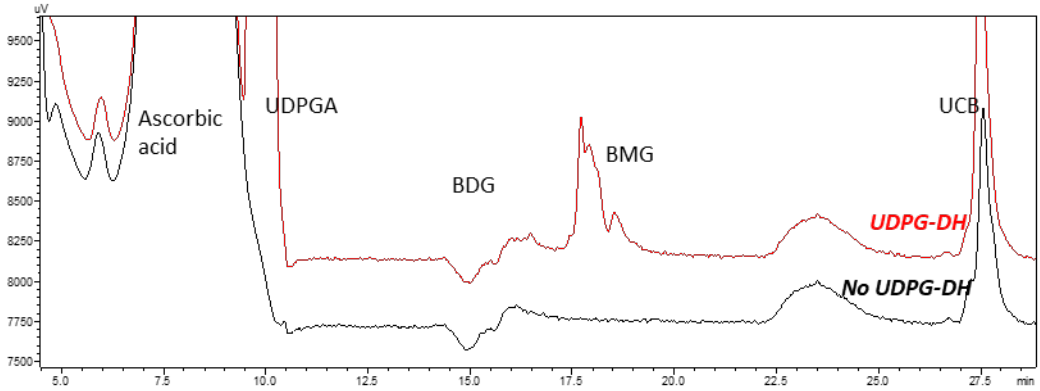

Figure 4-21. Chromatogram obtained at 262 nm till 12 min and then changed to 450 nm.

Development of Unified UDGPDH and UGT Enzymatic In Vitro Method: Levels of UDPGDH vary between people, and furthermore is dependent upon physiology stress and conditions. As such, efforts were placed towards finding a general ratio of UDPGDH to UGT that mimic the general trend of toxicity commonly seen with 6TP administration, that of increased UCB levels and decreased BMG levels which is solely responsible for bilirubin excretion. It is of note to mention that BMG1/2 are not excreted and does undergo de-glucuronidation resulting in increased UCB levels. After numerous attempted ratio levels of UDPGDH:UGT it was shown

that a ratio of 1:440 provided an accurate predictor of physiology conditions, and was reproducible **(Figure 4-22)**. While the high degree of ratio proportions is great, the velocity of the UDPGDH reaction is far greater than the UGT conjugation reaction (nearly 50-folds greater). Employing the individual methods for UDPGDH and UGT with the 1:440 UDPGDH:UGT enzymatic system, it was observed that UDPGA levels remained nearly constant with subjected to either 6TP or 6TU. While this seems to contradict our initial findings that 6TU inhibits UDPGDH greater than 6TP, the concentration of either purine was low enough to prove to be nearly non-interfering **(Figure 4-22 right)**. However, at these levels of 6TP and 6TU a clear difference in the formation of BDG can be observed, with 6TU showing lower amounts being formed at constant purine concentration. Thus suggesting, that minor changes in the physiology pool of UDPGA is great enough to translate into highly diminished levels of BDG for excretion, as shown in **Figure 4-22 left**. Presented within the supplemental chapter of this work are the other ratios of UDPGDH: UGT attempted and their levels of analyte formation.

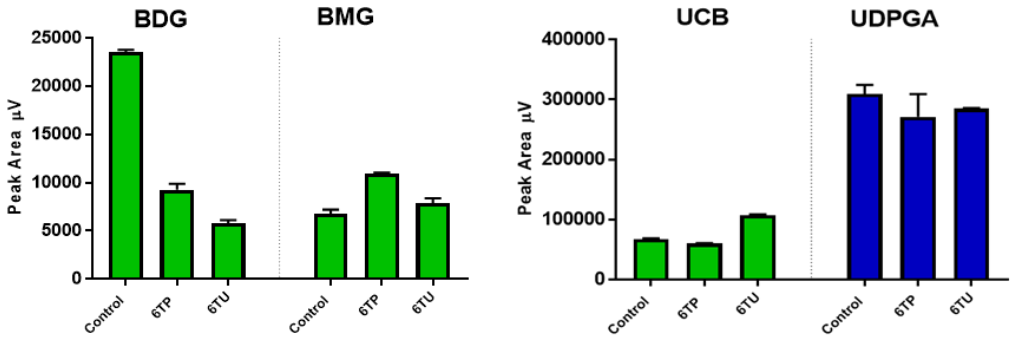

Figure 4-22 Overall effects of 1:440 ratio of UDPGDH: UGT with regards to UDPGA levels and BMG and BDG formation. Each analyte is an average of three independent runs with standard error bars

While a single method, that accurately reflects the physiology levels of both UDPGDH and UGT is not achievable, a ratio of 1:440 provides a good insight into the behaviors of 6TP and its

analogs/excretion metabolites and can be used as a general method for inhibition/activity studies towards the bilirubin pathway.

4.4. In Vivo Assessment of 6TP and Inhibition of UDPGDH and UGT

While our in vitro studies have shown that 6TP and its excretion metabolites do inhibit UDPGDH, level of inhibition per species was variable, we desired to proof our hypothesis in vivo. With the aid of collaborators at the University of Texas-Southwestern, rat liver hepatocytes were acquired and levels of UCB, BMG1/2 and BDG were assessed. Assessment of these species was done by our developed UGT HPLC method. Shown in **Figure 4-23** the control group shows higher levels of BMG, which is commonly reported, and was used to serve as the normalization point for the study. It is of interest to note that BDG is excreted, but healthy subjects do not commonly excrete BMG1/2. The treatment of the hepatocytes with 50 and 25 μM of 6TP resulted in nearly the same levels of decreased BDG formation. Relative the control, this depression was considered minor. On the contrary, when 10 and 5 μM of 6TU were employed a significant decrease in the levels of BMG was observed. While the decrease is assumed to originate from the inhibition of UDPGDH by 6TU by decreasing the liable pool of UDPGA and as such decreasing the conjugation of UCB, we cannot concretely make this claim. If the reduced BDG formation does in fact result from the decrease in UDPGA, the addition of UDPGA to the system should show a recovery of the system similar to the control group. The addition of 15 μM of UDPGA along with a high dose of 6TU (10 μM) resulted in the production of BDG similar to that of the control group. Thus, we can conclude that 6TU is in fact inhibiting UDPGDH, that results in lower levels of UDPGA and therefore preventing the conjugation of UCB to UDPGA for the formation of BDG. To ensure the UGT operating properly, as suggested by the control group, 10 μM of regorafenib was introduced and resulted in the near complete inhibition of UGT.

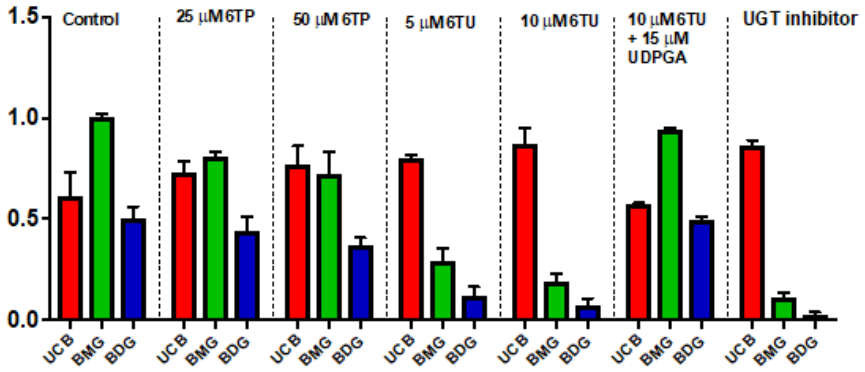

Figure 4-23. Hepatocyte studies with both high (50 and 10 μM) and low (25 and 5 μM) for 6TP and 6TU, respectively. Standard deviation is shown within the graph with a sample of n=4.

4.5. Synthesis of 6TP Analogs

Given the data collected, we can conclude that the C8 position of 6TP is the leading cause of inhibition towards UDPGDH. As such, we sought out to develop a synthetic route to gain access to analogs of 6TP that are substituted at the C8 position. Starting from 6-chloropurine (**28**) accessing 8-bromo-6-TP was accomplished over four steps in an overall 26% yield **(Figure 4-24)**. Evaluation of this analog as yet to be assessed in our HPLC and enzymatic methods, but it is envisioned to be done shortly. From this route, further analogs that are substituted at the C8 position can be accessed. To accomplish this, we propose that **32** can be elaborated onto a disulfide dimer. As such, the transformation of the bromine at C8 into its corresponding Grignard reagent can be performed, allowing for the introduction of other substituents at this position (Cl, F, Me, and deuterium). Reduction of the disulfide will afford new analogs of 6TP that are varied about the C8 position.

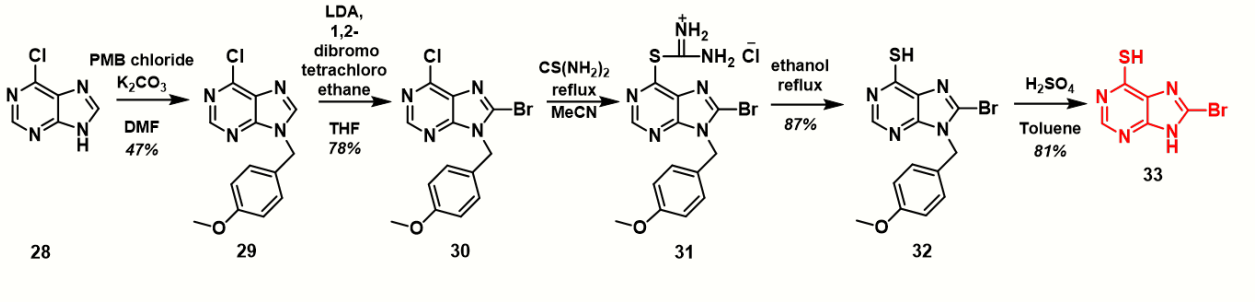

Figure 4-24. Synthetic route accessing 8-substituted 6TP analogs.

Chapter 5 - **Conclusion**

Acute lymphocytic leukemia (ALL) is one of the more than ten types of leukemias currently effecting both males and females in the United States. This form of leukemia comprises the nearly 6,000 new cases expected in 2017, with an estimate death rate of approximately 1,500. Currently, multiple drugs are being employed in the fight against these leukemias. Unfortunately, each of these treatments has failed to help decrease the projected death rates, mostly due to fatal toxicity associated with the treatments or discontinuation of treatments. 6-Thiopurine (6-TP) has a proven record in the remission of ALL mentioned previously, but also has a well-documented toxicity associated with its use. The major side effect associated with 6TP treatment is jaundice and hepatotoxicity, both of which comes from increased concentration of bilirubin within the blood. Because of this of this harmful condition, 6TP needs to be administrated in on- and off-treatment regimen to allow recovery from these toxic side-effects. However, said regiment greatly reduces 6TP effectiveness in the remission of leukemia. On the other hand, in excretion pathway, therapeutically inactive oxidative metabolites of 6TP such as 8-hydroxyl-6-thiopurine (6TP-8OH), 6-thioxanthine (6TX) and 6-thiouric acid (6TU) can be formed. It has been observed that 6TU is retained by the body well beyond 24-hour post 6TP treatment.

Noting that 6TP administration results in the onset jaundice, we hypothesize that this is from the direct inhibition of either/both enzymatic steps: 1) UDPGDH biological enzyme responsible for formation of UDPGA, or 2) UGT enzyme responsible for formation of bilirubin glucuronide and thereby decreasing the conjugation of bilirubin to its water-soluble glucuronide form for excretion.

To investigate the toxicity resulting from 6TP administration, inhibition analysis of these oxidative metabolites on UDPGDH were assessed using a robust UV-Vis method. The inhibition

profile made showed weak to no inhibition of 6TP towards UDPGDH with a K_i of 288 μM. However, 6TU, has increased inhibition towards UDPGDH with K_i of 7 μM. Inhibition was also observed with 6TXand 8-OH-6TP with K_i values 54 and 14 μM, respectively. To prevent the purines interference comes with UV-Vis method, the inhibition studies were carried out using a HPLC method that was developed and validated to separate all the analytes in the UDPGDH catalyzed reaction. Inhibition studies were performed via the HPLC method showed K_i values of 105 μM and 5 μM for 6TP and 6TU, respectively, towards UDPGDH.

To assess the inhibition studies towards the UGT enzyme, a HPLC method was developed for the simultaneous determination of bilirubin and its mono/diglucuronides. The inhibition studies were carried to assess the formation of glucuronides and consumption of UDPGA in the presence of the inhibitors using the HPLC method developed. Neither 6TP or 6TU were shown to inhibit UGT. In addition, inhibition studies were carried out in *in vivo* animal model that further confirmed that 6TP and 6TU do inhibit UDPGDH, but no effect on UGT activity. With these observations, we discovered that UDPGDH is inhibited by both 6TP and its oxidative metabolites. Furthermore, we can conclude that the C2 and C8 positions of 6TP are important for the associated of 6TP administration.

In the aim of developing a single method that analyze combined enzymatic system, another HPLC method was developed to assess the UDPGDH and UGT catalyze reactions together. This method also can be used as a common method to assess interference of any molecule on bilirubin excretion. Given the findings through SAR, efforts are being directed towards the synthesis of 8-substituted 6TP analogs. By blocking C8 position of 6TP, it can prevent the oxidation at C8. Therefore, it is expected that 6TP will greatly reduce its toxicities while retaining its therapeutic activity.

Final Notes:

Buffer A (imidazole and TBAHS) and methanol, acetonitrile was filtered through 0.2 μM nylon membranes prior to use it in HPLC. Before starting a HPLC run, first valve B was maintained with 80% methanol and valve A was maintained at 20% buffer A. Once the bottles were filled with solvents the entire HPLC system was purged. Then concentrations of methanol, buffer, or acetonitrile were adjusted according to the method and left the system in this stage for another 20 minutes until column get equilibrated before running the samples. When changing the HPLC system from methanol to acetonitrile, the system was equilibrated at 100% methanol concentration about 20 minutes and slowly switched it to 100% acetonitrile using the method gradient "100MeOH to 100MeCN". HPLC methods file used for analysis of UDPGDH, UGT and bi-enzymatic system are as followed. 1) CWI-106-method gradient 39, 2) CWI-300-method gradient 8, 3) CWI-353-combined 2. After each HPLC batch runs column was washed with 80% methanol with 20% water at 0.3 mL/min flow rate over night. Shorter column washes can cause building up column pressure.

To obtain ***N*-Para-methoxybenzyl-6-chloropurine (29)** K_2CO_3 was suspended in stirred solution of 6-choloropurine in DMF. To this was added 4-methoxy benzyl chloride. After 20 hours, reaction was quenched with 2 equivalents of water and extracted with ethyl acetate. The organic layer was dried over sodium sulfate and concentrated under reduced pressure. The remaining DMF was evaporated under vacuum overnight before running the column.

To obtain ***N*-Para-methyoxybenzyl-8-bromo-6-chloropurine (30)** addition of *n*-BuLi, compound 29 in THF, and dibromotrichlormethane should be done over 15-minute period slowly. The reaction was quenched with the addition of saturated ammonium chloride and was extracted with CH_2Cl_2 three times. The combined organic layers washed with brine, dried over anhydrous

sodium sulfate, concentrated, and the crude material was purified via flash silica gel chromatography (1:2 hexane:EtOAc).

To obtain ***N*-Para-methyoxybenzyl-8-bromo-6-thiopurine (32)**, compound **30**, thiourea, and acetonitrile and brought to reflux for 2 h. The solvent was removed to afford the thiourea purine (**31**), which was used without further purification. Ethanol was added to **31** and refluxed for 2 h. The reaction mixture was allowed to cool and was filtered to obtain a yellow precipitate, which was recrystallized with water to obtain pure **32**.

To obtain **8-Bromo-6-thiopurine (33),** PhMe and **32** and allowed to stir until the material dissolved and concentrated sulfuric acid was added and left to stir. After 2 h dark red oily solution will form and the PhMe was decanted from the mixture. Then diethyl ether was added and left to stir, which result in yellow precipitate. The precipitate filtered off and then dissolved in water. It was allowed to sit (2-3 h) that resulted in the formation of yellow crystals. These crystals were then recrystallized with methanol to afford the desired product.

Chapter 6 - **References**

1. American Cancer Society Acute Lyphocytic Leukemia. www.cancer.org (accessed 4 Feb).

2. Jabbour, E. J.; Faderl, S.; Kantarjian, H. M., Adult Acute Lymphoblastic Leukemia. *Mayo Clinic Proceedings* *80* (11), 1517-1527.

3. Fielding, A. K., Current treatment of Philadelphia chromosome-positive acute lymphoblastic leukemia. *Haematologica* **2010,** *95* (1), 8-12.

4. Tasian, S. K.; Loh, M. L.; Hunger, S. P., Philadelphia chromosome-like acute lymphoblastic leukemia. *Blood* **2017**.

5. Leoni, V.; Biondi, A., Tyrosine kinase inhibitors in BCR-ABL positive acute lymphoblastic leukemia. *Haematologica* **2015,** *100* (3), 295-299.

6. Ohanian, M.; Cortes, J.; Kantarjian, H.; Jabbour, E., Tyrosine kinase inhibitors in acute and chronic leukemias. *Expert Opinion on Pharmacotherapy* **2012,** *13* (7), 927-938.

7. Faderl, S.; O'Brien, S.; Pui, C.-H.; Stock, W.; Wetzler, M.; Hoelzer, D.; Kantarjian, H. M., Adult Acute Lymphoblastic Leukemia: Concepts and Strategies. *Cancer* **2010,** *116* (5), 1165-1176.

8. Kantarjian, H.; Thomas, D.; Jorgensen, J.; Kebriaei, P.; Jabbour, E.; Rytting, M.; York, S.; Ravandi, F.; Garris, R.; Kwari, M.; Faderl, S.; Cortes, J.; Champlin, R.; O'Brien, S., Results of Inotuzumab Ozogamicin, a CD22 Monoclonal Antibody in Refractory and Relapsed Acute Lymphocytic Leukemia. *Cancer* **2013,** *119* (15), 2728-2736.

9. Rowe, J. M.; Buck, G.; Burnett, A. K.; Chopra, R.; Wiernik, P. H.; Richards, S. M.; Lazarus, H. M.; Franklin, I. M.; Litzow, M. R.; Ciobanu, N.; Prentice, H. G.; Durrant, J.; Tallman, M. S.; Goldstone, A. H., Induction therapy for adults with acute lymphoblastic leukemia: results of more than 1500 patients from the international ALL trial: MRC UKALL XII/ECOG E2993. *Blood* **2005,** *106* (12), 3760-3767.

10. Puhalla, S.; Elmquist, W.; Freyer, D.; Kleinberg, L.; Adkins, C.; Lockman, P.; McGregor, J.; Muldoon, L.; Nesbit, G.; Peereboom, D.; Smith, Q.; Walker, S.; Neuwelt, E., Unsanctifying the sanctuary: challenges and opportunities with brain metastases. *Neuro-Oncology* **2015,** *17* (5), 639-651.

11. Gnekow, A. K.; Kortmann, R. D.; Pietsch, T.; Emser, A., Low Grade Chiasmatic-Hypothalamic Glioma - Carboplatin and Vincristin Chemotherapy Effectively Defers Radiotherapy within a Comprehensive Treatment Strategy. *Klin Padiatr* **2004,** *216* (06), 331-342.

12. Harmon, J. M.; Norman, M. R.; Fowlkes, B. J.; Thompson, E. B., Dexamethasone induces irreversible G1 arrest and death of a human lymphoid cell line. *Journal of Cellular Physiology* **1979,** *98* (2), 267-278.

13. Wheeler, G. E., CYclophosphamide-associated leukemia in wegener's granulomatosis. *Annals of Internal Medicine* **1981,** *94* (3), 361-362.

14. Verdier, E.; Carvalho, P.; Young, P.; Musette, P.; Courville, P.; Joly, P., Lymphangiosarcome traité par doxorubicine liposomale (Caelyx®). *Annales de Dermatologie et de Vénéréologie* **2007,** *134* (10, Part 1), 760-763.

15. Pieters, R.; Hunger, S. P.; Boos, J.; Rizzari, C.; Silverman, L.; Baruchel, A.; Goekbuget, N.; Schrappe, M.; Pui, C.-H., L-asparaginase treatment in acute lymphoblastic leukemia: a focus on Erwinia asparaginase. *Cancer* **2011,** *117* (2), 238-249.

16. Malagola, M.; Papayannidis, C.; Baccarani, M., Tyrosine kinase inhibitors in Ph+ acute lymphoblastic leukaemia: facts and perspectives. *Annals of Hematology* **2016,** *95* (5), 681-693.

17. Berkovitch, M.; Matsui, D.; Zipursky, A.; Blanchette, V. S.; Verjee, Z.; Giesbrecht, E.; Saunders, E. F.; Evans, W. E.; Koren, G., Hepatotoxicity of 6-mercaptopurine in childhood acute lymphocytic leukemia: Pharmacokinetic characteristics. *Medical and Pediatric Oncology* **1996,** *26* (2), 85-89.

18. Yang, X.-G.; Bao, Y.-L.; Huang, Y.-X.; Sun, L.-G.; Zhang, Y.-W.; Yu, C.-L.; Wu, Y.; Li, Y.-X., 6-[(1-naphthylmethyl)sulfanyl]-9H-purine induces G2/M phase arrest and apoptosis in human hepatocellular carcinoma HepG2 cells. *European Journal of Pharmacology* **2012,** *695* (1), 27-33.

19. Fujii, T., Ogawa, Kazuo,Itaya, Taisuke; Date, T.; Inagaki, J.-i.; Nohara, F., Purines. LXX. An Extension of the "Phenacylamine Route" to the Syntheses of the 7-N-Oxides of 6-Mercaptopurine and 6-Methylthiopurine, and Antileukemic Activity of Some Purine N-Oxides. *CHEMICAL & PHARMACEUTICAL BULLETIN* **1995,** *43* (3), 408-413.

20. Dervieux, T.; Blanco, J. G.; Krynetski, E. Y.; Vanin, E. F.; Roussel, M. F.; Relling, M. V., Differing Contribution of Thiopurine Methyltransferase to Mercaptopurine: Thioguanine Effects in Human Leukemic Cells. *Cancer Research* **2001,** *61* (15), 5810-5816.

21. Rowland, K.; Lennard, L.; Lilleyman, J. S., In vitro metabolism of 6-mercaptopurine by human liver cytosol. *Xenobiotica* **1999,** *29* (6), 615-628.

22. Clarke, D. A.; Philips, F. S.; Sternberg, S. S.; Stock, C. C., Effects of 6-mercaptopurine and analaogs on experimental tumors. *Annals of the New York Academy of Sciences* **1954,** *60* (2), 235-243.

23. Nelson, J. A.; Carpenter, J. W.; Rose, L. M.; Adamson, D. J., Mechanisms of Action of 6-Thioguanine, 6-Mercaptopurine, and 8-Azaguanine. *Cancer Research* **1975,** *35* (10), 2872-2878.

24. Haglund, S.; Taipalensuu, J.; Peterson, C.; Almer, S., IMPDH activity in thiopurine-treated patients with inflammatory bowel disease – relation to TPMT activity and metabolite concentrations. *British Journal of Clinical Pharmacology* **2008,** *65* (1), 69-77.

25. Tidd, D. M.; Paterson, A. R. P., A Biochemical Mechanism for the Delayed Cytotoxic Reaction of 6-Mercaptopurine. *Cancer Research* **1974,** *34* (4), 738-746.

26. Yan, T.; Berry, S. E.; Desai, A. B.; Kinsella, T. J., DNA Mismatch Repair (MMR) Mediates 6-Thioguanine Genotoxicity by Introducing Single-strand Breaks to Signal a G₂-M Arrest in MMR-proficient RKO Cells. *Clinical Cancer Research* **2003,** *9* (6), 2327-2334.

27. Karran, P.; Attard, N., Thiopurines in current medical practice: molecular mechanisms and contributions to therapy-related cancer. *Nat Rev Cancer* **2008,** *8* (1), 24-36.

28. Chouchana, L.; Fernández-Ramos, A. A.; Dumont, F.; Marchetti, C.; Ceballos-Picot, I.; Beaune, P.; Gurwitz, D.; Loriot, M.-A., Molecular insight into thiopurine resistance: transcriptomic signature in lymphoblastoid cell lines. *Genome Medicine* **2015,** *7* (1), 37.

29. Dervieux, T.; Brenner, T. L.; Hon, Y. Y.; Zhou, Y.; Hancock, M. L.; Sandlund, J. T.; Rivera, G. K.; Ribeiro, R. C.; Boyett, J. M.; Pui, C.-H.; Relling, M. V.; Evans, W. E., De novo purine synthesis inhibition and antileukemic effects of mercaptopurine alone or in combination with methotrexate in vivo. *Blood* **2002,** *100* (4), 1240-1247.

30. Carethers, J. M.; Hawn, M. T.; Chauhan, D. P.; Luce, M. C.; Marra, G.; Koi, M.; Boland, C. R., Competency in mismatch repair prohibits clonal expansion of cancer cells treated with N-methyl-N'-nitro-N-nitrosoguanidine. *Journal of Clinical Investigation* **1996,** *98* (1), 199-206.

31. Pacher, P.; Nivorozhkin, A.; Szabó, C., Therapeutic Effects of Xanthine Oxidase Inhibitors: Renaissance Half a Century after the Discovery of Allopurinol. *Pharmacological Reviews* **2006,** *58* (1), 87-114.

32. Hitchings, G. H.; Elion, G. B., Chemical suppresion of the immune response. *Pharmacological Reviews* **1963,** *15* (2), 365-405.

33. McLeod, H. L.; Krynetski, E. Y.; Relling, M. V.; Evans, W. E., Genetic polymorphism of thiopurine methyltransferase and its clinical relevance for childhood acute lymphoblastic leukemia. *Leukemia* **2000,** *14*, 567.

34. McCarthy, J. J.; Hilfiker, R., The use of single-nucleotide polymorphism maps in pharmacogenomics. *Nature Biotechnology* **2000,** *18*, 505.

35. SAHLIN, K.; BROBERG, S.; REN, J. M., Formation of inosine monophosphate (IMP) in human skeletal muscle during incremental dynamic exercise. *Acta Physiologica Scandinavica* **1989,** *136* (2), 193-198.

36. Peng, X.-X.; Shi, Z.; Damaraju, V. L.; Huang, X.-C.; Kruh, G. D.; Wu, H.-C.; Zhou, Y.; Tiwari, A.; Fu, L.; Cass, C. E.; Chen, Z.-S., Up-regulation of MRP4 and down-regulation of influx transporters in human leukemic cells with acquired resistance to 6-mercaptopurine. *Leukemia Research 32* (5), 799-809.

37. Kontorinis, N.; Agarwal, K.; Gondolesi, G.; Fiel, M. I.; O'Rourke, M.; Schiano, T. D., Diagnosis of 6 Mercaptopurine Hepatotoxicity Post Liver Transplantation Utilizing Metabolite Assays. *American Journal of Transplantation* **2004,** *4* (9), 1539-1542.

38. Present, D. H.; Meltzer, S. J.; Krumholz, M. P.; Wolke, A.; Korelitz, B. I., 6-mercaptopurine in the management of inflammatory bowel disease: Short- and long-term toxicity. *Annals of Internal Medicine* **1989,** *111* (8), 641-649.

39. Shorey, J.; Schenker, S.; Suki, W. N.; Combes, B., Hepatotoxicity of mercaptopurine. *Archives of Internal Medicine* **1968,** *122* (1), 54-58.

40. Björnsson, E. S.; Gu, J.; Kleiner, D. E.; Chalasani, N.; Hayashi, P. H.; Hoofnagle, J. H., Azathioprine and 6-Mercaptopurine Induced Liver Injury: Clinical Features and Outcomes. *Journal of clinical gastroenterology* **2017,** *51* (1), 63-69.

41. Wang, X.; Chowdhury, J. R.; Chowdhury, N. R., Bilirubin metabolism: Applied physiology. *Current Paediatrics* **2006,** *16* (1), 70-74.

42. Berk, P. D.; Howe, R. B.; Bloomer, J. R.; Berlin, N. I., Studies of bilirubin kinetics in normal adults. *Journal of Clinical Investigation* **1969,** *48* (11), 2176-2190.

43. Lauff, J. J.; Kasper, M. E.; Ambrose, R. T., Quantitative liquid-chromatographic estimation of bilirubin species in pathological serum. *Clinical Chemistry* **1983,** *29* (5), 800-805.

44. Ma, G.; Lin, J.; Cai, W.; Tan, B.; Xiang, X.; Zhang, Y.; Zhang, P., Simultaneous determination of bilirubin and its glucuronides in liver microsomes and recombinant UGT1A1 enzyme incubation systems by HPLC method and its application to bilirubin glucuronidation studies. *Journal of Pharmaceutical and Biomedical Analysis* **2014,** *92*, 149-159.

45. Egger, S.; Chaikuad, A.; Kavanagh, Kathryn L.; Oppermann, U.; Nidetzky, B., UDP-glucose dehydrogenase: structure and function of a potential drug target. *Biochemical Society Transactions* **2010,** *38* (5), 1378-1385.

46. Linster, C. L.; Schaftingen, E. V., Vitamin C. *The FEBS Journal* **2007,** *274* (1), 1-22.

47. Conway, J. G.; Kauffman, F. C.; Tsukuda, T.; Thurman, R. G., Glucuronidation of 7-hydroxycoumarin in periportal and pericentral regions of the lobule in livers from untreated and 3-methylcholanthrene-treated rats. *Molecular Pharmacology* **1988,** *33* (1), 111-119.

48. Reinke, L. A.; Belinsky, S. A.; Evans, R. K.; Kauffman, F. C.; Thurman, R. G., Conjugation of p-nitrophenol in the perfused rat liver: the effect of substrate concentration and carbohydrate reserves. *Journal of Pharmacology and Experimental Therapeutics* **1981,** *217* (3), 863-870.

49. Ma, G. L., Jiayuan.Cai, Weimin.Tan, Bo.Xiang, Xiaoqiang.Zhang, Ying.Zhang, Peng, Simultaneous determination of bilirubin and its glucuronides in liver microsomes and recombinant UGT1A1 enzyme incubation systems by HPLC method and its application to bilirubin glucuronidation studies. *Journal of Pharmaceutical and Biomedical Analysis* **2014,** *92*, 149-159.

50. Zhang, D.; Chando, T. J.; Everett, D. W.; Patten, C. J.; Dehal, S. S.; Humphreys, W. G., In vitro inhibition of UDP glucuronosyltransferase by atazanavir and other HIV protease inhibitors and the relationship of this property to in vivo bilirubin glucuronidation. *Drug Metabolism and Disposition* **2005,** *33* (11), 1729-1739.

51. Zhou, J.; Tracy, T. S.; Remmel, R. P., Correlation between Bilirubin Glucuronidation and Estradiol-3-Gluronidation in the Presence of Model UDP-Glucuronosyltransferase 1A1 Substrates/Inhibitors. *Drug Metabolism and Disposition* **2011,** *39* (2), 322-329.

52. Bartlett, M. G.; Gourley, G. R., Assessment of UGT Polymorphisms and Neonatal Jaundice. *Seminars in Perinatology* **2011,** *35* (3), 127-133.

53. Ma, G.; Wu, B.; Gao, S.; Yang, Z.; Ma, Y.; Hu, M., Mutual Regioselective Inhibition of Human UGT1A1-Mediated Glucuronidation of Four Flavonoids. *Molecular Pharmaceutics* **2013,** *10* (8), 2891-2903.

54. Fevery, J., Bilirubin in clinical practice: a review. *Liver International* **2008,** *28* (5), 592-605.

55. Bosma, P. J.; Chowdhury, N. R.; Goldhoorn, B. G.; Hofker, M. H.; Elferink, R. P. J. O.; Jansen, P. L. M.; Chowdhury, J. R., Sequence of exons and the flanking regions of human bilirubin-UDP-glucuronosyltransferase gene complex and identification of a genetic mutation in a patient with Crigler-Najjar syndrome, type I. *Hepatology* **1992,** *15* (5), 941-947.

56. Van Steenbergen, W.; Fevery, J.; De Groote, J., Thyroid hormones and the hepatic handling of bilirubin: II. Effects of hypothyroidism and hyperthyroidism on the apparent maximal biliary secretion of bilirubin in the Wistar rat. *Journal of Hepatology* **1988,** *7* (2), 229-238.

57. Rayner, H. L.; Schacter, B. A.; Israels, L. G., Effects of Drugs on Bilirubin Metabolism. In *Heme and Hemoproteins*, De Matteis, F.; Aldridge, W. N., Eds. Springer Berlin Heidelberg: Berlin, Heidelberg, 1978; pp 273-332.

58. Lankisch, T. O.; Moebius, U.; Wehmeier, M.; Behrens, G.; Manns, M. P.; Schmidt, R. E.; Strassburg, C. P., Gilbert's disease and atazanavir: From phenotype to UDP-glucuronosyltransferase haplotype. *Hepatology* **2006,** *44* (5), 1324-1332.

59. Ah, Y.-M.; Kim, Y.-M.; Kim, M.-J.; Choi, Y. H.; Park, K.-H.; Son, I.-J.; Kim, S. G., Drug-induced Hyperbilirubinemia and the Clinical Influencing Factors. *Drug Metabolism Reviews* **2008,** *40* (4), 511-537.

60. Hjelle, J. J., Hepatic UDP-glucuronic acid regulation during acetaminophen biotransformation in rats. *Journal of Pharmacology and Experimental Therapeutics* **1986,** *237* (3), 750-756.

61. Reen, R. K.; Jamwal, D. S.; Taneja, S. C.; Koul, J. L.; Dubey, R. K.; Wiebel, F. J.; Singh, J., Impairment of UDP-glucose dehydrogenase and glucuronidation activities in liver and small intestine of rat and guinea pig in vitro by piperine. *Biochemical Pharmacology* **1993,** *46* (2), 229-238.

62. Elion, G. B.; Burgi, E.; Hitchings, G. H., Studies on Condensed Pyrimidine Systems. IX. The Synthesis of Some 6-Substituted Purines. *Journal of the American Chemical Society* **1952,** *74* (2), 411-414.

63. Sariri, R.; Khalili, G., Synthesis of Purine Antiviral Agents, Hypoxanthine and 6-Mercaptopurine. *Russian Journal of Organic Chemistry* **2002,** *38* (7), 1053-1055.

64. Yu-qin, M.; Xing, Y.; Rong, D.; Xiao-guang, Y.; Yu-xin, L.; Ying, G.; Wen-liang, L., Synthesis, Anti-cancer Activity and Mechanism Study of 6-Mercapto-purine Derivatives. *Letters in Drug Design & Discovery* **2016,** *13* (6), 570-576.

65. Lewis, L. R.; Noell, C. W.; Beaman, A. G.; Robins, R. K., The Preparation and Antitumor Activity of Certain Derivatives of 6-Mercaptopurine. *Journal of Medicinal and Pharmaceutical Chemistry* **1962,** *5* (3), 607-617.

66. Koppel, H. C.; Robins, R. K., Potential Purine Antagonists. XIII. Synthesis of Some 8-Methylpurines1. *The Journal of Organic Chemistry* **1958,** *23* (10), 1457-1460.

67. Singh, J.; Schwarz, L. R.; Wiebel, F. J., A rapid enzymic procedure for the determination of picomole amounts of UDP-glucuronic acid. *Biochemical Journal* **1980,** *189* (2), 369-372.

68. Burrows, R. B.; Cintron, C., A microassay for UDP-glucose dehydrogenase. *Analytical Biochemistry* **1983,** *130* (2), 376-378.

69. Gainey, P. A.; Phelps, C. F., Interactions of urdine diphosphate glucose dehydrogenase with the inhibitor urdine diphosphate xylose. *Biochemical Journal* **1975,** *145* (2), 129-134.

70. Grubb, M. F.; Kasofsky, J.; Strong, J.; Anderson, L. W.; Cysyk, R. L., Serum stimulation of UDP-glucose dehydrogenase activity in Swiss 3T3 fibroblasts. *Biochem Mol Biol Int* **1993,** *30* (5), 819-827.

Appendix A - Supplemental

1. Information on Lineweaver-Burk curves Shown in Figure 4-1 & 4-3 with respect to UDP-glucose Saturation

Curve (UDPG saturation)	Equation	R^2
No 6TP	Y = 0.580*X + 3.348	0.9947
50 μM 6TP	Y = 0.674*X + 3.473	0.9986
100 μM 6TP	Y = 0.760*X + 3.633	0.9973
No 6TU	Y = 0.614*X + 4.536	0.9729
5 μM 6TU	Y = 0.685*X + 5.033	0.998
10 μM 6TU	Y = 0.765*X + 5.693	0.9734
No 6TX	Y = 25.63*X - 0.613	0.9963
20 μM 6TX	Y = 32.54*X + 34.96	0.9999
50 μM 6TX	Y = 43.54*X + 80.04	0.9997
No 8-OH 6TP	Y = 14.54*X + 24.08	0.9999
20 μM 8-OH-6TP	Y = 18.12*X + 29.88	0.9991
50 μM 8-OH-6TP	Y = 33.81*X + 80.85	0.9899

2. Information on Lineweaver-Burk curves Shown in Figure 4-1 & 4-3 with respect to NAD^+ Saturation

Curve (NAD^+ Saturation)	Equation	R^2
No 6TP	Y= 0.121*X+ 2.27	0.9879
50 μM 6TP	Y= 0.135*X+ 2.61	0.9961
100 μM 6TP	Y= 0.162*X+ 3.68	1
No 6TU	Y= 0.103*X+ 4.73	0.9798
5 μM 6TU	Y= 0.198*X+ 5.26	0.9732
10 μM 6TU	Y= 0.256*X+ 5.89	0.9853
No 6TX	Y= 0.117*X+ 4.93	0.9990
20 μM 6TX	Y= 0.152*X+ 6.18	0.9987
50 μM 6TX	Y= 0.222*X+ 10.7	0.9958
No 8-OH-6TP	Y= 0.936*X+ 22.5	0.9952
20 μM 8-OH-6TP	Y= 1.368*X+ 27.9	0.9984
50 μM 8-OH-6TP	Y= 3.422*X+ 54.2	0.9975

3. Gradient Profiles Tried for UDPGDH HPLC Method, Detection at 262 nm, Flow Rate 0.5 mL/min with an Imidazole/TBAHS Aqueous Phase and Methanol as Organic Phase

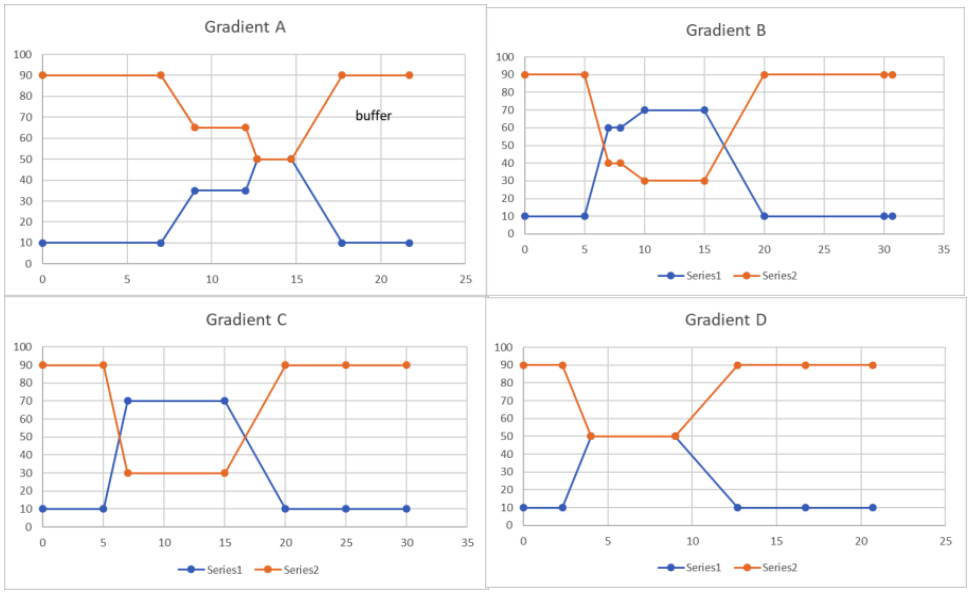

Buffer A *Methanol*

4. Summary Inhibition Curves Shown in Figure 4-11 & 4-12 with respect to NAD^+ Saturation

Curve (NAD^+ Saturation)	Equation	R^2
No 6TP	Y= 0.00003*X+ 0.008167	0.8301
50 μM 6TP	Y= 0.00005*X+ 0.009306	0.9349
100 μM 6TP	Y= 0.00006*X+ 0.009683	0.8683
No 6TU	Y= 0.00001*X+0.0067	0.848
5 μM 6TU	Y= 0.00002*X+ 0.0081	0.921
15 μM 6TU	Y= 0.00004*X+ 0.0096	0.883

5. Information on Lineweaver-Burk curves Shown in Figure 4-11 with respect to NAD^+ Saturation

1/[UDPG]	6TP Concentration μM		
	100	50	0
10	0.01003 ±0.0001	0.00954 ±0.0007	0.00809±0.0002
20	0.01150± 0.00002	0.01053± 0.00002	0.00882± 0.00031
40	0.01139± 0.0001	0.0115± 0.00002	0.00941± 0.00031
50	0.01258± 0.0004	0.01135± 0.0002	0.00941± 0.00041

6. Information on Lineweaver-Burk curves Shown in Figure 4-12 with respect to NAD^+ Saturation

1/[UDPG]	6TU Concentration µM		
	10	5	0
10	0.01162 ±0.001	0.00938 ± 0.0006	0.00734 ±0.00013
20	0.01164± 0.0003	0.00913±0.00041	0.00718± 0.0001
40	0.01045± 0.0007	0.00883± 0.0004	0.00712± 0.0001
50	0.01003± 0.0009	0.00823± 0.0005	0.0068± 0.0001

7. Gradient Profiles Tried for UGT HPLC Method, Detection at 450 nm, Flow Rate 0.5 mL/min with an Imidazole/TBAHS Aqueous Phase and Acetonitrile

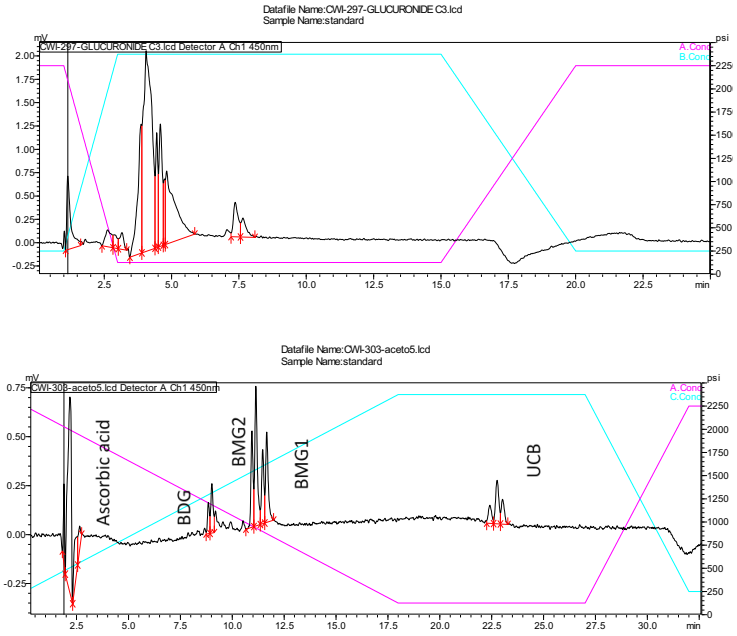

8. Inhibition Assessment of UGT1A1 with regards to Varying 6TP and 6TU Concentrations. Each data set was run in triplicate with standard deviation values given in parentheticals

Bilirubin Species	Control	50 μM 6TP	75 μM 6TP	50 μM 6TU	75 μM 6TU
UCB	3.72 μM (±0.38)	3.17 μM (±0.46)	4.35 μM (±0.87)	3.05 μM (±0.77)	3.49 μM (±0.54)
BMG1	1.82 μM (±0.04)	1.70 μM (± 0.14)	1.72 μM (± 0.34)	1.85 μM (± 0.21)	2.09 μM (± 0.03)
BMG2	4.24 μM (±0.34)	4.05 μM (±0.07)	4.61 μM (±0.86)	4.40 μM (±0.56)	5.21 μM (±0.30)
BDG	0.23 μM (±0.02)	0.23 μM (±0.13)	0.17 μM (±0..19)	0.19 μM (±0.23)	0.32 μM (±0.28)

9. Inhibition Assessment of UGT1A1 with regards to Varying 6TP and 6TU Concentrations as Quantified by UDPGA Consumption. Each data set was run in triplicate with standard deviation values given in parentheticals

	Duration of the Reaction		
	1-hour	**12-hour**	**15-hour**
UDPGA Control	241 μM (± 5.6)	110 μM (± 0.06)	17 μM (± 4.9)
RxN No Enzyme	252 μM (± 5.6)	243 μM (± 0.07)	253 μM (± 5.6)
Full RxN	251 μM (± 5.2)	245 μM (± 0.21)	252 μM (± 4.2)
75 μM 6TP	242 μM (± 3.4)	128 μM (± 3.08)	20 μM (± 3.5)
75 μM 6TU	241 μM (± 7.5)	125 μM (± 0.05)	16 μM (± 4.2)
50 μM 6TP	241 μM (± 1.7)	130 μM (± 0.05)	20 μM (± 2.1)
50 μM 6TU	243 μM (± 5.1)	128 μM (± 2.16)	20 μM (± 0.7)

10. Overall Effects of 1:2200 Ratio of UDPGDH: UGT with regards to UDPGA Levels and BMG and BDG Formation with UDPGDH Inhbitors

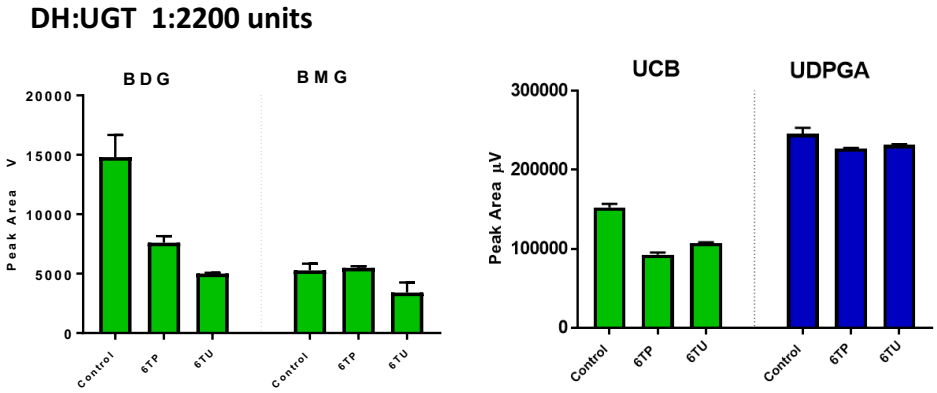

DH:UGT 1:2200 units	BDG	BMG	UCB	UDPGA
control	14801±1866	5604±710	152669±4399	245577±7824
6TP	7606±544	5485±140	92550±2810	227434±551
6TU	5008±62	3412±842	107482±936	231910±834

11. Information on Overall Effects of 1:440 Ratio of UDPGDH (Figure 4-22): UGT with regards to UDPGA Levels and BMG and BDG Formation with UDPGDH Inhibitors

DH:UGT 1:440 units	BDG	BMG	UCB	UDPGA
control	23730±517	6774±415	67398±1346	75204±1869
6TP	9257±626	10956±848	60482±455	293126±314
6TU	5578±217	7833±542	61860±776	285177±583

12. Overall Effects of 1:440 ratio of UDPGDH: UGT with regards to UDPGA Levels and BMG and BDG Formation with UGT Inhbitors

DH:UGT 1:440 units

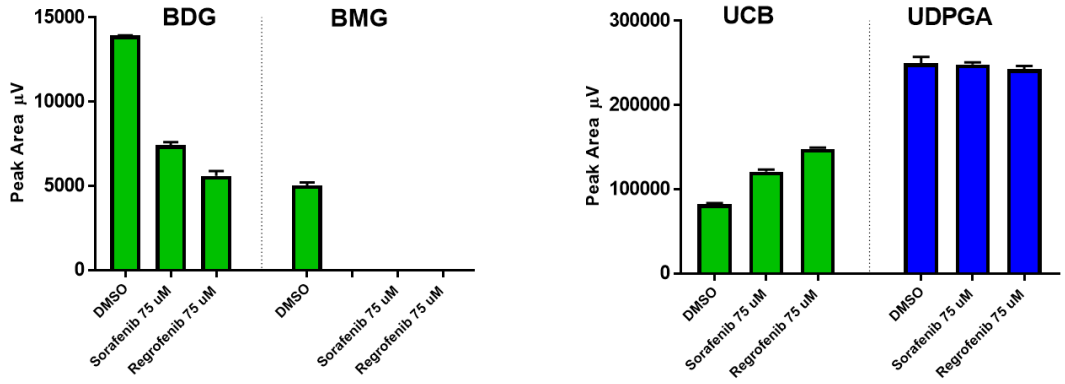

13. Information on Overall Effects of 1:440 ratio of UDPGDH: UGT with regards to UDPGA Levels and BMG and BDG Formation with UGT Inhibitors

DH:UGT 1:440 units	BDG	BMG	UCB	UDPGA
DMSO	13396±565	5032±175	83086±325	249518±7798
Sorafenib	7428±175	0±0	148031±1537	270444±38268
Regorafenib	5913±586	0±0	120883±2546	242623±583

14. Information on Inhibitor Assessment of known UGT Inhibitors Sorafenib and Regorafenib towards UGT and UDPGDH (Figure 4-19)

UGT	BMG+BDG
Control	**84112±2430**
DMSO	**60418±1126**
Sorafenib	**6813±723**
Regorafenib	**2648±275**

15. Information on Hepatocyte studies with both high (50 and 10 µM) and low (25 and 5 µM) for 6TP and 6TU, respectively (Figure 4-23)

	Control	[6TP]-low	[6TP]-high	[6TU]-low	[6TU]-high	UDPGA+[6TU] high	[UGT] Inhibitor	[UDPGA] +inhibitor
UCB	0.61	0.73	0.77	0.8	0.87	0.57	0.86	0.83
BMG	1	0.81	0.72	0.29	0.19	0.94	0.11	0.13
BDG	0.5	0.44	0.37	0.12	0.07	0.49	0.02	0.03

16. Synthesis of *N*-Para-methoxybenzyl-6-chloropurine (29) & NMR

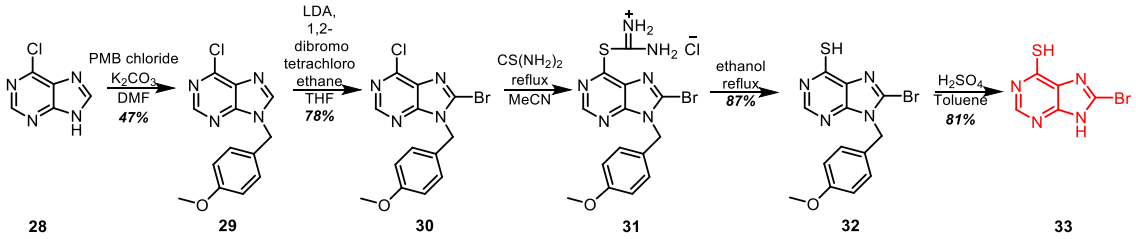

***N*-Para-methoxybenzyl-6-chloropurine (29):** To a round bottom flask (RBF) was added 6-chloropurine (**28**, 1g, 6.46 mmol) and left to stir until it dissolved at which time potassium carbonate (1.78 g, 12.9 mmol) and p-methoxybenzyl chloride was added. The reaction mixture was allowed to stir for 20 h at which time it was quenched with the addition of water (2 volume equivalents) and the mixture was extracted with ethyl acetate (x3). The organic layers were combined, dried over anhydrous sodium sulfate, concentrated, and the crude material was purified via flash silica gel chromatography (gradient 100% hexane to 1:15 hexane:EtOAc) to give 1.77 g of the desired product **29** in 47% yield. Isolation of the *N*7 protected 6-chloropurine was also achieved.

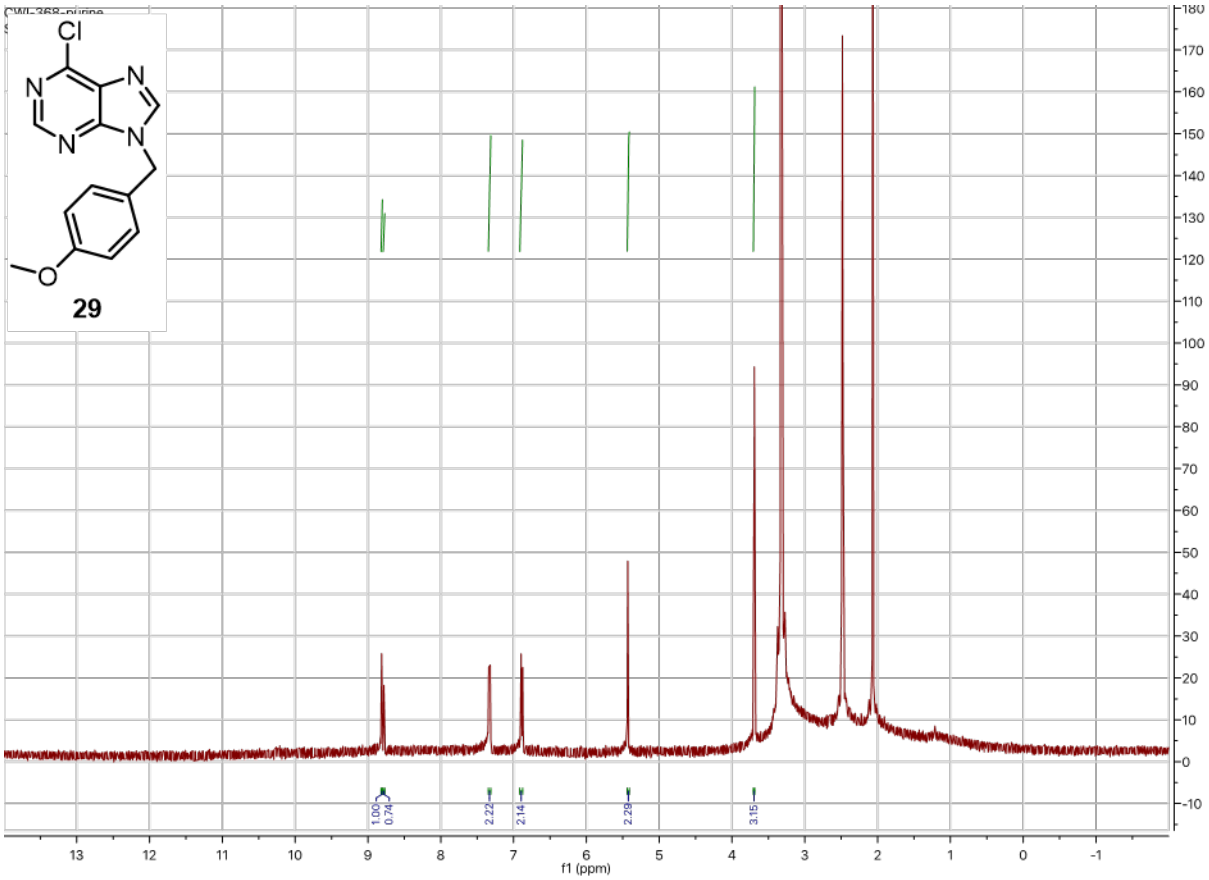

17. Synthesis of *N*-Para-methyoxybenzyl-8-bromo-6-chloropurine (30) & NMR

***N*-Para-methyoxybenzyl-8-bromo-6-chloropurine (30):** To a RBF charged with THF under an Argon atmosphere was added diisopropylamine (0.08 mL, 0.57 mmol) and the mixture was cooled to -78 °C at which time *n*-BuLi (1.5 M, 0.38 mL, 0.57 mmol) was added slowly and left to stir for 1 hour. Compound **29** (120 mg, 0.44 mmol) dissolved in THF (2 mL) was then added to the prepared LDA solution at -78 °C. After 1 h, dibromotrichlormethane (284 mg, 0.87 mmol) was added, and after 1 h the reaction was quenched with the addition of ammonium chloride and was extracted with CH_2Cl_2 (x3). The combined organic layers were combined, washed with brine, dried over anhydrous sodium sulfate, concentrated, and the crude material was purified via flash silica gel chromatography (1:2 hexane:EtOAc) to afford 120 mg of the desired product **30** in 78% yield.

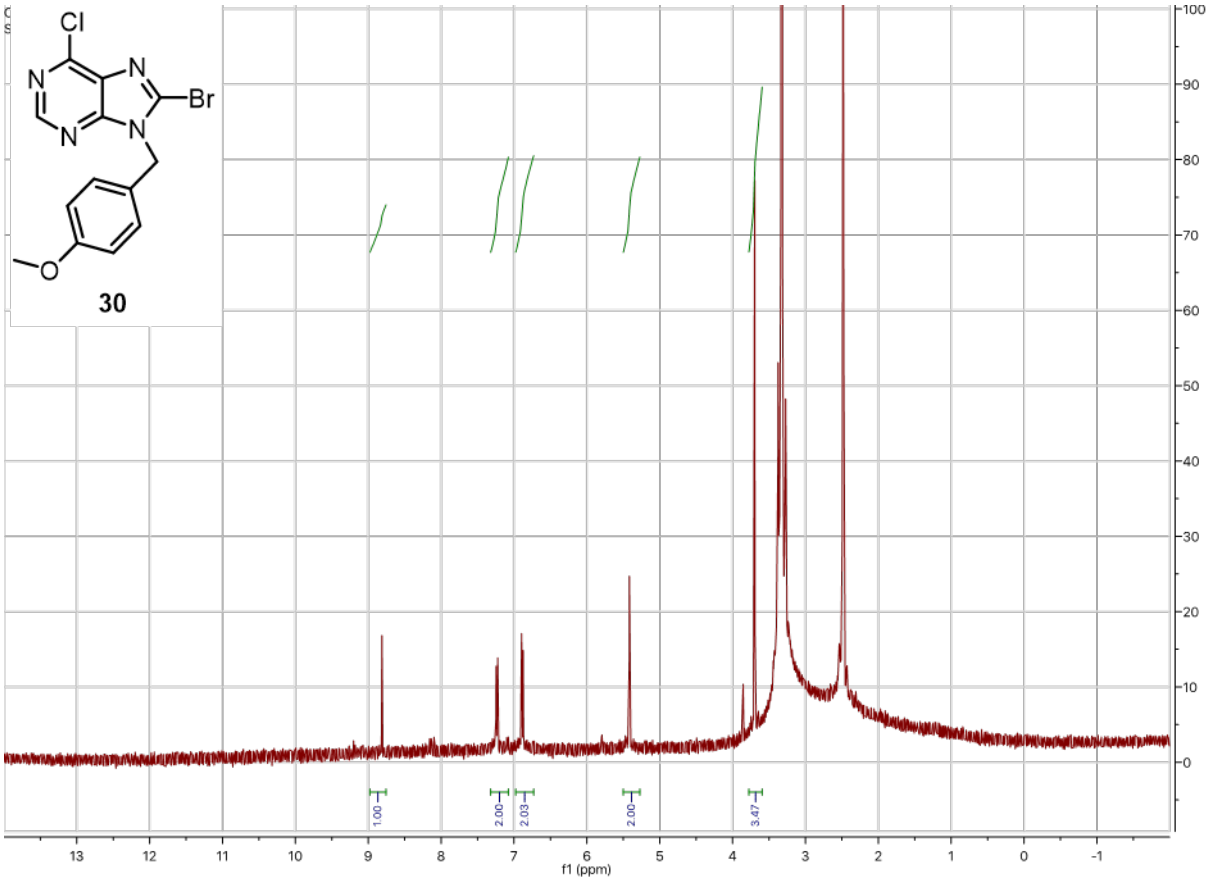

18. Synthesis of N-Para-methyoxybenzyl-8-bromo-6-thiopurine (32) & NMR

***N*-Para-methyoxybenzyl-8-bromo-6-thiopurine (32):** To a RBF was added **30** (170 mg, 0.39 mmol), thiourea (30 mg, 0.39 mmol), and acetonitrile (60 mL) and brought to reflux for 2 h. The solvent was removed to afford the thiourea purine (**31**), a species that was used without further purification. Ethanol (10 mL) was added to **31** and refluxed for 2 h. The reaction mixture was allowed to cool, which resulted in some of the desired compound recrystallizing from the solution that was removed via filtration. The addition of cold water resulted in a second recrystallization. Combining the material obtained from both filtrations gave 120 mg of the desired product **32** in 87% yield.

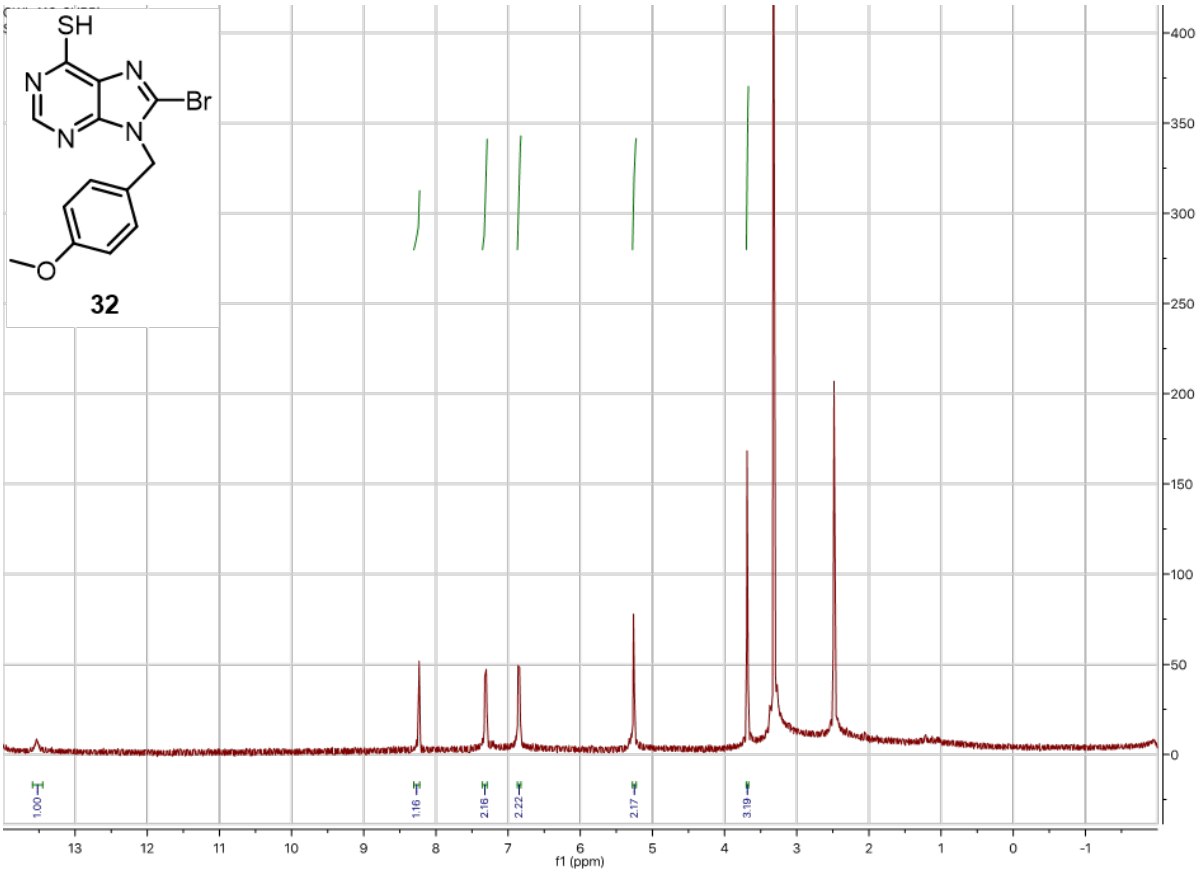

19. Synthesis of 8-Bromo-6-thiopurine (33) & NMR

8-Bromo-6-thiopurine (33): To a RBF was added PhMe (2 mL) and **32** (50 mg, 0.17 mmol) and allowed to stir until the material dissolved at which point concentrated sulfuric acid (18 µL) was added and left to stir. After 2 h the PhMe was decanted from the mixture and diethyl ether (4 mL) was added and left to stir. A precipitate forms, which was filtered off and then dissolved in water and allowed to sit (2-3 h) that resulted in the formation of crystals. These crystals were then recrystallized with methanol to afford 32 mg of the desired product in 81% yield.

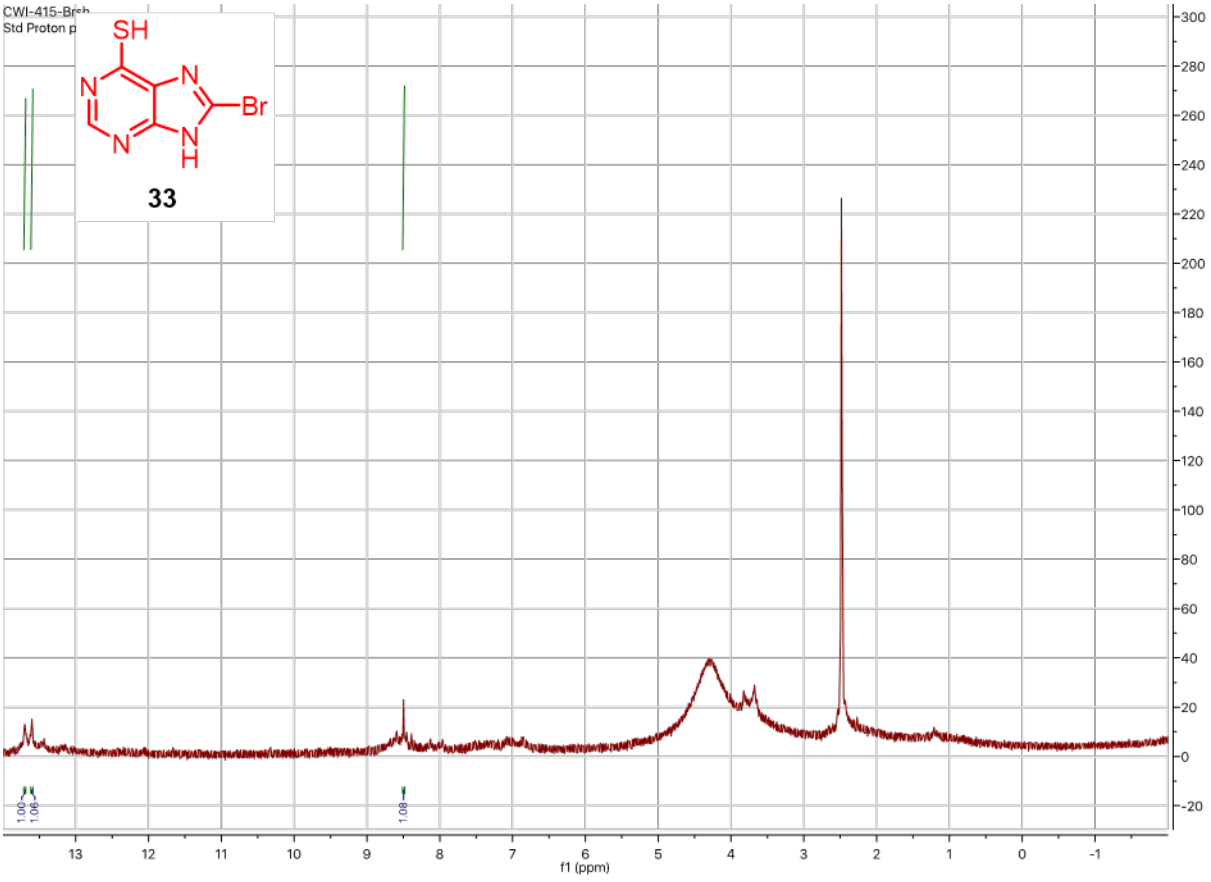

20. Statistical Calculations on Figure 4-18

Differences of trt Least Squares Means
Adjustment for Multiple Comparisons: Dunnett-Hsu

trt	_trt	Estimate	Standard Error	DF	t Value	Pr > |t|	Adj P	Alpha	Lower	Upper	Adj Lower	Adj Upper
									6		0	
756TP	control	1.3333	2.4060	8	0.55	0.5946	0.9449	0.05	-4.2149	6.8816	-5.9393	8.6060
756TU	control	0.6667	2.4060	8	0.28	0.7887	0.9953	0.05	-4.8816	6.2149	-6.6060	7.9393

Based on the analysis above, we use Dunnett adjustment. Since all adjusted P-values are larger than 0.05, we all fail to reject the Ho hypothesis. It further justifies our previous statement that there might be no difference among all of the treatment levels.

To complete the analysis, we provide interaction test for two treatments and comparisons between main effect with control:

Estimates

Label	Estimate	Standard Error	DF	t Value	Pr > |t|
50 vs control	1.5000	2.0837	8	0.72	0.4921
75 vs control	1.0000	2.0837	8	0.48	0.6441
6TP vs control	0.8333	2.0837	8	0.40	0.6997
6TU vs control	1.6667	2.0837	8	0.80	0.4469
Interaction test	-3.0000	3.4026	8	-0.88	0.4037

Since all adjusted P-values are larger than 0.05, we all fail to reject the Ho hypothesis. It indicates that there might be no interaction effect and no difference between main effects of treatments and control.

For 15 hour's design:

Type III Tests of Fixed Effects				
Effect	Num DF	Den DF	F Value	Pr > F
trt	4	4	2.79	0.1719

H0: there is no overall treatment effect
Ha: there is treatment effect

Since the P value for overall effect of trt is 0.1719>0.05, we fail to reject H0, which further means there might be no difference among all of the treatment levels. In order to answer the client's research question, we also have a look at the specific comparisons between treatment combinations and control (though theoretically speaking, it's not necessary since overall is not significant).

Table 2

Differences of trt Least Squares Means Adjustment for Multiple Comparisons: Dunnett-Hsu												
trt	_trt	Estimate	Standard Error	DF	t Value	Pr > |t|	Adj P	Alpha	Lower	Upper	Adj Lower	Adj Upper
506TP	control	4.0000	1.7029	4	2.35	0.0786	0.1974	0.05	-0.7281	8.7281	-2.5249	10.5249
506TU	control	3.0000	1.7029	4	1.76	0.1529	0.3595	0.05	-1.7281	7.7281	-3.5249	9.5249
756TP	control	3.0000	1.7029	4	1.76	0.1529	0.3595	0.05	-1.7281	7.7281	-3.5249	9.5249
756TU	control	-0.5000	1.7029	4	-0.29	0.7837	0.9932	0.05	-5.2281	4.2281	-7.0249	6.0249

Based on the analysis above, we use Dunnett adjustment. Since all adjusted P-values are larger than 0.05, we all fail to reject the Ho hypothesis. It further justifies our previous statement that there might be no difference among all of the treatment levels.

To complete the analysis, we provide interaction test for two treatments and comparisons between main effect with control:

Estimates

Label	Estimate	Standard Error	DF	t Value	Pr > |t|
50 vs control	3.5000	1.4748	4	2.37	0.0766
75 vs control	1.2500	1.4748	4	0.85	0.4444
6TP vs control	3.5000	1.4748	4	2.37	0.0766
6TU vs control	1.2500	1.4748	4	0.85	0.4444
Interaction test	-2.5000	2.4083	4	-1.04	0.3579

Since all adjusted P-values are larger than 0.05, we all fail to reject the Ho hypothesis. It indicates that there might be no interaction effect and no difference between main effects of treatments and control.

For 12 hours' design

Type III Tests of Fixed Effects

Effect	Num DF	Den DF	F Value	Pr > F
trt	4	5	0.29	0.8757

H0: there is no overall treatment effect
Ha: there is treatment effect

Since the P value for overall effect of trt is 0.8757>0.05, we cannot reject H0, which means there might be not significant difference among all of the treatment levels. In order to answer the client's research question, we also have a look at the specific comparisons between treatment combinations and control (though theoretically speaking, it's not necessary since overall is not significant)

Table 3

Differences of trt Least Squares Means
Adjustment for Multiple Comparisons: Dunnett

trt	_trt	Estimate	Standard Error	DF	t Value	Pr > |t|	Adj P	Alpha	Lower	Upper	Adj Lower	Adj Upper
506 TP	control	-1.0000	2.3664	5	-0.42	0.6902	0.9763	0.05	-7.0831	5.0831	-9.2255	7.2255
506 TU	control	-1.0000	2.3664	5	-0.42	0.6902	0.9763	0.05	-7.0831	5.0831	-9.2255	7.2255
756 TP	control	-1.0000	2.3664	5	-0.42	0.6902	0.9763	0.05	-7.0831	5.0831	-9.2255	7.2255
756 TU	control	-2.5000	2.3664	5	-1.06	0.3391	0.6928	0.05	-8.5831	3.5831	-10.7255	5.7255

Based on the analysis above, we use Dunnett adjustment. Since all adjusted P-values are larger than 0.05, we fail to reject the Ho hypothesis for all comparisons above. It further justifies our previous statement that there might be no difference among all of the treatment levels.

To complete the analysis, we provide interaction test for two treatments and comparisons between main effect with control:

Estimates

Label	Estimate	Standard Error	DF	t Value	Pr > |t|
50 vs control	-1.0000	2.0494	5	-0.49	0.6462
75 vs control	-1.7500	2.0494	5	-0.85	0.4322
6TP vs control	-1.0000	2.0494	5	-0.49	0.6462
6TU vs control	-1.7500	2.0494	5	-0.85	0.4322
Interaction test	-1.5000	3.3466	5	-0.45	0.6728

Since all adjusted P-values are larger than 0.05, we all fail to reject the Ho hypothesis. It indicates that there might be no interaction effect and no difference between main effects of treatments and control.

21. Statistical Calculations on Figure 4-16 and 4-17

EXPERIMENT 2

In the following analysis, I first analyze the outcome of

Type III Tests of Fixed Effects

Effect	Num DF	Den DF	F Value	Pr > F
trt	4	6	2.09	0.2003

H0: there is no overall treatment effect
Ha: there is treatment effect

Since the P value for overall effect of trt is 0.2003>0.05, we cannot reject H0, which means there might be not significant difference among all of the treatment levels. In order to answer the client's research question, we also do the interaction test for two treatments and comparisons between main effect with control, especially compare 6TP and 6TU with control (theoretically it's not necessary since overall test is not rejected.)

Table 4

Estimates

Label	Estimate	Standard Error	DF	t Value	Pr > |t|
50 vs control	-0.6150	0.3625	6	-1.70	0.1407
75 vs control	0.2000	0.3625	6	0.55	0.6011
6TP vs control	0.03750	0.3625	6	0.10	0.9210
6TU vs control	-0.4525	0.3625	6	-1.25	0.2584
Interaction test	-0.7400	0.7250	6	-1.02	0.3468

Since all P-values are larger than 0.05, we fail to reject the Ho hypothesis for all comparisons above. It further justifies our previous statement that there might be no difference among all of the treatment levels. The bar graph for estimate with confidence interval is also exhibited:

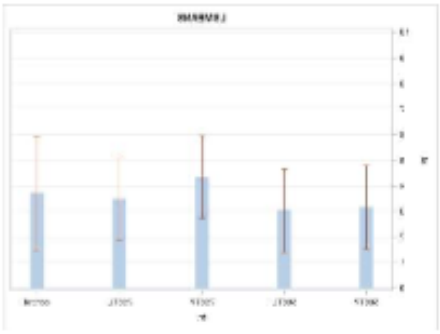

Now I do the analysis for outcome:

Type III Tests of Fixed Effects

Effect	Num DF	Den DF	F Value	Pr > F
trt	4	6	2.20	0.1860

H0: there is no overall treatment effect
Ha: there is treatment effect

Since the P value for overall effect of trt is 0.1860>0.05, we cannot reject H0, which means there might be not significant difference among all of the treatment levels. In order to answer the client's research question, we also do the interaction test for two treatments and comparisons between main effect with control, especially compare 6TP and 6TU with control (though theoretically speaking, it's not necessary since overall is not significant)

Table 5

Estimates

Label	Estimate	Standard Error	DF	t Value	Pr > |t|
50 vs control	-0.07250	0.4307	6	-0.17	0.8719
75 vs control	0.7775	0.4307	6	1.81	0.1211
6TP vs control	-0.04500	0.4307	6	-0.10	0.9202
6TU vs control	0.7500	0.4307	6	1.74	0.1323
Interaction test	0.6600	0.8614	6	0.77	0.4726

Since all P-values are larger than 0.05, we fail to reject the Ho hypothesis for all comparisons above. It further justifies our previous statement that there might be no difference among main effects with control. The bar graph for estimate with confidence interval is also exhibited:

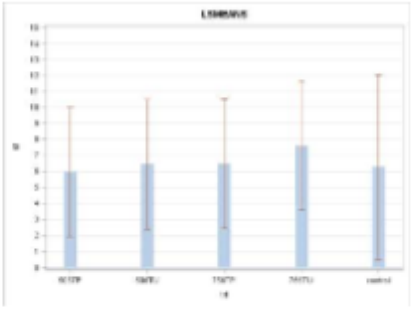

(In the second experiment, since we do not explore the all possible comparisons with control group, it's not necessary to do multiple comparison adjustment. One can definitely do Bonferroni adjustment in this experiment, which will still get a consistent conclusion to the analysis above)

Final conclusion

The analysis of all the experiments were done by analysis of variance (ANOVA), with two-way treatment structure (concentration with two levels * type of inhibitors with two+control) and randomized complete-block design(RCBD) structure. Dunnett adjustment was utilized to control the experimental error when all pairwise comparisons with control were conducted. For 1 hour, 12 hours, and 15 hours experiments, all multiple comparisons with control show that there might be no significant difference between each treatment combination and control (adjusted P-value>0.05), details in table 1, table 2, and table 3. The second set of experiments indicates that there might be no significant difference among 6TP with control, 6TU with control (P-value>0.05), details in table 4 and table 5. SAS is utilized to implement the analysis above.

########################## code for the first experiment

```
data cha;
input trial trt $ reps;
cards;
1 control 247
1 756TP  244
1 756TU 250
1 506TP 243
1 506TU 249
2 control 239
2 756TP  244
2 756TU 236
2 506TP 240
2 506TU 242
3 control 236
3 756TP  238
3 756TU 238
3 506TP 240
3 506TU 239
;
run;
proc print;
run;

data cha1;
input trial trt $ reps;
cards;
1 control 13
1 756TP  17
1 756TU 13
1 506TP 19
1 506TU 19
```

```
2 control 20
2 756TP  22
2 756TU 19
2 506TP 22
2 506TU 20
;
run;
proc print;
run;



*main analysis;
proc glimmix data=cha1 plots=studentpanel;
class trial trt;
model reps=trt/ddfm=kr;
random trial;
estimate '50 vs control' trt 0.5 0.5 0 0 -1;
estimate '75 vs control' trt 0 0 0.5 0.5 -1;
estimate '6TP vs control' trt 1 0 1 0 -2 /divisor=2;
estimate '6TU vs control' trt 0 1 0 1 -2 /divisor=2;
estimate 'Interaction test' trt 1 -1 -1 1 0;
lsmeans trt/diff=control('control') adjust=dunnett cl;
ods output lsmeans=lsmeans;
run;


*bar chart;
proc sgplot data=lsmeans noautolegend;
xaxis type=discrete;
needle x=trt y=estimate /lineattrs=(color=cxB9CFE7 thickness=20);
scatter x=trt y=estimate/markerattrs=(size=0) yerrorlower=lower yerrorupper=upper;
YAXIS LABEL = 'st' GRID VALUES = (200 TO 300 BY 1);
TITLE 'LSMEANS';
run;



data cha2;
input trial trt $ reps;
cards;
1 control 126
1 756TP  128
1 756TU 125
1 506TP 130
1 506TU 128
2 control 131
2 756TP  127
2 756TU 127
2 506TP 125
2 506TU 127
run;
proc print;
run;
```

```
*main analysis;
proc glimmix data=cha2 plots=studentpanel;
class trial trt;
model reps=trt/ddfm=kr;
random trial;
estimate '50 vs control' trt 0.5 0.5 0 0 -1;
estimate '75 vs control' trt 0 0 0.5 0.5 -1;
estimate '6TP vs control' trt 1 0 1 0 -2 /divisor=2;
estimate '6TU vs control' trt 0 1 0 1 -2 /divisor=2;
estimate 'Interaction test' trt 1 -1 -1 1 0;
lsmeans trt/diff=control('control') adjust=dunnett cl;
ods output lsmeans=lsmeans;
run;

*bar chart;
proc sgplot data=lsmeans noautolegend;
xaxis type=discrete;
needle x=trt y=estimate /lineattrs=(color=cxB9CFE7 thickness=20);
scatter x=trt y=estimate/markerattrs=(size=0) yerrorlower=lower
yerrorupper=upper;
YAXIS LABEL = 'st' GRID VALUES = (0 TO 150 BY 1);
TITLE 'LSMEANS';
run;
```

########################## code for the second experiment

```
data cha3;
input trial trt $ rep1 rep2;
cards;
1 control 3.41 7.28
1 756TP  3.74 7.49
1 756TU 3.11 8.06
2 control 4.59 5.68
2 756TP  4.97 5.51
2 756TU 3.88 7.19
1 control 3 7.36
1 506TP 3.5 5.94
1 506TU 2.5 7.16
2 control 3.9 4.82
2 506TP 2.84 6.02
2 506TU 3.6 5.73
run;
proc print;
run;



*main analysis;
proc glimmix data=cha3 plots=studentpanel;
class trial trt;
model rep2=trt/ddfm=kr;
random trial;
estimate '50 vs control' trt 0.5 0.5 0 0 -1;
estimate '75 vs control' trt 0 0 0.5 0.5 -1;
```

```
estimate '6TP vs control' trt 1 0 1 0 -2 /divisor=2;
estimate '6TU vs control' trt 0 1 0 1 -2 /divisor=2;
estimate 'Interaction test' trt 1 -1 -1 1 0;
lsmeans trt/diff=control('control') adjust=dunnett cl;
ods output lsmeans=lsmeans;
run;


*bar chart;
proc sgplot data=lsmeans noautolegend;
xaxis type=discrete;
needle x=trt y=estimate /lineattrs=(color=cxB9CFE7 thickness=20);
scatter x=trt y=estimate/markerattrs=(size=0) yerrorlower=lower
yerrorupper=upper;
YAXIS LABEL = 'st' GRID VALUES = (0 TO 15 BY 1);
TITLE 'LSMEANS';
run;
```

22. Publications

Journal of Pharmaceutical and Biomedical Analysis 151 (2018) 106–115

Contents lists available at ScienceDirect

Journal of Pharmaceutical and Biomedical Analysis

journal homepage: www.elsevier.com/locate/jpba

Inhibition of UDP-glucose dehydrogenase by 6-thiopurine and its oxidative metabolites: Possible mechanism for its interaction within the bilirubin excretion pathway and 6TP associated liver toxicity

Chamitha J. Weeramange[a], Cassie M. Binns[b], Chixiang Chen[c], Ryan J. Rafferty[a,*]

[a] Department of Chemistry, Kansas State University, 1212 Mid-Campus Drive North, 203 CBC Building, Manhattan, KS 66506, United States
[b] Department of Biochemistry, Kansas State University, 1711 Claflin Road, Manhattan, KS 66506, United States
[c] Department of Statistics, Kansas State University, 101 Dickens Hall, Manhattan, KS 66506, United States

ARTICLE INFO

Article history:
Received 5 October 2017
Received in revised form
24 December 2017
Accepted 29 December 2017
Available online 30 December 2017

Keywords:
6-Thiopurine
UDP-glucuronic acid
Glucuronidation
Drug metabolism
Jaundice

ABSTRACT

6-Thiopurine (6TP) is an actively prescribed drug in the treatment of various diseases ranging from Crohn's disease and other inflammatory diseases to acute lymphocytic leukemia and non-Hodgkin's leukemia. While 6TP has beneficial therapeutic uses, severe toxicities are also reported with its use, such as jaundice and liver toxicity. While numerous investigations into the mode in which toxicity originates has been undertaken. None have investigated the effects of inhibition towards UDP-Glucose Dehydrogenase (UDPGDH), an oxidative enzyme responsible for UDP-glucuronic acid (UDPGA) formation or UDP-Glucuronosyl transferase (UGT1A1), which is responsible for the conjugation of bilirubin with UDPGA for excretion. Failure to excrete bilirubin leads to jaundice and liver toxicity. We proposed that either 6TP or its primary oxidative excretion metabolites inhibit one or both of these enzymes, resulting in the observed toxicity from 6TP administration. Inhibition analysis of these purines revealed that 6-thiopurine has weak to no inhibition towards UDPGDH with a K_i of 288 μM with regard to varying UDP-glucose, but 6-thiouric (primary end metabolite, fully oxidized at carbon 2 and 8, and highly retained by the body) has a near six-fold increased inhibition towards UDPGDH with a K_i of 7 μM. Inhibition was also observed by 6-thioxanthine (oxidized at carbon 2) and 8-OH-6TP with K_i values of 54 and 14 μM, respectively. Neither 6-thiopurine or its excretion metabolites were shown to inhibit UGT1A1. Our results show that the C2 and C8 positions of 6TP are pivotal in said inhibition towards UDPGDH and have no effect upon UGT1A1, and that blocking C8 could lead to new analogs with reduced, if not eliminated jaundice and liver toxicities.

1. Introduction

Acute lymphocytic leukemia (ALL) and non-Hodgkin's leukemia represent two of the more than ten types of leukemia's currently affecting humans [1]. Together, these two forms comprise the nearly 80,000 new cases in 2016, with an approximate death rate of 22,000 in the United States. While current treatments have helped decrease this death rate compared to years past, the estimated 22,000 deaths still represent a large population of people seeking new treatments to help push them into remission. Multiple drugs are currently being employed in the treatment against these leukemias; such as, but not limited to: vincristine (oncovin), cytarabine (Cytosar), doxorubicin (adriamycin), etoposide (VP-16), teniposide (Vumon), methotrexate, cyclophosphamide (Cytoxan), and 6-thiopurine [2–9]. Unfortunately, each of these treatments have failed to decreased the projected 22,000 deaths, mostly due to fatal toxicity associated with the treatments or discontinuation of treatments. 6-Thiopurine (6TP, aka 6-mercaptopurine) has a proven record in the remission of both types of leukemia mentioned previously, but also has a well-documented toxicity associated with its use [9,10]. Through investigations into its mode of toxicity, it is envisioned that new classes/analogs that retain the potent therapeutic character of 6TP, but with greatly diminished if not eliminated toxicity, can be synthesized.

* Corresponding author at: Kansas State University, Department of Chemistry, 1212 Mid-Campus Drive North, Manhattan, KS, United States.
E-mail address: rjraff@ksu.edu (R.J. Rafferty).

https://doi.org/10.1016/j.jpba.2017.12.058
0731-7085/

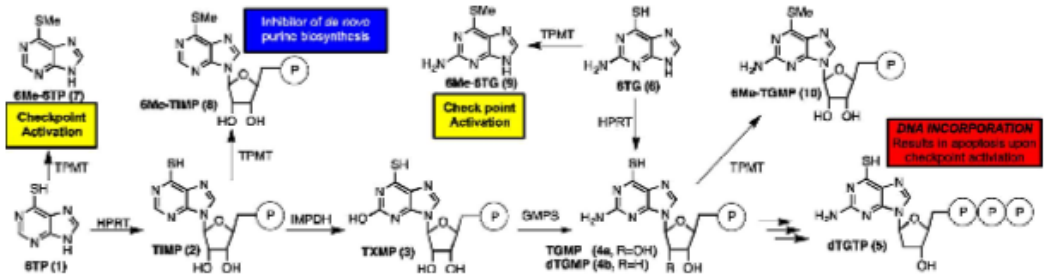

Fig. 1. Anabolic (therapeutic) metabolism of 6-thiopurine (**1**) and 6-thioguanine (**6**) into the dTGTP, a mimic of dGTP for DNA incorporation that results in cell death from base-pair mismatch. Various side metabolic routes of 6TP are presented: i) methylation forming 6-Me-6TP (**7**) and 6Me-6TG (**9**) that induces checkpoint activation triggering cell death from the dTGTP incorporation, and ii) methylation of TIMP (**2**) forming 6-MeTIMP (**8**) that inhibits *de novo* purine biosynthesis.

The therapeutic activity of 6TP (**1**) comes from two main routes: methylation of the thiol of 6TP (**7**) and formation of a deoxythioguanosine triphosphate mimic (dTGTP, **5**) illustrated in Fig. 1. The former metabolite is formed through the methylation of the thiol by thiopurine methyltransferase (TPMT), and has no direct therapeutic activity [11]. The latter is formed through a cascade starting with the phosphoribosylation of 6TP (**1**) by hypoxanthine-guanine phosphoribosyltransferase (HPRT) to access thioinosinic acid (TIMP, **2**). Two key-fates diverge from TIMP, both leading to the therapeutic efficacy [10,12]. En route to its primary therapeutic pathway, **2** is converted to thioxanthine monophosphate (**3**) by inosine monophosphate dehydrogenase (IMPDH). This is normally the rate-limiting step of the pathway, but it has been found that the activity of IMPDH is higher in malignant lymphoblasts and myeloblasts compared to normal lymphocytes [13]. Interestingly, 6TP has been shown to cause an induction of IMPDH which results in a four-fold increase of DNA incorporation of the deoxythioguanine mimic (**5**, *vide infra*). Formation of the thioguanine monophosphate nucleoside (**4a**) is accomplished by guanosine monophosphate synthetase (GMPS). This step also allows for the formation of the deoxyribose (**4b**) [10,12]. Kinase steps convert both **4a** and **4b** into their corresponding triphosphate forms of RNA and DNA (**5**), respectively. Cell death via 6TP administration occurs through the incorporation of the nucleotide **5**, which mimics and competes with endogenous guanosine nucleotides, into DNA. The incorporation of **5** into DNA results in base-pair mismatching and the cell undergoing apoptosis. However, cell death via this mechanism is not immediate [14]. Multiple passages of the S-phase are required to allow for sufficient dTGTP's to be incorporated into DNA; upon checkpoint activation, recognition of the mismatch base pairing is revealed [9,15]. Enhanced checkpoint activation with 6TP-adminstration comes from the methylated thiol species **7** and **9**, formed from the methylation of 6TP (**1**) and 6-thioguine (**6**, 6TG), respectively. Both methylated species have no cytotoxic properties themselves, but both induce checkpoint activation allowing for the identification of mismatching DNA sequences resulting in apoptosis [9]. In addition to methylation forming checkpoint activating species, the methylation of **2** by TPMT forms 6Me-TIMP (**8**), which has been proven to inhibit *de novo* purine biosynthesis [9,16]. Through this inhibition an increased cellular uptake of purines follows, which include 6TP. The increased influx of 6TP allows for increased DNA incorporation of **5** that increases the rate in which apoptosis occurs.

In conjunction to its therapeutic metabolism, there are also detoxification pathways operating simultaneously that greatly reduce the bioavailability of 6TP, shown in Fig. 2. En route to dTGTP (**5**), dTGMP (**4b**) can be used as a substrate for nucleotidases and nucleosidases that results in the formation of 6TG (**6**), which can further be converted to 6-thioxathine (**11**) by guanase. Xanthine oxidase (XO) then oxidizes the C8 position to form 6-thiouric acid (6TU, **12**), which is the terminal excretion metabolite of 6TP [17]. The formation of 6TU can be accomplished directly from 6TP through oxidation by XO, a species that is retained by the body well beyond 24-h post 6TP treatment [14]. It is through this pathway that an excess of 6TP can be redirected, thus preventing formation of 6Me-TIMP and dTGTP for therapeutic activity. Suppression in the formation of 6TU can be accomplished through a combination therapy with XO inhibitors, such as allopurinol [18]. However, said combination results in new and greater toxicity that requires a lower dosage of 6TP. Keeping in mind that high concentrations of dTGTP are required to cause cell death, the resulting 6TP decrease with the allopurinol co-treatment allows for cells to be rescued from this mode of cell death [18]. Likewise, the decreased administration of 6TP also directly reduces the *de novo* purine biosynthesis inhibition caused by 6Me-TIMP, further diminishing its therapeutic efficacy. As such, the combination therapy of XO inhibitors with 6TP fails to produce a beneficial treatment strategy.

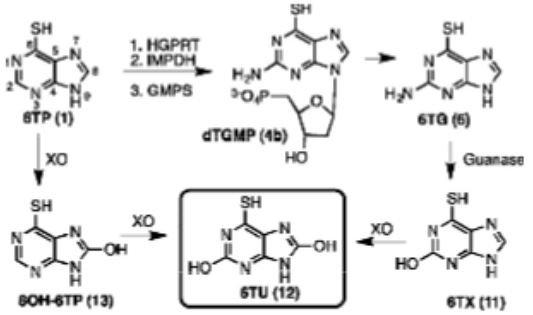

Fig. 2. Formation of 6-thiouric acid (**12**) through two pathways: from degradation of one of the intermediates of the therapeutic pathway (**4b**) and direct oxidation from 6TP by xanthine oxidase (XO).

One of the key toxic side effects of 6TP administration is jaundice; approximately 40% of those taking 6TP develop this life threatening side-effect [19]. The average person forms about 250–300 mg of bilirubin formed per day [20]. Failure to excrete bilirubin can cause jaundice, hyperbilirubinemia, kernicterus, Crigler-Najjar syndrome, Gilbert's syndrome and even death [21–23]. Jaundice results from the buildup of bilirubin within the body, most commonly from the failed detoxification of heme groups (**13**) post red blood cell senescence shown in Fig. 3 [24]. The heme group, comprised of a porphyrin and metal, of the former red blood cell must be degraded and excreted upon senescence of the erythrocyte, commonly referred to as the bilirubin pathway

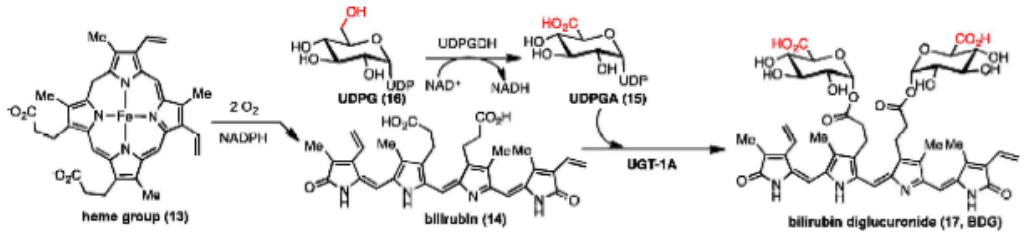

Fig. 3. Formation of the excretable bilirubin diglucuronide species from the conjugation of bilirubin with two UDPGA units.

(Fig. 3) [25]. The bilirubin (**14**) formed is a relatively large, non-polar molecule, whose characteristics make its excretion difficult but critical to prevent jaundice onset as well as liver toxicity. Excretion occurs with the direct conjugation with two UDP-glucuronic acids (**15**, UDPGA) via UDP-glucuronyl transferase (UGT-1A1) [26]. The UDPGA are formed from the oxidation of UDP-glucose (**16**, UDPG) by UDP-glucose dehydrogenase (UDPGDH) [27]. The resulting bilirubin diglucuronide (**17,** BDG) is more water-soluble and thus more easily excreted. The transferase enzyme responsible for this conjugation is located on the smooth and rough endoplasmic reticulum of the liver [28].

We postulate that it is through the inhibition UDPGDH and/or UGT1A1 that causes the severe reported toxicity from 6TP administration, namely jaundice. Furthermore, it is hypothesized that inhibition of one or both of these enzymatic steps is instigated by 6TP and its known excretion metabolites (**11, 12,** and **13**). This study outlines the work into investigating the possible route of toxicity resulting from 6TP administration about these two key enzymatic transformations.

2. Materials and methods

2.1. Chemicals and reagents

All standard chemicals used in this study were the highest grades available and were purchased through Sigma-Aldrich (Saint Louis, MO, USA), VWR (Radnor, PA, USA), or Fisher Scientific (Denver, CO, USA). Specialized reagents were purchased through specific vendors. Glycylglycine (gly-gly: G1127), ß-nicotinamide adenine dinucleotide (NAD^+: N1636), uridine 5′-diphosphoglucose (UDPG disodium salt: U4625), uridine 5′-diphosophoglucuronic acid (UDPGA: U6751), uridine 5′-diphosphoglucose dehydrogenases (UDPGDH: U6885), 6-thiopurine monohydrate (6TP), 6-thioguanine (6TG, A4882), 6-thioxanthine (6TX, T8125), bilirubin (including three mixed isomers, B4126), 4,5-diamino-6-hydroxypyrimidine hemisulfate salt (D19303), alamethicin (A5361), and pooled rat liver microsomes (M9066) were purchased from Sigma-Aldrich. 6-Mercaptopurine-2-ol (6-TX, QA-6668) was purchased from Combi-Blocks, and 6-thiouric acid (6-TU, SC-213040) from Santa Cruz Biotechnology. HPLC-grade water was obtained by passing distilled water through a reverse osmosis system followed by treatment with a Thermo Scientific Barnstead Smart2Pure 3UV purification system (Fisher, 10-451-045), herein referred to as nanopure water.

2.2. Equipment, supplies, data software, and statistical analysis

All standard consumable supplies used in this study were purchased from VWR or Fisher Scientific. Specific equipment utilized in this work are: 1) Hewlett-Packard 8452 Diode Array UV/Vis spectrophotometer (Palo Alto, CA, USA) equipped with a Lauda Brinkman Ecoline RE 106 E100 circulating water bath purchased from VWR, 2) HPLC system consisting of an CBM-20A/20Alite system controller, SIL-20AHT Auto sampler, SPD-20A, SPD-20AV UV–vis Detector, LC-20AT Solvent delivery module, CTO-20A Column Oven, DGU-20A3R Degassing unit and LC-20AD/20AT Gradient Valve Kit purchased from Shimadzu Scientific Instruments (Kyoto, Japan), and 3) all incubated reactions were performed with a Labcare America PRECISION water bath model 25 purchased from Fisher Scientific. All HPLC separations were performed on a Discovery C18 analytical column, 4.6 mm × 100 mm, 5 μm particle size (504955-30) along with the respective guard column (59576) purchased from Sigma-Aldrich. Data was processed and all figures and tables constructed via the program Prism 7.02 for Mac, GraphPad Software (La Jolla, CA, USA). All chemical structures were prepared with ChemDraw Professional 16.0 by PerkinElmer (Waltham, MA). All statistical calculations within this body of work was performed by the treatment of two-ay factorials (positive and negative controls, design structure of RCBD, and T-tests) with Statistical Analysis System (SAS) software for Windows (Cary, NC, USA).

2.3. UDP-glucose dehydrogenase activity assay

Standard preparation: A 0.50 M Gly–Gly buffer (pH 8.7 at 25 °C) was prepared by dissolving 1.62 g of Gly–Gly in 22 mL nanopure water, pH adjusted to 8.7 with 9 M potassium hydroxide and then diluted to 25 mL with nanopure water all while being shaken at 25 °C. Solutions of UDPG and NAD^+ were prepared by dissolving 1.7 mg and 4.5 mg, respectively, into nanopure water resulting in 2 mM and 10 mM solutions, respectively. Preparation of the 0.1 mM 6TU solution was done by dissolving 1.8 mg into 95.5 mL of nanopure water, pH was adjusted to 9.5 with a 2 M sodium hydroxide solution (for solubility), pH adjusted to 7.5 with a 0.5 M hydrochloric acid solution (a dilute solution of HCl is required to prevent thiol oxidation), and then diluted to 100 mL. In an analogous fashion, samples of 6TP, 6TX, and 8Me-6TP were prepared. A 5 unit/mL UDPGDH solution was prepared by dissolving 0.11 mg of UDPGDH in 0.8 mL of 0.5 M Gly–Gly while stirring; once dissolved, the solution was diluted to volume with gly–gly in a 1 mL volumetric flask. All solutions were kept at 4 °C when not in use.

2.3.1. Inhibitor assessment – general procedure

Spectrometric analysis was performed on a Hewlett-Packard 8452 Diode Array UV/Vis spectrometer equipped with a Lauda Brinkman Ecocline RE 106 E100 circulating water bath. The water bath was maintained at 25 °C and the diode array was set at 340 nm, both were allowed to warm up 10-min prior to analysis. To a 1 mL cuvette, 300 mL of 0.5 M Gly–Gly (0.15 M final concentration), nanopure water, varying NAD^+ and UDPG concentration in varying inhibitor concentrations were added and placed in the diode array for a 2 min thermal equilibration. Once 1.5 min elapsed, the instrument was zeroed to obtain an initial rate change in absorbance versus time. The reaction was initiated by addition of 20 μL of the UDPGDH solution. Thorough mixing by inversion of the cuvette was

performed as quickly as possible and then placed in the holder for analysis. The reaction was monitored from 20 to 120 s after enzyme addition, and the slope was calculated from 20 to 40 s using the diode array software.

Inhibitor Assessment – Saturating NAD^+ varying UDPG concentration: For each analysis, the cuvette was prepared in the same fashion as outlined above. The final concentration of the components of the mixture were 150 mM Gly-Gly, 0.1 unit/mL UDPGDH, 3 mM NAD^+ and varied concentrations of 0.1, 0.05, 0.025 and 0.02 mM of UDPG, obtained from stock solution addition. Nanopure water was used as a variable component to ensure that a final volume of 1 mL was obtained. Inhibitor analysis of the four purines was performed at two concentrations: 50 and 100 μM for 6TP, 20 and 50 μM for 6TX and 8OH-6TP, and 5 and 10 μM for 6TU, obtained from their corresponding stock solutions. Each assessment was performed in triplicate. The average of the three were plotted and the slopes were used to determined inhibition values.

Inhibitor Assessment – Saturating UDPG varying NAD+ concentration: In an analogous protocol as described for NAD^+ saturating conditions (above), inhibitor analysis of UDPGDH was performed under UDPG saturating conditions (0.6 mM) with varying concentrations of NAD^+.

2.4. UDP-glucuronosyltransferase activity assay

Standard preparation: A bilirubin stock solution was prepared by dissolving bilirubin in 100% dimethyl sulfoxide to yield a concentration of 2 mM, the stock solution was aliquoted, and stored at −70 °C until use. A 25 mM UDPGA stock solution was prepared by diluting 8 mg to 0.5 mL with nanopure water, and a 10 mg/mL alamethicin solution was prepared by taking 5 mg and diluting to 500 μL with methanol. Preparation of the 100 mM potassium dihydrogen phosphate buffer was done by dissolving 2.3 g of KH_2PO_4 into 80 mL of nanopure water, pH adjusted to 7.4 with 1 M HCl and diluted to volume in a 100-mL volumetric flask.

2.4.1. Chromatographic conditions – bilirubin and bilirubin glucuronide

Bilirubin and its glucuronide were separated on a Discovery C18 analytical column, 4.5 mm x 100 mm, 5 μM particle size with guard column. A dual mobile phase was employed; the aqueous phase consisted of an 8 mM imidazole & 2.5 mM tetrabutylammonium hydrogen sulfate (TBAHS) buffer at a pH of 6.5 in nanopure water and acetonitrile as the organic phase. A gradient elution profile was employed for full separation at a flow rate of 0.5 mL/min, the method begins at 10% acetonitrile and increases to 50% over 8 min, held for 5.5 min, increased to 95% over 4.5 min, held for 10 min, returned to 10% over 4 min and held at 10% for 2 min to allow for column regeneration. The detection wavelength was 450 nm with a sample injection volume of 5 μL. The combined peak area for bilirubin (sum of the three isomers) was plotted relative to the concentration prepared for the generation of a working standard curve.

Chromatographic Conditions – UDPGA: Chromatographic separations were performed on a Discovery C18 analytical column, 4.5 mm × 100 mm, 5 μm particle size (Supelco) with a guard column. UDPGA was separated under isocratic conditions, flow rate at 0.5 mL/min using a mobile phase comprised of 40% methanol and 60% buffer that was composed of 8 mM imidazole and 5 mM TBAHS at a pH of 6.5. The detection wavelength was 262 nm with a sample injection volume of 5 μL. Various concentrations of UDGPA were analyzed, and peak areas obtained were plotted relative to said concentrations to generate a working standard curve.

Quantification of Bilirubin, Mono/Di-glucuronide, and UDPGA Levels: Standard curves for both bilirubin and UDPGA were constructed and used for the quantification of each species. Bilirubin was quantified directly from the generated standard curve. A total of ten peaks for the glucuronide species, including their isomers were detected in the incubation samples. Peak assignment and identification of UCB, BMG1, BMG2, BDG and their isomers were based on their lipophilicity and polarity, as well as the elution pattern, chromatographic peak position and relative retention time from previous reports [21–23]. The calibration curves for bilirubin were used to determine the concentration of the mono- and di-glucuronide species employing the gradient HPLC bilirubin method described above. Quantification of UDPGA levels was determined through the use of the constructed standard curve within the isocratic HPLC method developed for UDGPA.

Bilirubin Glucuronide Formation: Bilirubin glucuronidation was performed at 37 °C in a shaking water bath. All steps taken were performed in the lowest light conditions possible; the glucuronide formed was found to be unstable to ambient lighting. The following was added to an Eppendorf tube to achieve the final concentrations indicated, final volume 200 μL: potassium phosphate buffer (50 mM, pH 7.4), bilirubin (10 μM), $MgCl_2{\cdot}6H_2O$ (0.88 mM), rat liver microsomes (RLM, 100 μg of protein/mL), alamethicin (22 μg/mL), and allowed to pre-incubated for 2 min. Addition of UDPGA (3.5 mM), referred to as the zero-time point, initiated the reaction. The mixture was allowed to shake at 37 °C for each of the time course experiments. To each reaction 600 μL of ice-cold methanol containing 200 mM ascorbic acid was added to terminate the enzymatic reaction, vortexed for 2 min, and then centrifuged at 12,000 rpm for 10 min. The supernatant was then analyzed by the developed gradient HPLC protocol for separation and quantification of UCB, BMG1, BMG2, and BDGs.

Validation of Bilirubin Glucuronide Formation: Quantification of UCB, BMG1&2 and BDGs were performed post the quenching of UGT1A1, which was performed by immersing the Eppendorf tube with the reaction mixture in a cold-water bath for two min. No ascorbic acid was used, as the residual material would quench the glucuronidase enzyme to be added. To this sample 0.1 mg/mL glucuronidase enzyme was added, inverted (x3), and then analyzed by the HPLC protocol developed to quantify the levels of bilirubin and BMG1&2 and BDGs for formation confirmation.

Inhibitor Assessment of Bilirubin Glucuronide Formation: Employing the same protocol delineated above for the formation of the bilirubin glucuronide species, inhibitor assessment was performed. To the Eppendorf tube, 6-thiopurine or 6-thiouric acid (50 and 75 μM final concentrations) was added alongside a control (no purine added) and allowed to pre-incubate for 2 min. Addition of UDPGA initiated the reaction for each of the time course experiments. The gradient HPLC method was employed for the 45-min time course experiments for the quantification of the glucuronide species. For experiments in which UDPGA was analyzed, the incubation protocol for the formation was altered as follows: 300 μL final volume, 2.5 μM of bilirubin, 260 μM of UDPGA was employed to start the reaction, no alamethicin, and the enzyme was quenched with heat (87 °C). Quantification of UDPGA for the 1, 12, and 15-h time course experiments was performed by the isocratic HPLC method described above.

2.5. Synthesis of 8-OH-6-Thiopurine

From commercially available 4,5-diamino-6-hydroxypyrimidine, thiol installation about the C6 position was accomplished under standard employed protocols with Lawesson's reagent [29] in a 43% yield. Following a Traube synthesis protocol [30], 4,5-diamino-6-thiopyrimidine was heated with urea in muffle furnace until the mixture underwent a molting process. The reaction was worked up under acid-base conditions followed by recrystallization to afford the desired 8OH-6-thiopurine in a 65% yield. The product matched reported

characterization data (NMR included within the Supplemental Material).

3. Results and discussion

3.1. Inhibition profiling of UDPGDH by 6TP, 6TU & 6TX

Assessment of activity/inhibition of NAD(P)-dependent dehydrogenase catalyzed reactions is commonly and routinely performed by UV/Vis spectrometry methods by monitoring absorbance changes at 340 nm [31]. The only caveat to performing assessment of activity in this fashion is that any substrate/inhibitors to be screened must not absorb at 340 nm. If wavelength overlap is present, it can make it difficult, or even impossible to determine if there are any substrate/inhibitor effects upon the enzymatic reaction. Purines, such as 6-thiopurine and its main excretion metabolites absorb at 340 nm and therefore prevent assessment of enzymatic activity in commonly employed assays. To overcome the interfering signal, we found that if the purines were screened in sufficiently low concentration, such that the magnitude of their absorbance at 340 nm is relatively non-interfering, that inhibition studies could be performed against UDPGDH in a rapid and reproducible fashion. Through spectral experimentation the following allowable maximum concentrations were found that had negligible interference at 340 nm: 100 μM for 6TP, 50 μM for 6TX, and 10 μM for 6TU. Lower concentrations were then analyzed for generation of inhibition profiles for 6TP, 6TU, and 6TX toward UDPGDH. Inhibition was assessed through saturation kinetics, in which either UDPG or NAD^+ was saturating while the other substrate concentration was variable.

Inhibition profiles for 6TP, 6TU, and 6TX against UDPGDH with varying UDPG and saturating NAD^+ is shown in Fig. 4A–C, and varying NAD^+ with saturating UDPG is presented in Fig. 4D–F. For each purine screened, three separate experiments were performed: no purine, and purine at both low and high concentration levels. From the analysis with no purine, under both varying UDPG and NAD^+ conditions, the K_m and V_{max} were calculated. The determination of the K_i was accomplished by plotting the slope from each independent analysis set versus the concentration of purine; calculation of the K_i was performed by taking the negative-inverse value of the x-intercept. Table insert within Fig. 4 summarizes the respective K_i, K_m, and V_{max} values for each purine in respect to both varying and saturating concentrations of UDPG and NAD^+ concentrations.

3.2. Synthesis of 8-OH-6-thiopurine and UDPGDH inhibition profiling

To assess the full effects of hydroxylation about the C2 and C8 positions (purine numbering shown in Fig. 4 table insert) of 6TP excretion metabolites, the synthesis of 8OH-6TP was undertaken from reported procedures in 28% yield over two-steps (Fig. 5) [30]. In an analogous fashion to the three purines described above, 8OH-6TP was assessed for inhibition towards UDPGDH. Fig. 6 outlines the inhibition of the C8 hydroxylated purine under varying UDPG concentration (Fig. 6A) and varying NAD^+ concentration (Fig. 6B). In regards to both, 8OH-6TP was found to inhibit UDPGDH more potently than 6TX (varying about the position of hydroxylation) and comparably to 6TU. The K_i with respect to varying UDPGA was found to be 14 μM and with respect to varying NAD^+ 32.5 μM.

3.3. Inhibition effects of 6TP and 6TU upon UGT1A1

Further investigation into the bilirubin detoxification pathway led to inhibition studies of 6TP and 6TU towards UGT1A1. Only 6TP and 6TU were screened, as they represented the two extremes of inhibition towards UDPGDH with regards to varying UDPGA concentrations. To assess inhibition, an HPLC method was developed that allowed for the separation and quantification of all substrates and products from the UGT1A1 reaction. While there are reported methods to assess the activity of this transferase reaction [21–23], our method developed includes universal applications of each, as well as new aspects. This method allows for the full separation and quantification for all bilirubin glucuronide species and unconjugated bilirubin, as well as applications into inhibition assessment.

Shown in Fig. 7-line A are the three isomers of unconjugated bilirubin (UCB) from 23.6–24.2 min. Line B the three isomers of the bilirubin diglucuronide (BDG) species at 11.2–11.4 mins and the various bilirubin monoglucuronides (BMG1&2) from 12.3–13.2 mins. To validate the formation of the various glucuronide species, a separate reaction was run and then treated with glucuronidase, which removes the glucuronic acid upon the various forms of the bilirubin glucuronide species forming unconjugated bilirubin and glucuronic acid. Line C is obtained post glucuronidase treatment of the formed glucuronide species from line B. With the results from Fig. 7, the formation of the glucuronide species is thereby confirmed and in extension confirms the validity of the method developed for separation of substrates and products [21].

Standard curves for both the mono- and di-glucuronide species was unattainable, given that both species are both light and thermally sensitive and have been found to degrade rapidly [21,22]. To this end, the bilirubin standard curve was employed given that the same chromophore species is present within UCB, BMG1&2, and BDG. Inhibition assessment of 6TP and 6TU was performed at 50 and 75 μM for both purines over a 45-min incubation period. Outlined in Fig. 8 are the levels of the BDG, the various BMG1&2, and UCB when treated with 50 and 75 μM of 6TP. Inhibition investigations by 6TU at the same conditions are shown in Fig. 9. The apparent values for the formation of BMGs, BDG, and remaining UCB showed no significant difference ($P > 0.05$) in the presence and absence of 6TP and 6TU. All statistical calculations are presented within the Supplementary Material. Stability of the glucuronide species could present doubt in the accuracy of the quantification and in turn the validity of the inhibition profiles obtained. Therefore, assessment of inhibition by indirect means of a stable species could further validate the findings from the glucuronide study.

3.4. 6TP & 6TU inhibition of UGT1A1 via UDPGA quantification

Due to the well reported and documented instability of the glucuronide species, activity of UGT1A1 was assessed by monitoring and quantifying UDPGA levels. The previous HPLC method for glucuronide quantification was not applicable for UDPGA quantification due to the elution of UDPGA at a gradient point in the method. Therefore, an isocratic HPLC assay with UV detection at 262 nm was developed for quantification of UDPGA that allows for the indirect quantification of BMG1&2 and BDG formation. Successful conjugation of bilirubin to either one or two UDPGAs will form the desired glucuronide species, and upon any degradation of these thermally and light reactive species will result in the return of UCB and glucuronic acid. The glucuronic acid will have a different retention factor in comparison to UDPGA. Therefore, any decrease in UDPGA levels directly corresponds to the formation of the glucuronide species. A standard curve for UDPGA was generated to access concentration in this work (presented in the supplemental material). Thermal stability of UDPGA is key for this method, and was determined by incubating UDPGA in the reaction media over a 15-h period (shown in Fig. 10 with comparison between UDPGA and mixture with no enzyme added at 37 °C).

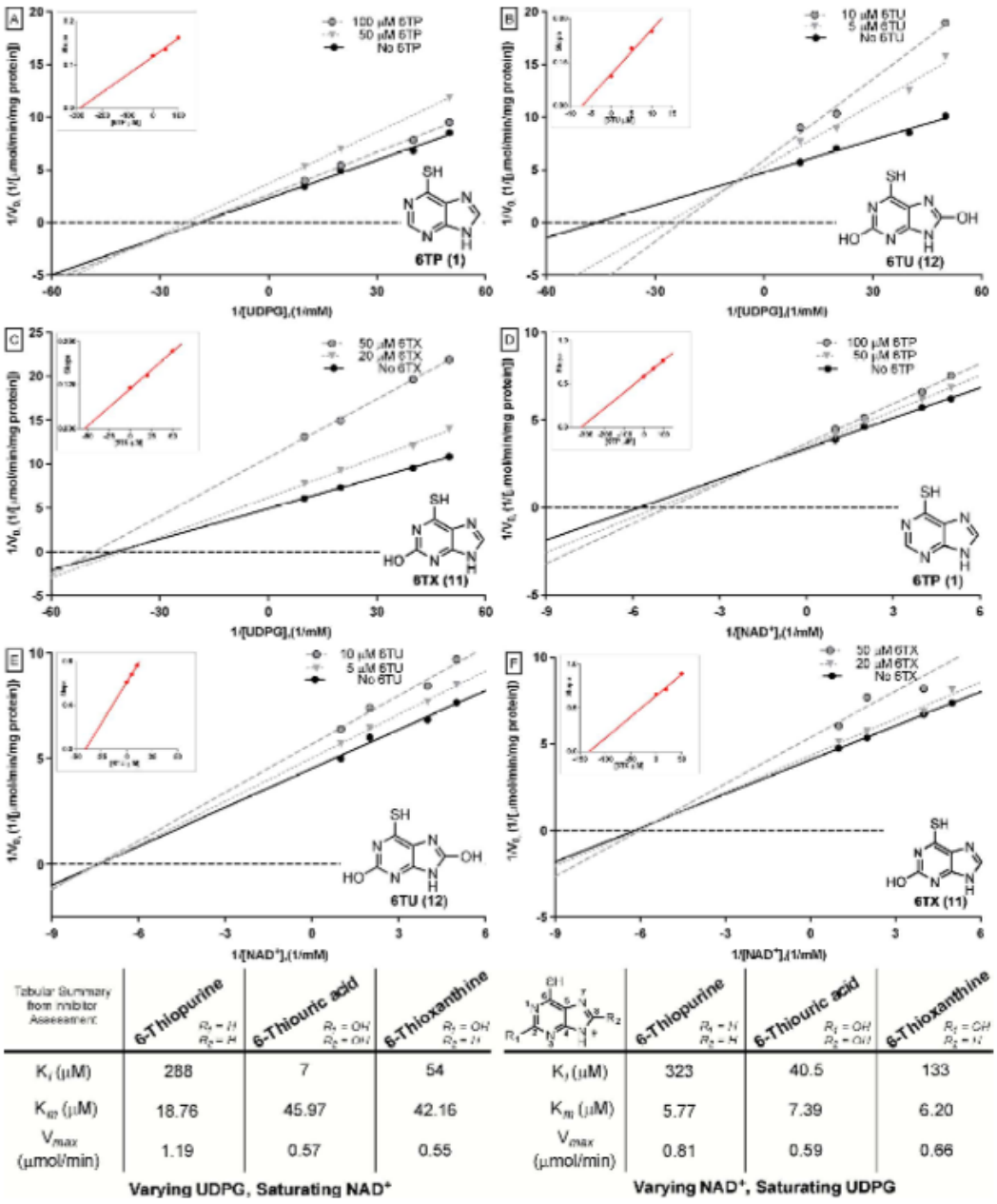

Tabular Summary from Inhibitor Assessment	6-Thiopurine (R_1 = H, R_2 = H)	6-Thiouric acid (R_1 = OH, R_2 = OH)	6-Thioxanthine (R_1 = OH, R_2 = H)
K_i (µM)	288	7	54
K_m (µM)	18.76	45.97	42.16
V_{max} (µmol/min)	1.19	0.57	0.55
Varying UDPG, Saturating NAD+			

	6-Thiopurine (R_1 = N, R_2 = H)	6-Thiouric acid (R_1 = OH, R_2 = OH)	6-Thioxanthine (R_1 = OH, R_2 = N)
K_i (µM)	323	40.5	133
K_m (µM)	5.77	7.39	6.20
V_{max} (µmol/min)	0.81	0.59	0.66
Varying NAD+, Saturating UDPG			

Fig. 4. Inhibition assessment towards UDP-glucose dehydrogenase by various 6TP excretion metabolites through Lineweaver-Burk plot analysis under UDPG varying NAD^+ saturating conditions. A) Concentrations of 6TP, varying UDPG, screened were 0, 50, & 100 µM with slopes of each line 0.121, 0.135, 0.1623 respectively. Plotting slopes versus concentration afforded a regression line of y = 0.000413x + 0.1188. B) Concentrations of 6TU, varying UDPG, screened were 0, 5, & 10 µM with slopes of each line 0.103, 0.198, 0.2565 respectively. Plotting slopes versus concentration afforded a regression line of y = 0.0154x + 0.1091. C) Concentrations of 6TX, varying UDPG, screened were 0, 20, & 50 µM with slopes of each line 0.117, 0.152, 0.223 respectively. Plotting slopes versus concentration afforded a regression line of y = 0.0021x + 0.1143. D) Concentrations of 6TP, varying NAD^+, screened were 0, 50, & 100 µM with slopes of each line 0.580, 0.674, 0.760 respectively. Plotting slopes versus concentration afforded a regression line of y = 0.0018x + 0.5813. E) Concentrations of 6TU, varying NAD^+, screened were 0, 5, & 10 µM with slopes of each line 0.614, 0.685, 0.765 respectively. Plotting slopes versus concentration afforded a regression line of y = 0.0154x + 1091. F) Concentrations of 6TX, varying NAD^+, screened were 0, 20, & 80 µM with slopes of each line 0.655, 0.708, 0.891 respectively. Plotting slopes versus concentration afforded a regression line of y = 0.0048x + 6387.

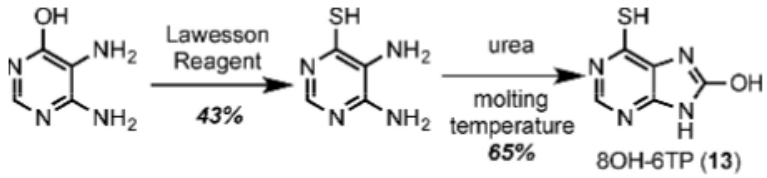

Fig. 5. Synthesis of 8OH-6TP via a modified Traube approach. Thiol installation through Lawesson reagent upon commercially available 4,5-diamino-6-hydroxylpyrimidine with subsequent purine formation via condensation with urea.

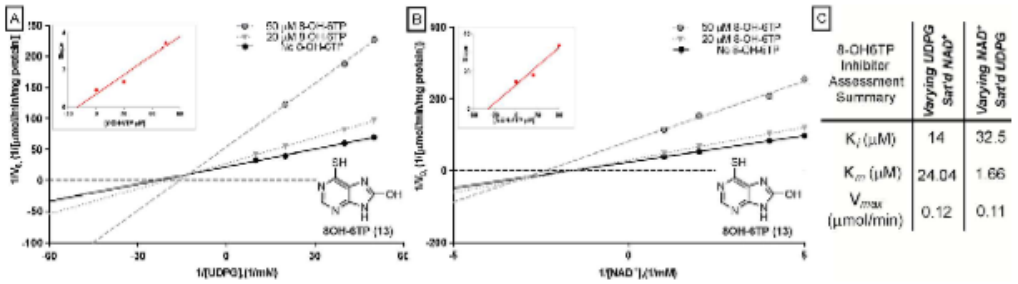

Fig. 6. Lineweaver-Burk inhibitor assessment of 8OH-6TP under varying UDPG saturating NAD^+ conditions (left), varying NAD^+ saturating UDPG (center), and inhibitor summary (right). Concentrations of 8OH-6TP screened were 0, 20, & 50 μM under both condition with slopes of each line for varying UDPG 0.9365, 1.368, 3.422, respectively, and varying NAD^+ 14.54, 18.12, 33.81, respectively. Plotting slopes versus concentration afforded a regression line of y = 0.0512x + 0.7142 for varying UDPG and y = 0.3963x + 12.91 for NAD^+.

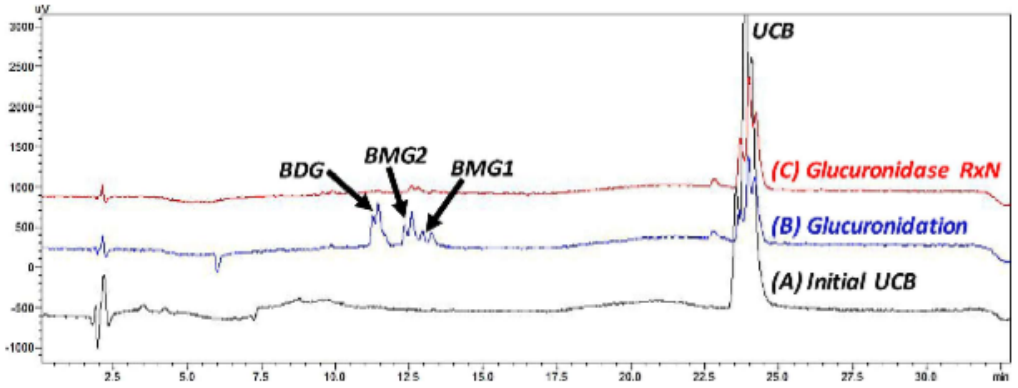

Fig. 7. Chromatograms showing the standard unconjugated bilirubin (line A), formation of the glucuronide bilirubin species (line B), and the UCB obtained post glucuronidase treatment of a sample containing BMG1&2 and BDG for validation of glucuronide formation. The gradient HPLC method was employed with a detection of 450 nm.

Three time-course experiments were performed (1, 12 & 15-h) in which UDPGA concentrations were determined by HPLC analysis (Fig. 10). When the reaction was performed in the absence of any inhibitors, concentrations of UDPGA dropped to 241 μM after 1-h, 110 μM after 12-h, and 17 μM after 15-h from the initial 260 μM (validated by aliquot removal prior to the start of the reaction). Levels of UDPGA were found to be relatively the same when testing inhibition by 50 and 75 μM of 6TP: 241 & 242 for 1 h, 130 & 128 for 12 h, and 20 & 20 for 15 h, respectively. Inhibitor assessment of 6TU towards UGT1A1 afforded similar results to 6TP and the control when screened at 50 and 75 μM of 6TU: 243 & 241 for 1 h, 128 & 125 for 12 h, and 20 & 16 for 15 h, respectively. The apparent UDPGA levels at the end of the reaction showed no significance difference ($P > 0.05$) in the presence and absence of 6TP and TU. All statistical calculations are presented within the Supplementary Material.

4. Conclusion

In the study presented, we have investigated the possible correlations between the excretion metabolites (6TX, 8-OH-6TP, and 6TU) associated with 6TP and the severe toxicities resulting from its administration. These side-effects are so potent that as a result, the

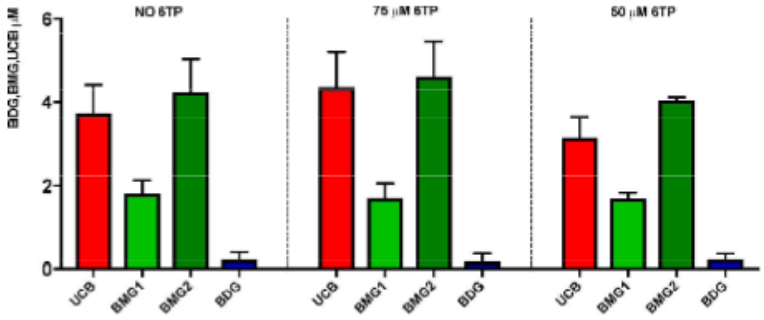

Fig. 8. Inhibition studies of UDP-glucuronosyl transferase (UGT1A1) by 6TP at 50 and 75 μM. Levels of unconjugated bilirubin (UCB), monoglucuronide bilirubin (BMG1 & BMG2), and diglucuronide bilirubin (BDG) quantified through the bilirubin standard curve (presented in the supplemental material). Each analyte is an average of three independent runs with standard error bars.

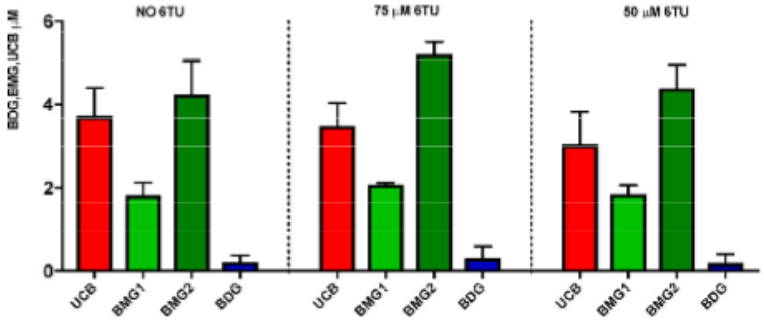

Fig. 9. Inhibition studies of UDP-glucuronosyl transferase (UGT1A1) by 6TU at 50 and 75 μM. Levels of unconjugated bilirubin (UCB), monoglucuronide bilirubin (BMG1 & BMG2), and diglucuronide bilirubin (BDG) quantified through the bilirubin standard curve (presented in the supplemental material). Each analyte is an average of three independent runs with standard error bars.

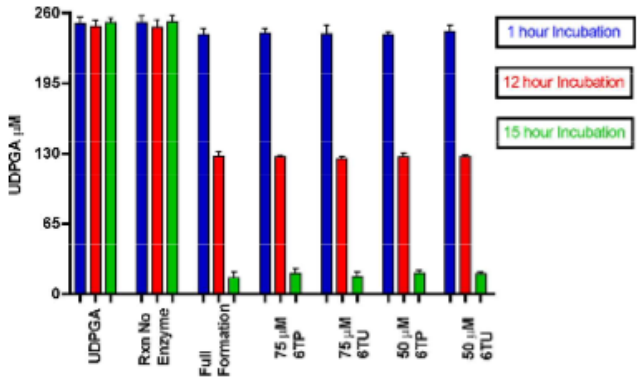

Fig. 10. Assessment of UGT1A1 inhibition by 6TP and 6TU at 75 and 50 μM over three time-course experiments of 1, 12 and 15-h. One-hour incubations are triplicates of triplicates, 12-h are triplicates, and 15-h are triplicates of duplicates.

administration of the drug is given in an on/off strategy allowing time for said toxic species to be cleared by the body. Unfortunately, this greatly reduces the therapeutic efficacy. Severe liver damage is commonly associated with 6TP administration, and given the degree of red blood senescence within leukemia, it is proposed that liver toxicity results from the failed clearance of bilirubin. The two key reactions responsible for bilirubin excretion are: 1) UDPGA formation from UDPG via UDP-glucose dehydrogenase (UDPGDH), and 2) bilirubin conjugation with UDPGA forming the excretable species via UDP-glucuronosyl transferase. As described above, in addition to the therapeutic pathway for 6TP, there is an excretion pathway operating concurrently and at a faster rate. These excretion metabolites are proposed to be responsible for the associated toxicity, specifically through inhibition of UDPGDH and/or UGT1A1.

Table 1
Inhibition assessment of UGT1A1 with regards to varying 6TP and 6TU concentrations. Each data set was run in triplicate with standard deviation values given in parentheticals.

Bilirubin Species	Control	50 μM 6TP	75 μM 6TP	50 μM 6TU	75 μM 6TU
UCB	3.72 μM (±0.38)	3.17 μM (±0.46)	4.35 μM (±0.87)	3.05 μM (±0.77)	3.49 μM (±0.54)
BMG1	1.82 μM (±0.04)	1.70 μM (±0.14)	1.72 μM (±0.34)	1.85 μM (±0.21)	2.09 μM (±0.03)
BMG2	4.24 μM (±0.34)	4.05 μM (±0.07)	4.61 μM (±0.86)	4.40 μM (±0.56)	5.21 μM (±0.30)
BDG	0.23 μM (±0.02)	0.23 μM (±0.13)	0.17 μM (±0.19)	0.19 μM (±0.23)	0.32 μM (±0.28)

Inhibition of UDPGDH by 6TP, 6TX, and 6TU was performed via a new UV/Vis method that was developed. The K_i values were determined for both UDPG and NAD^+ under varying concentrations; given the endogenous concentrations of NAD^+, only the varying UDPG K_i values are discussed. It is of note that the K_i values found upon varying NAD^+ conditions followed the same pattern as those of varying UDPG. The K_i values from these three purines revealed a fascinating pattern of hydroxylation and corresponding inhibition properties. It was found that 6-thiopurine possessed low inhibition character towards UDPGDH with a K_i of 288 μM. Interestingly, it was observed that 6-thiouric acid, the terminal excretion metabolite, possessed the greatest inhibition towards UDPGDH with a K_i of 7 μM in comparison to 288 μM for 6TP. This data set suggests that hydroxylation about the C2 and C8 positions might be pivotal in the inhibition of UDPGDH. Strikingly, when C2 is hydroxylated, inhibition is reduced by three-fold as observed with 6-thioxanthine.

To reveal the entire picture of hydroxylation effects about C2 and C8 with regards to UDPGDH inhibition, the assessment of 8OH-6TP was performed. While this compound is commercially available, its cost is academically prohibitive, and therefore a synthetic route was established. With a synthetic route in place, inhibition towards UDPGDH was performed, and it was found to have a K_i of 14 μM relative to varying UDPG concentration. Correlating the K_i values of the four excretion metabolites to the hydroxylation patterns suggests that the C8 hydroxyl has a greater inhibition character than C2 towards UDPGDH.

Inhibition assessment of these excretion metabolites towards UGT1A1 could not be accomplished through the same UV/Vis method. As such, a method was developed that allowed for baseline separation of all substrates and all glucuronide species. Illustrated in Fig. 7 line B shows the baseline separation of all substrates and products from UGT1A1 at 450 nm. The peaks for each bilirubin species is due to the multiple isomers of bilirubin; 3 for UCB, 2 for BMG1, 2 for BMG2, and 3 for BDG. To confirm that BMG1&2 and BDG are in fact the mono- and di-glucuronide species, a glucuronidase reaction was performed. In this, glucuronide groups are hydrolyzed to afford glucuronic acid and UCB, in this case. As observed in Fig. 7 line C, the glucuronidase experiment upon a pre-formed reaction mixture (Fig. 7 line B) showed the absences of any of the proposed glucuronide species that were previously observed, thereby confirming that the glucuronide formation was successful and that the method is sound. Additional confirmation on the identity of these peaks was drawn from other published methods [31–34].

With a method in place, inhibition screening by the excretion metabolites was undertaken. The bilirubin standard curve generated was found to have a linearity range of 2.5 μM to 8.5 μM. Quantification of bilirubin was accomplished from this standard curve with great accuracy and sensitivity. It is well documented that the glucuronide species formed from bilirubin are light sensitive, and prone to rapid degradation [21–23]. As such, generation of a standard curve of these species can be problematic and thereby prevent proper assessment of activity of UGT1A1 in the presence of our proposed inhibitors. This issue was circumnavigated given that the detectable moiety within these species is the bilirubin core; therefore, quantification of these species could be done through the bilirubin standard curve. Inhibition assessment of UGT1A1 by 6TP and 6TU was performed at two concentrations, but 6TX and 8OH-6TP were not screened, as 6TP and 6TU represent the two extremes of inhibition with regard to UDPGDH. The concentrations of the various bilirubin species were determined after a 45-min period at the varied purine concentration summarized in Table 1. From this, it can be concluded that there is no inhibition of UGT1A1 by either purine at varying concentrations over a 45 min period.

Table 2
Inhibition assessment of UGT1A1 with regards to varying 6TP and 6TU concentrations as quantified by UDPGA consumption. Each data set was run in triplicate with standard deviation values given in parentheticals.

	Duration of the Reaction		
	1-h	12-h	15-h
UDPGA Control	241 μM (±5.6)	110 μM (±0.06)	17 μM (±4.9)
RxN No Enzyme	252 μM (±5.6)	243 μM (±0.07)	253 μM (±5.6)
Full RxN	251 μM (±5.2)	245 μM (±0.21)	252 μM (±4.2)
75 μM 6TP	242 μM (±3.4)	128 μM (±3.08)	20 μM (±3.5)
75 μM 6TU	241 μM (±7.5)	125 μM (±0.05)	16 μM (±4.2)
50 μM 6TP	241 μM (±1.7)	130 μM (±0.05)	20 μM (±2.1)
50 μM 6TU	243 μM (±5.1)	128 μM (±2.16)	20 μM (±0.7)

It is well documented that 6TU remains in the body for more than 24 h post 6TP administration, and as such, one must consider that inhibition of the UGT1A1 occurs well beyond the 45-min experiment described above. Performing the inhibition experiment outlined previously through the quantification of the glucuronide species is not feasible due to the extreme sensitivity of the glucuronide compounds. Therefore, an indirect method to assess inhibition was undertaken through the quantification of UDPGA. Inhibition assessment was performed at the same concentrations of each purine as within the bilirubin assessment, but at varied reaction times of 1, 12, and 15 h. Statistical analysis of all inhibition studies towards UGT1A1 was performed, and it was concluded that all adjusted P-values are larger than 0.05, which indicates that there might be no difference between main effects of treatments and control, thereby verifying that 6TP and 6TU possess no inhibition properties towards UGT1A1 (Table 2).

In summary, we have proposed that the toxic side-effects associated with 6TP administration arises from the inhibition of either or both UDP-glucose dehydrogenase (UDPGDH) or UDP-glucuronosyl transferase (UGT1A1) by 6TP and/or its main excretion metabolites 6TU, 6TG, and/or 6TX. We directed our study towards the clearance of bilirubin, given that liver toxicity is one of the most commonly reported toxicities associated with 6TP administration. As such, the bilirubin pathway was investigated, and no inhibition was observed by both 6TP and 6TU over a 15-h period at concentrations that exceed drug dosing towards UGT1A1. However, inhibition by these purines, as well as the other excretion metabolites towards UDPGDH, was observed. Through these inhibition studies it was discovered that the hydroxylated C2 and C8 positions, namely 6TU, resulted in the greatest inhibition. Said inhibition will directly impact the levels of UDPGA that, in turn, will affect bilirubin conjugation and excretion. While C2 shows inhibition, no alteration at this site is possible as it is directly required for the formation of the nucleotide mimic for DNA incorporation – the primary therapeutic metabolite. The C8 position, on the contrary, can be studied for possible analog construction in the aims of reducing, if not eliminating, the toxicity associated from 6TP administration. Currently

work is being directed in the synthesis of new analogs about the C8 position that hopefully will possess reduced inhibition towards UDPGDH, but retain the therapeutic efficacy of 6-thiopurine.

Funding sources

This work could not have been undertaken without the gracious financial support from the Johnson Cancer Center of Kansas State University and Startup Capital from Kansas State University.

Conflict of interest

The authors declare that they have no conflicts of interest with the contents of the article.

Author contributions

CJW conducted nearly all of the experiments, analyzed the results, and helped write the manuscript. CMB helped with the initial stages of the bilirubin assay development. CC performed all statistical calculations for inhibitory assessment of UGT1A1. RJR conceived the idea for the project, helped with initial training, and wrote the paper; all authors edited and approved the manuscript.

Acknowledgements

We would like to thank Dr. James Mott of Shimadzu Scientific Instruments, Inc. for invaluable discussions on HPLC method development and instrument parameters. We would also like to thank Olivia Haney for technical writing aspects of this manuscript. This paper is dedicated in the memory of Lanny Rafferty.

Appendix A. Supplementary data

Supplementary data associated with this article can be found, in the online version, at https://doi.org/10.1016/j.jpba.2017.12.058.

References

[1] J.M. Torpy, C. Lynm, R.M. Glass, Acute lymphoblastic leukemia, JAMA 301 (4) (2009) 452.
[2] T. Tsuruo, H. Iida, S. Tsukagoshi, Y. Sakurai, Overcoming of vincristine resistance in P388 leukemia in vivo and in vitro through enhanced cytotoxicity of vincristine and vinblastine by verapamil, Cancer Res. 41 (5) (1981) 1967–1972.
[3] P.A.J. Speth, Q.G.C.M. van Hoesel, C. Haanen, Clinical pharmacokinetics of doxorubicin, Clin. Pharmacokinet. 15 (1) (1988) 15–31.
[4] K.R. Hande, Etoposide: four decades of development of a topoisomerase II inhibitor, Eur. J. Cancer 34 (10) (1998) 1514–1521.
[5] N.S. Elbarbary, E.A.R. Ismail, R.K. Farahat, M. El-Hamamsy, ω-3 fatty acids as an adjuvant therapy ameliorates methotrexate-induced hepatotoxicity in children and adolescents with acute lymphoblastic leukemia: a randomized placebo-controlled study, Nutrition 32 (1) (2016) 41–47.
[6] A.d.B. Tiphaine, L.L. Hjalgrim, J. Nersting, J. Breitkreutz, B. Nelken, M. Schrappe, M. Stanulla, C. Thomas, Y. Bertrand, G. Leverger, A. Baruchel, K. Schmiegelow, E. Jacqz-Aigrain, Evaluation of a pediatric liquid formulation to improve 6-mercaptopurine therapy in children, Eur. J. Pharm. Sci. 83 (2016) 1–7.
[7] A.F. Hawwa, J.S. Millership, P.S. Collier, K. Vandenbroeck, A. McCarthy, S. Dempsey, C. Cairns, J. Collins, C. Rodgers, J.C. McElnay, Pharmacogenomic studies of the anticancer and immunosuppressive thiopurines mercaptopurine and azathioprine, Br. J. Clin. Pharmacol. 66 (4) (2008) 517–528.
[8] X. Yuan, E. Gavriilaki, J.A. Thanassi, G. Yang, A.C. Baines, S.D. Podos, Y. Huang, M. Huang, R.A. Brodsky, Small-molecule factor D inhibitors selectively block the alternative pathway of complement in paroxysmal nocturnal hemoglobinuria and atypical hemolytic uremic syndrome, Haematologica 102 (2017) 466–475.
[9] P. Karran, N. Attard, Thiopurines in current medical practice: molecular mechanisms and contributions to therapy-related cancer, Nat. Rev. Cancer 8 (1) (2008) 24–36.
[10] K. Rowland, L. Lennard, J.S. Lilleyman, In vitro metabolism of 6-mercaptopurine by human liver cytosol, Xenobiotica 29 (6) (1999) 615–628.
[11] T. Dervieux, J.G. Blanco, E.Y. Krynetski, E.F. Vanin, M.F. Roussel, M.V. Relling, Differing contribution of thiopurine methyltransferase to mercaptopurine: thioguanine effects in human leukemic cells, Cancer Res. 61 (15) (2001) 5810–5816.
[12] J.A. Nelson, J.W. Carpenter, L.M. Rose, D.J. Adamson, Mechanisms of action of 6-thioguanine, 6-mercaptopurine, and 8-azaguanine, Cancer Res. 35 (10) (1975) 2872–2878.
[13] S. Haglund, J. Taipalensuu, C. Peterson, S. Almer, IMPDH activity in thiopurine-treated patients with inflammatory bowel disease –relation to TPMT activity and metabolite concentrations, Br. J. Clin. Pharmacol. 65 (1) (2008) 69–77.
[14] D.M. Tidd, A.R.P. Paterson, A biochemical mechanism for the delayed cytotoxic reaction of 6-mercaptopurine, Cancer Res. 34 (4) (1974) 738–746.
[15] L. Chouchana, A.A. Fernández-Ramos, F. Dumont, C. Marchetti, I. Ceballos-Picot, P. Beaune, D. Gurwitz, M.-A. Loriot, Molecular insight into thiopurine resistance: transcriptomic signature in lymphoblastoid cell lines, Genome Med. 7 (1) (2015) 37.
[16] T. Dervieux, T.L. Brenner, Y.Y. Hon, Y. Zhou, M.L. Hancock, J.T. Sandlund, G.K. Rivera, R.C. Ribeiro, J.M. Boyett, C.-H. Pui, M.V. Relling, W.E. Evans, De novo purine synthesis inhibition and antileukemic effects of mercaptopurine alone or in combination with methotrexate in vivo, Blood 100 (4) (2002) 1240–1247.
[17] J.M. Carethers, M.T. Hawn, D.P. Chauhan, M.C. Luce, G. Marra, M. Koi, C.R. Boland, Competency in mismatch repair prohibits clonal expansion of cancer cells treated with N-methyl-N′-nitro-N-nitrosoguanidine, J. Clin. Invest. 98 (1) (1996) 199–206.
[18] P. Pacher, A. Nivorozhkin, C. Szabó, Therapeutic effects of xanthine oxidase inhibitors: renaissance half a century after the discovery of allopurinol, Pharmacol. Rev. 58 (1) (2006) 87–114.
[19] M. Einhorn, I. Davidsohn, Hepatotoxicity of mercaptopurine, JAMA 188 (9) (1964) 802–806.
[20] S.P. Roche, R. Kobos, Jaundice in the adult patient, Am. Fam. Physician 69 (2) (2004) 299–308.
[21] G. Ma, J. Lin, W. Cai, B. Tan, X. Xiang, Y. Zhang, P. Zhang, Simultaneous determination of bilirubin and its glucuronides in liver microsomes and recombinant UGT1A1 enzyme incubation systems by HPLC method and its application to bilirubin glucuronidation studies, J. Pharm. Biomed. Anal. 92 (2014) 149–159.
[22] D. Zhang, T.J. Chando, D.W. Everett, C.J. Patten, S.S. Dehal, W.G. Humphreys, In vitro inhibition of UDP glucuronosyltransferase by atazanavir and other HIV protease inhibitors and the relationship of this property to in vivo bilirubin glucuronidation, Drug Metab. Dispos. 33 (11) (2005) 1729–1739.
[23] J. Zhou, T.S. Tracy, R.P. Remmel, Correlation between bilirubin glucuronidation and estradiol-3-gluronidation in the presence of model UDP-glucuronosyltransferase 1A1 substrates/inhibitors, Drug Metab. Dispos. 39 (2) (2011) 322–329.
[24] M. Vögelin, L. Biedermann, P. Frei, S.R. Vavricka, S. Scharl, J. Zeitz, M.C. Sulz, M. Fried, G. Rogler, M. Scharl, The impact of azathioprine-associated lymphopenia on the onset of opportunistic infections in patients with inflammatory bowel disease, PLoS One 11 (5) (2016) e0155218.
[25] E.A. Hullah, P.A. Blaker, A.M. Marinaki, M.P. Escudier, J.D. Sanderson, A practical guide to the use of thiopurines in oral medicine, J. Oral Pathol. Med. 44 (10) (2015) 761–768.
[26] P.P. Siva, K.M. Murali, A. Deepak, S. Murali, S. Michael, M. Sandhya, A novel liquid chromatography tandem mass spectrometry method for the estimation of bilirubin glucuronides and its application to in vitro enzyme assays, Drug Metab. Lett. 10 (4) (2016) 264–269.
[27] N.R. Beattie, N.D. Keul, A.M. Sidlo, Z.A. Wood, Allostery and hysteresis are coupled in human UDP-glucose dehydrogenase, Biochemistry 56 (1) (2017) 202–211.
[28] M. Kakehi, Y. Ikenaka, S.M.M. Nakayama, Y.K. Kawai, K.P. Watanabe, H. Mizukawa, K. Nomiyama, S. Tanabe, M. Ishizuka, Uridine diphosphate-glucuronosyltransferase (UGT) xenobiotic metabolizing activity and genetic evolution in pinniped species, Toxicol. Sci. 147 (2) (2015) 360–369.
[29] Z. Kaleta, B.T. Makowski, T. Soós, R. Dembinski, Thionation using Fluorous Lawesson's reagent, Org. Lett. 8 (8) (2006) 1625–1628.
[30] H.C. Koppel, R.K. Robins, Potential purine antagonists. XIII. Synthesis of some 8-methylpurines1, J. Organ. Chem. 23 (10) (1958) 1457–1460.
[31] T.K. Tam, B. Chen, C. Lei, J. Liu, In situ regeneration of NADH via lipoamide dehydrogenase-catalyzed electron transfer reaction evidenced by spectroelectrochemistry, Bioelectrochem. (Amsterdam, Netherlands) 86 (2012) 92–96.

JOURNAL OF NATURAL PRODUCTS

Article

Cite This: J. Nat. Prod. 2017, 80, 3234−3240

pubs.acs.org/jnp

Total Synthesis of Reniochalistatin E

Anthony Fatino, Giovanna Baca, Chamitha Weeramange, and Ryan J. Rafferty*

Department of Chemistry, Kansas State University, Manhattan, Kansas 66506, United States

Supporting Information

ABSTRACT: Reniochalistatin E (**1**) is one of the five related cyclic peptides isolated from the marine sponge *Reniochalina stalagmitis*. The discovery of these compounds resulted from a screening program directed toward the identification of proline-rich bioactive compounds. Reniochalistatin E is the only member of the family to possess a tryptophan amino acid residue. Given the cytotoxicity observed for **1**, efforts were directed toward developing a synthetic route to **1**. The first total synthesis of **1** has been accomplished in a 15-step route in an overall 5.0% yield. The synthetic sample of reniochalistatin E was shown to have similar activity toward HeLa and RPMI-8226 cell lines compared to the natural sample, with IC_{50} values of 16.9 vs 17.3 μM and 4.5 vs 4.9 μM, respectively. Interestingly, both of the fully deprotected octapeptides constructed toward the synthesis of reniochalistatin E were shown to have cytotoxicity. The route provides a means to probe the structure−activity relationship of **1** and further biological investigations.

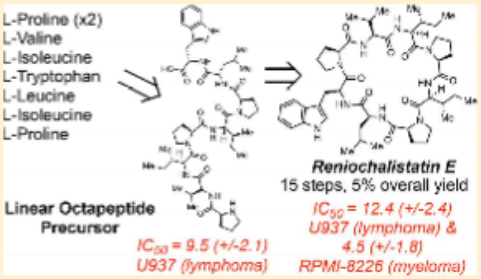

The reniochalistatin family of cyclic peptides was isolated from the marine sponge *Reniochalina stalagmitis* near Yongxing Island in the South China Sea in 2014 by Lin and co-workers.[1] The family was discovered as part of a screening program designed to find new bioactive cyclic peptides from marine sponges in the South China Sea.[2−5] Cyclic peptides that are proline-rich have been shown to have a variety and wide scope of biological activity, such as antiviral, antitumor, antimicrobial, and general cytotoxic properties.[6−8] The members of the reniochalstatin family were found to be proline-rich and composed of apolar and aromatic amino acid residues. Leucine and isoleucine are present in all five members, along with multiple proline units (two within reniochalistatins A, B, and C and three within D and E). The aromatic amino acid residue varies among the members of the family; B, C, and D contain phenylalanine, whereas E is the only one with a tryptophan residue.[8] Reniochalistatins A through D are cyclic heptaptides, whereas E is the only cyclic octapeptide that was isolated. Only reniochalistatin E showed biological activity, with cytotoxicity toward myeloma (RPMI-8226, IC_{50} of 4.9 μM) and gastric (MGC-803, IC_{50} of 9.7 μM) cancer cell lines. It was the activity toward myeloma that drew the attention of our laboratory and resulted in a total synthesis campaign to be undertaken.

We envisioned that **1** could be synthesized via successive amino acid couplings in tandem with selective deprotection steps. The cyclic compound could be obtained from the coupling and macrocyclization of the two desired tetrapeptides (**2** and **3**). Each of these tetrapeptides could be constructed from their corresponding commercially available L-amino acids, with selective protection about either the free carboxylic acid or amine (Scheme 1).

According to the retrosynthetic plan outlined in Scheme 1, efforts were directed toward the construction of tetrapeptide **2** (Scheme 2). Starting from the Boc-protected L-isoleucine (**4**) an amidation was performed though a benzotriazole-L-yl-oxy-tris-pyrrolidino-phosphonium hexafluorophosphate (PyBOP)-mediated coupling with the methyl ester of L-proline (**5**), affording the dipeptide **6** in 92% yield. Analogously, Boc-L-leucine (**7**) was coupled to the methyl ester of L-tryptophan (**8**) under the same conditions to access dipeptide **9** in 97% yield. Saponification of dipeptide **6** furnished the free acid **10**, and Boc deprotection of **9** accessed the amine hydrochloride salt **11**. Both reactions provided quantitative yields. The coupling of these two dipeptides was accomplished with PyBOP under standard conditions to give tetrapeptide **2** in 55% yield. Employing 1-ethyl-3-(3′-dimethylaminopropyl)carbodiimide hydrochloride (EDC·HCl) with HOBt as the coupling conditions, yields were optimized at 86%.

With tetrapeptide **2** in hand, efforts were directed toward the construction of tetrapeptide **3** (Scheme 3), which will allow for access to **1**. The coupling of Boc-L-proline (**12**) to the methyl ester of L-leucine (**13**) was performed with PyBOP to furnish the dipeptide **14** in 97% yield. Saponification of **14** gave access to the free acid dipeptide **15** in quantitative yields. The second half of the tetrapeptide was accessed from the Boc deprotection of dipeptide **6** in quantitative yield. The coupling of **15** to **16** under the previously employed PyBOP conditions afforded the desired tetrapeptide **3**, but unfortunately as an impure mixture based upon the ^{1}H NMR spectrum obtained. All attempts at

Received: July 29, 2017
Published: December 8, 2017

DOI: 10.1021/acs.jnatprod.7b00656
J. Nat. Prod. 2017, 80, 3234−3240

Scheme 1. Retrosynthetic Approach to Reniochalistatin E

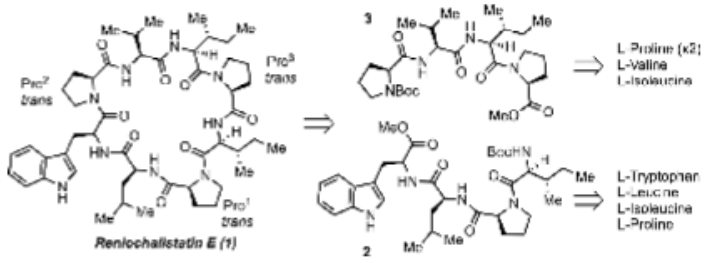

Scheme 2. Assembly of Tetrapeptide 2 with Successive PyBOP Coupling and Deprotection Steps

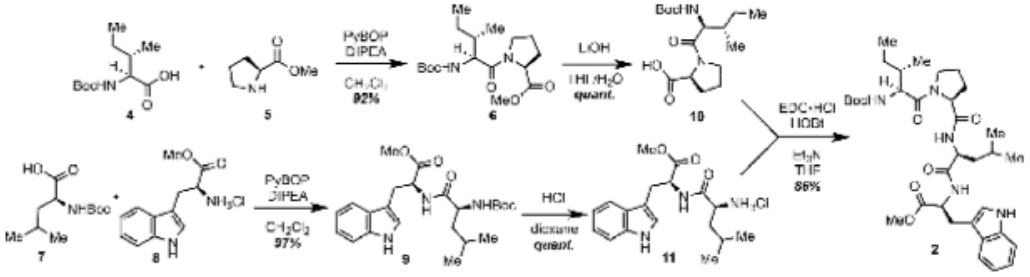

Scheme 3. Construction of Tetrapeptide 3 through Successive Amide Forming Coupling Reactions along with Deprotection Steps

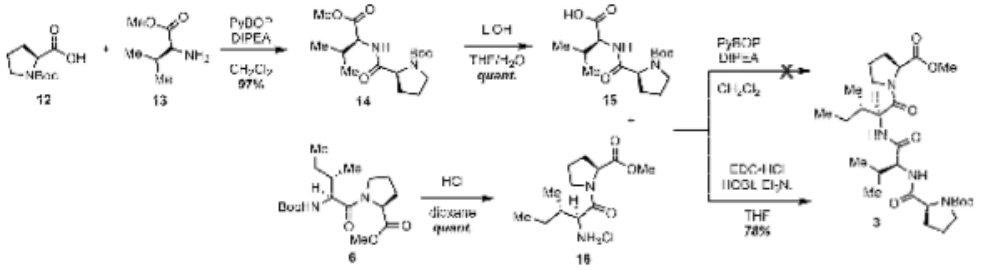

Scheme 4. Tetrapeptide Couplings and Cyclization Strategies Accessing Reniochalistatin E (1)

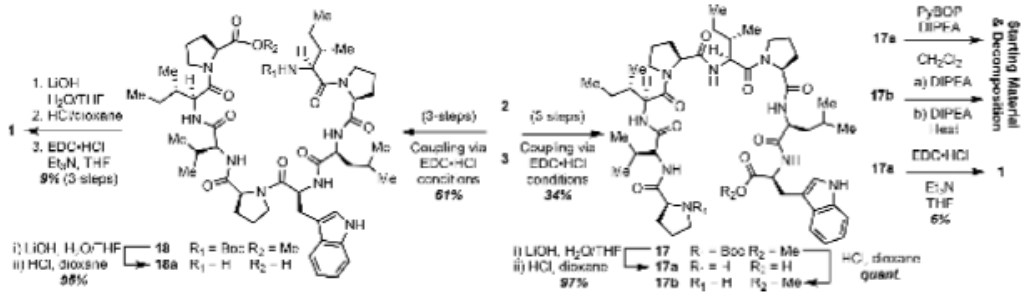

purification (workup procedures, chromatographic eluents, and silica) of this material continued to provide the same contaminant peaks within the acquired ^{1}H NMR spectrum. When this material was carried forward, either through saponification or Boc deprotection, none of the desired material was collected. Pure tetrapeptide **3** was successfully accessed through the use of EDC·HCl and HOBt in 78% yield.

DOI: 10.1021/acs.jnatprod.7b00656
J. Nat. Prod. 2017, 80, 3234−3240

Having accessed both of the desired tetrapeptides **2** and **3**, the coupling and macrocyclization were performed. The initial approach to the linear octapeptide of **1** was through the saponification of **2** and the Boc deprotection of **3**. Coupling of the free acid of **2** to the free base of **3** with EDC·HCl furnished octapeptide **17** in 34% yield over three steps (Scheme 4). Compound **17** was subjected to saponification followed by Boc deprotection to afford its fully deprotected form **17a** in 97% yield. The attempted macrocyclization of this material under PyBOP conditions failed to provide any of the desired product, but rather resulted in the return of starting material (55%) and decomposition. It is hypothesized that the bulk of both the secondary amine within the proline residue and the BOP-activated ester of the tryptophan residue could provide sufficient steric congestion, thereby preventing cyclization from occurring. To reduce the steric hindrance about these centers, aminolysis was then attempted for ring closure. For this, the Boc group on **17** was removed to afford **17b**, with the methyl ester intact. Unfortunately, all attempts at cyclization in this fashion failed to provide **1** and resulted in the return of starting material (67%) and decomposition. Recognizing the difficulty in macrocyclization of these two sterically encumbered proline and tryptophan residues of **17a**, it was envisioned that coupling of these two centers to access the linear octapeptide would be more attainable followed then by macrocyclization. As such, **2** was saponified to its free acid and Boc deprotection of **3** afforded the free amine, both accomplished in quantitative yields. The EDC·HCl coupling of these two units furnished the linear octapeptide **18** in 61% yield over three steps. Compound **18** was transformed into its free acid and free amine counterpart in 95% yield and then subjected to EDC·HCl coupling conditions to afford the desired natural product **1** in 9% yield. The ^{1}H and ^{13}C NMR spectra as well as the MS data of the synthesized **1** match with the literature data (see the Supporting Information). Confirmation of the *trans* prolines within **1** was confirmed based on the comparison of the reported $\Delta\delta_{C\beta\text{-}C\gamma}$ values of proline residues (4.9, 4.2, and 4.1 ppm for Pro,[1] Pro,[2] and Pro,[3] respectively). The successful macrocyclization of the free acid/amine of **18** with EDC·HCl on the first attempt led us to attempt the same conditions for cyclization upon the unsuccessful closure of the free acid/amine of **17**. To our surprise, treating **17a** with EDC·HCl afforded reniochalistatin E in 6% yield. All spectroscopic (NMR and IR) and MS data matched both the literature and the previously synthesized material.

Screening various coupling reagents and conditions was then performed to increase the yield of **1** (Table 1). Entries 1 and 9 highlight the coupling affording **1** outlined in Scheme 4 from **17a** and **18a**, respectively. The attempted PyBOP-mediated coupling of **18a** (entry 8) provided only recovered starting material (78%) and decomposition. Employing HOBt, a commonly used additive in peptide couplings, with EDC·HCl to cyclize **17a** and **18a** (entries 2 and 10) resulted in low yields of **1** of 2% and 6%, respectively. Entry 10 reflects the highest yield of **1** in our synthetic approach via **18a**. Next, macrocyclization was attempted employing 3-(diethoxyphosphoroyloxyl)-1,2,3-benzotriazine-4(3*H*)-one (DEPBT), a reagent that has been successful in the cyclization of similar amino acid based macrocycles.[9] Unfortunately, all attempts at cyclization with this reagent of **17a** and **18a** (entries 3 and 11) as well as using cesium chloride as an additive to promote carbonyl coordination (entries 4 and 12) failed to provide **1** in any increased yield. Uronium-based coupling reagents are well reported for their success in macrocyclizations, and as such, *N,N,N′,N′*-tetramethyl-*O*-(1*H*-benzotriazol-1-yl)uronium hexafluorophosphate (HBTU)[10−13] and *N,N,N′,N′*-tetramethyl-*O*-(1*H*-benzotriazol-1-yl)uronium tetrafluoroborate (TBTU)[13−16] were both attempted with **17a** and **18a** in the absence and presence of 4-(dimethylamino)pyridine (DMAP).[17,18] In all attempted cyclizations, these uronium-based reagents provided either none or low yields of **1**. Employing HBTU with DMAP to cyclize **18a** provided a 13% yield of **1** (entry 14), but in our hands, EDC·HCl with HOBt gave the best, albeit low, 15% yield of the natural product.

Table 1. Screening of Coupling Conditions of Fully Deprotected 17a and 18a

entry	cmpd	coupling agent	additive	result
1	**17a**	EDC·HCl	N/A	6%
2		EDC·HCl	HOBt	8%
3		DEBPT	N/A	
4		DEBPT	CsCl	
5		HBTU	N/A	
6		HBTU	DMAP	4%
7		TBTU	DMAP	trace
8	**18a**	PyBOP	N/A	trace
9		EDC·HCl	N/A	9%
10		EDC·HCl	HOBt	15%
11		DEBPT	N/A	
12		DEBPT	CsCl	5%
13		HBTU	N/A	
14		HBTU	DMAP	13%

With reniochalistatin E and numerous di-, tetra-, and octapeptides in both fully protected and deprotected states in hand, all compounds were screened for general cytotoxicity against six human cancer cell lines (A549, lung; HeLa, cervical; MiaPaca, pancreatic; U937, lymphoma, RPMI-8226, myeloma; and MM.1R, multiple myeloma). None of the di- or tetrapeptides in protected and partial deprotected states were found to have IC_{50} values lower than 30 μM against these cell lines. Our synthetic sample of reniochalistatin E possessed approximately the same IC_{50} value toward the HeLa and RPMI-8226 cell lines: IC_{50} of 16.9 μM ($\pm$1.9) relative to the reported 17.3 μM in HeLa and an IC_{50} of 4.5 ($\pm$2.2) relative to the reported 4.9 μM in RPMI-8226 (Table 1). Reniochalistatin E lacked cytotoxicity against all of the tested cell lines (cytotoxicity = IC_{50} < 10 μM). Both **17** and **18**, diprotected octapeptides, were shown to have no cytotoxicity. Interestingly, the free acid/amine **17a** was shown to have borderline cytotoxicity toward the U937 cell line with an IC_{50} of 9.5 $\pm$ 2.1 μM. In comparison to the free acid/amine **18a**, no cytotoxicity was observed. No further investigational studies at this time have been performed that could draw conclusions regarding structure−activity relationships based upon the results obtained.

In conclusion, we have accomplished the first total synthesis of reniochalistatin E in 15 steps with an overall 5.0% yield from commercially available materials. Cytotoxicity studies with reniochalistatin E and all intermediates accessed within the route revealed a general lack of cytotoxicity. However, the synthetic and isolated reniochalistatin E are shown to possess nearly the same activity toward the HeLa cervical cancer cell line, further supporting the total synthesis outlined herein. In addition, an interesting and unexpected cytotoxicity was observed for the free acid/amine of **17a** (linear octapeptide precursors to the natural product) toward the U937 cell line. With a route established to this cyclic octapeptide, efforts are

DOI: 10.1021/acs.jnatprod.7b00656
J. Nat. Prod. 2017, 80, 3234−3240

Table 2. Evaluation of Reniochalistatin E and Linear Octapeptides for Cytotoxicity

	observed IC_{50} (μM)[a]					
cmpd	A549	HeLa	MiaPaca	U937	RPMI-8226	MM.1R
1	>20	16.9 ± 1.9	>20 μM	12.4 ± 2.4	4.5 ± 1.8	>11.2 ± 1.0
17	>20	>20	19.1 ± 1.3	>20	>20	>20
17a	>20	>20	>20	9.5 ± 2.1	>20	>20
18	>20	>20	>20	>20	>20	>20
18a	>20	18.4 ± 1.7	>20	>20	16.4 ± 3.5	>20

[a]Cytotoxicity evaluated in 384-well plates, 1500 (2000 U937) cells/well, 72 h incubation period, and evaluated via Alamar Blue.

currently being pursued toward probing the effects of single amino acid variations as well as the transposition of phenylalanine for tryptophan. The resulting analogues of **1** will be evaluated for cytotoxicity.

EXPERIMENTAL SECTION

General Experimental Procedures. Optical rotations were measured on an Atago Polax-2L polarimeter with a sodium lamp. IR spectra were recorded on a Cary 630 FT-IR spectrometer as thin films. Only the strongest and/or structurally important absorptions of IR spectra were reported in wavenumbers (cm^{-1}). ^1H (400, 500 MHz) and ^{13}C (100, 151 MHz) spectra were obtained on Varian and Bruker-Ascend spectrometers. The chemical shifts are given in parts per million (ppm) relative to residual $CHCl_3$ at δ 7.26 ppm for proton spectra and relative to $CDCl_3$ at δ 77.23 ppm for carbon spectra, unless otherwise noted. High-resolution mass spectra were obtained using an LCT Premier time-of-flight mass spectrometer. Flash column chromatography was performed with silica gel grade 60 (230–400 mesh). Dichloromethane (CH_2Cl_2), tetrahydrofuran (THF), toluene (PhMe), *N*,*N*-dimethylformamide (DMF), CH_3CN, triethylamine (Et_3N), and MeOH were all degassed with argon and passed through a solvent purification system containing alumina or molecular sieves. All commercially available reagents were used as received.

***N*-Boc-L-Ile-L-Pro-OMe (6).** To a stirring solution of *N*-Boc-L-isoleucine (**4**; 1.0 g, 4.16 mmol, 1.0 equiv) in CH_2Cl_2 (42 mL) were added PyBOP (2.27 g, 4.37 mmol, 1.05 equiv) and iPr_2EtN (1.09 mL, 6.24 mmol, 1.5 equiv). To a separate round-bottom flask (RBF) were added L-proline methyl ester (**5**; 1.03 g, 6.24 mmol, 1.5 equiv), iPr_2EtN (2.17 mL, 12.48 mmol, 3.0 equiv), and CH_2Cl_2 (6.3 mL). Both reaction mixtures were left to stir for 1 h, at which time they were combined and left to stir overnight at room temperature (rt). The reaction was quenched with 1 M HCl (1 vol equiv), and the product was extracted with CH_2Cl_2 (×2), washed with $NaHCO_{3(satd)}$, dried over sodium sulfate, and concentrated under reduced pressure. The crude material was purified via flash silica gel chromatography (1:2 EtOAc/hexane) to afford **6** (1.30 g, 92% yield): $[\alpha]_D^{25}$ +40.3 (*c* 1.23, $CHCl_3$); IR (film) ν_{max} 3436, 2973, 1746, 1642, 1436, 1217 cm^{-1}; ^1H NMR ($CDCl_3$, 400 MHz) δ 5.11 (d, *J* = 9.5 Hz, 1H), 4.52–4.44 (m, 1H), 4.24 (dd, *J* = 9.5, 7.2 Hz, 1H), 3.80–3.73 (m, 1H), 3.66 (s, 3H), 3.65–3.58 (m, 1H), 2.22–2.12 (m, 1H), 2.01–1.90 (m, 3H), 1.71 (ddq, *J* = 10.3, 6.5, 3.5 Hz, 1H), 1.53 (td, *J* = 7.2, 6.6, 3.2 Hz, 1H), 1.37 (s, 9H), 1.07 (ddd, *J* = 13.4, 6.7, 2.3 Hz, 1H), 0.96 (d, *J* = 6.8 Hz, 3H), 0.86 (t, *J* = 7.4 Hz, 3H); ^{13}C NMR ($CDCl_3$, 101 MHz) δ 172.64, 171.65, 156.01, 79.70, 59.04, 56.46, 52.35, 47.42, 38.13, 29.29, 28.56, 25.17, 24.38, 15.47, 11.46; HRESIMS *m*/*z* 343.2193 $[M + H]^+$ (calcd for $C_{17}H_{30}N_2O_5$, 343.2188).

***N*-Boc-L-Leu-L-Trp-OMe (9).** To a stirring solution of compound *N*-Boc-L-leucine (**7**; 1.0 g, 4.32 mmol, 1.0 equiv) in CH_2Cl_2 (43 mL) were added PyBOP (2.36 g, 4.54 mmol, 1.05 equiv) and iPr_2EtN (1.13 mL, 6.48 mmol, 1.5 equiv). To a separate RBF were added L-tryptophan methyl ester (**8**; 1.65 g, 6.48 mmol, 1.5 equiv), iPr_2EtN (2.26 mL, 12.96 mmol, 3.0 equiv), and CH_2Cl_2 (6.5 mL). Both reaction mixtures were left to stir for 1 h, at which time they were combined and left to stir overnight at rt. The reaction was quenched with 1 M HCl (1 vol equiv), and the product was extracted with CH_2Cl_2 (×2), washed with $NaHCO_{3(satd)}$, dried over sodium sulfate, and concentrated under reduced pressure. The crude material was purified via flash silica gel chromatography (1:1 EtOAc/hexane) to afford **9** (1.81 g, 97% yield): $[\alpha]_D^{25}$ +27 (*c* 0.15, $CHCl_3$); IR (film) ν_{max} 3418, 3018, 2872, 1739, 1513, 1215 cm^{-1}; ^1H NMR (400 MHz, DMSO-d_6) δ 10.85 (s, 1H), 8.06 (d, *J* = 7.4 Hz, 1H), 7.45 (d, *J* = 7.9 Hz, 1H), 7.31 (d, *J* = 8.1 Hz, 1H), 7.13 (d, *J* = 2.4 Hz, 1H), 7.07–7.02 (m, 1H), 6.96 (td, *J* = 7.5, 6.9, 1.1 Hz, 1H), 6.82 (d, *J* = 8.5 Hz, 1H), 4.51 (q, *J* = 7.1 Hz, 1H), 3.98 (td, *J* = 8.7, 6.0 Hz, 1H), 3.55 (s, 3H), 3.13–3.05 (m, 2H), 1.53 (dd, *J* = 13.6, 6.9 Hz, 2H), 1.35 (s, 9H), 1.26 (s, 1H), 0.84 (d, *J* = 6.6 Hz, 3H), 0.81 (d, *J* = 6.5 Hz, 3H); ^{13}C NMR (101 MHz, $CDCl_3$) δ 172.99, 172.44, 155.95, 136.45, 127.76, 123.62, 122.15, 119.58, 118.63, 111.71, 109.49, 80.22, 53.46, 53.29, 52.54, 41.55, 28.52, 27.81, 24.92, 23.18, 22.04; HRESIMS *m*/*z* 454.2308 $[M + Na]^+$ (calcd for $C_{23}H_{33}N_3O_5Na^+$, 454.2312).

***N*-Boc-L-Ile-L-Pro-OH (10).** To a stirring solution of **6** (556 mg, 1.62 mmol, 1.0 equiv) in 1:1 THF/H_2O (16 mL) was added LiOH (194 mg, 8.12 mmol, 5.0 equiv). The mixture was left to stir at rt for 5 h. The reaction was quenched with 1 M HCl (1 vol equiv), and the product was extracted with CH_2Cl_2, washed with $NaHCO_{3(satd)}$, dried over sodium sulfate, and concentrated under reduced pressure. The product **10** was obtained in quantitative yield as an oily residue, which was used without further purification. IR (film) ν_{max} 3456, 3304, 2977, 1704, 1314 cm^{-1}; ^1H NMR (400 MHz, $CDCl_3$) δ 8.31 (s, 1H), 5.35 (d, *J* = 9.5 Hz, 1H), 4.57 (t, *J* = 6.4 Hz, 1H), 4.32–4.25 (m, 1H), 3.82 (dt, *J* = 9.6, 7.2 Hz, 1H), 3.64 (ddd, *J* = 9.7, 7.5, 5.4 Hz, 1H), 2.18 (dd, *J* = 10.0, 3.9 Hz, 2H), 2.07–1.99 (m, 2H), 1.76 (td, *J* = 7.0, 3.4 Hz, 1H), 1.64–1.48 (m, 2H), 1.41 (d, *J* = 7.7 Hz, 9H), 0.95 (d, *J* = 6.7 Hz, 3H), 0.87 (t, *J* = 7.2 Hz, 3H).

***N*-Boc-L-Leu-L-Trp-OH (11).** To a RBF was added 1 M HCl in dioxane (4.6 mL), which cooled to 0 °C, at which point **9** (500 mg, 1.16 mmol) was added. The reaction was allowed to stir for 1.5 h. The solvent was removed under reduced pressure to afford a crude white solid (**11**), which was used without further purification. IR (film) ν_{max} 3416, 2879, 1651, 1176 cm^{-1}; ^1H NMR (400 MHz, DMSO-d_6) δ 9.04 (d, *J* = 7.2 Hz, 1H), 8.25 (s, 3H), 7.49 (d, *J* = 7.8 Hz, 1H), 7.35 (dt, *J* = 8.1, 1.0 Hz, 1H), 7.24 (d, *J* = 2.3 Hz, 1H), 7.07 (ddd, *J* = 8.1, 7.0, 1.3 Hz, 1H), 7.00 (ddd, *J* = 8.0, 7.0, 1.1 Hz, 1H), 4.63–4.54 (m, 1H), 3.81 (t, *J* = 7.2 Hz, 1H), 3.58 (s, 3H), 3.21–3.13 (m, 2H), 1.68 (dt, *J* = 13.3, 6.6 Hz, 2H), 1.57 (s, 2H), 0.90 (dd, *J* = 7.9, 6.4 Hz, 6H).

***N*-Boc-L-Ile-L-Pro-L-Leu-L-Trp-OMe (2).** Compound **10** (1.32 g, 4.02 mmol, 1 equiv), compound **11** (1.08 g, 2.94 mmol, 1 equiv), and HOBt (473 mg, 3.09 mmol, 1.05 equiv) were dissolved in dry THF (40 mL) at rt under an argon atmosphere. The solution was cooled to 0 °C and stirred for 20 min, after which Et_3N (1.43 mL, 10.29 mmol, 3.5 equiv) was then added and stirred. Lastly, 20 min later EDC·HCl (592 mg, 3.09 mmol, 1.05 equiv) was added, and the reaction mixture was left to stir overnight. The reaction was quenched with H_2O (1 vol equiv), and the product was extracted with CH_2Cl_2, dried over sodium sulfate, and concentrated under reduced pressure. The crude material was purified via flash silica gel chromatography (3:1 EtOAc/hexane) to give afford **2** (2.22 g, 86% yield) as a clear liquid: $[\alpha]_D^{25}$ +48.1 (*c* 1.75, $CHCl_3$); IR (film) ν_{max} 3305, 3017, 2876, 1741, 1631, 1506, 1392, 1215 cm^{-1}; ^1H NMR ($CDCl_3$, 400 MHz) δ 8.29 (s, 1H), 7.51 (d, *J* = 8.6 Hz, 1H), 7.33 (d, *J* = 8.0 Hz, 1H), 7.16 (td, *J* = 8.2, 7.6, 1.3 Hz, 1H), 7.13–7.05 (m, 1H), 7.03 (d, *J* = 2.4 Hz, 1H), 6.97 (d, *J* = 7.8 Hz, 1H), 6.70 (d, *J* = 7.9 Hz, 1H), 5.20 (d, *J* = 9.4 Hz, 1H), 4.90 (dt, *J* = 7.9, 5.5 Hz, 1H), 4.37 (d, *J* = 6.0 Hz, 1H), 4.27 (dd, *J* = 9.3, 7.0 Hz, 1H), 3.71 (d, *J* = 8.9 Hz, 1H), 3.66 (s, 3H), 3.60–3.51 (m, 1H), 3.30 (d, *J* = 5.5 Hz, 2H), 2.12–1.87 (m, 3H), 1.73–1.56 (m, 5H), 1.43 (s, 9H), 1.13–1.05 (m, 1H), 0.92 (d, *J* = 6.8 Hz, 3H), 0.90–0.80 (m, 11H); ^{13}C NMR ($CDCl_3$, 101 MHz) δ 172.86, 172.49, 172.08, 171.74, 156.08, 136.32, 127.75, 123.57, 122.11,

DOI: 10.1021/acs.jnatprod.7b00656
J. Nat. Prod. 2017, 80, 3234–3240

119.61, 118.60, 111.55, 109.58, 79.89, 60.26, 56.61, 52.95, 52.56, 52.15, 47.99, 41.15, 37.95, 28.60, 25.58, 27.76, 25.31, 24.79, 24.42, 23.10, 23.05, 22.06, 15.65, 11.31; HRESIMS m/z 642.3817 $[M + H]^+$ (calcd for $C_{34}H_{52}N_5O_7$, 642.3822).

***N*-Boc-L-Pro-L-Val-OMe (14).** Compounds **12** (3.0 g, 13.94 mmol, 1 equiv) and **13** (2.34 g, 13.94 mmol, 1 equiv) were added to a stirring solution of HOBt (2.24 g, 14.63 mmol, 1.05 equiv) in dry THF (139 mL) at rt under an argon atmosphere. The solution was then cooled to 0 °C and stirred for 20 min, after which Et_3N (6.8 mL, 48.79 mmol, 3.5 equiv) was added. After an additional 20 min of stirring EDC·HCl (2.8 g, 14.63 mmol, 1.05 equiv) was added, and the reaction mixture was left to stir overnight. The reaction was quenched with H_2O (1 vol equiv), and the product was extracted with CH_2Cl_2, dried over sodium sulfate, and concentrated under reduced pressure. The crude material was purified via flash silica gel chromatography (1:1 EtOAc/hexane) to give **14** (4.45 g, 97% yield) as a clear liquid: $[\alpha]_D^{25}$ = +80.8 (c 2.05, $CHCl_3$); IR (film) ν_{max} 3680, 3323, 3415, 2973, 2879, 1740, 1681, 1216 cm^{-1}; ^1H NMR ($CDCl_3$, 400 MHz) δ 4.50 (dd, J = 8.6, 5.1 Hz, 1H), 4.32 (s, 1H), 3.72 (s, 3H), 3.42 (s, 2H), 2.29 (s, 1H), 2.15 (pd, J = 6.9, 5.1 Hz, 2H), 1.95−1.84 (m, 3H), 1.48 (s, 9H), 0.92 (dd, J = 8.3, 6.8 Hz, 6H); ^{13}C NMR (DMSO-d_6, 101 MHz) δ 172.71, 78.98, 59.71, 58.16, 52.30, 47.18, 31.67, 30.41, 28.80, 28.68, 23.61, 19.77, 18.99, 14.76; HRESIMS m/z 329.2025 $[M + H]^+$ (calcd for $C_{16}H_{29}N_2O_5$, 329.2032).

***N*-Boc-L-Pro-L-Val-OH (15).** To a stirring solution of **14** (360 mg, 1.1 mmol, 1 equiv) in 1:1 THF/H_2O (4.4 mL) was added LiOH (131 mg, 5.5 mmol, 5 equiv), and the mixture was left to stir at rt for 3 h. The reaction was quenched with 1 M HCl (1 vol equiv), and the product was extracted with CH_2Cl_2, washed with $NaHCO_{3(sat'd)}$, dried over sodium sulfate, and concentrated under reduced pressure. Crude **15** was obtained in quantitative yield as an oily residue and was used without further purification: IR (film) ν_{max} 3410 (b), 1676 cm^{-1}; ^1H NMR ($CDCl_3$, 400 MHz) δ 10.37 (s, 1H), 7.51 (s, 1H), 4.50 (s, 1H), 4.40−4.19 (m, 1H), 3.50−3.28 (m, 2H), 2.31−2.09 (m, 3H), 1.94−1.79 (m, 2H), 1.43 (s, 9H), 0.91 (dd, J = 9.9, 6.9 Hz, 6H).

***H*$_2$*N*-L-Leu-L-Trp-OMe (16).** To a RBF containing **6** (857 mg, 2.5 mmol) was added 1.0 M HCl in dioxane (10 mL), and the mixture was cooled to 0 °C. The reaction mixture was allowed to stir at the same temperature for 3 h. The solvent was removed under reduced pressure to afford crude **16** in quantitative yield as a white solid, which was used without further purification. IR (film) ν_{max} 3416, 2879, 1651, 1454 cm^{-1}; ^1H NMR ($CDCl_3$, 400 MHz) δ 8.34−8.27 (m, 3H), 4.61 (dd, J = 8.5, 5.3 Hz, 1H), 4.25 (s, 1H), 3.97 (s, 1H), 3.68 (s, 3H), 3.52 (d, J = 9.0 Hz, 1H), 2.28 (s, 1H), 2.05−1.91 (m, 4H), 1.68 (ddd, J = 13.5, 7.5, 3.3 Hz, 1H), 1.35 (ddd, J = 13.3, 10.0, 7.1 Hz, 1H), 1.12 (d, J = 6.8 Hz, 3H), 0.94 (t, J = 7.3 Hz, 3H); HSESIMS m/z 243.1658 $[M + H]^+$ (calcd for $C_{12}H_{23}N_2O_3$, 243.1664).

***N*-Boc-L-Pro-L-Val-L-Ile-L-Pro-OMe (3).** Compounds **16** (1.71 g, 7.06 mmol, 1 equiv) and **15** (2.24 g, 7.13 mmol, 1 equiv) were added to a stirring solution of HOBt (1.13 g, 7.41 mmol, 1.05 equiv) and dry THF (71 mL) at rt under an argon atmosphere. The solution was cooled to 0 °C and stirred for 20 min, after which Et_3N (3.46 mL, 24.71 mmol, 3.5 equiv) was added. After an additional 20 min of stirring, EDC·HCl (1.42 g, 7.41 mmol, 1.05 equiv) was added, and the mixture was stirred overnight. The reaction was quenched with H_2O (1 vol equiv), and the product was extracted with CH_2Cl_2, dried over sodium sulfate, and concentrated under reduced pressure. The crude material was purified via flash silica gel chromatography (7:1 EtOAc/hexane) to give **3** (1.52 g, 78% yield) as a clear liquid: $[\alpha]_D^{25}$ +72.3 (c 3.21, $CHCl_3$); IR (film) ν_{max} 3673, 3412, 3306, 2879, 1743, 1632, 1368 cm^{-1}; ^1H NMR ($CDCl_3$, 400 MHz) δ 7.48 (s, 1H), 6.65 (s, 1H), 6.42 (s, 1H), 4.58 (t, J = 8.2 Hz, 1H), 4.47 (dd, J = 8.6, 4.9 Hz, 1H), 4.31 (s, 1H), 4.26 (dd, J = 8.6, 5.6 Hz, 1H), 3.81 (dt, J = 9.8, 6.3 Hz, 1H), 3.68 (s, 3H), 3.64−3.59 (m, 1H), 3.46−3.28 (m, 2H), 2.33 (s, 1H), 2.19 (ddq, J = 12.9, 6.8, 3.7 Hz, 2H), 2.02−1.79 (m, 8H), 1.43 (s, 9H), 0.97 (d, J = 6.8 Hz, 3H), 0.89−0.80 (m, 9H); ^{13}C NMR ($CDCl_3$, 101 MHz) δ 172.63, 172.40, 171.29, 171.25, 170.63, 80.70, 61.37, 59.96, 59.00, 58.70, 55.04, 52.35, 47.51, 47.25, 37.65, 31.41, 30.58, 29.29, 28.55, 25.17, 24.52, 19.50, 17.45, 15.41, 11.30; HSESIMS m/z 561.3198 $[M + H]^+$ (calcd for $C_{27}H_{46}N_4O_7Na$, 561.3264).

***H*$_2$*N*-L-Ile-L-Pro-L-Leu-L-Trp-OMe (Free Amine of Tetrapeptide 2).** To a RBF containing **2** (1.03 g, 1.6 mmol) was added 1.0 M HCl in dioxane (6.4 mL), and the solution was cooled to 0 °C. The reaction mixture was allowed to stir at the same temperature for 3 h. The solvent was removed under reduced pressure to afford a crude white solid (free base of **2**), which was used without further purification. IR (film) ν_{max} 3323, 3018, 2879, 1633, 1449, 1216 cm^{-1}; ^1H NMR ($CDCl_3$, 400 MHz) δ 8.17 (d, J = 44.9 Hz, 2H), 7.51 (d, J = 7.7 Hz, 1H), 7.32 (d, J = 8.0 Hz, 1H), 7.14 (t, J = 7.5 Hz, 1H), 7.10−7.05 (m, 2H), 6.83 (d, J = 8.3 Hz, 1H), 4.96 (d, J = 7.8 Hz, 1H), 4.83−4.63 (m, 4H), 4.42 (q, J = 7.8 Hz, 2H), 3.91 (d, J = 8.3 Hz, 1H), 3.79−3.70 (m, 2H), 3.65 (s, 5H), 3.30 (d, J = 6.0 Hz, 2H), 2.96 (ddt, J = 22.3, 10.3, 6.4 Hz, 2H), 1.95−1.81 (m, 7H), 1.29−1.22 (m, 3H), 0.89−0.76 (m, 22H).

***N*-Boc-L-Pro-L-Val-L-Ile-L-Pro-OH (Free Acid of Tetrapeptide 3).** To a stirring solution of **3** (200 mg, 0.37 mmol, 1 equiv) in 1:1 THF/H_2O (1.5 mL) was added LiOH (45 mg, 1.86 mmol, 5 equiv), and the solution was left to stir at rt for 3 h. The reaction was quenched with 1 M HCl (1 vol equiv), and the product was extracted with CH_2Cl_2, washed with $NaHCO_{3(sat'd)}$, dried over sodium sulfate, and concentrated under reduced pressure. The crude material (free acid of **3**), obtained in quantitative yield as an oily residue, was used without further purification. IR (film) ν_{max} 3311, 3016, 2965, 1632, 1215 cm^{-1}; ^1H NMR ($CDCl_3$, 400 MHz) δ 7.50 (s, 0H), 4.63 (t, J = 8.9 Hz, 0H), 4.41 (d, J = 65.5 Hz, 4H), 3.88 (d, J = 10.7 Hz, 1H), 3.67 (s, 2H), 3.43 (s, 2H), 2.16 (s, 7H), 1.96−1.74 (m, 5H), 1.46 (s, 9H), 1.21−0.74 (m, 12H).

Octapeptide *N*-Boc-L-Pro-L-Val-L-Ile-L-Pro-L-Ile-L-Pro-L-Leu-L-Trp-OMe (17). Free base of **2** (915 mg, 1.69 mmol, 1 equiv), free acid of **3** (784.5 mg, 1.5 mmol, 1 equiv), and HOBt (240 mg, 1.56 mmol, 1.05 equiv) were dissolved in dry THF (17 mL) at rt, under an argon atmosphere. The solution was then cooled to 0 °C and stirred for 20 min, after which Et_3N (0.731 mL, 5.25 mmol, 3.5 equiv) was added. After an additional 20 min of stirring, EDC·HCl (299 mg, 1.56 mmol, 1.05 equiv) was added, and the mixture was left to stir overnight. The reaction was quenched with H_2O (1 vol equiv), and the product was extracted with CH_2Cl_2, dried over sodium sulfate, and concentrated under reduced pressure. The crude material was purified via flash silica gel chromatography (1:9 EtOAc/MeOH) to afford **17** (605 mg, 34% yield) as an amber liquid: $[\alpha]_D^{25}$ −26 (c 0.21, MeOH); ^1H NMR ($CDCl_3$, 400 MHz) δ 7.50 (d, J = 7.9 Hz, 1H), 7.31 (d, J = 8.0 Hz, 1H), 7.13 (t, J = 7.2 Hz, 1H), 7.10−7.03 (m, 2H), 6.82 (s, 1H), 4.97 (s, 1H), 4.65 (s, 2H), 4.42 (s, 2H), 4.25 (s, 1H), 3.88 (d, J = 9.4 Hz, 1H), 3.69 (s, 2H), 3.66 (s, 3H), 3.30 (d, J = 4.9 Hz, 2H), 2.07 (d, J = 145.9 Hz, 24H), 1.44 (s, 4H), 1.31−1.21 (m, 1H), 0.90−0.75 (m, 25H); ^{13}C NMR ($CDCl_3$, 101 MHz) δ 17.38, 172.39, 151.82, 142.80, 140.68, 136.40, 127.78, 122.15, 119.63, 118.69, 111.44, 52.59, 48.15, 28.55, 24.87, 24.87, 23.06, 23.06, 19.62, 19.62, 15.33, 11.24; HRESIMS m/z 1070.6253 $[M + H]^+$ (calcd for $C_{55}H_{85}N_9O_{11}Na$, 1070.6267).

***H*$_2$*N*-L-Pro-L-Val-L-Ile-L-Pro-OMe (Free Amine of Tetrapeptide 3).** To an RBF containing **3** (151 mg, 0.28 mmol) was added 1.0 M HCl in dioxane (1.1 mL), and the solution was cooled to 0 °C. The reaction was allowed to stir at the same temperature for 3 h. The solvent was removed under reduced pressure, forming a crude white solid (free base **3**), which was used without further purification. IR (film) ν_{max} 3323, 2878, 1742, 1633, 1216 cm^{-1}; ^1H NMR ($CDCl_3$, 400 MHz) δ 10.92 (s, 1H), 8.76 (s, 1H), 8.16 (s, 1H), 7.83 (d, J = 9.0 Hz, 1H), 4.92 (s, 1H), 4.76−4.68 (m, 1H), 4.52−4.35 (m, 2H), 3.87 (s, 2H), 3.69 (d, J = 2.2 Hz, 3H), 3.64 (dd, J = 8.5, 5.1 Hz, 1H), 3.44 (s, 3H), 2.63 (s, 1H), 2.46−2.17 (m, 5H), 2.00 (dd, J = 18.0, 6.0 Hz, 10H), 1.52−1.39 (m, 2H), 1.01−0.79 (m, 13H).

***N*-Boc-L-Ile-L-Pro-L-Leu-L-Trp-OH (Free Acid of Tetrapeptide 2).** To a stirring solution of **14** (100 mg, 0.16 mmol, 1 equiv) in 1:1 THF/H_2O (640 mL) was added LiOH (19 mg, 0.78 mmol, 5 equiv), and the solution was left to stir at rt for 3 h. The reaction was quenched with 1 M HCl (1 vol equiv), and the product was extracted with CH_2Cl_2, washed with $NaHCO_{3(sat'd)}$, dried over sodium sulfate, and concentrated under reduced pressure. Crude **15** was obtained in quantitative yield as an oily residue, which was used without further purification. IR (film) ν_{max} 3311 (bs), 2965, 1632, 1215 cm^{-1}; ^1H NMR ($CDCl_3$, 400 MHz) δ 8.42 (s, 1H), 7.57 (d, J = 7.9 Hz, 1H), 7.31 (s, 1H), 7.12 (dq, J = 24.7, 9.6, 7.3 Hz, 3H), 5.22 (s, 1H), 4.83 (d, J = 7.5 Hz, 1H), 4.31 (d, J = 41.9 Hz, 2H), 3.73 (s, 2H), 3.54 (s, 1H), 3.30 (s, 2H), 2.08−1.72 (m, 0H), 1.43 (s, 9H), 1.10−0.57 (m, 12H).

DOI: 10.1021/acs.jnatprod.7b00656
J. Nat. Prod. 2017, 80, 3234−3240

Octapeptide *N*-Boc-L-Ile-L-Pro-L-Leu-L-Trp-L-Pro-L-Val-L-Ile-L-Pro-OMe (18). Free acid of **2** (137 mg, 0.31 mmol, 2.1 equiv) and free base of **3** (92 mg, 0.15 mmol, 1 equiv) were added to a stirring solution of HOBt (25 mg, 0.16 mmol, 1.05 equiv) in dry THF (3.1 mL) at rt under an argon atmosphere. The solution was cooled to 0 °C and stirred for 20 min, after which Et_3N (0.07 mL, 0.53 mmol, 3.5 equiv) was added and stirred. After an additional 20 min of stirring, EDC·HCl (31 mg, 0.16 mmol, 1.05 equiv) was added and the reaction mixture was left to stir overnight. The reaction was quenched with H_2O (1 vol equiv), and the product was extracted with CH_2Cl_2, dried over sodium sulfate, and concentrated under reduced pressure. The crude material was purified via flash silica gel chromatography (9:1 EtOAc/MeOH) to afford **18** (198 mg, 61% yield) as an amber liquid: $[\alpha]_D^{25}$ −29 (*c* 0.78, MeOH); IR (film) ν_{max} 3423, 2925, 1741, 1687, 1612, 1452 cm^{-1}; ^1H NMR ($CDCl_3$, 400 MHz) δ 8.67 (s, 1H), 7.67 (d, J = 7.8 Hz, 1H), 7.62−7.27 (m, 4H), 7.20−6.85 (m, 6H), 5.21 (d, J = 9.3 Hz, 1H), 5.01 (q, J = 7.2 Hz, 1H), 4.75−4.00 (m, 10H), 3.80 (dt, J = 35.8, 5.2 Hz, 3H), 3.72−3.66 (m, 3H), 3.58 (s, 3H), 3.18 (d, J = 7.3 Hz, 1H), 2.36−1.85 (m, 16H), 1.42 (d, J = 4.6 Hz, 9H), 1.04−0.83 (m, 24H); ^{13}C NMR ($CDCl_3$, 101 MHz) δ 172.76, 171.84, 171.74, 171.58, 170.90, 156.03, 136.30, 124.14, 123.58, 121.96, 119.58, 118.68, 111.55, 109.77, 79.70, 77.52, 77.04, 60.50, 60.27, 59.34, 59.11, 56.57, 55.13, 55.03, 52.31, 52.26, 52.10, 51.68, 48.01, 47.63, 47.55, 41.19, 37.93, 37.59, 37.53, 30.91, 30.26, 29.26, 28.58, 28.56, 28.11, 27.78, 25.36, 25.18, 24.80, 24.59, 24.53, 23.32, 23.01, 21.92, 19.59, 19.04, 18.36, 15.70, 15.60, 15.39, 11.33, 11.27; HSESIMS m/z 1070.6253 $[M + H]^+$ (calcd for $C_{55}H_{83}N_9O_{11}Na$, 1070.6267).

Reniochalistatin E (1) via 18. To a stirring solution of **18** (470 mg, 0.45 mmol, 1 equiv) in a 1:1 THF/H_2O (1.8 mL) was added LiOH (54 mg, 2.24 mmol, 5 equiv), and the solution was left to stir at rt for 3 h. The reaction was quenched with 1 M HCl (1 vol equiv), and the product was extracted with CH_2Cl_2, dried with brine, dried over sodium sulfate, and concentrated under reduced pressure to afford the free acid of **18**, which was used without further purification. The free acid of **18** (365 mg, 0.72 mmol) was added to an RBF, and the flask was cooled to 0 °C, to which was added 1.0 M HCl in dioxane (2.9 mL). The reaction mixture was stirred for 3 h at rt. The solvent was removed under reduced pressure to afford the crude material **18a**, a white/orange solid that was used without further purification. Compound **18a** (115 mg, 0.12 mmol, 1 equiv) was added to a stirring solution of HOBt (18 mg, 0.12 mmol, 1 equiv) in dry THF (12 mL) at rt under an argon atmosphere. The solution was cooled to 0 °C and stirred for 20 min, after which Et_3N (0.06 mL, 0.42 mmol, 3.5 equiv) was added. After an additional 20 min of stirring, EDC·HCl (25 mg, 0.13 mmol, 1.05 equiv) was added and the reaction mixture was left to stir overnight. The reaction was quenched with H_2O (2 vol equiv), and the product was extracted with CH_2Cl_2, dried over sodium sulfate, and concentrated under reduced pressure. The crude material was purified via flash silica gel chromatography (85:15 EtOAc/MeOH) to afford **1** (39 mg, 9% yield): $[\alpha]_D^{25}$ −100 (*c* 0.16, MeOH); IR (film) ν_{max} 3290, 2960, 2927, 1670, 1615, 1501, 1445 cm^{-1}; ^1H NMR ($CDCl_3$, 500 MHz) δ 10.96−10.84 (m, 1H), 8.11−7.78 (m, 1H), 7.52 (dd, J = 24.5, 7.9 Hz, 2H), 7.40 (d, J = 8.2 Hz, 1H), 7.32 (t, J = 8.7 Hz, 1H), 7.02−6.92 (m, 2H), 4.38−4.33 (m, 1H), 3.36 (s, 23H), 3.33−3.22 (m, 1H), 2.48 (s, 1H), 1.99−1.70 (m, 2H), 1.24 (s, 2H), 0.96−0.75 (m, 8H), 0.83 (s, 27H); ^{13}C NMR (DMSO-d_6, 126 MHz) δ 172.37, 171.88, 171.81, 171.48, 171.31, 170.58, 170.22, 169.58, 136.59, 127.36, 124.18, 121.21, 118.60, 118.38, 111.71, 111.57, 61.20, 60.67, 59.59, 56.74, 55.85, 54.61, 54.39, 54.22, 47.81, 47.55, 47.41, 38.21, 37.49, 35.09, 33.21, 30.01, 23.92, 29.31, 29.28, 25.22, 25.12, 24.95, 24.83, 24.10, 23.77, 22.71, 20.87, 19.21, 18.88, 15.69, 15.10, 11.50, 9.81; HRESIMS m/z 938.5475 $[M + H]^+$ (calcd for $C_{49}H_{73}N_9O_8Na$, 938.5473).

Reniochalistatin E via 17. To a stirring solution of **17** (249 mg, 0.24 mmol, 1 equiv) in 1:1 THF/H_2O (1 mL) was added LiOH (29 mg, 1.2 mmol, 5 equiv), and the mixture was left to stir at rt for 3 h. The reaction was quenched with 1 M HCl (1 vol equiv), and the product was extracted with CH_2Cl_2, washed with brine, dried over sodium sulfate, and concentrated under reduced pressure. The crude material (free acid of **17**) was obtained in 68% yield as a white powder, which was used without further purification. The free acid of **17** (167 mg, 0.16 mmol) was added to an RBF, and the flask was cooled to 0 °C, to which 1.0 M HCl in dioxane (0.64 mL) and 1 mL of dioxane were added. The reaction mixture was stirred for 3 h at the same temperature, then allowed to warm to rt overnight. The solvent was removed under reduced pressure to afford the crude material **17a**, a white/orange solid that was used without further purification. Compound **17a** (152 mg, 0.16 mmol, 1 equiv) was added to the stirring solution of HOBt (25 mg, 0.16 mmol, 1 equiv) in dry THF (16 mL) at rt under an argon atmosphere. The solution was cooled to 0 °C and stirred for 20 min, after which Et_3N (0.08 mL, 0.56 mmol, 3.5 equiv) was added. After an additional 20 min of stirring, EDC·HCl (32 mg, 0.17 mmol, 1.05 equiv) was added, and the reaction mixture was left to stir overnight. The reaction was quenched with H_2O (1.5 vol equiv), and the product was extracted with CH_2Cl_2, washed with brine, dried over sodium sulfate, and concentrated under reduced pressure. The crude material was purified via flash silica gel chromatography with a gradient solvent system (9:1 EtOAc/MeOH; 7:3 EtOAc/MeOH) to afford **1** (8.6 mg, 6% yield). All NMR and MS data matched those of **1** accessed via **18**.

Biological Assays. *Cell Culture Information.* Cells were grown in media supplemented with fetal bovine serum (FBS) and antibiotics (100 μg/mL penicillin and 100 U/mL streptomycin). Specifically, experiments were performed using the following cell lines and media compositions: HeLa, A549, RPMI-8226, MM.1R, and U-937 (RPMI-1640 + 10% FBS) and Mia PaCa-2 (DMEM + 10% FBS). Cells were incubated at 37 °C in a 5% CO_2, 95% humidity atmosphere for all experiments.

IC_{50} Value Determination for Adherent Cells Using Alamar Blue. Adherent cells were added to a 384-well plate (1500 cells/well) in 10 μL of media and were allowed to adhere for 2−3 h. Compounds were solubilized in DMSO (10 μM stock solutions) and added to a 96-well plate over a range of concentrations (31.6 nM to 200 μM) with media, and 40 μL was added to the 384-well plate in triplicate for each concentration of compound. After 69 h of continuous exposure, 5 μL of Alamar Blue was added to each well, and the cells were allowed to incubate for an additional 3 h. The plates were then read for fluorescence intensity with an excitation of 560 nm and emission of 590 nm on a BioTek Synergy H1 plate reader. Doxorubin and etoposide were both used as positive death controls, and wells with no compounds added as negative death controls. IC_{50} values were determined from three or more independent experiments using GraphPad Prism 7.0. (LaJolla, CA, USA)

IC_{50} Value Determination for Nonadherent Cells Using Alamar Blue. The same procedure for adherent cells was used, with the following modifications. Cells (2000 cell/well) in media (10 μL) were added after 40 μL of compound in media was added to the 384-well plate. No time was given to allow cells to adhere.

■ ASSOCIATED CONTENT

Supporting Information

The Supporting Information is available free of charge on the ACS Publications website at DOI: 10.1021/acs.jnatprod.7b00656.

^1H NMR and ^{13}C NMR spectra for all new compounds (PDF)

■ AUTHOR INFORMATION

Corresponding Author

*E-mail (R. J. Rafferty): rjraff@ksu.edu. Phone: 785-532-6624.

ORCID

Ryan J. Rafferty: 0000-0002-4835-6343

Notes

The authors declare no competing financial interest.

■ ACKNOWLEDGMENTS

This work could not have been undertaken without the gracious financial support from the Johnson Cancer Center of Kansas State University and Startup Capital from Kansas State University. This paper is warmly dedicated to Professor Richard

M. Hyslop in recognition of his mentorship, guidance, and friendship.

REFERENCES

(1) Zhan, K.-X.; Jiao, W.-H.; Yang, F.; Li, J.; Wang, S.-P.; Li, Y.-S.; Han, B.-N.; Lin, H.-W. *J. Nat. Prod.* **2014**, *77*, 2678−2684.
(2) Tabudravu, J.; Morris, L.; Kettenes-van den Bosch, J. J.; Jaspars, M. *Tetrahedron Lett.* **2001**, *42*, 9273−9276.
(3) Song, J.; Jeon, J.-e.; Won, T.; Sim, C.; Oh, D.-C.; Oh, K.-B.; Shin, J. *Mar. Drugs* **2014**, *12*, 2760.
(4) Napolitano, A.; Bruno, I.; Rovero, P.; Lucas, R.; Peris, M. P.; Gomez-Paloma, L.; Riccio, R. *Tetrahedron* **2001**, *57*, 6249−6255.
(5) Vera, B.; Vicente, J.; Rodríguez, A. D. *J. Nat. Prod.* **2009**, *72*, 1555−1562.
(6) Fang, W.-Y.; Dahiya, R.; Qin, H.-L.; Mourya, R.; Maharaj, S. *Mar. Drugs* **2016**, *14*, 194.
(7) Ibrahim, S. R. M.; Min, C. C.; Teuscher, F.; Ebel, R.; Kakoschke, C.; Lin, W.; Wray, V.; Edrada-Ebel, R.; Proksch, P. *Bioorg. Med. Chem.* **2010**, *18*, 4947−4956.
(8) Blunt, J. W.; Copp, B. R.; Keyzers, R. A.; Munro, M. H. G.; Prinsep, M. R. *Nat. Prod. Rep.* **2012**, *29*, 144−222.
(9) Liu, M.; Tang, Y. C.; Fan, K. Q.; Jiang, X.; Lai, L. H.; Ye, Y. H. *J. Pept. Res.* **2005**, *65*, 55−64.
(10) Schmidt, R.; Neubert, K. *Chem. Biol. Drug Design* **1991**, *37*, 502−507.
(11) Tang, Y.-C.; Gao, X.-M.; Tian, G.-L.; Ye, Y.-H. *Chem. Lett.* **2000**, *29*, 826−827.
(12) Ye, Y.-h.; Gao, X.-m.; Liu, M.; Tang, Y.-c.; Tian, G.-l. *Lett. Pept. Sci.* **2003**, *10*, 571−579.
(13) Abdelmoty, I.; Albericio, F.; Carpino, L. A.; Foxman, B. M.; Kates, S. A. *Lett. Pept. Sci.* **1994**, *1*, 57−67.
(14) Grabowska, K.; Puszko, A. K.; Lipiński, P. F.; Laskowska, A. K.; Wileńska, B.; Witkowska, E.; Perret, G. Y.; Misicka, A. *Bioorg. Med. Chem.* **2017**, *25*, 597−602.
(15) Gholap, S. S.; Ugale, S. R. *Chem. Sel.* **2017**, *2*, 7445−7449.
(16) Jou, G.; González, I.; Albericio, F.; Lloyd-Williams, P.; Giralt, E. *J. Org. Chem.* **1997**, *62*, 354−366.
(17) Bastiaans, H. M. M.; van der Baan, J. L.; Ottenheijm, H. C. J. *J. Org. Chem.* **1997**, *62*, 3880−3889.
(18) Tang, Y. c.; Xie, H. b.; Tian, G. l.; Ye, Y. H. *J. Pept. Res.* **2002**, *60*, 95−103.

DOI: 10.1021/acs.jnatprod.7b00656
J. Nat. Prod. 2017, 80, 3234−3240

23. Research Proposition Oral Examination Report

Novel combination therapy targeting Hedgehog signaling pathway inhibition induced autophagic cell death in breast cancer.

Research Proposition Oral Examination

Chamitha J. Weeramange

Major Adviser: Dr. Ryan J. Rafferty

08/18/2017

Department of Chemistry

Kansas State University

Table of Contents

1. Specific aims.

Breast cancer is the second leading cause of cancer related death among women in United States [1-3]. It starts when cells in the breast undergo uncontrolled cell division and eventually these overgrown cells form a tumor that can be felt as a lump. These malignant tumors can invade the surrounding tissues and spread through the different areas of the body. If these conditions left untreated, it can cause death either through organ failure or infection. Even though, there are many early detection and therapeutic strategies, the heterogeneity and complexity of tumor biology within the patients with similar diagnosis might have different response to treatment[4, 5]. Thus, better understanding of the tumor properties and new therapeutic strategies are necessary. With that being said, one of the most profound findings in terms of breast cancer therapy includes targeting cells with regarding to specific signaling pathway to kill the cancer cells as upregulation of many signaling molecules highly activate the abnormal cell proliferation causing the tumorigenesis. The Hedgehog signaling pathways (HH) is one of these well-known pathways that allows for targeting. This pathway plays a key role in regulation of embryonic development, cell proliferation, differentiation and tissue patterning[6, 7]. In addition, in recent years, many oncogenic genes have been identified that are directly regulated by HH pathway. Upregulation of HH pathway components, such as ***Smoothened (SMO)*** and ***Gli*** has been shown in their relevance in many cancer types such as breast cancer, glioma, medulloblastoma, neuroblastoma, leukemia, gastric cancer[8-10]. In addition to the signaling pathway role, the HH pathway also regulates autophagy process which is self-destruction of the cell. Further, the upregulation of HH pathway has been observed to dysregulate autophagy process in cells by discontinuing the synthesis of autophagosomes [8, 11, 12]. Similarly, it has been discovered that deletion of HH pathway transcription regulators, such as the up-regulator ***Gli*** proteins involved in increasing the level of autophagic process in cells [11]. Autophagic cell death is one type of programmed cell death that is essential for maintenance of homeostasis and protection against disease by removing cells destroy by cancer. Since dysregulation of HH pathway, induces autophagy process naturally in breast cancer cells, it can be considered as better strategy to eliminate cancer cells by autophagic cell death. In this method, the

inhibition of HH signaling can be achieved by inactivating the components of HH pathway such as ***Gli*** transcription factors and HH ligand[11]. This will increase the autophagy process in the cell naturally and the excessive autophagy can be achieved by introducing an autophagy activator that will lead cells to die via autophagic cell death. Though this method has been experimented in several studies, a major limitation to this application is selectivity, as both cancerous and noncancerous cells are affected. But if only cancer cell can be targeted with this combination therapy, it can be a promising therapeutic approach for cancer. This can be easily achieved by targeting cancer cell specific regulator of HH pathway.

Within the past several years, a truncated variant of the ***Gli1*** protein (***tGli1***) has been found within the breast cancer cells, but not in non-cancerous cells of breast tissues[6, 13, 14]. It has been observed that ***tGl1*** promotes cell migration, invasion and angiogenesis in higher rate compared to the ***Gli1*** protein express in tumor cells and upregulate more oncogenic genes than ***Gli1*** does by getting activated through HH signaling pathway [12]. Therefore, inhibition of HH pathway by primarily focusing on targeting ***tGli1*** can be a better therapeutic approach considering its unique distribution pattern and the oncogenic effect. Since ***Gli*** protein inhibition causes the downregulation of the HH pathway and activate the autophagy process in cancer cells including breast cancer [11], and since ***tGli1*** promotes same oncogenic genes that ***Gli*** protein regulates[5], it can be hypothesized that down regulation of this ***tGli1*** protein can inhibits the HH signaling and upregulate autophagy process like the full length ***Gli*** protein would do.

Therefore, a combinational therapy is proposed that includes monoclonal antibody for the specific targeting of ***tGli1*** and an autophagic activator to increase the rate of programmed cells death. In that way, it's expected the HH signaling cascade will be inhibited and autophagy will get activated. This synergistic method will be affected by cancerous cells among the non-cancerous cells and since this is a combination therapy, higher dosage of the drugs can be reduced and that will lower down the side effects and toxicities while maximize the therapeutic benefits.

Specific Aim 1:

Design of a monoclonal antibody which binds the ***tGli1*** protein, present within cancer cells and not non-cancerous cells, in the HH signaling pathway.

Specific Aim 2:

Design of a small molecule to activate autophagic process by targeting ULK1 protein kinase domain based on the binding interactions with the important amino acid residues from computational docking study.

Specific Aim 3:

In vitro evaluation of ***tGli*** antibody, autophagy activator and combined therapy in breast cancer cells lines.

2. Background and significance

2.1. Hedgehog (HH) signaling pathway

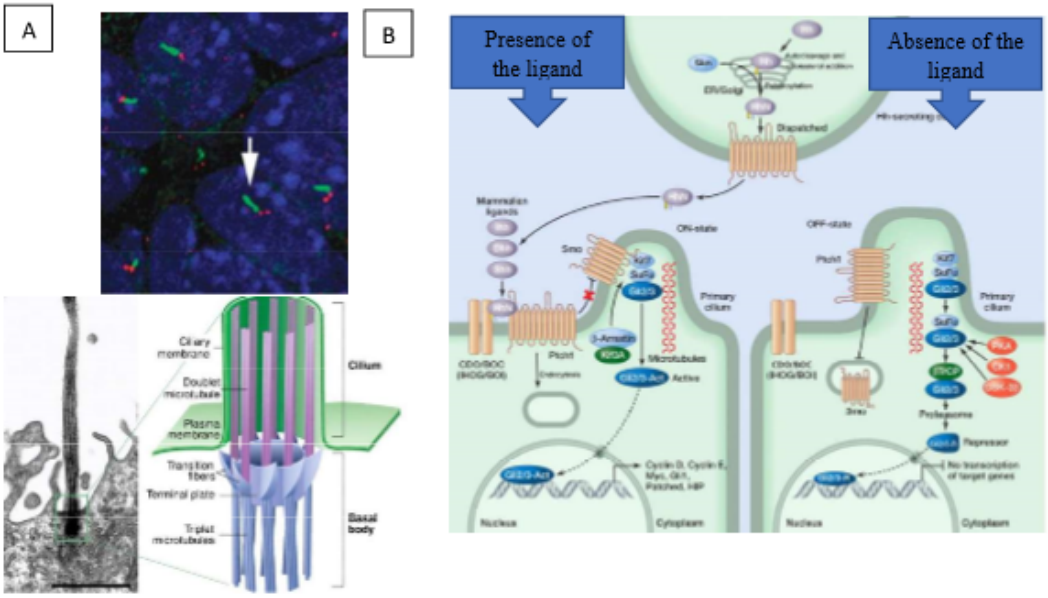

Figure 1: Illustration of primary cilium (A)[15];Signaling molecules involves in HH pathway (B)[16]

There are three hedgehog proteins that are expressed in mammals; Sonic hedgehog (SHH), Indian hedgehog (IHH), and Desert hedgehog (DHH). These Hedgehog proteins (HH proteins) are synthesized as approximately 45 kDa pro-proteins and eventually undergoes autocleavage to give the amino terminal

polypeptide, HH-NH_2 , which has all the signaling activity[16]. The HH signaling takes place selectively in the primary cilium (figure 1A), which is a solitary organelle that comes out from the cell surface of the most mammalian cell types during growth arrest[15]. When looking at the pathway there are three main components that contributes the signaling; the HH receptor ***Patched*** (***Ptc***), signal transducer ***Smoothened*** (***SMO***) and bifunctional transcriptional factors or ***Gli* proteins**. The main response of cells to HH signaling is the activation of target genes by these ***Gli*** proteins. As shown in figure 1B, in the absence of the ligand, ***Ptc*** localizes to the primary cilium base and inhibit ***SMO*** travel in to the top of the primary cilium through some protein-protein interactions. At the same time, the ***Gli*** full length transcription factors form a complex with *sufu* and *Kif7* (members of kinesin family) which leads to phosphorylates ***Gli*** proteins by *protein kinase A*, *Ck1* and *glycogen synthase kinase one-3 beta*. Phosphorylation of ***Gli*** proteins recruit ubiquitin ligase, *Beta-TrC*" (Beta transducing repeat containing proteins) that is ubiquitinating ***Gli*** proteins and marking it for proteosomal degradation. The importance of this step is, the degradation only occurs partially that result half of the ***Gli*** proteins which act as repressors. These repressors don't allow the transcription of the target genes, so that the gene regulation downstream of the signaling pathway is inhibited. All these process is because the *Ptc* has localized to the cilium. In the presence (figure 1B left side) of the ligand or HH protein, it binds to *Ptc* and exits the cilium. After *Ptc* leaves the cilium, ***SMO*** is transported to the top of the primary cilium and inserted in to the membrane of the primary cilium. This transportation is facilitated by the *Beta-Arrestin* and *Kif3A*. Then the ***SMO*** promotes the disassembly of *Sufu- Gli* complex which prevents ***Gli*** proteins get phosphorylated and release the full-length active ***Gli*** transcription factors that can be entered in to the nucleus and act as transcription factors to activates the transcription of targeted genes which regulates the cellular growth.

The functions of HH pathway remains one of the important signaling pathway in adults for many reasons. The HH pathway regulate the proliferation of the adult stem cells from various tissues such as hematopoietic cells[17], mammary[18] and neural stem cells[19].

2.2. Autophagy and it's regulation in the mammalian cell

Autophagy has been identified as a cell survival mechanism in different conditions. It can help to degrades the unwanted proteins and organelles to supply energy to the ells when cells are nutrient deficient and it is important to degrade the infectious particles in the cells[15, 20-23]. On the other hand, excessive level of autophagy has been recognized as a form of cells death[22, 24-26]. To avoid the confusion in between the two-contrasting processes, autophagy mediated cell death is termed "autophagic cell death". Herein, the mechanism of action of autophagy and its regulation is discussed.

Autophagy is important catabolic process that delivers cytoplasmic material to the lysosomes for degradation[27-29]. When looking at the mechanism of action, it involves membrane formation and fusion. First an isolation membrane also known as *phagophore*, must be initiated from a membrane source known as phagophore assembly site (PAS) (figure 2A). It's suggested that SER, mitochondria, plasma membrane could supply membrane for formation of autophagosomes under different conditions[24]. This isolation membrane can elongate and surrounds cargo that makes a double membrane autophagosome. Once this is formed, it fuses with lysosome to form autolysosome in which lysosomal enzymes degrade the cargo. As shown in figure 2A, autophagy is regulated by three protein complexes in mammals;ULK1 and its interacting protein complex,VPS34 and its interacting protein complex and two ubiquitin like conjugation system. Upon activation of ULK 1 protein complex it activates class III PI3Kinase complex consisting lipid kinase VPS34 and these two-protein complex function to generate phosphatidyl inositol 3-phosphate in early autophagosome formation[24]. This leads the recruitment of two ubiquitin like conjugation systems containing ATGs, which control the elongation and closure of the autophagopore.

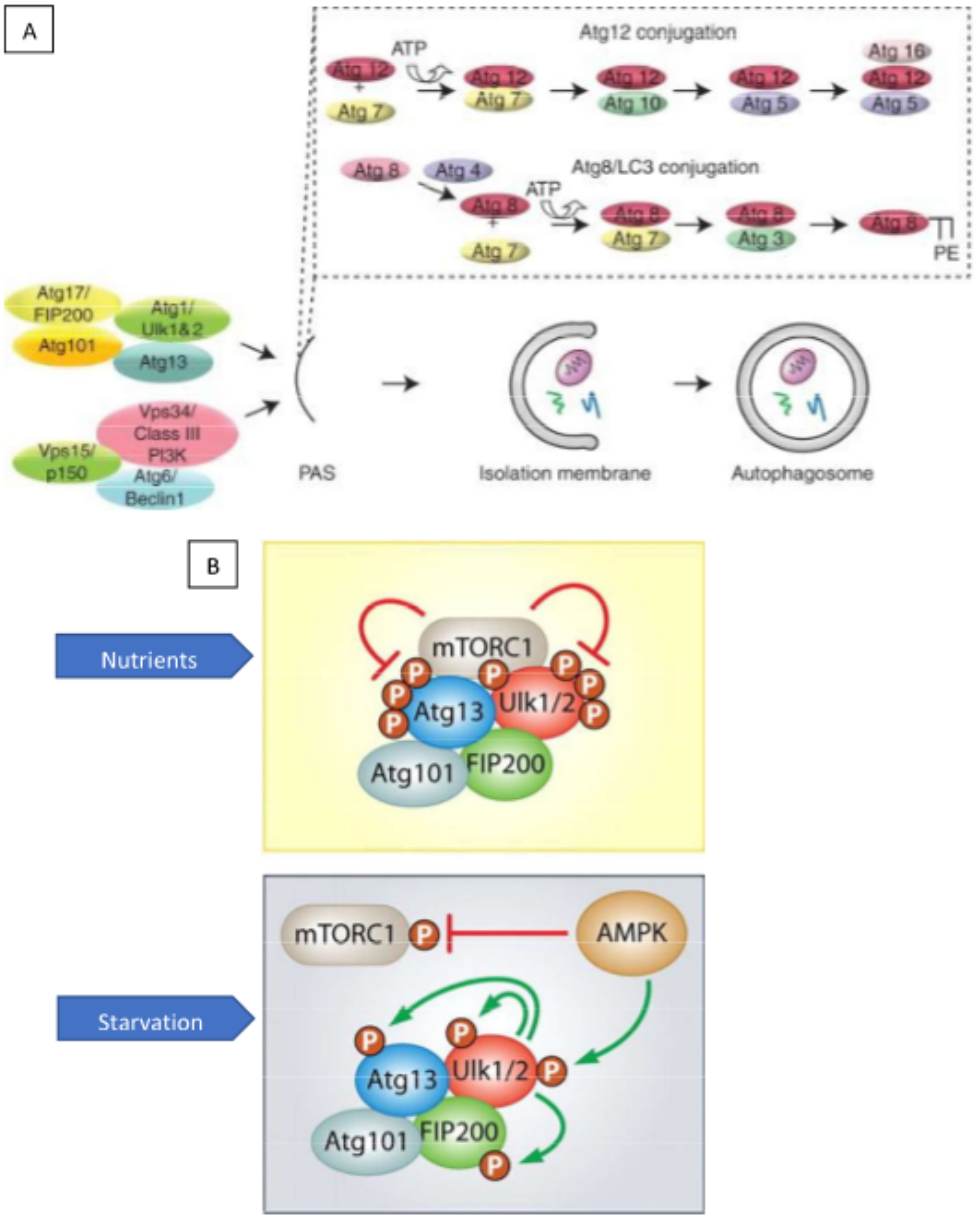

Figure 2: Autophagy mechanism (A)[27] and its regulatory protein complexes (B)[28].

There are two proteins that is important in regulating autophagy (figure 2B); AMPK (activated protein kinase) which can be activated in low energy condition that leads to induction of autophagy[24]. The second protein is called mTOR (mammalian target of rapamycin) which can be activated in diverse positive signal

such as high energy levels, normoxia, high amino acids, which leads to inhibition of autophagy[24]. When looking at the mechanism of autophagy regulation in detail, under fed condition mammalian target of rapamycin or mTORC1 will phosphorylate ULK1 and its regulating protein complex and inhibit it. On the other hand, when cells have insufficient nutrients or upon starvation, AMPK kinase plays the role in inhibiting mTORC1 complex and that will relief the inhibition on the autophagy complex (ULK1 and its regulatory proteins containing complex) by mTORC1. This will result the autophosphorylation of ULK1 protein and it will phosphorylate the other regulating proteins in the complex which will activate the autophagy process. It regulates the survival during short starvation by sustaining the energy in the cell. In addition, it is important in organelle turnover, protection against metabolic stress and DNA damage, clearance of aggregate- prone proteins, regulation of cell size, longevity, programmed cell death, defense against intracellular pathogens etc[24].

In advanced cancer, autophagy can benefit the progression of tumor as it is protecting cells against apoptosis by providing nutrients to the cells[29]. However, autophagy can also cause cell death in apoptosis-defective cells[30]

2.3. The hedgehog signaling pathway regulates autophagy in breast cancer

Much research has been conducted that provide insight in to the connection between HH and autophagy and its activation via downregulation of HH signaling resulting in breast cancer[11, 31-33]. In these experiments, autophagy process was measured using LC3-II levels in cells. During the formation of autophagosome membranes, cytosolic LC3 is conjugated to phosphatidylethanolamine (LC3-II) which can be specifically bound to autophagosome membrane[34]. Therefore, LC3-II can be utilized in western blot to identify number of autophagosomes which corresponds to level of autophagy process in the cell.

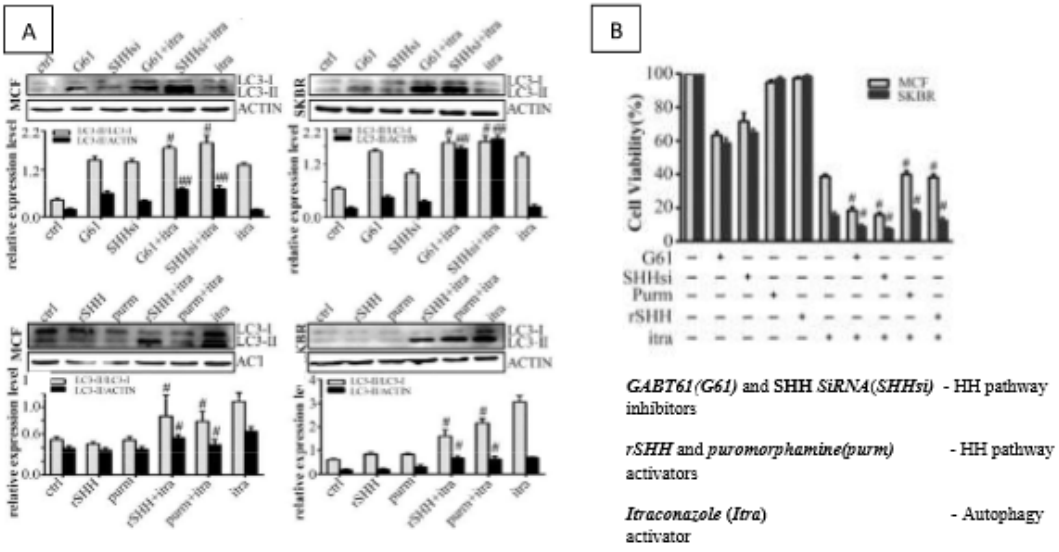

Figure 3: LC3 levels in breast cancer cell line after indicated treatments (A) and cell viability with indicated treatments (B)[11]

As shown in figure 3A when *GABT61*(*G61*) or *SHH siRNA*(*SHHsi*) (HH inhibitors) treatment alone moderately increased the LC3 levels which indicates that HH pathway inhibition induces the autophagy process. Similarly, when cells are treated with HH activators *rSHH* and or *purmorphamine* alone, the LC3 levels went down as expected. However, when cells are co-treated with HH inhibitors and *itraconazole* (autophagy activator) LC3 level were shown to increase more showing that combination treatment causing excessive autophagy activation. At the same time, cell viability assay shows higher cell death in this combined treatment compared to the other treatments indication in figure 3B.

Furthermore, the HH inhibitor use in this study, *G61* is inhibiting the HH pathway through inhibiting ***Gli*** transcription factors[6]. Therefore these results suggest that inactivation of HH signaling by inhibiting ***Gli*** transcriptional factor, leads to activation of autophagy process which can cause death of the cell.

2.4. A novel splice variant, *tGli1* only presence in cancer cells and activates HH signaling

The transcriptional factors downstream of HH signaling pathway, ***Gli1*** proteins belong to zinc finger transcriptional factors that regulate the expression of number of genes associated with cellular functions[35]. In past years, a novel splice variant of ***Gli1*** protein called ***tGli1*** protein has been discovered by Lo and co-workers [13]. This protein is made with deletion of 123 base pairs of ***Gli1,*** but has entire exon 3 and part of exon 4 of the ***Gli1*** gene. The ***tGli1*** shows similar function as ***Gli1*** proteins downstream of HH pathway. However, its expression result in high mortality and an increase in invasiveness of cancer cells by differentially expressing more than 100 genes compared to ***Gli1*** proteins[14]. The other important fact that ***tGli1*** attract much attention is, it is specifically expressed in cancer cells including breast cancer cells but not in normal healthy cells [6, 14]. This open-up a new pathway to specifically detect cancer cells among the noncancerous cells.

3. Research proposal

When looking at the treatments for cancer, programmed cell death is an important step to control cancer progression. Autophagy is one of the three types of programmed cell deaths[11] and it can be described as a more successful application among other two types: apoptosis and necrosis as there are many evidence that shows excess activation of autophagy lead to cell death[24-26].

Thus far, antiproliferation of cancer cells by this combination therapy of impairing HH signaling and activating autophagic cell death together, has been studied by few researchers. However, when it comes to the down regulation of the HH signaling pathway by inhibition of ***Gli*** transcriptional factor, it also influences on the functions of ***Gli*** in normal healthy cells such as tissue specification, upregulation of anti-apoptotic proteins etc. However, if we can specifically target inhibition of HH pathway in cancer cells and activate autophagic cell death simultaneously, it can be a more promising approach towards treatment of cancer with less side effects.

As mentioned above, since ***tGli1*** belongs to zinc family proteins like ***Gli*** and it has the same function as ***Gli1*** protein downstream of HH pathway, it can be hypothesized that inhibition of ***tGli1*** protein in cancer cells can down regulates the HH signaling pathway. If it is true, oncogenic HH signaling pathway in cancer cells can be specifically targeted. At the same time, since HH inhibition result in upregulation of autophagy process, an autophagy activator can be introduced to elevate the rate of autophagic cell death. Herein, it is proposed a combine treatment of monoclonal antibody that specifically binds to ***tGli1*** protein and a small molecule activator that induces ULK1 protein complex that leading to autophagic cell death in cancer cells. Furthermore, it is expected that binding of ***tGli1***-antibody to ***tGli1*** protein will inactivate its function and downregulates HH pathway while activating autophagy in cancer cell specific manner. In addition, the autophagy activator will increase the autophagic process excessively which will lead the autophagic cell death.

4. Method and design

4.1. Generation of monoclonal antibody against *tGli1* transcriptional factor

Monoclonal antibody therapy is a form of immunotherapy that uses to identify different antigens by an antibody. Whenever pathogens invade our body, it brings along other proteins which known as antigens. Once these antigens are present, a specialized type of B lymphocyte known as plasma cells, produce antibodies which are highly specific to these antigens and their influence inside the body can be inhibited. An antibody is a 'Y' shape structure which consist of two regions: variable region and constant region. The variable region consists of a cleft that has the amino acid sequence for specific antigen[36]. These sites are known as antigen binding site. When an antibody binds to the specific antigen, it can inactivate the antigen and prevent it from continuing its normal function inside the cells[37]. Antibodies are divided in to five classes; IgG, IgM, IgA, IgE and IgD base on the number of 'Y' like units and the type of heavy chain polypeptide they contain. The classes can have divided in to sub classes with unique structural feature of the antibody[36]

Different plasma cells produce polyclonal antibodies, and bind to different places of a single antigen. In contrast, monoclonal antibody forms from a single type of plasma cell and always bind to a single specific region of an antigen[38]. Since there are many types of ***Gli*** protein isoforms regulates canonical HH signaling, using a monoclonal antibody for the full length of the protein, will be useful for the isoform specific inhibition of ***tGli1*** activity in cancer cells.

Inside any organism, there are different types of plasma cells that can make antibodies and to harvest specific type of antibody, specific plasma cells need to be isolated from the organisms. However, the problem associates with isolating plasma cells is that, they die quickly following removal from the organism. As a solution to this matter, the plasma cells that produce the specific antibody can be turned in to cancer cells to make them immortal cells [30]. In that way, these cells can be grow outside the organism in a media with nutrients. The same concept will be followed to mass produce antibody against ***tGli1*** protein. Here "Antibodies: A Laboratory Manual, second edition"[36] by Dr. Edward A. Greenfield and "Generation of monoclonal antibodies against chemokine receptors"[39] by Leonor Kremer were referred to make the following protocol to generate the ***tGli1***-antibody.

4.1.1. Generation of general transfected cell line to express ***tGli1*** protein (antigen)

Transfected cells that express protein of interest can be used as antigen to produce specific antibodies. To prepare a transfectant cell line expressing ***tGli1***, the cDNA sequence of this protein (Homo sapiens truncated GLI1 (***tGLI1***) mRNA, GenBank: GQ890670.2)[40] can be cloned in a plasmid which is then can be transfected to an appropriate cell line. Here, pCIneo expression vector (gene sequence from *Promega*)[41] is used to clone ***tGli1*** gene and *Biolab molecular cloning technical guide* [42] was followed for the plasmid construction. After finding out that NheI and NotI restriction enzyme sites of the vector are not present in the gene of interest, these two restriction enzyme sites were selected as the cloning sites. Before ligating the gene and the vector, there need to be the same sticky ends at the ends of the ***tGli1*** gene and vector cloning sites. Therefore, NheI and NotI restriction sites need to be introduced to ***tGli1*** gene as well. This can be done with suitable primers (single strand DNA sequence design to locate the target DNA

fragments). Following is the forward and reverse primers made to insert the restriction sites of interest in to the gene ends.

A

Forward primer
5'GCATGAGCTAGCATGATGTTCAACTCGATGACCCCACCA3'
Reverse Primer
5'TGCTTAGCGGCCGCTTAGGAGGCACTAGAGTTGAGGAATTCTGTT3'

B

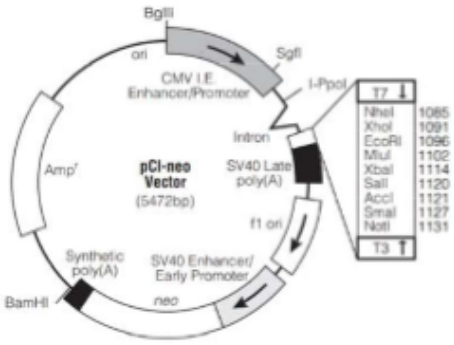

Figure 4: sequence reference points (A) and pCI-neo vector circle map (B)[41]

Once the correct primers are made target gene can be amplified using PCR (polymerase chain reaction). This technique is used in molecular biology to amplify a DNA sequence in million folds. The PCR reaction can be performed in a PCR machine which carries out temperature cycles. To PCR the ***tGli1*** with primers the samples should be included these ingredient: 10X PCR buffer, 2 mM dNTP mix (mix of nucleotides, which are the building blocks if new DNA strands), Forward and reverse primers, taq DNA polymerase, 25 mM $MgCl_2$ (cofactor for DNA polymerase) and the template DNA (***tGli1*** gene). The PCR program can be setup at 94 ^{0}C for 5 min to activate taq DNA polymerase enzyme and 30 seconds at 94^{0}C to make single stranded DNA from double stranded DNA fragments. Then the annealing of the primers and DNA by making H bonds can be done by keeping it for 30 seconds at 65^{0}C and to synthesize the new DNA strand using the enzyme it can be programed for 30 seconds at 72^{0}C. These steps represent a one cycle and it can be continued for 30 more cycles. Finally, it can be set at 72^{0}C for 5 min to ensure remaining single strands are fully extended at the end, the machine need to be held at 4^{0}C to deactivate the taq polymerase enzyme. With this technique, the number of target DNA can be increased in to million copies and afterwards PCR

product can be run on 1% agarose gel to identify whether the product is formed. After confirmation, the remainder can be purified to remove salts, extra dNTPs etc.

The next step is to ligate the ***tGli1*** gene in to the pCI-neo vector. Firstly, both vector and the insert need to be cut in the same restriction sites. Here, restriction enzyme site digestion with NheI and NotI enzymes can be carried out. The purpose of this step is to cut both the insert and the vector in the restriction enzyme sites and the reaction mixture can be made as follow: DNA 50 μL, NheI and NotI, optimal buffer (NEB4) dilute final concentration of 1X, 10XBSA dilute to final concertation of 1 X, H_2O bring up to final volume 50 μL -100 μL. This reaction mixture should be incubated at 37 c^0 water bath for at least 2 hours. After this step the digested products (insert and vector separately) can be run through agarose gel (gel purification) and the DNA fragment can be cut off from the gel and it should be further purified using a gel purification kit. To do the ligation or combine two DNA fragments (***tGli1*** and the vector) reaction mixture can prepare as follow: vector 2 μL, ***tGli1*** 6 μL, T4 DNA ligase 1 μL, ligase buffer 1 μL, 10 uL final volume. This reaction mixture can be incubated at room temperature overnight. After ***tGli1*** is cloned in to pCIneo vector, the plasmid can be transferred to the rat HEK 293T cells by mixing 20 μg of plasmid with $10x10^4$ cells/mL cells for 5 minutes and followed by electroporation technique. Then the stable transfected cells can be selected for the immunization.

4.1.2. Immunization

The stable transfectant cell lines can be used as the immunogen. Firstly, the HEK 293T cells can be cultured and harvest when they are 90% viable. Once the cells are harvested they can be centrifuged and the supernatant can be removed. Then cells can be washed and resuspend with PBS buffer and injected in to 10-week-old Lou rats as a 20 x 10^6 cells/0.3 mL sterile PBS cell lysate intraperitoneally or subcutaneously. After 7 to 10 days of each injection or once good humoral response (titer) has appeared rat serum samples can be collected. These serum samples can be tested for antibody of interest by indirect antibody capture assay: for an example ELISA (enzyme linked immunosorbent assay). This assay can be carried out in the multi-well plate so that dilution of the test sample can be easily prepared. Then ***tGli1*** or

the antigen can be coated to bottom of the well plate to make them immobilized. Then antibody of interest in the plasma sample can be bound to the antigen forming the immune complex. After washing the well with buffer unbound antibodies can be removed and the remaining immune complex is then detected by secondary mouse antibody conjugated to an enzyme label followed by a wash. Finally, solution of color producing enzyme substrate can be introduced to interact with the enzyme bound to secondary antibody. This process will show a visible color that can be detected by naked eye or quantify by electronic plate reader.

To do the ELISA assay firstly, ***tGli1*** (antigen) solution need to be prepared in PBS buffer to a concentration of 1 μg/mL. then 100 μL of the diluted antigen can be added to 96-well microtiter plate. The palate can be sealed and incubate it overnight at 4 ^{0}C overnight and protein solution can be removed followed by a addition of 250 μL blocking buffer (BSA/PBS-1-2%) to add proteins to the unoccupied binding sites on the solid support. After one-hour incubation blocking buffer can be removed and 100 μL diluted serum sample with antibody in blocking buffer can be added in to the well plate. After several washes, 100 μL of AP-conjugated goat anti-mouse IgG Fc can be added to each well and incubate for 1 hour. After several washes, the developing solution can be added and incubate for 1 hour prior to quench the reaction with H_2SO_4. Then the developed color can be read with a plate reader. In that way efficiency of immunization process can be determined and mouse can be injected again with ***tGli1***-trnasfectant cell lysate before one month of the final boost.

4.1.3. Cell fusion and production of positive Hybridomas

Once the antibody screening is positive, the spleen and the peripheral nodes of the rats can be harvested by scarifying rats with CO_2 inhalation. The organ removal must be done with aseptic techniques. Then the antibody screening cells can be prepared from the organs and mixed with myeloma cells. After the fusion, cells can be plated in multiwall plate with selective medium. Myeloma cells does not express the gene hypoxanthine-guanine phosphoribosyl transferase enzyme, which support the salvage pathway of nucleotide synthesis when the normal pathway is blocked. Therefore, after fusion of myeloma and

lymphocytes, addition of azaserine drug can be used to selectively isolate hybrid cells. Because, azaserine blocks the de novo nucleotide synthesis and forcing the myeloma cell fusion lymphocyte cells to use the salvage nucleotide synthesis pathway. Therefore, the single myeloma cells will be dead while hybridoma cells are remaining in the medium. After one week after the fusion, cells can be tested for positive hybridomas (using the ELISA assay). Firstly, plamacytoma cells can be mixed with DMEM medium in 2 X 10^6 cells/mL concentration while rats spleen and lymph nodes tease apart in petri dish containing 6 mL DMEM. Then, filter the cell suspension and transfer in to falcon tube followed by the centrifugation. The pellet can be resuspended with 0.83% ammonium chloride and incubate at 37^0C for few minutes. Then the lysed erythrocytes can be resuspended in 10 mL medium and myeloma and lymphocytes can be mixed in 1:4 ration. After several washing procedures by centrifugation and resuspending with serum free media, 1 mL of warmed (37^0C) PEG 4000 can be added to the lymphocyte-myeloma cell mixture. The cells can be cultured in a flask 24 h at 37^0C and then can be resuspended in media containing 0.1 mM hypoxanthine and 10 μM azaserine (0.5-1 X 10^5 cells/mL) and plate them in 96 well plate (200 μL/well). The plates can be incubated in 37 ^{0}C with 5% CO_2 while changing the media every 4 days. Supernatant with the cells for the hybridomas can be tested with ELISA assay after 10 to 14 days. Positive hybridoma colonies (cover more than 10 % of the well bottom) then can transfer in to 24 well plate future assays.

4.1.4. Large scale production of ***tGli1*** antibody and its characterization

The positive hybridomas then can be overgrown in culture medium to produce the antibodies in large scale (5-60 μg/mL). The purification of antibodies can be done by precipitate them with 50 % ammonium sulfate and finally the antibody affinity can be tested with ELISA assay. The final collection of antibody can be stored in -20^0C.

4.2. ULK1 activation for autophagic cell death

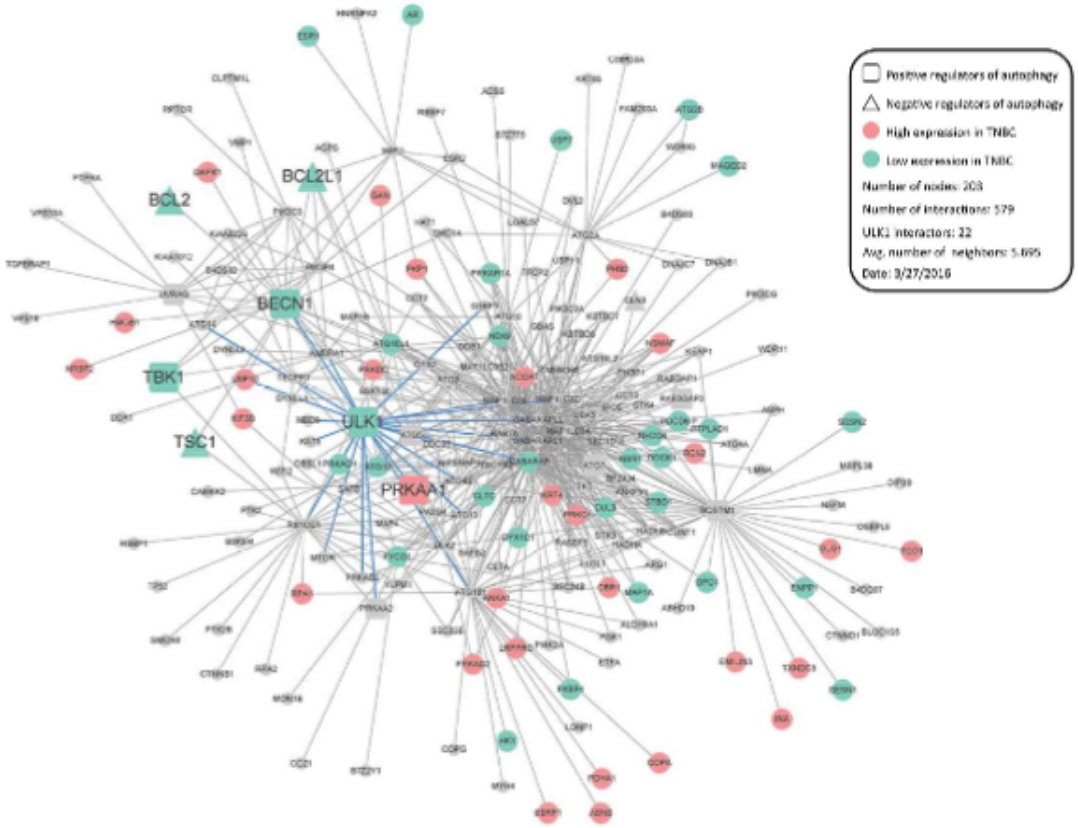

Figure 5: ULK1 networking with autophagic process(TNBC-Triple negative breast cancer)[43].

When looking at the autophagy mechanism, there are many autophagy regulating proteins that can be targeted to achieve autophagic cell death. Among them, ULK1 modulated autophagy can be a promising approach as for several reasons; ULK1 is the important regulatory protein in the ULK1 complex that is essential for autophagy induction[43]. In addition, ULK1 has been shown to down regulate in many cancer types including triple negative breast cancer[44]. Most of all, according to Liu and group's findings, ULK1 act as a hub protein in the core autophagic network which shows connections with 22 interactors(figure 5) [43]. This number is higher than the average number of interactors for a specific protein. This is suggesting that ULK1 is promising protein target as positive autophagy regulator.

4.2.1. Activation mechanism of ULK1

In 2017, Bo Liu and co-workers recently identified a ULK1 activator through in silico high throughput screening and chemical synthesis. They eventually discovered a ULK1 agonist, LYN-1604 (figure 6A) and for this synthesis, they have hypothesized that ATG 13 and FIP200 bind to the hydrophobic pocket of ULK1 and it will alter the confirmation of the kinase domain of ULK1 to the on state(figure 6B)[43]. Upon synthesis of LYN 1604 molecule, they could lock in this binding interaction in between these protein complexes and three amino acid residues (Lys50, Leu53, Tyr89) have been found as the key activation sites in between the protein and the agonist. Furthermore, they have demonstrated that LYN-1604, could significantly inhibit the growth of triple negative breast cancer in LYN-1604 treated mice by ULK1 modulated autophagic cell death[44].

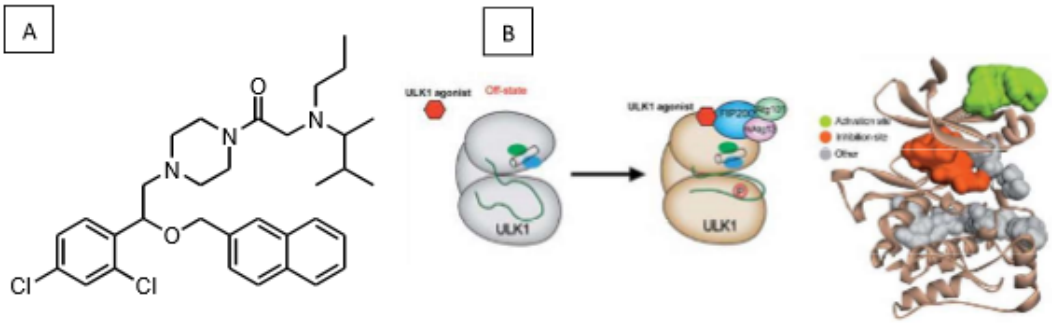

Figure 6: Structure of LYN1604 (A), Schematic drawing of the activation mechanism of ULK1 agonist and candidate binding pockets in the structure of the kinase domain of ULK1. The inhibitor pocket is shown in red and the virtual screening pocket is shown in green**[43]**

Even though, LYN-1604 shows binding interactions with the above-mentioned residues in the binding pocket of ULK1 kinase domain, this molecule violates two rules out of five Lipinski rules[45]. To synthesis a better drug molecule with structural properties for better absorption, Lipinski rules have been used for many years and the impact of these rules have been more effective. The Lipinski rules states that poor absorption and permeation of a drug molecule is more likely when: 1) there are more than 5 H bond donors,

2) molecular weight greater than 500, 3) logP greater than 5, 4) there are more than 10 H bond acceptors, and 5) substrate for biological transporters are exceptions for this rule[45].

LYN-1604 has it molecular weight at 584.63 and calculated logP value (log P= 7.54) is higher than what a better drug molecule supposed to have (The logP value is a partition coefficient which indicates molecule's distribution in octanol to water). This indicates the higher hydrophobicity and low bioavailability of this molecule. Therefore, it's suggested to look in to more synthetic routs towards novel effective ULK1 activators.

4.2.2. Discovery of small molecule targeting ULK1 modulated autophagic cell death

Based on the Bo Liu results on autophagy activation, the core structural scaffold of LYN1604 and its binding affinity to active site of ULK1, (Lys50, Leu53, Tyr89) is studied for the analog synthesis. To make possible small molecule activators for ULK1, a structural scaffold is proposed base on the expected interactions with the three amino acids of interest and it is proposed by following Lipinski rules to estimates the drug like structural, physiochemical, and biochemical properties to overcome the barriers to drug exposure in living system.

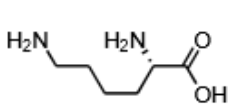

lysine

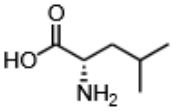

leucine

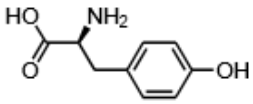

tyrosine

To overcome the high hydrophobicity and make it more cell permeable and soluble, the compound U1 (figure 7A) is proposed with an indole ring which is a mimicry of a purine and H-bond donor and acceptor groups. The oxygens within the ether carbonyl's will act as H-bond acceptors while the amide and indole NH groups can serve as H bond donors. These H acceptors are expected to make H bonding with lysine (Lys50) and tyrosine (Tyr89). Further, a benzene moiety is attached to one end of the molecule that is expected to interact with the phenyl ring of Tyr89 to make π-π interactions. In addition, the molecule is

made with hydrophobic groups expecting the hydrophobic interactions with side chain of leucine residue (Leu53) in the binding pocket.

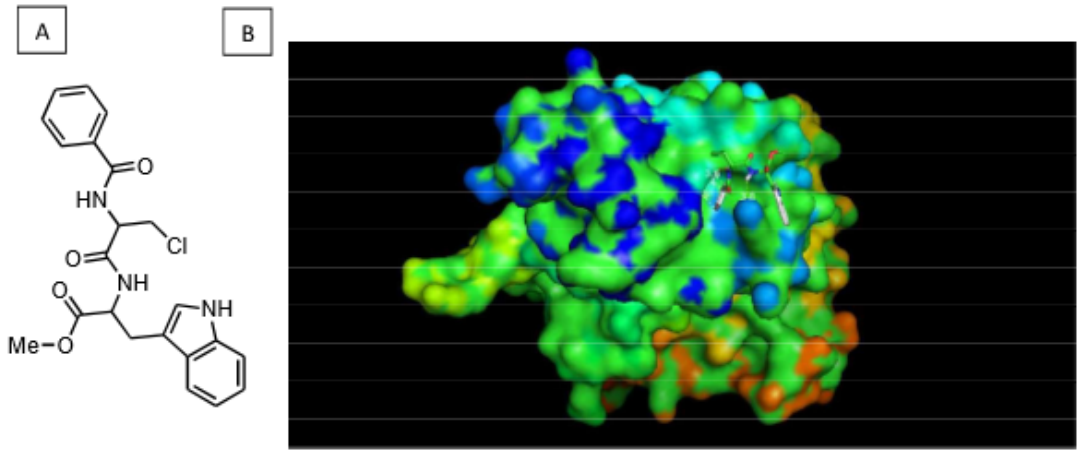

Figure 7: Representation of proposed U1 compound (A) Docking confirmation of compound U1 with ULK1 protein (protein PDB code 4WNP) surface view (B)

Computational docking experiments were used to see the actual binding interactions of the molecule with ULK1 and AutoDock Vina computational docking program software was used as the method. First the protein data bank PDB file for ULK1 protein (ID: 4WNP) was uploaded to the docking software and the compound was drawn in Chem3D. The lowest energy confirmation of the ligand was considered in the process of docking. Upon the docking studies, the carbon group attached to 2H and a Cl was initially being a methyl group and the methyl attached to ester group of the indole ring was a H atom. But changing a one H to a Cl group and ester H to a methyl group respectively, support it to go inside the binding pocket further.

The molecular docking program gave nine lowest binding energies for the compound U1 binding to the ULK1 kinase binding domain. The first confirmation gave the lowest binding energy which is -6.2 kcal/mol. But confirmation 6 (-5.8 kcal/mol) is selected as it covers the three amino acid residues deeply in the biding domain (figure 7B).

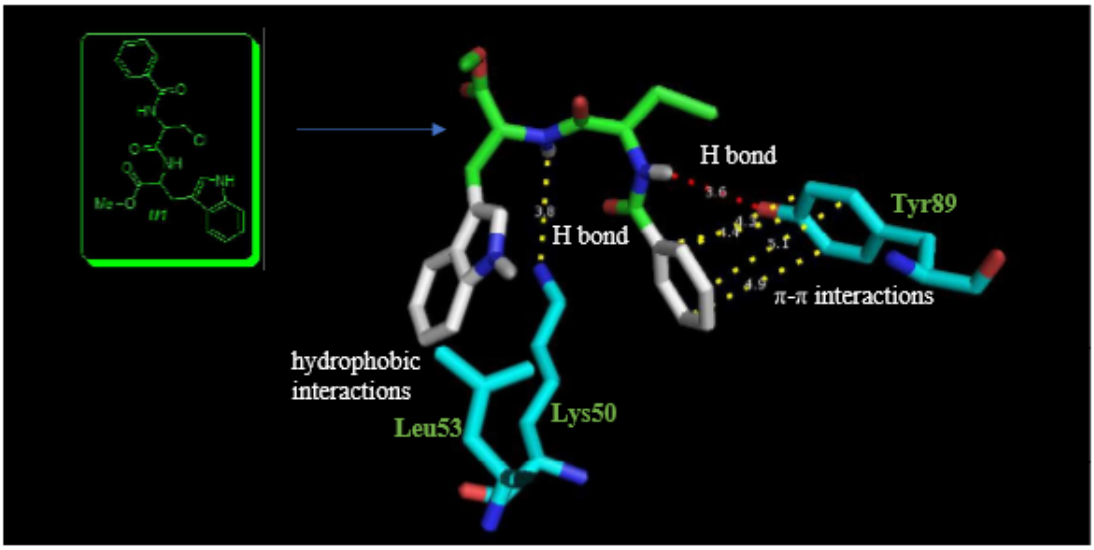

Figure 8: Close-up structure of docking conformation showing the H bonding and hydrophobic interactions with compound U1 with ULK1 protein (PDB code: 4WNP). Binding distances are given in Å.

The docking results shows strong interaction between the compound U1 and the amino acids of interest. As expected, the NH hydrogens in the molecules make strong hydrogen bonds with the N group of lysine side chain and also with to oxygen atom in the tyrosine residue. At the same time, the phenyl ring in the tyrosine residues make π-π interactions with the benzene moiety in the molecule. On the other hand, leucine side chain residue makes hydrophobic interactions with indole ring. These docking studies shows that compound U1 is interacting with all the three amino acids (figure 8). In addition, U1 molecular weight and logP are calculated at 427.89 and 2.63 respectively. Therefore, it can be considered as a promising drug candidate and that is capable of acting as an autophagy activator by setting the ULK1 and its interacting protein complex on state.

4.2.3. Synthesis route of ULK1 activator.

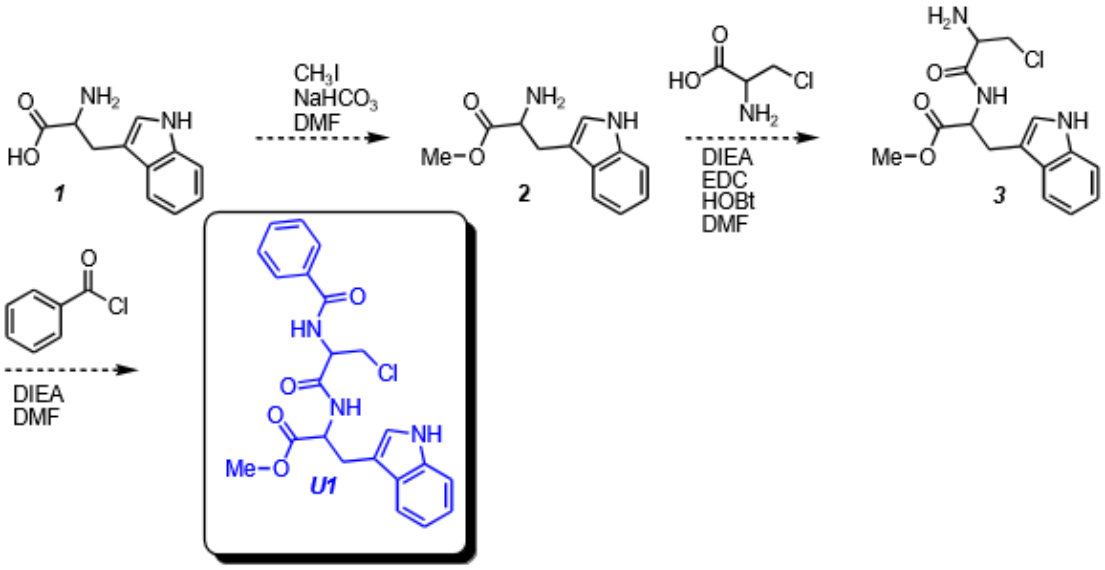

Scheme 1: Synthesis of compound U1

In the proposed synthesis in scheme 1 first, commercially available compound 1 can undergo Williamson synthesis to obtain the ether product (compound 2)[46]. Then to a solution of compound 2 in DMF, the coupling reagent EDC can be added followed by the activating reagent HOBt and 3-chloro alanine to obtain compound 3[47]. Next, to a stirring solution of compound 3 in DMF, DIEA can be added in followed by the benzoyl chloride. The reaction mixture can be stirred at room temperature until the compound U1 is made[48].

4.3. Biological evaluation of *tGli1* antibody and the autophagy activator

The antiproliferation effect of ULK1 activator-induced autophagic cell death and ***tGli1*** antibody induced HH pathway inhibition can be confirmed by the following assays. In addition, the effect of the combined treatment induced autophagic cell death along with HH pathway inhibition can be tested to see whether this synergistic method enhances cell cytotoxicity.

4.3.1. In vitro evaluation of autophagy activator

ULK1 activator induce autophagic cell death can be tested using western blot. LC-II the protein embedded in autophagosome membrane and this protein is directly proportional to formation of autophagosomes. This indicates the level of autophagic process in the cells. In this procedure, breast cancer cells can be treated with ULK1 activator and incubated at 37^0C for certain time. Then the cells can be lysed with a lysis buffer and supernatant can be used for the further analysis after the centrifugation. The cellular proteins can be separated using SDS page gel and it can be transferred in to PVDF membrane. The membrane can be incubated with primary antibody overnight and secondary antibody for one hour before visualizing the protein band[11].

On the other hand, process LC3 proteins in the autophagic puncta can be observed by immunofluorescence assay using confocal microscopy. Here the control and treated cells can be stained with anti-LC3 primary antibody and fluorescence labeled secondary antibody before visualize using confocal microscopy[11]. In this assay, if the autophagy activator induces the autophagic process in the cells, it is expected higher level of LC3-II proteins is made. In that case, the following western blot and immunofluorescence results are expected.

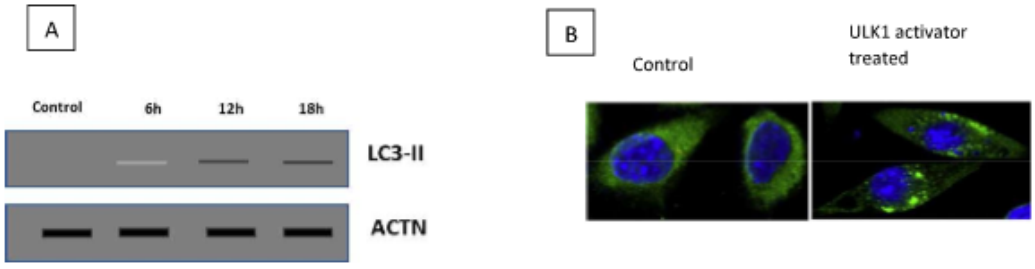

Figure 9: Illustration of expected western blot images of ULK1 activator treated cancer cells (A). Expected immunofluorescences image of autophagic punctate with LC3 proteins in cancer cells (B)[11]

4.3.2. In vitro evaluation of ***tGli1*** antibody

SHH protein is the ligand that activates HH pathway. Therefore, the SHH ligand is directly proportional to the process of HH signaling. To see whether ***tGli1*** antibody is a good candidate to inhibit the signaling pathway, SHH protein levels in the antibody treated cancer cell can be measured with western blot. If it inhibits the HH pathway, decreasing SHH levels can be observed as following graphs depicts.

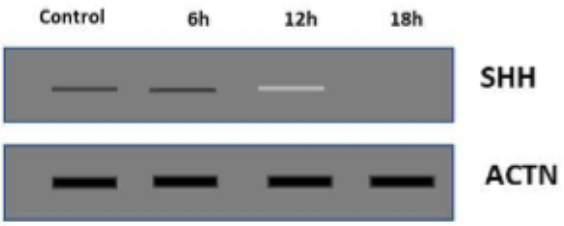

Figure 10: Illustration of expected western blot image of SHH protein in ***tGli1*** antibody treated cancer cells and the quantification of SHH

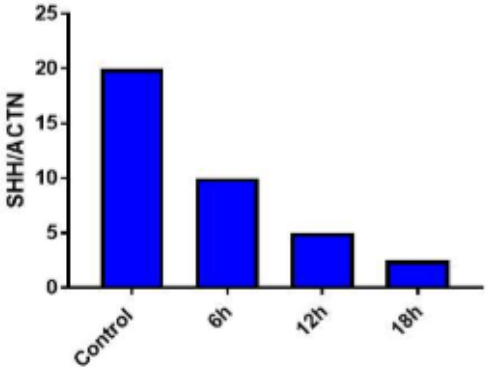

4.3.3. In vitro evaluation of combine treatment with Autophagy activator and ***tGli1*** protein

After confirmation of HH pathway inhibition by ***tGli1*** antibody and autophagic cell death is upregulate by the ULK1 activator, cell viability assay can be carried out to see if it kills the breast cancer cells when the both treatments are combined. To perform the cell viability testing, MTT assay can be performed in 96 well plates. First cells can be seeded in 96 well plates (5000 cells/well). After some incubation cell can treated with ***tGli*** antibody, autophagy activator (U1), and with both antibody and the U1. Breast cancer cells can be incubated with the treatment for about 48 hours prior to adding MTT reagent. MTT, a yellow

tetrazole will turn in to purple formazan in living cells by mitochondrial reductase and absorbance value for the purple formazan at wavelength 570 nm is directly proportional to the live cells[49] The absorbance values can be determined using electronic plate reader.

As expected, if ***tGli1*** inhibiting HH pathway and ULK1 activator induces autophagic cell death the results from the cell viability assay can be observed as follow.

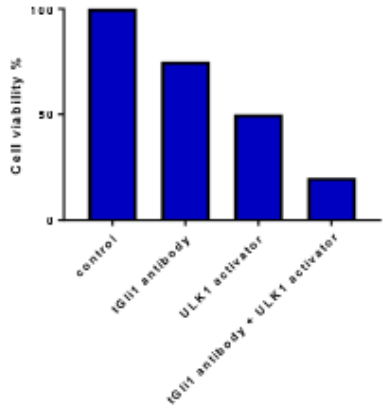

Figure 11: Expected cell viability when cells are treated as indicated.

5. Conclusion:

The upregulation of autophagy via inhibition of hedgehog signaling was confirmed with ***Gli*** protein inhibitors in previous studies. Thus, antiproliferation of breast cancer cells have been achieved by inhibiting HH pathway and activating autophagic cell death by introducing HH inhibitor and an autophagy activator synergistically. But this method can also increase the cytotoxicity in normal cells. Therefore, this research is focused on the development of novel HH pathway inhibitor that targeting cancer cell specific component of HH signaling which is ***tGli*** protein. In that way, it's expected that HH signaling will be downregulated and eventually induces autophagy process in cancer cells. In addition, this research is focused on developing an effective autophagy activator which can aid the HH pathway inhibition induced autophagic cell death when treating synergistically.

Here, we have proposed a monoclonal antibody which will binds to ***tGli1*** protein and downregulates its function in HH pathway. On the other hand, we have proposed an autophagy activator (**U1**) which is targeting ULK1 protein kinase domain. This molecule is proposed considering the three amino acid residues that is important for on state activity of ULK1 and its interacting proteins. The molecular docking data of this molecule and the ULK1 kinase domain shows that proposed compound U1 has better binding interactions. Therefore, it can be expected this molecule can act as a better autophagy activator.

However, when thinking about the possible problem that could rise with this method, the instability and the cell impermeability of the naked antibody are considerable issues[50, 51]. The instability issue of the naked antibody treatment can be overcome by pH optimization, molecular stabilizers, buffer optimization. In addition, cell impermeability can be overcome by developing conjugation chemistries where antibody is attached to carrier molecule for the intracellular delivery[52] [51]. So far there have been many conjugation technologies that can enhance the target delivery in the circulation to limit off-target toxicity. These findings have been beneficial for high selectivity with favorable pharmacokinetics profiles of monoclonal antibodies. Therefore, to enhance the efficacy of the ***tGli1*** antibody, a carrier molecule can be attached to make a immunoconjugate that can specifically target cancerous cells. pH-Lip is a known carrier molecule that can specifically target tumor microenvironment and this delivery molecule is capable of delivering cell-impermeable molecules in to the cells in tumor microenvironment base on the acidity[53].Since cancer cell environment is acidic, this method can be used to deliver the ***tGli1*** antibody, directly to the cancer cells to expand its therapeutic efficacy. On the other hand, same method can be applied to the U1 molecule for delivering it to vicinity of tumor environment. Furthermore, it's crucial to develop and validate the appropriate in vitro test with the combination therapy on human blood and tissues and have predictive tests before administration on human.

In conclusion, the ***tGli1*** antibody induced inhibition of HH pathway, combine with an autophagy activator to destroy the cancer cell via autophagic cell death, in cancer cell specific manner may be a novel therapeutic strategy for breast cancer prevention.

6. References

1. Haukaas, T.H., et al., *Metabolic Portraits of Breast Cancer by HR MAS MR Spectroscopy of Intact Tissue Samples.* Metabolites, 2017. **7**(2): p. 18.
2. Wang, T.-W., et al., *Tailored design of multifunctional and programmable pH-responsive self-assembling polypeptides as drug delivery nanocarrier for cancer therapy.* Acta Biomaterialia, 2017.
3. Siegel, R.L., K.D. Miller, and A. Jemal, *Cancer statistics, 2017.* CA: A Cancer Journal for Clinicians, 2017. **67**(1): p. 7-30.
4. Yu, Y., et al., *HOTAIR may regulate proliferation, apoptosis, migration and invasion of MCF-7 cells through regulating the P53/Akt/JNK signaling pathway.* Biomedicine & Pharmacotherapy, 2017. **90**: p. 555-561.
5. Dagenais, M., et al., *The Interleukin (IL)-1R1 pathway is a critical negative regulator of PyMT-mediated mammary tumorigenesis and pulmonary metastasis.* OncoImmunology, 2017. **6**(3): p. e1287247.
6. Rimkus, T.K., et al., *Targeting the Sonic Hedgehog Signaling Pathway: Review of Smoothened and GLI Inhibitors.* Cancers, 2016. **8**(2): p. 22.
7. Quaranta, R., et al., *Maml1 acts cooperatively with Gli proteins to regulate sonic hedgehog signaling pathway.* Cell Death Dis, 2017. **8**: p. e2942.
8. Milla, L.A., C.N. González-Ramírez, and V. Palma, *Sonic Hedgehog in cancer stem cells: a novel link with autophagy.* Biological Research, 2012. **45**: p. 223-230.
9. Cao, X., et al., *Upregulation of VEGF-A and CD24 Gene Expression by the tGLI1 Transcription Factor Contributes to the Aggressive Behavior of Breast Cancer Cells.* Oncogene, 2012. **31**(1): p. 104-115.
10. Carpenter, R.L. and H.-W. Lo, *Identification, Functional Characterization, and Pathobiological Significance of GLI1 Isoforms in Human Cancers.* Vitamins and hormones, 2012. **88**: p. 115-140.
11. Wang, X., et al., *Anti-proliferation of breast cancer cells with itraconazole: Hedgehog pathway inhibition induces apoptosis and autophagic cell death.* Cancer Letters, 2017. **385**: p. 128-136.
12. Jimenez-Sanchez, M., et al., *The Hedgehog signalling pathway regulates autophagy.* Nature Communications, 2012. **3**: p. 1200.
13. Lo, H.-W., et al., *A novel splice variant of GLI1 that promotes glioblastoma cell migration and invasion.* Cancer research, 2009. **69**(17): p. 6790-6798.
14. Zhu, H., et al., *The GLI1 Splice Variant TGLI1 Promotes Glioblastoma Angiogenesis and Growth.* Cancer letters, 2014. **343**(1): p. 10.1016/j.canlet.2013.09.014.
15. Singla, V. and J.F. Reiter, *The Primary Cilium as the Cell's Antenna: Signaling at a Sensory Organelle.* Science, 2006. **313**(5787): p. 629-633.
16. Ingham, P.W., *Hedgehog Signaling.* Cold Spring Harbor Perspectives in Biology, 2012. **4**(6).
17. Bhardwaj, G., et al., *Sonic hedgehog induces the proliferation of primitive human hematopoietic cells via BMP regulation.* Nat Immunol, 2001. **2**(2): p. 172-180.
18. Liu, S., et al., *Hedgehog Signaling and Bmi-1 Regulate Self-renewal of Normal and Malignant Human Mammary Stem Cells.* Cancer research, 2006. **66**(12): p. 6063-6071.
19. Ahn, S. and A.L. Joyner, *In vivo analysis of quiescent adult neural stem cells responding to Sonic hedgehog.* Nature, 2005. **437**(7060): p. 894-897.
20. Reggiori, F. and D.J. Klionsky, *Autophagy in the Eukaryotic Cell.* Eukaryotic Cell, 2002. **1**(1): p. 11-21.
21. Deretic, V., et al., *Autophagy in Immunity Against Mycobacterium tuberculosis: a Model System to Dissect Immunological Roles of Autophagy.* Current topics in microbiology and immunology, 2009. **335**: p. 169-188.

22. Cuervo, A.M., et al., *Autophagy and Aging: The Importance of Maintaining "Clean" Cells.* Autophagy, 2005. **1**(3): p. 131-140.
23. Stolz, A., A. Ernst, and I. Dikic, *Cargo recognition and trafficking in selective autophagy.* Nat Cell Biol, 2014. **16**(6): p. 495-501.
24. Das, G., B.V. Shravage, and E.H. Baehrecke, *Regulation and Function of Autophagy during Cell Survival and Cell Death.* Cold Spring Harbor Perspectives in Biology, 2012. **4**(6).
25. Tavassoly, I., et al., *Dynamic Modeling of the Interaction Between Autophagy and Apoptosis in Mammalian Cells.* CPT: Pharmacometrics & Systems Pharmacology, 2015. **4**(4): p. 263-272.
26. Chen, H., et al., *Cyclic Mechanical Stretching Induces Autophagic Cell Death in Tenofibroblasts Through Activation of Prostaglandin E2 Production.* Cellular Physiology and Biochemistry, 2015. **36**(1): p. 24-33.
27. Das, G., B.V. Shravage, and E.H. Baehrecke, *Regulation and Function of Autophagy during Cell Survival and Cell Death.* Cold Spring Harbor perspectives in biology, 2012. **4**(6): p. 10.1101/cshperspect.a008813 a008813.
28. Alers, S., et al., *Role of AMPK-mTOR-Ulk1/2 in the Regulation of Autophagy: Cross Talk, Shortcuts, and Feedbacks.* Molecular and Cellular Biology, 2012. **32**(1): p. 2-11.
29. Takahashi, H., et al., *Autophagy is required for cell survival under L-asparaginase-induced metabolic stress in acute lymphoblastic leukemia cells.* Oncogene, 2017. **36**(30): p. 4267-4276.
30. Law, B.Y.K., et al., *N-Desmethyldauricine Induces Autophagic Cell Death in Apoptosis-Defective Cells via Ca(2+) Mobilization.* Frontiers in Pharmacology, 2017. **8**: p. 388.
31. Hanna, A. and L.A. Shevde, *Hedgehog signaling: modulation of cancer properies and tumor mircroenvironment.* Molecular Cancer, 2016. **15**: p. 24.
32. Gonnissen, A., S. Isebaert, and K. Haustermans, *Targeting the Hedgehog signaling pathway in cancer: beyond Smoothened.* Oncotarget, 2015. **6**(16): p. 13899-13913.
33. Abdal Dayem, A., et al., *The Anti-Cancer Effect of Polyphenols against Breast Cancer and Cancer Stem Cells: Molecular Mechanisms.* Nutrients, 2016. **8**(9): p. 581.
34. Tanida, I., T. Ueno, and E. Kominami, *LC3 and Autophagy*, in *Autophagosome and Phagosome*, V. Deretic, Editor. 2008, Humana Press: Totowa, NJ. p. 77-88.
35. Kinzler, K.W., et al., *The GLI gene is a member of the Kruppel family of zinc finger proteins.* Nature, 1988. **332**(6162): p. 371-374.
36. *Antibodies: A Laboratory Manual edited by Edward A. Greenfield.* The Quarterly Review of Biology, 2015. **90**(2): p. 228-228.
37. Scott, A.M., J.D. Wolchok, and L.J. Old, *Antibody therapy of cancer.* Nat Rev Cancer, 2012. **12**(4): p. 278-287.
38. Lipman, N.S., et al., *Monoclonal Versus Polyclonal Antibodies: Distinguishing Characteristics, Applications, and Information Resources.* ILAR Journal, 2005. **46**(3): p. 258-268.
39. Kremer, L. and G. Márquez, *Generation of Monoclonal Antibodies Against Chemokine Receptors*, in *Cell Migration in Inflammation and Immunity: Methods and Protocols*, D. D'Ambrosio and F. Sinigaglia, Editors. 2003, Humana Press: Totowa, NJ. p. 243-260.
40. (NCBI), N.c.f.b.i., *Homo sapiens truncated GLI1 (tGLI1) mRNA, GenBank: GQ890670.2.* 2017.
41. Promega. *pci-neo-mammalian-expression-vector-protocol*. [cited 2017 6 Aug]; Available from: https://www.promega.com/-/media/files/resources/protocols/technical-bulletins/0/pci-neo-mammalian-expression-vector-protocol.pdf.
42. BioLab.Inc, *Molecular cloning technical guide.* 2017.
43. Zhang, L., et al., *Discovery of a small molecule targeting ULK1-modulated cell death of triple negative breast cancer in vitro and in vivo.* Chemical Science, 2017. **8**(4): p. 2687-2701.
44. Ouyang, L., et al., *A small-molecule activator induces ULK1-modulating autophagy-associated cell death in triple negative breast cancer.* Autophagy, 2017. **13**(4): p. 777-778.

45. Lipinski, C.A., et al., *Experimental and computational approaches to estimate solubility and permeability in drug discovery and development settings.* Advanced Drug Delivery Reviews, 1997. **23**(1): p. 3-25.
46. Koert, U., *Stereoselective Synthesis of Oligo-Tetrahydrofurans.* Synthesis, 1995. **1995**(02): p. 115-132.
47. Alexander, M.D., et al., *Mk2 inhibitors and uses thereof*. 2014, Google Patents.
48. Mevellec, L.A., et al., *SUBSTITUTED 4,5,6,7-TETRAHYDRO-PYRAZOLO[1,5-a]PYRAZINE DERIVATIVES AND 5,6,7,8-TETRAHYDRO-4H-PYRAZOLO[1,5-a][1,4]DIAZEPINE DERIVATIVES AS ROS1 INHIBITORS*. 2015, Google Patents.
49. Tominaga, H., et al., *A water-soluble tetrazolium salt useful for colorimetric cell viability assay.* Analytical Communications, 1999. **36**(2): p. 47-50.
50. Hansel, T.T., et al., *The safety and side effects of monoclonal antibodies.* Nat Rev Drug Discov, 2010. **9**(4): p. 325-338.
51. Beck, A., et al., *Strategies and challenges for the next generation of antibody-drug conjugates.* Nat Rev Drug Discov, 2017. **16**(5): p. 315-337.
52. Goswami, S., et al., *Developments and Challenges for mAb-Based Therapeutics.* Antibodies, 2013. **2**(3): p. 452.
53. Thévenin, D., M. An, and D.M. Engelman, *pHLIP-mediated Translocation of Membrane Impermeable Molecules into Cells.* Chemistry & biology, 2009. **16**(7): p. 754-762.